Doctoral Thesis ETH No. 16783

Self-Assembly of Functionalized Nanoparticles into Microarrays and Gradients

A dissertation submitted to the

SWISS FEDERAL INSTITUTE OF TECHNOLOGY ZURICH

for the degree of

Doctor of Sciences

presented by

Christoph Huwiler
Dipl. Werkstoff-Ing. ETH
born on January 5, 1975
citizen of Hasle (LU)

accepted on the recommendation of

Prof. Dr. Janos Vörös, examiner
Prof. Dr. Marcus Textor, co-examiner
Prof. Dr. Heinrich Hofmann, co-examiner
Dr. Erik Reimhult, co-examiner

November 9, 2006

For My Parents

Abstract

The general trend in the development of new technological innovations in numerous, if not most fields of research remained the same for the last few years: smaller, faster and cheaper. Driven by the semiconductor industry[1] and many others, the urge to fabricate precise structures in the nanometer[2] range is steadily increasing and techniques to do so are rapidly evolving.

With decreasing feature sizes[3], a lot of these traditional "top-down" technologies[4] reach their physical limits and new concepts for the fabrication of structures and devices in the nanometer range are needed. A very intriguing possibility to form such hierarchical, complex nanostructures is the idea to let the structures assemble by themselves *in situ*, which is then termed a "bottom-up" approach. Obviously, this idea of "self-assembly" is inspired by nature, where such processes are omnipresent.[5]

This thesis describes various methods to produce such self-assembled nanostructures and analyzes the processes involved in their fabrication. The building blocks which were self-assembled on a (patterned) surface are colloidal particles in the nanometer range (40 and 73 nm silica nanoparticles). In a first step, these particles were assembled on a substrate as a linear colloidal gradient, continuously changing the particle density on these chips over several cm. The presented method offers an essentially material independent approach for the production of colloidal gradients and has the

[1] Moore's Law may be mentioned here, which predicts that the number of transistors per chip increases exponentially over time (http://en.wikipedia.org/wiki/Moore's_law)

[2] 10^{-9} m, a millionth of a meter

[3] Intel's Dual Core processors are currently produced with a 90 nm pitch line width

[4] Referring to techniques that "carve" structures into the substrate (such as photolithography, stamping techniques, etc.)

[5] The self-assembly of biomolecules (proteins) into complex supramolecular structures with great accuracy and high efficiency is one prominent example

additional advantage of being able to tailor the properties of the adsorbed colloidal particles by the application of a suitable heat treatment step.

Wettability contrast patterns were produced using a micro-fabrication method developed *in-house* on which silica nanoparticles were forming selective colloidal assemblies. The processes involved in the formation of these colloidal patterns were investigated. Capillary forces acting between particles during the drying process were responsible for the pattern formation arranging close-packed particle layers on the hydrophilic areas and leaving no particles on the hydrophobic background. Different methods of drying the suspension on the pattern were examined as well as the influence of a variety of parameters was studied. Generally, removing the patterned substrate at controlled conditions from the suspension leads to more controlled array formation,[6] while drying of a drop of suspension was less controllable but revealed interesting insight in the mechanisms responsible for the pattern formation.

To further increase the application potential of such nanoparticles, functionalization concepts were investigated that enhance the properties of these particles. Coating the nanoparticles with a functional co-polymer (PLL-*g*-PEG) not only acts as a sterical stabilizer for the nanoparticle suspension but also rendered these particles non-interacting with biomolecules and PLL-*g*-PEG-coated substrate surfaces, a very advantageous property for future applications of such particles in functional biosensing devices. It was demonstrated, how biotinylated PEG-side chains offer a convenient way to bind these particle to biotinylated PLL-*g*-PEG surface spots (via a streptavidin linker).[7] The parameters governing the assembly of these functionalized nanoparticle arrays on micron sized structures using the streptavidin-biotin interaction were studied and furthermore, ideas were presented how such particle arrays can be bi-functionalized[8] for specific applications in biosensing devices, where good control of the surface chemistry combined with the high surface area of nanoparticles might be a useful combination.

To conclude, a variety of different patterning approaches for nanoparticles on (patterned) substrates were examined and developed in this thesis and the mechanisms and parameters influencing these processes were investigated. Furthermore, func-

[6] Lower removal speeds and higher particle concentrations let to thicker colloid layer on the hydrophilic structures

[7] These spots were produced using a micro-fabrication technique developed *in-house*

[8] Adding a second function on the particle beside the biotin, which may then act as a capturing agent for a specific biomolecule

tionalization concepts for such nanoparticles were presented to increase the usefulness of these nanoparticle (arrays) for applications in the field of biotechnology.

Seite Leer /
Blank leaf

Zusammenfassung

Seit geraumer Zeit ist in vielen Wissenschafts- und Forschungsbereichen ein genereller Trend auszumachen: kleiner, leistungstärker, schneller und zugleich billiger müssen neuentwickelte technologische Innovationen sein. Massgeblich angetrieben von der Halbleiter-Industrie, aber auch vielen anderen Bereichen, werden immer filigranere und präziser gefertigte Strukturen gefordert, was zu einer Zunahme von Technologien geführt hat, die in der Lage sind solche Nanostrukturen herzustellen.

Mit zunehmender Miniaturisierung geraten aber viele herkömmliche, "Top-down"[9] Fabrikationsmethoden an ihre physikalischen Grenzen und in absehbarer Zeit werden neue Konzepte für die Herstellung von Nanostrukturen und -komponenten benötigt. Ein faszinierender Weg solche hierarchischen, komplexen Nanostrukturen zu produzieren, sehen Wissenschaftler in der Möglichkeit diese Strukturen sich selber "zusammenbauen" zu lassen. Diese Idee der "Selbstorganisation" ist ein sogenannter "Bottom-up"-Ansatz, wobei kleine Einzelteile automatisch zu einem grösseren Ganzen werden. Dieser Ansatz hat sich die Natur zum Vorbild genommen, wo solche Selbstorganisationsprocesse an der Tagesordnung sind.[10]

In dieser Doktorarbeit werden verschieden Wege beschrieben, wie man solche Selbstorganisationsprocesse auf technische Systeme übertragen kann und die Prozesse, die zu dieser Selbstorganisation führen werden untersucht und beschrieben. Die Bausteine, die hierfür verwendet werden, sind Nanopartikel aus Silikondioxid (mit einer Grösse von 40 und 73 nm). In einem ersten Schritt wird eine Methode präsentiert, welche es erlaubt diese colloidalen Nanopartikel so auf einer Oberfläche

[9] Als "Top-down" werden Methoden bezeichnet, wo die feinen Strukturen aus einem grossen Ganzen gefertigt werden, die Strukturen als eingebrannt, eingeätzt, gestempelt, o.ä. werden.

[10] Als Beispiel seien hier supramolekulare Biomoleküle genannt, welche spontan aus vielen Proteinen mit grosser Präzision und Effizient zusammengesetzt werden

anzuordnen, dass ein Gradientmaterial entsteht, welches auf der einen Seite eine hohe Partikeldichte aufweist und dessen Partikeldichte sich zur anderen Seite hin kontinuierlich verändert. Diese Methode ist materialunabhängig – mit gewissen Einschränkungen — und erlaubt es in einem einfachen Prozess Partikelgradientmaterialien herzustellen, welche in verschiedensten Bereichen Anwendungen finden können. Auch kann die Morphologie der Nanopartikel auf der Oberfläche mit einem Sinterprozess effizient beeinflusst werden, was eine weitere Möglichkeit zur Anpassung dieser Gradienten an viele Anwendungsprofile ermöglicht.

Weiter wird demonstriert, wie Nanopartikel auf mikrostukturierten Oberflächen gezielt angeordnet werden können. Dazu werden mikrostrukturierte Oberflächen mit unterschiedlichen Benetzbarkeiten in einem institutsinternen Verfahren hergestellt auf welchen dann die Nanopartikel sich selbst organisieren. Diese Selbstorganisation und die Prozesse die dazu führen, werden untersucht und beschrieben. Dabei zeigte sich, dass in diesem Fall Kapillarkräfte hauptverantwortlich für die Selbstorganisation der Partikel sind. Sie sorgen dafür, dass die Nanopartikel während dem Trocknungsprozess auf den wasseranziehenden (hydrophilen) Stukturen dichtgepackt angeordnet werden, während der wasserabweisende Hintergrund frei von Partikeln bleibt. Im Laufe der Arbeit wurden verschiedene Trocknungsarten und der Einfluss diverser Faktoren auf die Selbstorganisation der Kolloide untersucht. Als grundsätzlich beste Methode erwies sich dabei das kontrollierte Herausziehen der strukturierten Proben aus der Partikelsuspension, was zu besser kontrollierbaren Partikelstrukturen auf den hydrophilen Strukturen sorgt.

Mit der Absicht die Anwendbarkeit solcher Nanopartikel weiter zu steigern, wurden auch Methoden untersucht und entwickelt, welche die Funktionalisierung dieser Partikel erlauben. Die Partikel wurden dabei mit einem speziellen Co-Polymer (PLL-*g*-PEG) beschichtet, welches auf der einen Seite zu einer Stabilisierung der Partikelsuspension führt, es aber hauptsächlich ermöglicht, diese Partikel resistent gegen jede Adsorption von Biomolekülen zu machen. Solche proteinresistenten Oberflächen finden verbreitet Anwendung in vielen biotechnologischen Anwendungen und die Entwicklung von proteinresistenten Partikeln mit der zusätzlichen Möglichkeit diese Partikel auf Oberflächen gezielt anzuordnen, könnte mithelfen, dass solche Nanopartikel in der Konstruktion von zukünftigen Biosensorikgeräten eingesetzt werden, um die Empfindlichkeit dieser Geräte zu verbessern. In dieser Arbeit wurde gezeigt, welche Prozesse verantwortlich sind um diese funktionalisierten Partikel auf strukturierten Oberflächen anzuordnen. Die mit PLL-*g*-PEG/PEG-biotin beschichteten

Partikel werden dabei auf mikrostrukturierte Oberflächen gebunden. Die Nanopartikel, die nicht nur proteinresistent sind, sondern auch eine Biotin Funktion auf ihrer Oberfläche haben, werden dabei einfach auf Oberflächenregionen gebunden, auf denen Streptavidin vorhanden ist. Die Bindung zwischen Biotin und Streptavidin wird ausgenützt, um die funktionalisierten Nanopartikel gezielt auf Oberflächen zu organisieren. Desweiteren werden neue Konzepte präsentiert, welche in Zukunft auch die Funktionalisierung von Nanopartikeln mit zwei verschiedenen Funktionen ermöglichen soll. Diese bi-funktionalisierten Partikel könnten dann einst in Proteinsensorikgeräten zur Anwendung kommen, wo solche mehrfach-funktionalisierten Nanopartikel interessante Anwendungsmöglichkeiten finden.

Contents

1 Scope of the Thesis **1**

2 Introduction to the Field **5**

2.1 Motivation, Focus and Scientific Background of Thesis 5

2.2 Colloidal Particles and their Interaction with Interfaces 8

2.2.1 Interfaces and Colloids: Definitions 9

2.2.2 Stability of Colloidal Suspensions 10

2.2.3 Molecular Interaction Energies 12

2.2.4 Repulsive Electrostatic Forces 18

2.2.5 Electric Double Layers 22

2.2.6 DLVO-Theory 30

2.2.7 Repulsive Steric Forces 34

2.3 Capillary Forces 36

2.3.1 Interfacial Tension / Surface Free Energy 37

2.3.2 Capillary Forces in Three-Phase-Systems 38

2.3.3 Capillary Forces Between Particles 41

2.4 Immobilizing Colloids on a Surface: Strategies 45

2.4.1 Electrostatic Adsorption 45

2.4.2 Capillary Forces 46

2.4.3 Specific Binding of Colloidal Particles 47

2.5 Self-Assembling of Colloidal Particles on Patterned Surfaces 47

2.5.1 Surface Pre-Patterning and Particle Self-Assembly 48

2.5.2 Particle-Assembly by Electrostatic Adsorption 49

2.5.3 Particle-Assembly using Capillary Forces 49

2.5.4 Particle-Assembly via Specific Binding 53

2.5.5 Potential Applications of Nanoparticle Arrays 54

Bibliography 60

3 Methods and Materials Characterization 69

3.1 Characterization Techniques 69

3.1.1 ζ-potential measurements 69

3.1.2 X-ray Disc Centrifuge (XDC) 70

3.1.3 Contact Angle Analysis / Microdroplet Density measurements 72

3.1.4 Optical Waveguide Lightmode Spectroscopy (OWLS) 72

3.1.5 Scanning Electron Microscopy (SEM) 76

3.1.6 Ellipsometry 77

3.2 Materials Characterization 79

3.2.1 Colloidal Silica Particles 79

3.2.2 Polymers 83

3.2.3 Alkane Phosphate SAMs 87

3.2.4 Biomolecules 87

3.2.5 Buffer solutions 89

3.3 Photolithography for SMAP and MAPL 89

3.4 Production of Wettability Contrast Pattern (SMAP) 90

3.5 Production of Patterned Surfaces for Specific Binding of Colloidal Particles (MAPL) 91

Bibliography 93

4 Colloidal Gradients on Metal Oxide Surfaces 95

4.1 Introduction 95

4.2 Experimental 97

4.3 Results and Discussion 99

4.3.1 Adsorption of Colloidal Particles on Charged Surfaces 99

4.3.2 Colloidal Gradients 106

4.3.3 Heat Treatment of Nanoparticle Gradients 114

4.4 Conclusions 118

Bibliography 121

5 Nanoparticles Self-Assembly on Wettability Pattern 123

5.1 Introduction 123

5.2 Experimental 124

5.3 Results and Discussion 126

5.3.1 Wettability Contrast Characterization 126
5.3.2 Nano Colloidal Arrays on Wettability Contrast Pattern 130
5.3.3 Capillary and Hydrodynamic Forces in the Self-Assembly Process of Particles on a Wettability Pattern 142
5.4 Conclusions 151
Bibliography 153

6 Particle Assemblies using Specific Binding Systems 155
6.1 Introduction 155
6.1.1 Biotin-Streptavidin System 157
6.2 Experimental 158
6.3 Results and Discussion 161
6.3.1 Coating of Nanoparticles with PLL-*g*-PEG 161
6.3.2 Adsorption Behavior of Coated and Uncoated Silica Particles . 163
6.3.3 Production of Functionalized Nanoparticle Arrays using MAPL168
6.4 Conclusions 175
Bibliography 177

7 Bi-Functionalization of Colloidal Particles 179
7.1 Introduction 179
7.1.1 Colloidal Nanoparticles and Proteomics? 179
7.2 Experimental 180
7.2.1 Colloid Assembly Experiments 180
7.3 Results and Discussion 181
7.3.1 Increasing Sensitivity by Increased Surface Area of Particle Layers 181
7.3.2 Protein Resistance of PLL-*g*-PEG/PEG-biotin coated particle layers 183
7.4 Bi-Functionalization of Colloidal Particles 189
7.5 Conclusions 194
Bibliography 197

8 Conclusions and Outlook 199
8.1 Nanoparticle Gradients 199
8.2 Particle Self-Assembly by Capillary Forces 200
8.3 Functionalizing Nanoparticles 201

8.4 Arrays of Functionalized Particles 202
8.5 Outlook 202
8.5.1 Nanoparticle Gradients 203
8.5.2 Silica Nanoparticle Assemblies 204
8.5.3 Functionalized Nanoparticles 205
Bibliography 207

Curriculum Vitae **213**

CHAPTER 1

Scope of the Thesis

This thesis was motivated by the desire to exploit the many interesting properties of nanoparticles in a controlled way. To do so, in many cases, it is necessary to immobilize these nanoparticles on a — possibly structured — surface rather than keeping them in a suspension. The study of particle-surface interactions, the understanding of particle self-assembly on surfaces and the control of the drying process are technological key elements in this context. The potential approaches of increasing the functionality of such particle assemblies on surfaces are therefore the main topics of this thesis. From a fundamental point of view, it is explored what forces govern the assembly of colloidal particles on surfaces — patterned and unpatterned — and how particle organization on a surface can be controlled. A second objective of this thesis is the tailoring of the nanoparticles functionality in order to develop systems and strategies of potential interest as platforms for a range of applications. An example it the use of such functionalized particle arrays in biosensing devices, where particle surface chemistry and particle array formation on the surface have to be carefully and simultaneously controlled. In the following section the scope of the thesis is outlined in more detail.

Overview of Thesis Chapters

Chapter 2 starts with an overview of the most important forces involved in the interaction between colloidal particles and (patterned) surfaces. This theoretical introduction provides the basic of understanding of how particles interact with a each other and with a surface. Two main contributions are identified that govern

the particle assembly on surfaces: attractive forces (mainly of electrostatic nature) that may attract and adsorb particles to a surface in suspension and capillary forces that act between particles on a surface during the drying process. The interplay between these main forces determines the outcome of a particle array on homogeneous or patterned substrates and the tailoring of these forces will be an important task in the following chapters. Furthermore, an overview of present methods for the production of particle arrays found in the literature is provided in *Chapter 2*, discussing the different methods, that have been or are being developed to produce self-organized particle assemblies. *Chapter 3* provides information on all the experimental techniques including micro-fabrication methods used in this thesis, as well as a detailed characterization of the particles and the particle coating protocols and other information on materials and methods.

Chapter 4 introduces a new and universal method for the production of gradients in particle surface density. Controlling the adsorption kinetics of nanoparticles during a dip-coating process on a substrate leads to distinct particle gradients with a linear change in particle density on the surface with tunable density profiles. A subsequent sintering process of the particle gradients allows further tailoring of the gradient properties. Using a surface patterning technique developed in-house termed SMAP, silica nanoparticle assemblies are produced using capillary forces as the driving force in *Chapter 5*. Besides providing fundamental insight in the self-assembly process of nanoparticles on a patterned surface, this method furthermore offers the straightforward possibility of generating large-scale nanoparticle assemblies without geometrical restrictions. While such arrays may be useful on their own, it was aimed at developing an assembly technique that relies on tailored, specific (rather than difficult to control quantitatively, unspecific) interactions, by corresponding functionalization of both particle and substrate. Thus, in *Chapter 6* particle arrays based on coating the particles with a biotinylated polymer and assembling them with spatial control on a pattern of streptavidin through exploitation of the biotin-streptavidin linkage system. The final results chapter (*Chapter 7*) sketches ways how to use nanoparticle arrays as developed in *Chapter 6* in biosensing devices, where the properties of these arrays may shine the most. The colloidal assemblies are shown to be resistant to protein adsorption (as is the surface pattern); as shown in *Chapter 7*, preliminary results prove that it is possible to add a specific second function to the nanoparticle surface which will, for example, provide a way of capturing target

molecules from a biological sample; the increased surface area of the nanoparticle array will thereby increase the detection sensitivity of such a bioaffinity assay.

Seite Leer /
Blank leaf

CHAPTER 2

Introduction to the Field

2.1 Motivation, Focus and Scientific Background of Thesis

Functional materials with topographically or chemically complex (e.g. hierarchical) surfaces in the nanometer range are currently developed in view of their promising new or improved optical or electronical properties that find potential applications in biosensing or (opto-)electronic devices. The still-emerging field of nanotechnology is in need of reliable, fast (and therefore parallel), economical and versatile methods for structuring surfaces with controlled surface chemistry and topography in the nanometer range. A very intriguing possibility to form such hierarchical, complex nanostructures is the idea to let such structures assemble by themselves *in situ*. Obviously, this idea of "self-assembly" is inspired by nature, where such processes are omnipresent. One of the most prominent examples for such a process is nature's capability of self-assembling specific biomolecules (proteins) into complex supramolecular structures with great accuracy and high efficiency. In a way, the analogy to building a car engine is not far-fetched. A molecular "car-engine" (e.g. the motor-protein complex of certain bacteria) is simply "self-assembled" *in situ* by nature from its components. It is certainly a tempting idea to throw the motor components in a room where they "self-assemble" into the ready-to-use car-engine without any outside work needed! With that example, inescapably, one of the most prominent concepts in nanotechnology has been introduced, the "bottom-up approach". Its counterpart, the "top-down approach" describes the formation of

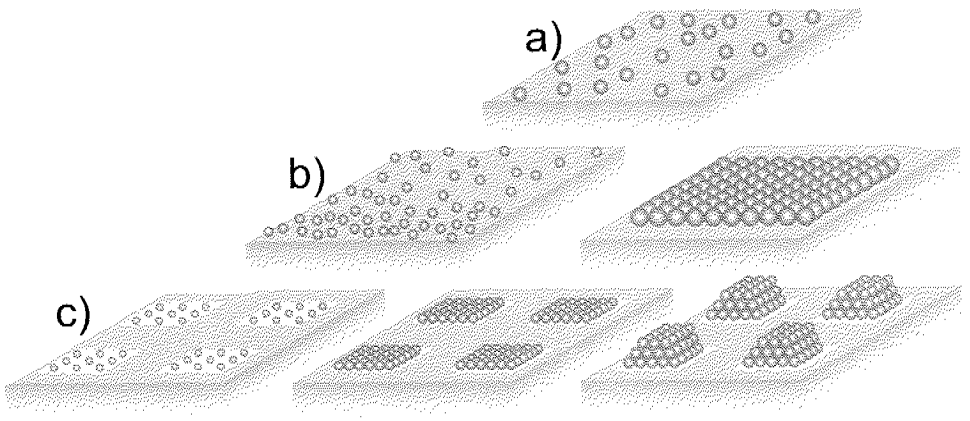

Figure 2.1: a) random adsorption of particles on a surface b) modification of surface properties or adsorption conditions may lead to the formation of a monolayer or controlling the adsorption kinetics on a substrate (see Chapter 4) a colloid density gradient. c) prepatterning of the substrate opens new possibilities to self-assemble colloidal particles in specific configurations.

(nano-)structures by "carving" out topographical or chemical structures with macroscopic means. Most conventional fabrication techniques belong to this realm.[1] For nanotechnolgical applications, the concept of self-assembly (= the "bottom-up approach") is indeed very intriguing, since building structures in the nanometer range is not a trivial task for obvious reasons.[2] Thus, a lot of scientific effort has been put forward to learn about self-assembly processes and adopting them for technological applications. Among the best-known of these self-assembly processes are arguably molecular self-assembly techniques, where specific molecules[3] form stable, well-ordered molecular monolayers on a surface. These so-called self-assembled monolayers (SAMs) are an often used way to specifically modify the chemical surface properties.[1–3] Such self-assembly techniques are not restricted to molecular species, it is also possible to spontaneously self-assemble more complex, mesoscale and even millimeter-sized 3D objects into different structures.[4–6]

In recent years, spherical colloids have attracted considerable interest in such self-assembly experiments due to numerous advantageous properties (controllable size and surface properties, well-defined shapes, narrow size distributions, variety of materials available).[7] For example, the potential of colloidal nanoparticles to form

[1] Photolithography, etching techniques, printing techniques, etc.

[2] Given the very small size at which one has to operate and the vast number of repeating structuring elements that have to be fabricated on a small area.

[3] For example alkane thiols or alkane phosphates

functional assemblies on patterned substrates let to the development of different methods using colloidal particles as building blocks for such self-assembly processes. Furthermore, methods are also developed to form colloidal assemblies that carry a certain (often biological) function towards possible applications of such arrays in biotechnology. More specifically, substantial effort has been put into self-assembling colloidal particles into various structures, for example 3D crystals,[8–11] monolayers [12] and patterned particle arrays [7, 13 20]. The progress in this field will be addressed further in this introductory Chapter. Fig. 2.1 depicts schematically some general possibilities of how self-assembly of particles may be used to form different structures on a surface. Undirected adsorption of colloidal particles is shown in Fig. 2.1a), where particles simply adsorb to a surface randomly by electrostatic interactions. Directing this process (or changing the surface properties in a specific way) may lead to structures as shown in Fig. 2.1b): formation of close-packed self-assembled colloidal monolayers (on the right) or of colloidal particle gradients (on the left). The production of such particle gradients, where the particle density may be changed over the length of the substrate, is presented in Chapter 4 of this thesis. Fig. 2.1c) finally shows different possibilities of how colloidal particles may be self-assembled on patterned substrates (Chapters 5 and 6). In this case, pre-patterning of the surface (in the micron-scale) provides a template to which the particles react and structures as depicted may be achieved.

The focus in this thesis will be on the production of different colloidal structures assembled on a surface, with special emphasis on the formation of nano colloidal assemblies of particles on patterned substrates. The precise control of particle positioning, however, is often not sufficient as the particles ideally have to carry a given function, which make them interesting for the use in biotechnological applications. Chapter 4 will introduce the formation of colloidal gradients on a homogeneous surface. There, it is discussed how the control of particle adsorption kinetics and the control of particle interaction with the substrate can produce particle gradients that have a very low concentration of particles at one end of the sample and contain a full monolayer on the other end of the sample (the typical length of such a gradient can be varied between a few mm and a few cm). Then, in Chapters 5 and 6, surface patterning methods developed in our group are used as a basis for the self-assembly of particles onto these patterns. Two inherently different mechanisms of producing such nano colloidal arrays are developed and compared in these chapters. As mentioned, functionalization of particles may offer an interesting way to expand the

usefulness of nanoparticles in such colloid arrays. Chapter 7 shows an collection of ideas and first results how such particles carrying different functional units may help in the production of better and more sensitive biosensing devices (for example for proteomic applications).

It is therefore the aim of this introductory chapter to provide the reader with the necessary background knowledge from a theoretical point of view to understand how particles interact with surfaces and what forces determine the outcome of, say, structures depicted in Fig. 2.1c) as well as give a comprehensive overview of current literature in this field including possible applications of such hierarchical colloidal arrays. Thus, in the following sections, the most important theoretical concepts in interfacial and colloidal science are summarized and also, the origin of capillary forces in such processes and some immobilization strategies for colloidal particles on surfaces are discussed. In the end of this section, the different forces involved in the production of colloidal assemblies on patterned surfaces should be identified, allowing an approximate prediction of how these particle arrays develop depending on the properties of the colloidal suspension and the structured surface.

2.2 Colloidal Particles and their Interaction with Interfaces

Producing nano colloidal arrays on a (structured) surface (Fig. 2.1c) (as accomplished in this thesis) involves several important steps: 1. a stable colloidal suspension must be formed and maintained. 2. interactions of the colloidal particles in the suspension with the substrate surface must be controlled / tailored and 3. the drying of the suspension must be accomplished without an unwanted impact on the final structure. Thus, the study of interactions of colloidal particles with solid surfaces and liquids is a key element and a recurrent topic in this work. Processes occurring in steps 1 and 2 are directly related to the properties of the interfaces involved. The other important part in this work (phase 3) involves drying of the colloidal particles on a (structured) surface, which leads to a second important effect that affects the outcome of such a particle array: capillary forces. In this section, the focus will be on particle-surface interactions in suspension (steps 1 and 2 as mentioned before), thus discounting capillary forces, which will be discussed in Section 2.3, for the moment. To start with, some basic definition of this field are given:

2.2.1 Interfaces and Colloids: Definitions

The general term "interface" denotes a boundary between two phases (liquid-liquid, solid-liquid, liquid-gas, etc.), while a "surface" refers specifically to a boundary between a solid and a gas or a liquid (colloidal particles therefore have surfaces). Phenomena directly related to the properties of these interfaces (e.g. in colloidal systems) play an important role in a myriad of events in every-day life. A few classical examples are mentioned here in no particular order: dissolving fat molecules from dishes / cloth using soap, but also our bodies ability to metabolize fat, production of inks and colors, properties of soil, creation of water-repellent surfaces, the formation of river deltas by the sedimentation of small particles or weather phenomena (fog, smog, smoke). These are all processes where the interface plays a dominant role. Two main phenomena are responsible for the relevance of interfaces in so many processes[21]: the interfacial tension and the occurrence of adsorption. Both aspects will be discussed later.

Table 2.1: Colloidal Systems

Continuous Medium	**Dispersed Medium**		
	Gas	**Liquid**	**Solid**
Gas	**non (all soluble)**	**(liquid)aerosol** (fog, mist)	**(solid) aerosol** (smoke, dust)
Liquid	**foam** (whipped cream)	**emulsion** (milk, blood)	**sol** (paint, ink)
Solid	**(solid) foam** (styrofoam,metallic foams)	**gel** (gelatin,cheese)	**(solid) sol** ruby glass

The term "colloid" is somewhat less strictly defined. It was introduced in 1861 by Scottish scientist Thomas Graham and originates from the Greek word $\kappa o\lambda\lambda\alpha$, meaning "glue". Usually, a colloid refers to an entity having a dimension (in at least one direction) between 1 and 1000 nm which is dispersed in a medium. Based on that general definition, one can imagine different kinds of colloidal systems depending on whether the colloid is solid, liquid or gaseous and in what kind of medium it is dispersed. An overview of colloidal systems is given in Table 2.1. Looking at this definition for "colloid", it becomes evident that colloid and interfaces are closely related due to the fact that colloidal systems exhibit very large surface areas per given volume (since their size is so small) and surface effects are pre-eminent.[22]

Interfacial properties therefore govern the properties of colloidal systems to a large extent.

2.2.2 Stability of Colloidal Suspensions

One of the basic problem in colloid science is the stability of colloidal suspension. Why do small solid particles not agglomerate and sediment as one would expect from a thermodynamical point of view? First, we can therefore note that using the term "stability" to describe the ability of a colloidal suspension to remain its dispersed state is somewhat misleading, because the thermodynamically stable situation for a colloidal suspension would be its agglomerated form. A dispersed colloidal system represents a high energy situation which is thermodynamically extremely unfavorable. Colloidal particles, that are not soluble in the medium, would therefore like to minimize the surface area exposed to the medium: this situation would be reached in the agglomerated state. A "stable" suspension is thus — thermodynamically correctly speaking — in a "metastable" state. However, there is an energy barrier that the particles must overcome to move from the dispersed state to its agglomerated state as discussed in section 2.2.6. This energy barrier can be so high, that in a given time interval no agglomeration occurs: each particle has an average energy of $\frac{3}{2}kT$, the "height" of the energy barrier can vary over a wide range. But no matter how high this barrier is, a few particles will have the needed energy to overcome it and agglomerate. If the energy barrier is at least around 10 times higher then the energy of a particle, a suspension is usually considered "stable".[23] But again, stability in this sense is a purely kinetic idea and a very relative term that must always be regarded in the context of the application. For certain applications a suspension which does not agglomerate for a day might be considered as "stable", while other suspensions might be kept for more then 100 years without particles flocculating.[4] Colloid stability is therefore mainly a question of how fast or how slow the kinetics of agglomeration are. It is one of the main tasks of colloidal science to find ways to manipulate that energy barrier and find models and equations that describe these barriers and interaction curves. In the following paragraphs the basic ideas of "colloidal stability" will be reviewed. Generally, two kinds of colloidal particles can be distinguished, which differ largely in the way they interact with the surrounding

[4]Faraday's famous gold sols[24] are still kept in suspension today

media. This difference also has the consequence that the way they can be stabilized differs substantially:[21]

hydrophilic colloids In this case the colloids (e.g. polymer molecules, proteins, micells etc.) are soluble in the solvent (e.g. water) and the colloid suspension forms spontaneously. These colloid suspensions are inherently stable because their affinity to the solvent is much higher then to themselves. Thus, it is seldom this class of colloids that is referred to when the term "colloid" is used. Also, the whole discussion of stability of colloidal suspension is in this case not necessary, since the dispersed state is for this class of colloid the thermodynamically stable state. Instead of hydrophilic, the term lyophilic (which is more general and not restricted to water-based systems) is used.

hydrophobic colloids The medium is not a solvent for the colloids in this case. Most metal and metal oxide colloidal particles belong to this category and the stability of such suspensions is not as easily achieved and maintained, since here, colloidal particles in the dispersed state are not in their thermodynamical equilibrium and clever strategies (or lucky coincidence...) have to be used to form a "stable" suspension (which is always only metastable, correctly speaking). Similarly to hydrophilic colloids, hydrophobic colloids are also called lyophobic in a more general context.

It is very important to note, that the terms hydrophilic and hydrophobic in this case are not used in their more common meaning (describing the wetting behavior of a surface or more general the affinity of water to that substance). "Hydrophobic colloids" are just in as so far "hydrophobic" as they are not soluble in water (water is not a good solvent for these particles), they still often have a "hydrophilic" surface (which is associated with a low water contact angle, as discussed in Section 2.3). In context of this work, the focus lies on lyophobic colloids (e.g. silica nanoparticles in aqueous media) and factors governing their stability are discussed. Again, silica particles are a good example for "hydrophobic colloids" (they are not dissolved by water) which have a hydrophilic surface (a very low water contact angle).

Colloidal particles interact with each other in various ways in the suspension. Usually, these forces are divided into the following main categories:

- Van der Waals or dispersion forces (attractive)

- electrostatic interactions (in charged particle systems), also called double layer forces (repulsive)
- steric interactions (repulsive)
- chemical interactions (e.g. formation of chemical bonds) (attractive)
- gravitational forces (if particles are sufficiently large and / or have a high density)[5]

It is the superposition of all these attractive and repulsive forces that determines for how long (if at all!) a colloidal suspension can maintain its stability.

2.2.3 Molecular Interaction Energies

This section deals with intermolecular forces that have an important influence on colloid stability. There are two main contribution to the interaction potential of colloidal particles by molecular forces. On the one hand, Van der Waals forces, attractive forces due to uneven charge distributions in molecules, are always present and are to a large part responsible for the attraction of colloidal particles. On the other hand, when two molecules approach each other, electron shells of the one molecule will start to interact with the other. Electron orbital overlap is not possible, thus molecules will heavily repel each other at very close distances. These two effects are commonly referred to as molecular interactions and they will be discussed in the next paragraphs.

Van der Waals Forces

The attractive part between two particles in a colloidal suspension is termed Van der Waals interactions and was postulated by J.D. van der Waal in 1873.[25] In his semi-empirical equation of state describing deviations from the ideality in gases the term a describes the attractive force between two molecules (b is the intrinsic volume of the molecules, n the number of moles):

[5]Obviously, gravitational forces are not strictly interparticle forces, but still are a contributing force that influences the stability of a colloidal suspension

$$(p + an^2/V)(V - nb) = nRT \tag{2.1}$$

Van der Waals forces are a result of an uneven distribution of positive and negative charges in a molecule. If such an uneven distribution is found in a molecule also in its isolated state, it is called polar and if two such molecules approach each other, attractive orientations are energetically more likely and stable: as a consequence, two polar molecules attract each other. Keesom found the r^{-6} dependence of this kind for polar attraction. But also a polar and an apolar molecule attract each other in a similar way because the polar molecule induces an uneven charge distribution in the apolar molecule. It was Debye who realized this process and thus, Debye-Van der Waals forces have to be added to the Keesom-Van der Waals forces. They also scale with r^{-6}. These two contributions can be derived using classical electrostatics but there is a third (and for colloidal science) very important term in Van der Waals forces which is of quantum mechanical nature: the London-Van der Waals or dispersion forces.[26] These forces operate between two non-polar molecules and quantum mechanical perturbation theory is needed to solve this problem. We can imagine these forces if we look at a molecule as a stable nucleus surrounded by electrons, which circulate with very high frequencies around the nucleus ($10^{15}s^{-1}$). Thus, at every moment, the molecule is "polar", but this polarity changes with the frequency very rapidly. But still, if two such non-polar molecules approach, they will have a higher probability for attractive configurations and thus an attractive force evolves between the two molecules. One effect of these dispersion forces is that they are "retarded" when the molecules are far apart. The information, where the electrons in the molecules are has to be transported to the other molecule and the further apart they are, the "less" correct this information is (because transporting this information (via electromagnetic waves) needs a finite amount of time). Thus, at larger distances, dispersion forces scale with r^{-7} instead of the usual r^{-6} dependence. In this context, this semi-classical analogy shall suffice to give a "feeling" for this kind of Van der Waals forces. Thus, we may write:

$$u(r) = -(\beta_K + \beta_D + \beta_L)/r^6 \tag{2.2}$$

where β_K is the contribution of the Keesom-Van der Waals forces, β_D those of the Debye-Van der Waals forces and β_L those of the London-Van der Waals forces. Note

that 2.2 is derived for vacuum, e.g. no medium between two molecules. If a medium (such as water) is between the two molecules, the Van der Waals forces are reduced because the dielectric screening from the medium. Obviously this screening effect is particularly strong for water with its high dielectric constant. The energy of the Van der Waals interactions (for all three types) is around 1 $kJmol^{-1}$ where as a covalent bond has a binding energy of around 150 to several hundreds $kJmol^{-1}$ (hydrogen bonds, for comparison, have typical energies of around 50 $kJmol^{-1}$). This also means, that Van der Waals interactions are only relevant at relatively low temperatures or for large molecules and — as described below — for macroscopic objects.

The energy curve $u(r)$ for the Van der Waals force between two molecules decreases with r^{-6} for not too great distances between the interacting molecules. The attractive force $F(r)$ therefore decreases with r^{-7} since the following relations between the force F (for conservative forces) and the energy u hold:[6]

$$F = -\mathrm{d}u/\mathrm{d}r \tag{2.3}$$

Van der Waals Forces of Colloidal Particles

To determine the Van der Waals forces between two macrobodies (e.g. colloids), instead of two molecules, several theories have been developed, that of Hamaker and De Boer and that of Lifshitz[27][7] being the most common. Due to its nature, London-Van der Waals forces are in principle the only relevant contribution to the Van der Waals forces in this situation. Pairwise addition[8] of all interactions in the two considered macrobodies yields the following expression for the London-Van der Waals interaction energy for two spheres of radius a_1 and a_2 (Fig. 2.2a):

$$U(r) = -\frac{A}{6}\left[\frac{2a_1a_2}{r^2-(a_1+a_2)^2} + \frac{2a_1a_2}{r^2-(a_1-a_2)^2} + ln\left[\frac{r^2-(a_1+a_2)^2}{r^2-(a_1-a_2)^2}\right]\right] \tag{2.4}$$

[6]In conservative forces, the work needed to go from A to B is equal to the difference in potential energy, e.g. no energy is dissipated. Van der Waals, electric and gravitational forces are examples.

[7]The most significant difference between the two is, that the Lifshitz theory also includes retardation effects, which are neglected by Hamakers theory

[8]Assumptions: every atom of particle 1 interacts with all atoms of particle 2, no screening effects occur (e.g. no medium is present), retardation is neglected and instead of summing up all contributions the integral is taken

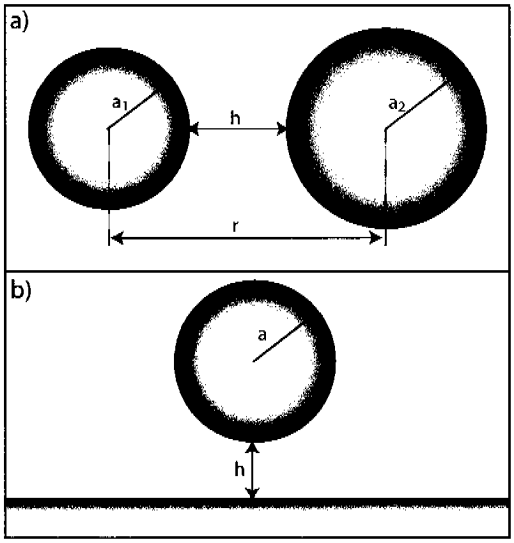

Figure 2.2: Schematic illustration of two spheres (radius a_1 and a_2) separated by a distance h (a) and a sphere (radius a) and a flat plate separated by the distance h (b).

where A is the Hamaker constant and r is $h + a_1 + a_2$ as seen in Fig. 2.2a). The Hamaker constant describes the attraction between the two bodies 1 and 2 (across a medium 3) and values for this constant can be calculated[28, 29] ($A_{12(3)}$ is abbreviated for convenience to A). The Hamaker constant is a convenient and conventional way to estimate the magnitude of the attractive Van der Waals forces.[29] For two equal spheres $a = a_1 = a_2$), Eq. 2.4 reduces to:[9]

$$U(r) = -\frac{A}{6}\left[\frac{2a^2}{h^2+4ah} + \frac{2a^2}{h^2+4ah+4a^2} + ln\left[\frac{h^2+4ah}{h^2+4ah+4a^2}\right]\right] \tag{2.5}$$

For the interesting region where the two particles come very close together, e.g. $h << a_1, a_2$ (for Eq. 2.4) and $h << a$ (Eq. 2.6), we get the two expressions for the interaction energies between two spheres (Eq. 2.6) and two equal spheres (Eq. 2.7):

$$U(r) = -\frac{Aa_1a_2}{6h(a_1+a_2)} \tag{2.6}$$

$$U(r) = -\frac{Aa}{12h} \tag{2.7}$$

[9]Here, we use h instead of r (as defined before), because h is the parameter which is relevant in calculating interaction energies, as done later

In this case, the interaction energy $U(r)$ is in J instead of J/m^2, an indication that Eq. 2.7 considers the complete interaction energy between two particles of radius a. In the course of this work, not only the interaction between two particles are of interest but also the interaction of a colloidal particle with a flat surface (see Fig. 2.2). This is the limiting case of Eq. 2.4 where $a_1 = a$ and $a_2 \rightarrow \infty$ and we can thus derive:

$$U(r) = -\frac{A}{6}\left[\frac{a}{h} + \frac{a}{h+2a} + ln\left[\frac{h}{h+2a}\right]\right] \tag{2.8}$$

For small distances between the sphere and the flat substrate ($h << a$) we get:

$$U(r) = -\frac{Aa}{6h} \tag{2.9}$$

which is very similar to the decay behavior between two spheres. $U(r)$ is here again in J indicating that it is the total interaction energy between a sphere of radius a and a the flat substrate. Lastly, the potential energy for two flat plates with separation distance h is given by:[23]

$$U(r) = -\frac{A}{12\,\pi\,h^2} \tag{2.10}$$

Note, that in this case, the interaction energy $U(r)$ is calculated in energy per unit area (J/m^2).

Recall, that the decay behavior between to molecules in vacuum scales with r^{-6} while in the case of two particles (or a particle and a flat surface) the decay behavior changes drastically (scaling with r^{-1}), which is due to the nature of the London-Van der Waals forces. These forces gain of importance as soon as we look at macroscopic objects and the decay of these attractive forces is much smaller compared to that of atoms or molecules. While the equations presented before are derived for vacuum conditions it is shown, that the same equations also remain valid in the presence of a medium between the two objects. The only thing that changes is the Hamaker constant A, which will then also reflect the attractive forces between the objects and the medium. For two objects of the same material, the Hamaker constant will always be positive (or 0), which states that two objects of the same material will always attract each other. It may happen in the case of two objects of different material

that they will repel each other. This is not because the London-Van der Waals forces are repulsive but because the attraction of one object to the medium is larger then to the other object, which is then excluded. Calculated and experimental values for Hamaker constants for a variety of materials can readily be found in literature.[29, 30]

Repulsive Molecular Forces

If two molecules come to close vicinity of each other, their electron shells will start to overlap. This, however, is energetically extremely unfavorable (Pauli's law prohibits, that two electrons in the same state occupy the same space). This repulsion is also called "hard core" or "Born" repulsion. There exists no generally valid law, but it is agreed that the decay of that repulsion energy is very steep. The most common notation is a r^{-12} law.

Lennard-Jones pair interaction

If we now consider the attractive molecular interaction energy (Van der Waals attraction) and the repulsion energy originating from the molecules being "hard spheres", we can write the total molecular interaction energy between two molecules as the sum of the two. This expression is commonly known as the Lennard-Jones pair potential.

$$u(r) = 4u_m \left[\left(\frac{s}{r}\right)^{12} - \left(\frac{s}{r}\right)^{-6} \right] \tag{2.11}$$

The Lennard-Jones interaction energy curve is schematically depicted in Fig. 2.3. There, the equilibrium distance r_m can be identified as the distance between the two molecules, where the Lennard-Jones interaction energy curve $u(r)$ has its lowest negative value $-u_m$. This point of maximum attraction is the equilibrium distance that the two molecules will occupy if no other influence (temperature, other forces) are involved. If the distance is smaller than r_m, the two molecules repel each other heavily due to the repulsive force from overlapping electron orbitals. At larger distances then r_m, the molecules will be attracted towards r_m due to the attractive r^6 term in Eq. 2.11 originating from the London-Van der Waals interaction.

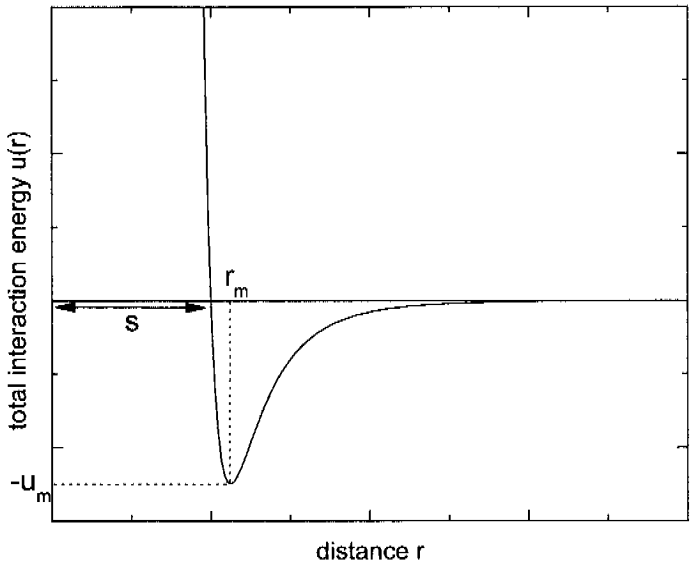

Figure 2.3: Schematic illustration of the Lennard-Jones interaction energy curve $u(r)$ is given in equation 2.11. The large r^{-12} term is responsible for the high repulsive potential at close separation distances between two molecules. At a given distance r_m, the total interaction energy has its local minima $-u_m$. This point is the equilibrium separation distance that two molecules will have.

2.2.4 Repulsive Electrostatic Forces

Electrostatic Interactions

Charges are omnipresent in (solid) colloidal systems and influence the properties of such a system drastically. They are mainly introduced by ionization of surface groups (e.g. hydroxyl groups) or the adsorption of charged molecules or ions on the particles heavily depending on the conditions of the system (such as ionic strength or pH). The reason why electrostatic effects play such an important role in colloidal systems lies in their relatively long range character. The Coulomb force between two charges decays with r^{-2} while e.g. attractive Van der Waals forces between two molecules decay much faster (with a scaling factor of r^{-7} as discussed previously). When looking at a colloidal system from an electrochemical point of view, this system can be treated in different ways. Often it is sufficient to look at such a system by treating the solvent as homogeneous isotropic medium only affecting electrochemical process through its dielectric permittivity. This primitive approach[31] works fine for relatively long distances but obviously breaks down when molecular dimensions are reached and the solvent cannot be treated as a homogeneous entity. This is

also the reason why classical models (such as the Debye-Hückel theory, the Gouy-Chapman theory and the DLVO theory, which will be discussed in Section 2.2.6) have their limitations under these circumstances.

Ions in solutions are usually the charge carriers in colloidal systems and their presence gives rise to a number of important electrochemical effects, that are closely related to colloidal stability. As a whole, the suspension is electroneutral, containing an equal number of positive and negative ions, thus the space charge density ρ is 0. Locally, however, ρ can deviate substantially from 0. Near a surface, ρ is not equal to zero because surfaces usually also have a surface charge density σ and counterions (carrying the opposite charge than the surface) are enriched making ρ non-zero. Specifically, around a charged colloidal particle, the ion distribution is different from the bulk distribution: counterions are enriched and co-ions are depleted near the surface. This effect — in short — is referred to as the electrical double layer (EDL). The details of this EDL, however, are more complex and will be discussed Section 2.2.5. It is safe to say, that the formation of the EDL near a surface is one of the oldest and still controversially discussed problems of interface and colloid science. It is also mentioned at this point, that both ρ and σ are macroscopic quantities. This means we have to look at a sample with a large enough volume and a large enough time scale (since ions usually are mobile) to average the charges in this volume during the time period. Since we look at ions and charge densities often in such a macroscopic way, we have to expect deviations from these models if we approach molecular length scales (where ions have to be treated as individual charge carrier). The presence and distribution of these ions and the influence of the surface charge density on the stability of a colloidal system are the topics of this next few paragraphs.

Debye-Hückel theory

Ions in solution — due to their charge — attract or repel each other by Coulomb interactions. These attractions lead to a certain ordering in a solution, because around a cation there is on average more negative charge then in the bulk. The cation carries an "atmosphere" of anions around itself. It was Debye and Hückel[32] who formulated a theory describing how ions interact with each other in a solvent. They derived a linear differential equation for the potential $\psi(r)$ at a given distance r from the ion:

$$\frac{1}{r^2}\frac{d}{dr}\left[r^2\frac{d\psi(r)}{dr}\right] = \kappa^2\psi(r) \tag{2.12}$$

To get the analytically soluble expression in Eq. 2.12, Debye and Hückel had to approximate the exact differential equation (by what is known as the Debye-Hückel approximation) and which has the consequence that Eq. 2.12 remains only valid in case of very dilute electrolyte solutions. In the above equation, the parameter κ is given by:

$$\kappa^2 = \frac{F^2\sum_j z_j^2 c_j(\infty)}{\epsilon_0\epsilon RT} \tag{2.13}$$

z_j is the charge of the ion j and $c_j(\infty)$ is the bulk ion concentration of species j and F the Faraday constant. Since κ has the dimensions of a reciprocal length, κ^{-1} is a length and is known as Debye-length. It was mentioned before, that the Debye-Hückel theory assesses the charge "atmosphere" around an ion. The Debye-length now is a means to describe the thickness of this atmosphere and is a measure for the screening of the potential of the central ion by surrounding counterions. We can now also define the ionic strength:

$$I = \frac{1}{2}\sum_j z_j^2 c_j \tag{2.14}$$

For monovalent salts, the ionic strength is equal to the salt content in M. This leads — together with Eq. 2.13 — to:

$$\kappa^2 = \frac{2F^2 I}{\epsilon_0\epsilon RT} \tag{2.15}$$

If the values for the natural constants (F, ϵ_0 and R) are inserted and an aqueous solution at $T = 298°C$ is considered, we get:

$$\kappa^2 = 10.822\, I \tag{2.16}$$

Values for the Debye length calculated from Eq. 2.16 are shown in Fig. 2.4. High ionic strength solutions decrease κ^{-1} drastically, thus shielding the charge of an ion efficiently. Also, higher valent electrolytes shield charges more efficiently. This

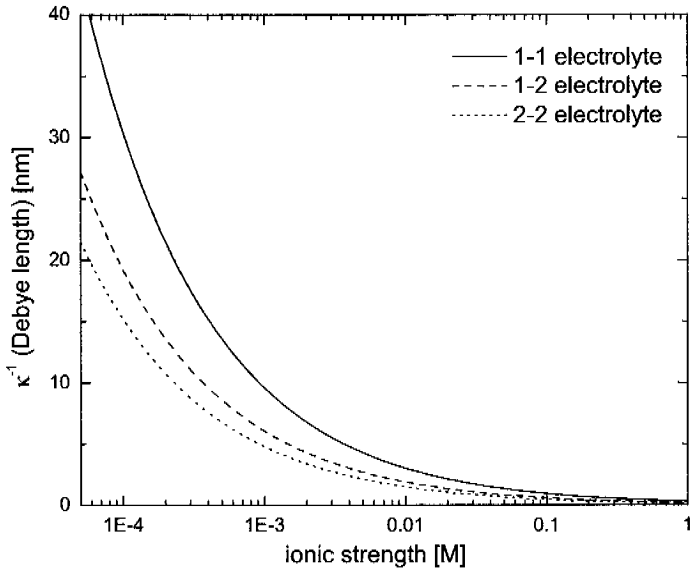

Figure 2.4: Calculated values for the Debye length κ^{-1} from Eq. 2.16 for different electrolyte systems (the numbers in the graph indicate valencies of the electrolyte). Values are calculated for aqueous solutions at $25°C$. Low values for κ^{-1} indicate a large shielding effect: ions surrounding the central ion shield the potential of this ion more efficiently. This is the case for high-valent electrolytes or high salt concentrations.

result will later lead to the general conclusion that colloidal particles are less stable in high salt suspension. In such suspension the surface charge of a particle is shielded efficiently by the high number of ions around the particle and the electrostatic repulsion force is active for much shorter length scales then in low salt solutions.

The only physically meaningful solution for Eq. 2.12 is:

$$\psi(r) = \frac{Ce^{-\kappa r}}{r} \tag{2.17}$$

Thus, the potential at a distance r from the ion decays with an exponential function. How steep that decrease is, is determined by the Debye length κ^{-1}. For the constant C, the following expression can be deducted using electroneutrality as a boundary condition (a_i is the distance of closest approach between two ions in solution):[31]

$$C = \frac{z_i e\, e^{\kappa a_i}}{4\pi\epsilon_0\epsilon\,(1+\kappa a_i)} \tag{2.18}$$

The Debye-Hückel theory thus gives expressions for how the potential around a center ion develops, how surrounding ions shield this potential and also how surrounding

charges are distributed. However, it must be kept in mind, that the Debye-Hückel theory is based on relatively basic principles: it studies completely dissociated ions as hard spheres with a point charge and the surrounding medium is an isotropic and homogeneous dielectric. Therefore, a number of possible interactions are neglected within the Debye-Hückel theory. Among these are solvation processes, solvent structure-originated interactions, incomplete dissociation of ions, dispersion forces (only Coulomb interactions are considered). And also, phenomena originating from the heterogeneous and molecular structure of the media are not considered. However, the Debye-Hückel theory predicts many observed effects correctly and is still the basis of more advanced or more general theories used in colloidal science.

2.2.5 Electric Double Layers

In the previous section, it was discussed how charges are of great importance in aqueous colloidal suspensions and basic properties of ions in solution were discussed (leading to the Debye-Hückel theory). There, it was discussed how the potential around an ions develops and how surrounding counterions shield the charge of that center ion (the center ion carrying an counterion "atmosphere" around itself). This is a basic example of an electric double layer (EDL). In fact, this picture can be expanded to most aqueous solid colloidal suspensions, where the particle usually carries a surface charge. The classical (and for this work relevant) example are metal oxide particles in water, which — depending on the exact condition — may take up H^+ ions from solution and incorporate these charges into surface hydroxyl groups (at low pH) or release H^+ ions from the surface (at high pH). These charges on the particle lead to an enrichment of counterions near the surface as schematically shown in Fig. 2.5.

The formation of the electric double layer is an exothermic (spontaneous) process, because ΔG is negative as a whole. This negative ΔG originates from a positive part ΔG_{el} which describes the electrical (coulombic) part of the electric double layer and a large negative part ΔG_{non-el}, which summarizes the non-electrostatic interactions (adsorption of species on the surface, which is energetically favorable). The positive sign in ΔG_{el} originates from the fact, that charging a surface with species of the same sign is not an energetically favorable process. Therefore, the exact charge distribution on a surface is very much dependent on the affinity of ions to adsorb to a surface. If only electric contributions were considered, no electric

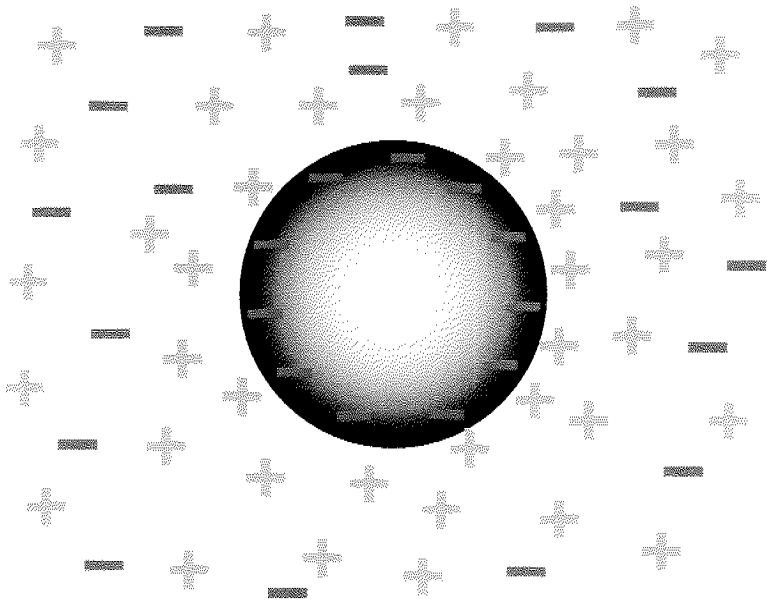

Figure 2.5: Schematic illustration of a negatively charged colloidal particle in an electrolyte suspension. Positive ions are accumulated near the particle surface. Anions are depleted in that regions. This effect is referred to as the electric double layer (Eq. 2.11).

double layers would form. Only the affinity of for example H^+ ions for a metal oxide surface makes charging of a surface an exothermic process and the formation of electric double layers possible. In the following sections, the formation of this electric double layer and the models describing it are discussed.

The Stern layer and the diffuse part of the double layer

Ions which adsorb to the surface of a particle "specifically" are found in a thin layer on the surface. "Specifically" in this case means, that the ion species adsorbs to the surface not only by electrostatic interactions but also has a natural affinity to the surface (e.g. due to its chemical composition or the radius of the ion) and the adsorbing ion is not surrounded by hydrating water molecules. In case of metal oxide surfaces, the ionic species, that adsorb specifically, are hydrogen atoms and the degree to which these hydrogen atoms adsorb to the surface defines the surface charge density σ. Obviously, the more hydrogen atoms cover the metal oxide surface (Γ_{HCl} describing the coverage of the surface with H^+ ions[10]), the more positive σ

[10]It is written HCl because for electroneutrality reasons with every adsorbing H^+ ion, a Cl^- counterions is positioned in the electric double layer

gets. The degree to which H^+ ions adsorb to the particle surface depends mainly on the concentration of the hydrogen ions in solution, i.e. the pH. σ is usually positive at low and negative at high pH. Therefore, at a given pH, which is referred to as the point of zero charge (PZC), σ equals 0. If a specific ion species, as the hydrogen ions in metal oxide systems, is responsible for the surface charge of the particle, this ion is called the charge-determining ion. We can summarize these observations in the following way:

$$\sigma = F(\Gamma_{HCl} - \Gamma_{NaOH}) \tag{2.19}$$

where Γ_{HCl} and Γ_{NaOH} are the concentrations of H^+ and OH^- on the surface (with $NaCl$ as the salt) and F is the Faraday constant. This adsorbed layer of ions on the surface consisting of bound ions, is commonly not treated as part of the electric double layer on the solution side of the particle. Hydrogen atoms, as the charge-determining ions, are considered as part of the metal oxide surface and are responsible for the surface charge. However, counterions are attracted to that charged surface (which might for example be Cl^--ions) and form a thin layer of counterions on the charged surface. This thin layer is often referred to as the Stern layer. More over, not only a Stern layer forms around a charged particle but also an ion cloud that has the same charge as the Stern layer and which is surrounding the particle surface. This outer section of the electric double layer is usually termed diffuse part of the electric double layer (see Fig. 2.6 for a schematic sketch of this situation). In this diffuse part of the double layer, counterions are enriched and co-ions are depleted as sketched in Fig. 2.5. Both of these effects make up the total charge in the diffuse part: for example, a surplus of Cl^- ions and a deficit of Na^+ ions result in a charge of the diffuse double layer of the charge of the Cl^- ions plus the negative amount of Na^+ ions. The reason for the formation of this diffuse double layer can be qualitatively described as an equilibrium between the minimum energy situation (which would want all counterions — due to electrical attraction — as near as possible to the surface) and the maximum entropy situation (which would like to have all ions homogeneously distributed).[33] As discussed later, it is found that the ion distribution in the diffuse part of the double layer follows a Boltzmann distribution and thus decays exponentially from the surface ion concentration value to the bulk ion concentration value (Eq 2.21).

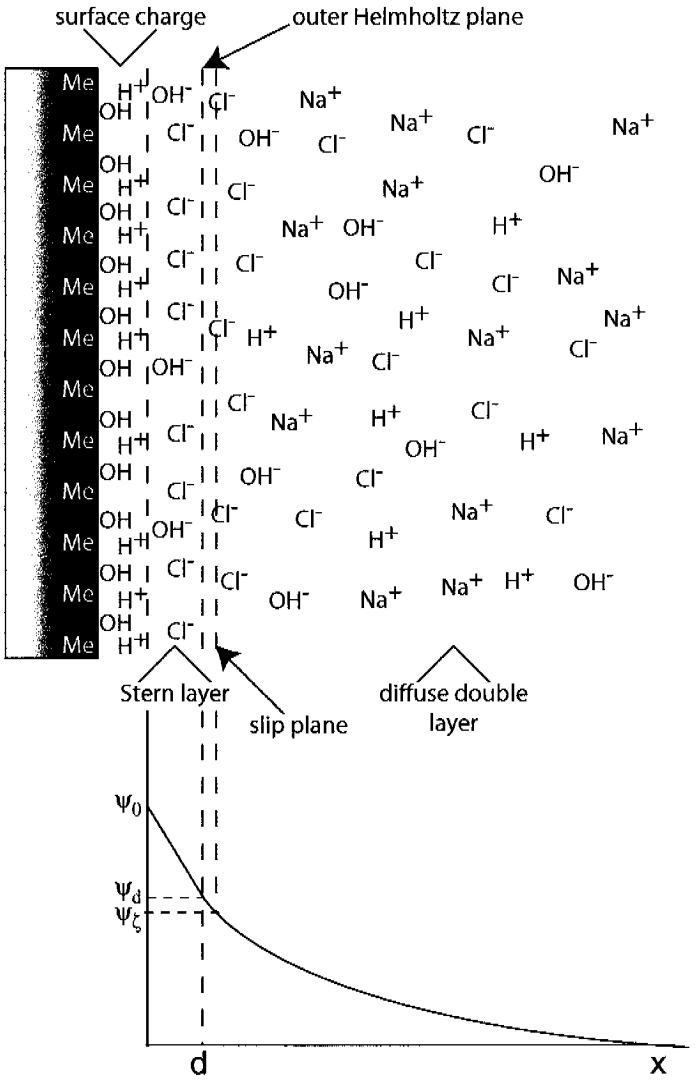

Figure 2.6: Sketch of a metal oxide surface in aqueous NaCl solution and the corresponding potential curve. a) At a pH lower than the IEP, an excess of H^+ ions protonates the surface, charging the surface positively. As a consequence, counterions (from salt and water) are attracted to the surface. According to the Stern-model, a thin layer of counterions adsorbs strongly to the surface. The surface potential ψ_0 drops in this layer linearly to the value of the stern layer (ψ_d). In the diffuse part of the double layer, the potential $\psi(x)$ drops according to Eq. 2.24. Note that the ζ-potential ψ_ζ has a value close but normally slightly higher than that of ψ_d. The ζ-potential indicates the potential at the slip plane of the particle. The slip plane indicates what part of the double layer "moves" with the particle if the particle is moved in the suspension. In this sketch, the division of the Stern layer into two parts, an inner part where ions without water shell adsorb and an outer part, where coions with their water shell adsorb is not shown. This inner part corresponds to the distance m as indicated in the text and the outer part of the Stern layer corresponds to the distance d.

Dividing the electric double layer in these two parts offers some advantages. The most important is, that — if the Stern layer is treated separately — the diffuse part can be modelled much better.[11] The borderline between the Stern and the diffuse part of the double layer is called the outer Helmholtz plane (Fig. 2.6). As sketched in Fig. 2.6, the Helmholtz plane is often very close to the ζ-potential of a surface / particle, which makes it an important experimentally accessible parameter.

One of the most common modelling approaches for the diffuse part of the electric double layer is that of Gouy and Chapman. In this theory, the diffuse part of the double layer of a flat substrate is treated very similar to that of an ion in the Debye-Hückel theory. This is the main difference between the two theories: the Debye-Hückel theory models the double layer of an ion and in the Gouy-Chapman theory, instead of an ion, a flat surface and its surrounding diffuse electric double layer is modelled. The general assumptions are the same in both theories: ions are point charges, the solvent is a homogeneous entity with macroscopic properties and only electrostatic interactions are considered.

Generally, to derive the potential ψ at a distance of x from the surface, the Poisson equation (Eq. 2.20) is used to link the space charge density ρ to the potential ψ.

$$\frac{d^2\psi(x)}{dx^2} = -\frac{\rho(x)}{\epsilon\epsilon_0} \tag{2.20}$$

The Gouy-Chapman model assumes that counterions (and co-ions) are attracted to the surface by electrostatic attraction but at the same time exhibit thermal motion. This assumption leads to a Boltzmann-distribution for the concentration of the counterions and co-ions in equilibrium:

$$c_i(x) = c_\infty e^{\frac{-z_i F\psi(x)}{RT}} \tag{2.21}$$

Here, c_∞ is the bulk concentration of the ions, z the charge of the ion and F the Faraday constant. For the space charge density $\rho(x)$, which is needed to find $\psi(x)$, the following equation can be derived if we consider both, the excess of counterions and the deficit of co-ions:

[11] The used models become exact at sufficiently large distances form the surface which is the case if a Stern layer is considered, also the potentials are relatively low at some distance from the surface so only minor deviations from ideality are observed

$$\rho(x) = F \sum_i z_i c_i(x) \tag{2.22}$$

Since we know $c_i(x)$ from Eq. 2.21, we can insert Eq. 2.21 in Eq. 2.22 and thus modify the Poisson-equation (Eq. 2.20) to get the Poisson-Boltzmann equation, which describes the electrostatic potential in ionic solutions:

$$\frac{d^2\rho(x)}{dx^2} = -\frac{zFc}{\varepsilon_0\varepsilon}(e^{\frac{-zF\rho(x)}{RT}} - e^{\frac{zF\rho(x)}{RT}}) \tag{2.23}$$

Eq. 2.23 can be solved analytically using appropriate substitutions.[31] Presenting only the result of that process, the following expression for $\psi(x)$ can be found:

$$\psi = \psi_0 e^{-\kappa x} \tag{2.24}$$

Note that Eq. 2.24 is the linearized form of the analytically correct solution for the Poisson-Boltzmann equation. This linearization is also known as the Debye-Hückel approximation. It is valid for not too high potentials on the surface. Eq. 2.24 indicates (in accordance to the Debye-Hückel theory) that the potential in the diffuse double layer decreases exponentially. It reduces to ψ_0/e at a distance κ^{-1}. This again shows how the reciprocal Debye-length κ^{-1} is an good indicator for the double layer thickness. This relation, however, is only valid for small potentials and for flat surfaces (e.g. not too small colloidal particles).[31] Note that in Eq. 2.24, the countercharge that is responsible for the potential drop of ψ consists of both, an excess of counterions and a deficit of co-ions. If we look at both of these charge carriers separately, two expressions for σ_+^{dp} and σ_-^{dp}[12] (the total charge present in the diffuse double layer) can be found:

$$\sigma_+^{dp} = \frac{2czF}{\kappa}[e^{-z\psi/2} - 1] \tag{2.25}$$

$$\sigma_-^{dp} = \frac{2czF}{\kappa}[1 - e^{z\psi/2}] \tag{2.26}$$

Combining a Stern-layer of finite thickness d with a Gouy-Chapman type of modelling for the diffuse part of the double layer leads to a situation as sketched in

[12] "dp" stands for "diffuse part"

Fig. 2.6. The potential $\psi(x)$ drops linearly from $x = 0$ to $x = d$. In some cases, the distance from $x = 0$ to $x = d$ is further divided into a value $x = m$ which is between 0 and d. The distance m would be associated with specifically bound counterions, which do not have a water shell around themselves. Such un-hydrated ions can move closer to the surface due to the lack of surrounding water molecules. For simplicity, $x = m$ is not shown in Fig. 2.6. d is the distance of closest approach for a *hydrated* ion. Since m is the distance of closest approach of an un-hydrated counterion, it looses its meaning in systems, where no such specifically adsorbing ions are present. In such a case, there are no charges at all between $x = 0$ and $x = d$. Equation 2.24 remains valid for the outer part of the double layer ($x \geq d$) and only x has to be replaced by $x - d$. The potential $\psi(x)$ drops linearly between $x = 0$ and $x = m$ (if m is existing) according to:

$$\psi_0 - \psi_m = -\frac{\sigma_0}{\epsilon_m \epsilon_0} m \tag{2.27}$$

and between $x = m$ and $x = d$:

$$\psi_m - \psi_d = -\frac{\sigma_m}{\epsilon_s \epsilon_0}(m - d) \tag{2.28}$$

These equation are not as straight-forward to solve, since the values for ϵ_s and ϵ_m are not easily identifiable. They describe the dielectric constants at the distance m and d from the surface, a value which is not accessible. It is certainly much lower than that for bulk water due to water structuring in this sub-nanometer regime. For the distances m and d the values for the ion radii can be chosen, either for the hydrated case (d) or for the case without a water shell (m).

Note, that with the introduction of a Stern-layer in the system, Eq. 2.24 is generally a very good approximation for the "true" potential $\psi(x - d)$, because the Stern-layer does reduce the surface potential (according to Eq. 2.27 and 2.28), which makes the Debye-Hückel approximation even more accurate. In real systems, it is often sufficient to consider only d, the Stern layer thickness and m can be disregarded.

The surface charge (σ_0) is exactly compensated by the total charge in the double layer due to the requirement of electroneutrality in the system.

$$\sigma_0 = -(\sigma_d + \sigma_{dp}) \tag{2.29}$$

σ_0, the surface charge, is compensated by the charge present in the diffuse part of the double layer (σ_{dp}) and the charge present in the adsorbed layer (Stern-layer) close to the surface (σ_d). Also, we can write for the surface charge σ_0 the following relation (note again, that if no specifically adsorbing layer of ions is present σ_m becomes 0 and the Stern layer only consists of a layer of counterions at a distance d from the surface):

$$\sigma_0 - \sigma_d = \epsilon\epsilon_0\kappa\psi_d \tag{2.30}$$

Thus, if σ_0 and σ_d are known or measured, the whole potential progression of $\psi(x)$ can be deduced. For a lot of systems, σ_0 can be measured by titration experiments using the charge-determining ions and σ_d can often be set equal or close to the ζ-potential which is also an accessible parameter (in Fig. 2.6, ψ_d and ψ_ζ are drawn close together as it is the case for most system, ψ_ζ being generally slightly lower than ψ_d).

In conclusion, the Gouy-Chapman-Stern-theory describes how the potential decays across an electric double layer present on a charged particle. It does include the possibility of an adsorbed ionic species close to the surface (the Stern-layer) and assumes a linear decay of the potential in this region. In the region after the Stern-layer, the decay of the potential is described in an exponential way (Eq. 2.25). The presented model is applicable in a rather large regime of ionic strength (between 0.1 and 10^{-4}M).[33]

Point of Zero Charge and Isoelectric Point

The point of zero charge (PZC) of a surface is simply defined as the condition where the surface has no net charge ($\sigma_0 = 0$). The PZC is associated with a given pH value, where the conditions are such that on average protonation and deprotonation of surface hydroxyl groups is compensated. The isoelectric point (IEP) is where $\sigma_{ek} = 0$. σ_{ek} can be identified with the slip plane, where under shear the electric double layer is sheared with respect to the surface. The position of this slip plane is not generally established [31] but in most cases, σ_{ek} can be identified with σ_d, the charge of the outer Helmholtz plane. For this charge, we can write:

$$\sigma_{ek} \approx \sigma_d = -(\sigma_0 + \sigma_m) \tag{2.31}$$

σ_m is the charge of the specifically adsorbed ions on the surface. Eq. 2.31 already indicates that if there are no specifically adsorbing ions, the PZC is equal to the IEP. This means in a salt free suspension the PZC is always equal to the IEP, because at the PZC there is no surface charge and no charges from salt can adsorb. As soon as say $-$ anions adsorb specifically the situations changes. Adsorbing anions induces a positive surface charge thus the PZC is no longer at the same pH. We have to add more (charge-determining) anions (e.g. more OH^-) to bring the surface charge back to 0. This is equal to increasing the pH. Specifically adsorbing anions means the pH of the PZC must shift upwards and vice versa for the adsorption of cations. The IEP, however, shifts in the opposite direction of the PZC. If anions adsorb specifically ($\sigma_m < 0$) the surface charges positively ($\sigma_0 > 0$). At the IEP, the condition $\sigma_0 = \sigma_m$ must be fulfilled and more cations (H^+ in our case) have to be adsorbed on the surface to completely compensate σ_m. Thus, the IEP shifts to lower values. As soon as the IEP (usually measured with ζ-potential measurements) and the PZC (measured with titration experiments) are different (or move in different directions upon addition of certain ions), this is a direct proof that ions have specifically adsorbed on the surface of the colloidal particle.

2.2.6 DLVO-Theory

The electric double layer around a charged particle (as described in Section 2.2.5) results in a repulsive force between two (equally charged) particles in a suspension. At the same time, London-Van der Waals forces attract the same two particles (section 2.2.3). Obviously, superposition of these repulsive and attractive forces — depending on their relative strength — results in a total interaction energy curve as a function of the separation distance between two particles with distinct minima (points of maximum attraction) and maxima (points of maximum repulsion). The DLVO-theory is the most prominent model that describes this superposition. It was developed by Deryaguin and Landau in Russia and Verwey and Overbeek in the Netherlands in the forties of the last century.[34] This superposition of ΔG_{VdW} (attractive Van der Waals potential energy) and ΔG_{EDL} (the repulsive electrostatic energy term stemming from the electric double layer) leads to the total interaction energy between two particles:

$$\Delta G_{tot} = \Delta G_{VdW} + \Delta G_{EDL} \tag{2.32}$$

First, we get the energy of attraction due to Van der Waals dispersion forces (ΔG_{VdW}) from Eq. 2.10:

$$\Delta G_{VdW} = -\frac{A}{12\pi h^2} \tag{2.33}$$

with the Hamaker constant A and the separation distance between the two spherical particles h (see Fig. 2.2). The equation for two flat plates may be chosen over that for two particles because the interaction length (a few nm) is generally small compared to the radius of particles (above a few dozen nanometers) such that the two particles may be treated as two approaching "walls".

The double layer contribution to the free energy is not as straightforward to calculate. Phenomenologically, if two particles start to approach each other, the electric double layers start to overlap and a repulsive force acts on the particles due to the increase of counterions which decreases their degree of freedom and thus their entropy. Thus, the potential energy of ΔG_{EDL} is increased. It is intuitive that ΔG_{EDL} should increase exponentially with decreasing separation distance of the particles, since the EDL decreases exponentially with increasing distance from the surface of the particle as seen in Eq. 2.24. However, the details of the derivation of these equations is not given here. The reader is directed for example to the text books of Norde and Russel.[22, 33] There and elsewhere, a variety of solutions for the interaction energy due to the overlapping electric double layer are given, depending on specific boundary conditions (e.g. assumption of constant potentials or constant charge), approximations and geometries that were used to obtain them.[22, 23, 33, 35] Norde derives in his book the following equations for two flat plates and two equal spherical particles:[33]

$$\Delta G_{EDL} = \left(\frac{64\, c_0\, RT\, \gamma_d^2}{\kappa}\right) e^{-\kappa h} \tag{2.34}$$

h is the separation distance between the two and γ_d is a related to ψ_d (see below). For two spherical particles with radius a, ΔG_{EDL} becomes:

$$\Delta G_{EDL} = \left(\frac{64\pi\, c_0\, RT\, a\, \gamma_d^2}{\kappa^2}\right) e^{-\kappa h} \tag{2.35}$$

For surface potentials of less then about 50 mV and a 1:1 electrolyte, γ_d is related to the ψ_d, the Stern-layer potential according to:

$$\gamma_d = \frac{z\,F\,\psi_d}{4\,R\,T} \tag{2.36}$$

For two flat plates with a separation distance h in an electrolyte with ion concentration c_0 (and under the assumption of constant charge) the following expression is also found elsewhere:[23]

$$\Delta G_{EDL} = \left(\frac{64\,c_0\,kT}{\kappa}\right)e^{-\kappa h} \tag{2.37}$$

Another common approach to derive analytical expressions for the repulsive electric potential was introduced by Derjaguin. He introduced an approximation which allows the derivation of an expression for the interaction potential for two spherical particles from two flat plate interaction energies under constant potential conditions:[22]

$$U(x) = 2\pi\epsilon_0\epsilon\left(\frac{kT}{ze}\right)^2 a\psi^2 ln(1 + e^{-\kappa h}) \tag{2.38}$$

Combining Eq. 2.37 and an appropriate selection of Eq. 2.34-2.36 leads to an expression for the total interaction energy as a function of separation distance of two particles according to:

$$\Delta G_{tot} = \left[2\pi\epsilon_0\epsilon\left(\frac{kT}{ze}\right)^2 a\psi^2 ln(1 + e^{-\kappa h})\right] - \frac{A}{12\pi h^2} \tag{2.39}$$

Two main contributors to the overall interaction energy can be identified in Eq. 2.39. It is mainly the Debye-length κ^{-1} that determines the strength of the repulsive term. Thus, the electrolyte concentration and valency of the electrolyte play a very dominant role in colloidal stability (according to Eq. 2.16). The influence of the electrolyte concentration is shown in Fig. 2.7c), where it becomes obvious that for high salt concentrations, repulsion is only effective over a very short range. Also, the value of the Hamaker constant is of importance, governing the attractive term in Eq. 2.35. Large Hamaker constants indicate high attractive forces and such suspensions will be much harder to stabilize (Fig. 2.7a). Fig. 2.7d) schematically depicts three typical curves obtained from Eq. 2.39 for different parameters. It is obvious, that for high repulsive energies a situation as shown in Fig. 2.7d), curve 1 evolves, where a large energy barrier hinders particles from reaching their primary

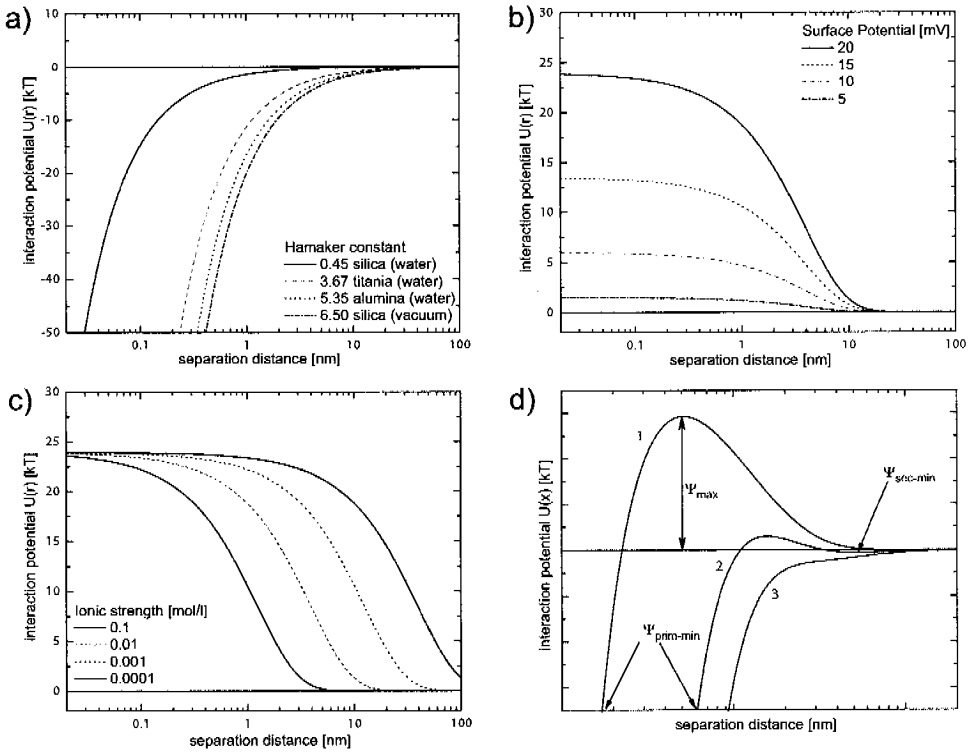

Figure 2.7: Calculations of various interaction potentials. a) attractive interaction potentials due to dispersions forces (Van der Waals forces) between two particles calculated from Eq. 2.5. The large dependence on the Hamaker constant is clearly seen. Silica particles exhibit rather low attractive potentials from Van der Waals forces, which benefits the stabilization of colloidal silica suspension. Different values for Hamaker constants are taken from Bergström.[29] b) Influence of surface potential on repulsive double layer forces according to Eq. 2.38. Ionic strength was fixed at 0.01 mol. The repulsive potential increases with increasing surface charge, a fact that for example explains why colloidal suspension tend to agglomerate near the IEP of a suspension (where the active charge vanishes). c) Influence of ionic strength of electric double layer potentials. Surface potential is fixed at 20 mV. The charge-shielding effect of ionic species as discussed in section 2.2.5 becomes obvious. In a 0.1 mol salt suspension, the electric double layer is only effective over a very short range, while at suspension containing only little salt, electrostatic repulsion is effective over a much wider distance. d) Schematic representation of DLVO-interaction potentials as obtained from Eq. 2.39. Superposition of attractive Van der Waals-potentials (as shown in a) and repulsive forces due to surface charges (as shown in b) and c) lead to situations as sketched in d). Curve 1 shows a case, where large repulsive forces (e.g. high surface potentials and low salt concentrations) dominate in the suspension. A high ψ_{max} (typically exceeding $10kT$) inhibits agglomeration in the primary minimum near the surface. This energy barrier shows, that no suspension is in its thermodynamic equilibrium rather it is in a kinetically stable situation because particles can not overcome the high energy barrier and agglomerate. Curve 2 shows a situation where a secondary minimum is visible and only a low energy barrier hinders particles from reaching their primary minimum. In the first place, particles will flocculate very weakly by moving in the secondary minimum (this flocculation can usually be reversed by stirring of the suspension because the secondary minimum is only very shallow and little energy is needed to redisperse the particles). Given some time, it is very likely that this suspension agglomerates, because particles will overcome the relatively low energy barrier and find their primary minimum. In curve 3, an unstable colloid suspension is sketched (with e.g. high Hamaker constants, low salt or low surface potentials). No energy barrier prevents the particles from coagulation and the suspension will agglomerate rapidly.

minimum. Such a suspension will be stable over long time intervals. If the repulsive term is smaller or the attractive Van der Waals energy term larger (e.g. due to a high Hamaker constant), the particles can not be stabilized and they will move into their primary minimum (agglomeration)(Fig. 2.7d), curve 2). Also, situations can occur, where a secondary minimum exists (Fig. 2.7d), curve 3. Then, particles will preferentially move into this secondary minimum and reside there. They will form a loosely agglomerated structure. However, a suspension that is agglomerated in such a way can be redispersed very easily, since only little energy is necessary to move the particles out of the secondary minimum (stirring by hand is often enough). All these curves shown in Fig. 2.7d) can be encountered in real systems and the fact that the DLVO-theory predicts these situations correctly is one indication why it is still of such importance even 60 years after its invention. Also, the DLVO-theory shows the importance of charged surfaces and the influence of ion concentration for colloid stabilization. The DLVO-theory, and this is probably the most important advantage, is able to quantitatively predict numerous effects and experimental observations found in colloidal science, based on experimentally measurable parameters only (ζ-potential (approximately equal to ψ_d), radius of the spheres, salt concentration, Hamaker constant, dielectric permittivity...)

2.2.7 Repulsive Steric Forces

In addition to electrostatic repulsive forces, steric (or entropic) repulsion is the second main force that might be responsible for the stabilization of a colloidal suspension. In this case, a lyophilic entity (most commonly an organic (macro-)molecule) adsorbs to a colloidal particle and provides a repulsive force termed steric or entropic repulsion.[23] These adsorbing molecules often have a dual chemical character: one part of the molecule has low affinity for the medium (or a high affinity to the colloid) and is thus adsorbing readily to the particle, while the other part of the molecule generally has a high affinity for the medium and thus forms a thick protective layer with good solubility for the medium which helps to stabilize the colloid. Two effects are responsible for the repulsive effect of this phenomenon:[36, 37]

osmotic effect Upon approach of two particles coated with a polymer, the concentration of the adsorbed molecules increases in the region of the polymer layer. This is an energetically unfavorable situation and solvent molecules try

to minimize the concentration difference by diluting the overlapping layer and separating it by moving into the area between the particles (as indicated with arrows in Fig. 2.8a). This gives rise to a repulsive osmotic force.[38]

entropic effect The overlapping of the adsorbed molecules of two particles leads to a decrease of the degree of freedom for the adsorbed polymer molecules. This loss of entropy is also unfavorable and particles try to regain the lost entropy by increasing the separating distance (see Fig. 2.8b). This effect is also referred to as volume restriction effect.[36, 39]

From these descriptions it is obvious, that the solvent quality plays a crucial role in steric stabilization. If the medium is a "good" solvent[13] for the adsorbed polymer, the adsorbed polymer will be well-hydrated and a thick polymer coating on the particle evolves with extended, random-coil like polymer chains extending from the particle surface into the medium. If the solvent is "bad", the polymer chains will collapse because the medium does not interact with the polymer. However, if solubility is too good, the polymer may desorb from the surface. This is the reason why many protective polymers exhibit a dual chemical character mentioned above.

Generally, the higher the molecular weight of the adsorbing polymer is, the better the steric stabilization, because longer polymer chains result in a thicker, well-hydrated layer (if the solvent is good). At very high molecular weights, however, possible complications can be expected such as bridging. Bridging describes the fact that one polymer chain is able to adsorb to more than one particle at the same time (provided the polymer is structured such that several adhesive sites exist on the particle surface). This obviously exerts a strong attractive force which will lead to flocculation. Another potential hazard in steric stabilization processes with polymer molecules appears, when the polymer is only weakly attached to the surface. In this case, the polymer might desorb if two particles approach each other, because the force that normally would lead to steric stabilization is high enough to remove the polymer from the surface. Note, that also free polymer in solution affects particles in suspension. In this case, the free polymer is squeezed out of the area where two particles approach each other. This also produces an attractive osmotic pressure that may lead to coagulation.[22]

[13]Solvent molecules interact preferably with the adsorbed polymers. In a "bad" solvent, polymer molecules interact preferentially with themselves as does the solvent

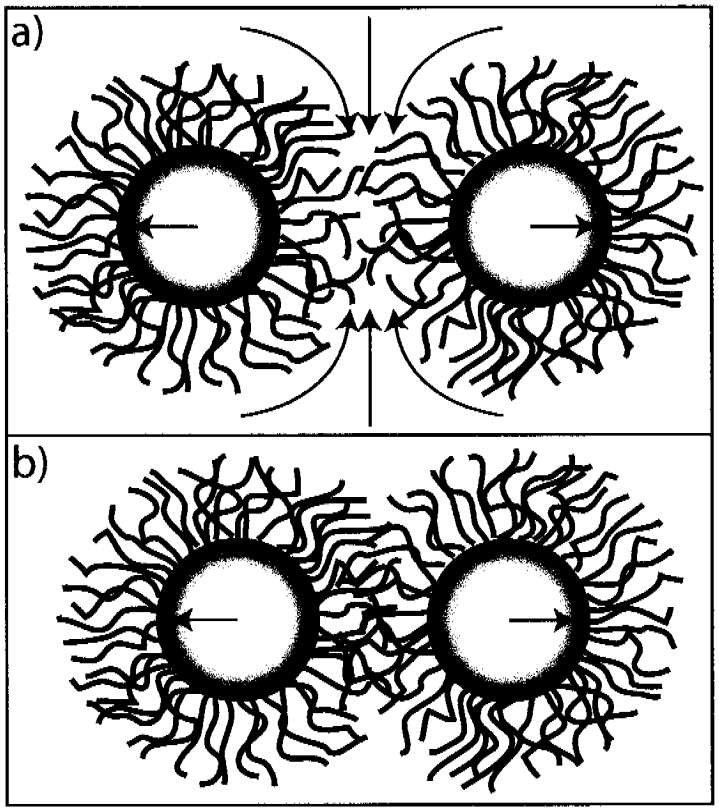

Figure 2.8: Schematic representation of steric stabilization of particles by the adsorption of polymeric molecules. In the sketch, one-end adsorption of the polymer is assumed. a) osmotic repulsion effect: an increase in polymer concentration between two approaching colloids leads to a flow of solvent molecules that tries to minimize this concentration increase. Inflow of solvent molecules is indicated by arrows. b) entropic / volume restriction effect: when the polymer layer of two particles start to overlap, the entropy is decreasing because the polymer chains loose some of their degrees of freedom. The particles try to counteract that loss by increasing their separation distance.

2.3 Capillary Forces

In all colloidal self-assembly fabrication techniques, a suspension of colloidal particles is a prerequisite to form the desired colloid structure on the surface. Drying of the solvent is therefore an inherent part in such a process and mainly due to the small size of the colloidal particles, capillary forces may play in important role and determine the final outcome of the adsorbed colloid structure. In fact, we can classify two main categories of production methods: those using capillary forces to form the intended structure and those using alternative methods for assembling colloidal particles into useful structures (and thus trying to avoid unwanted impact of capillary forces). A straightforward example for those two processes is that of

colloidal crystals. They can readily be formed by sedimentation,[40–42] building the colloidal crystal in suspension, or they can be formed by self-assembly processes that utilize attractive capillary forces during the evaporation phase.[8, 12, 43, 44] But capillary forces play an important role in the production of patterned colloidal arrays as they were developed in this thesis. Similar to the example just given, systems can be created to pattern colloidal particles where the attractive nature of capillary forces is used (Chapter 5 of this thesis) and others that try to minimize those forces during the evaporation process (Chapter 6). The basic physical principles that lead to the occurrence of capillary forces in colloidal systems during drying are assessed and reviewed in this section.

2.3.1 Interfacial Tension / Surface Free Energy

An interface is inherently a region of positive free energy. If it would not be such, brownian motion, for example, could simply distort and convolute the interface until the phase boundaries become mixed (since there would be no energy barrier preventing that). The positive free energy nature of an interface has the consequence that in a given system, interfacial areas are minimized (if possible), e.g. spherical air bubbles form in water and these bubbles coalesce over time. Thus, high surface area materials (or emulsions) are inherently metastable, because they are not in their thermodynamical equilibrium state. However, kinetically, it is possible to "stabilize" such a system to consider it (kinetically) stable for the interesting time intervals (as discussed for a colloidal suspension).

The reason for the positive free energy of an interface or surface lies in the fact, that surface atoms exhibit a different force field than atoms in the bulk of the material: surface atoms "lost" some of their interaction possibilities (compared to an atom in the bulk), which increases the energy of surface atoms. Obviously, the surface free energy increase depends on the surface area produced, the more atoms are surface atoms, the higher the surface free energy.[14] Surface atoms have a net positive attraction toward the bulk, which results in a state of lateral tensions along the surface. It is therefore the excess surface free energy of an interface that gives rise to interfacial tension.[15]

[14]The surface free energy will also depend on the separation distance of the separated surfaces but becomes constant if the two surfaces can be considered separated "infinitely"

[15]Units of surface tension and surface free energy are equal (usually mJ/m^2) and in case of liquid and its vapor also numerically equal

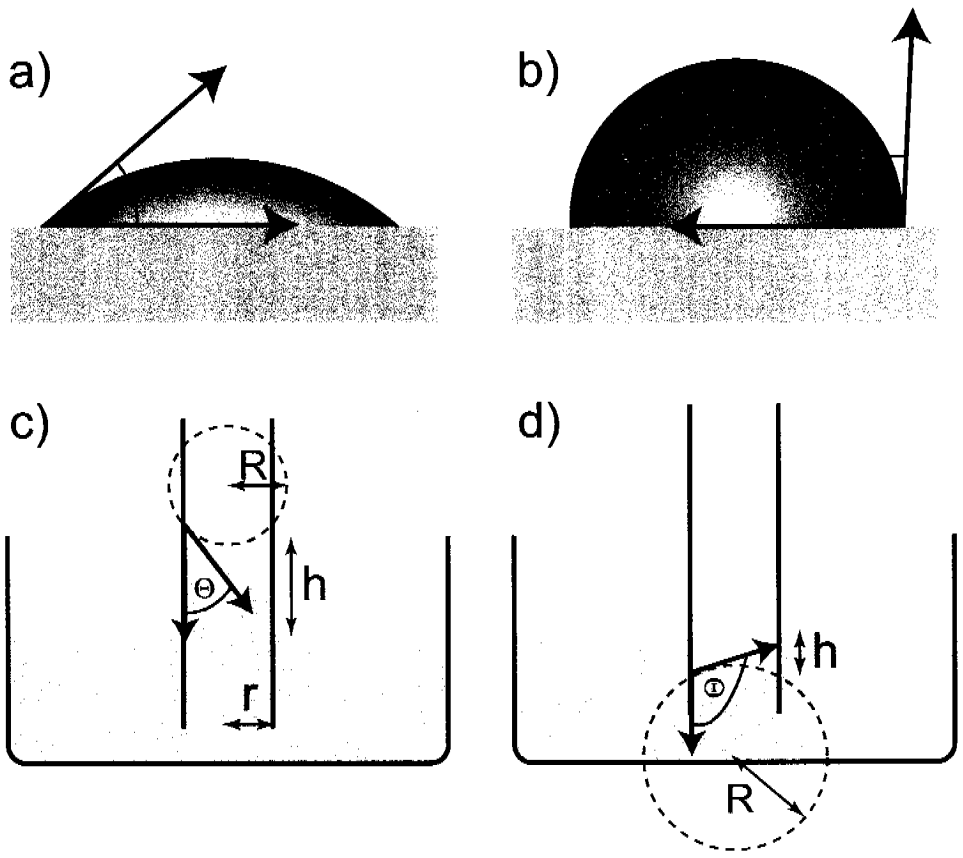

Figure 2.9: The contact angle Θ of water on a surface. a) hydrophilic contact angle (<90 degree) and b) an example for a hydrophobic surface (>90 degree). c) and d) show the rise (or fall) of a water column in a small capillary of radius r, termed the "capillary rise". This effect originates from the wetting properties of the capillary. In a hydrophilic capillary (c) (the contact angle Θ is indicated), the water rises to a certain height h, while a hydrophobic capillary (d) decreases the water level in the capillary by a given height h. The calculations for the capillary rise are given in the text.

2.3.2 Capillary Forces in Three-Phase-Systems

As a result of interfacial free energy and the resulting interfacial tension, capillary effects occur in systems containing phase boundaries. Capillary effects are of special importance in systems which contain three-phase boundaries, e.g. contain solid surfaces, a liquid and a gas phase. The simplest of these cases is a liquid drop on a flat surface. There will be three types of interfacial energies: the solid-vapor interfacial free energy γ_{SV}, that of the solid-liquid interface (γ_{SL}) and that of the liquid-vapor interface (γ_{LV}). If the drop has reached its equilibrium state, the change in surface free energy will be zero and Young's equation can be derived:[33]

$$\cos\Theta = \frac{\gamma_{SV} - \gamma_{SL}}{\gamma_{LV}} \tag{2.40}$$

Θ is the contact angle that evolves between the surface and the drop as shown in Fig. 2.9. Depending on the values of the respective interfacial free energies the contact angle will vary over a wide range. If the surface free energy (γ_{SV}) is higher than the interfacial free energy between liquid and vapor (γ_{LV}) the liquid will spread on the surface resulting in a low contact angle (Fig. 2.9a), in the reverse case, the liquid will form a drop with a contact angle larger than 90° (Fig. 2.9b). A surface is "wetted" if the contact angle is 0° (or below a given, small angle) and generally it is often spoken of the "wettability" of a surface: better wettability is corresponding to a smaller contact angle. However, no clear definition of the terms non-wetting, partially wetting and wetting is given, so some caution in their use is appropriate.[33] Another direct consequence of surface tension at interfaces is the fact, that a capillary pressure evolves if a liquid-liquid or liquid-vapor boundary is curved. It is this curvature and the pressure difference that arises that is responsible for capillary flow effects. Because of the pressure difference, liquid flows in capillary systems to counteract that pressure difference. In systems, where no curved interfaces exist, no capillary flow will occur. Laplace derived an equation that describes this pressure difference across a liquid-fluid[16] interface depending on the radius of curvature R of that interface. For spherical surfaces, the following expression is found:

$$\Delta P = \frac{2\gamma}{R} \tag{2.41}$$

Thus, the inside of a curved surface (e.g. an air bubble in water) will have a higher capillary pressure then its outside medium. A traditional example of capillary forces in a three-phase system is the rise of a water column in a capillary of radius r as depicted in Fig 2.9 c) and d). A small capillary is in contact with a liquid, and depending on the contact angle Θ, a curved meniscus will form which gives rise to a water column in the capillary. We can immediately derive the following from geometrical considerations: the radius of curvature R in the capillary with radius r depends on the contact angle Θ ($R = r/\cos\Theta$)(see sketch in Fig. 2.9 c) and d). Thus, the capillary pressure in the capillary will be — according to Eq. 2.41 —

[16]Fluid is considered any non-solid, thus may be a liquid or vapor phase

$2\gamma \cos\Theta/r$. The liquid will rise in the capillary until it is in equilibrium with the hydrostatic counterforce. This can be expressed as follows:

$$\Delta pgh = \frac{2\gamma \cos\Theta}{r} \tag{2.42}$$

Here, Δp is the difference in density between liquid and fluid, g is the acceleration due to gravity and h the height of the meniscus as depicted in Fig. 2.9. Eq. 2.42 is in theory an easy way to determine the interfacial energy of a liquid experimentally.

Contact Angles and Capillary Flow in Real Systems

Some important deviations from the ideal situations described in the above paragraph need to be mentioned. First, contact angles are — in principle - material constants. As such, they should be constant, whether the contact angle is measured on a freshly cleaned sample (referred to as advancing contact angle (Θ_a) or on a sample that was exposed to the liquid before (termed receding contact angle (Θ_r). The difference between the two is called contact angle hysteresis. These deviations may have different origins, most commonly they are due to heterogeneities in the surface composition, surface roughness, residual solvent on the surface or in the surface cavities. Surface roughness, for example, leads not only to such hysteresis effects but also to the fact that the apparent contact angle may differ from the "real" one.[33]

Also, capillary flow may not be as ideal as described before. Most notably, the surface tension (which is assigned a constant value) might change over time due to various effects and more importantly from point to point. If the surface tension is different from point to point, liquid flows from regions with low surface tension to regions with high surface tensions. If liquid flows due to a surface tension gradient, this is commonly referred to as "Marangoni flow". The reason for the evolution of such gradients may be mainly two-fold. For one, a local increase in temperature leads to a lower surface tension at this point and consequently an out-flow of liquid to regions with higher surface tensions. Also, for multi-component systems, adsorption-related phenomena or differences in evaporation rates may lead to such surface tension gradients. If a two-component system consists of a high and a low surface tension component, often, the low surface tension liquid adsorbs preferentially at the liquid-fluid interface and lowers the surface tension. If this component is more

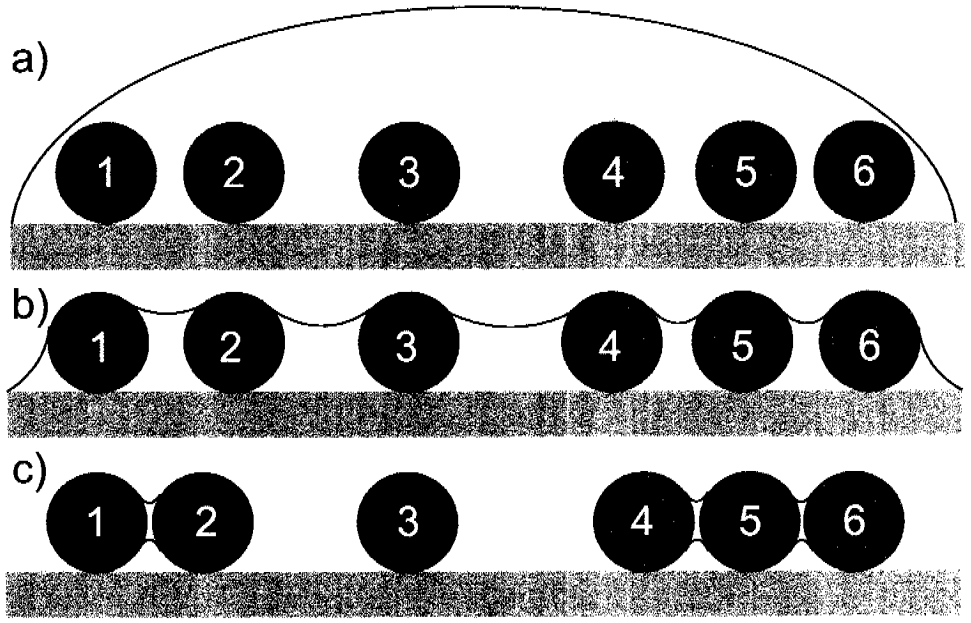

Figure 2.10: Schematic representation of the evolution of capillary forces in adsorbed particles. a) Particles adsorb to the substrate in suspension (e.g. via electrostatic interactions). b) Upon evaporation of the solvent, particles are at a given point only partially immersed in the solvent, giving rise to a three-phase contact line. Due to the low contact angle between solvent and particle (assuming hydrophilic particles), the meniscus between the particles is curved, which gives rise to attractive capillary forces. c) Depending on the separation distance of the particles and the relative strength of the particle-substrate interaction, the attractive capillary forces are strong enough to bring adjacent particles in close contact and only a small liquid bridge between particles in contact remains (which dries off eventually).

volatile, it evaporates faster and the surface tension will increase which leads to local composition differences. In-flow of liquid is the consequence in this case.

2.3.3 Capillary Forces Between Particles

The right hand side of Eq. 2.42 describes the capillary pressure that leads to a water column "climbing up" in a small capillary. It is, on the other hand, also a measure of the attractive force that the liquid in the capillary exerts on the walls of the capillary. If the capillary depicted in Fig. 2.9 c) and d) had "moveable" walls, the capillary pressure would contract those walls (or two plates, for that matter) instead of rising in the capillary.[17] It now becomes obvious, that capillary forces start to act in a particle system as soon as the particles are only immersed partially

[17]It only contracts the two plates if the contact angle is smaller than 90°! Above 90° the walls would be separated because the capillary pressure is then positive

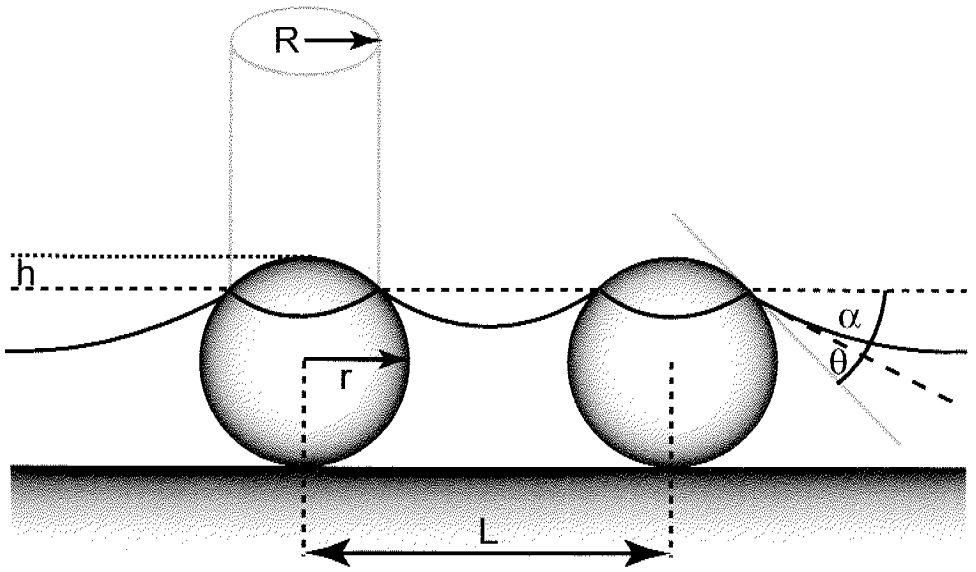

Figure 2.11: Two nanoparticles partially immersed in a thin liquid film. Attractive immersion capillary forces evolve between the two, depending on the contact angle Θ, the separation distance L and the particle radius r as described in the text.

in the water film. Apparently, this situation will inevitably occur at one point during the drying process. In Fig. 2.10 such a situation is schematically depicted. In the beginning, particles adsorb in suspension on the surface (e.g. by electrostatic forces) (Fig. 2.10a). As the solvent evaporates, the particles on the surface begin to show three-phase contact lines (Fig. 2.10b). Between individual particles a curved water meniscus forms (which depends on the contact angle between particle and solvent and exerts an attractive capillary force according to Eq. 2.42 (right hand side). Before, it was noted that the radius of the water meniscus R depends on the radius of the capillary r. Accordingly, particles which are inherently closer in contact to a neighboring particle will be exposed to higher capillary pressure (in the sketch, capillary forces between 1-2, 4-5,5-6 will be higher then those between 2-3 and 3-4). Consequently, particles 1-2, 4-5-6 will move towards each other and form a cluster on the surface, whereas particle 3 remains on the surface as a single particle.

The situation where the water film thickness is less then a particle diameter and the particles protrude out of the water film and form menisci is again depicted in Fig. 2.11. This type of capillary force acting between two particles is termed immersion forces. Immersion forces differ from "floating capillary forces", which act on particles floating on a liquid film. Floating capillary forces are of gravitational origin, they depend on the weight of the particle that deforms a liquid film and produces in

this way a curved liquid film. Therefore, such floating capillary forces have no effect on very small particles (because gravity does not affect them much). Immersion forces on the other hand act also on very small particles down to 10 nm [45] and are essentially originating from the wetting behavior of the particles. To illustrate this, in Fig 2.11 the contact angle Θ is shown and geometrical considerations suggest, that changing the contact angle must play an important role in the formation of the water meniscus. From the sketch in Fig. 2.11 it is also obvious that immersion capillary forces even exist if the contact angle Θ is 0. This would not be the case for floatation capillary forces since particles that have such a low contact angle will sink into the liquid and cannot float.[46] Several theoretical papers derived analytical expression for the lateral capillary forces in situation as shown in Fig. 2.11 using either an energy or a force equilibrium approach.[12, 45–48] Kralchevsky et. al propose the following, analytical expression for the lateral capillary forces between two particles on a surface:[46, 47]

$$F = 2\,\pi\,\gamma\,Q_1 Q_2\,q\,K_1(qL) \tag{2.43}$$

where L is the separation distance of the particles, γ is the surface tension and K_1 is a modified Bessel function of first order and Q_i is defined as follows:

$$Q_i = R_i \sin(\alpha_i) \tag{2.44}$$

here, R is the radius of the contact line (of particle 1 and 2) and α is the meniscus slope angle as shown in Fig. 2.11. q in Eq. 2.43 is the inverse capillary length, a measure of how far the capillary attraction is active (in a sense comparable to the Debye length introduced earlier). It is defined as follows:

$$q^{-1} = \left(\frac{\gamma}{\Delta\rho\,g}\right)^{1/2} \tag{2.45}$$

Under the assumption that $R << L << q^{-1}$, Eq. 2.43 simplifies to:

$$F = 2\,\pi\,\gamma\,\frac{Q_1 Q_2}{L} \tag{2.46}$$

whose similarity to the Coulomb law of electricity is obvious. Therefore, Q_i is also referred to as the "capillary charge" of particle i. The higher Q_i, the more can

particle i deform the liquid meniscus and therefore increase the capillary force. The radius of the contact line R can be approximated by:[48]

$$R = \sqrt{h(2r - h)} \tag{2.47}$$

where h is the distance the particles protrude out of the liquid film (Fig. 2.11). And also for α, the angle of the meniscus, an approximation can be found relating α to the contact angle Θ:

$$\alpha = \arcsin(\frac{R}{r}) - \Theta \tag{2.48}$$

With those equations, the capillary force between two particles can be expressed as a function of only particle size r, contact angle Θ, surface tension γ, immersion height h and separation distance L under some restrictions (following from Eq. 2.46 and using Eq. 2.44, 2.47 and 2.48). For the capillary force between two particles we find in conclusion:[12]

$$\Delta G = 2\,\pi\,\gamma\,\frac{R^2\,\sin^2(\alpha)}{L} \tag{2.49}$$

For the interaction energy of the capillary attraction, Aizenberg uses the following expression:[18][14]

$$\Delta G = 2\,\pi\,\gamma\,\frac{R^2\,\sin^2(\alpha)\,r}{L - 2r} \tag{2.50}$$

For a more detailed discussion on capillary forces, the reader is directed to two reviews published by Kralchevsky.[49, 50]

[18]Note that using L instead of $L - 2r$ does not lead to a significant change of the results since one of the restriction is, that $r << L$ and therefore somewhat "arbitrarily".

2.4 Immobilizing Colloids on a Surface: Strategies

As elaborated from a theoretical point in the previous sections, there are only a few fundamentally different ways to immobilize particles on a surface. These main principles are shortly reviewed in this section.

2.4.1 Electrostatic Adsorption

Colloidal particles in a suspension usually carry charges. These charges provide stability for the colloid suspension (repulsion between equally charged molecules) but also offer a way to adsorb colloids to a oppositely charges surface (see Chapter 4). Charged particles will adsorb to oppositely charged surfaces and a large number of papers exists that study such systems.[51, 52] A vast number of methods exist today to charge a surface such that it is suitable for particle adsorption experiments. Typically, particles will adsorb randomly on an oppositely charged surface as described by the random sequential adsorption (RSA) model. Specific properties of such systems (particle density on the surface, clustering, number of layers on the surface, etc.) are relatively easily controlled by changing salt concentration and pH (as the most important). As a rule of thumb, going to high salt concentration suspensions with a pH close to the IEP of the suspension will lead to the formation of densely packed mulilayer particle assemblies, while a pH far a way from the IEP and no salt produces generally particle assemblies with only a few particles per area adsorbed. These simple parameters allow a good control of the particle arrays therefore electrostatic interactions are probably the most widely used means to adsorb particles on surfaces. Also, there is generally no principal difference between particles adsorbing on a homogeneous substrate or on a patterned surface. In both cases, electrostatic interactions are rather predictable and a pattern on the surface (for example, of positively and negatively charged regions) will cause the particle suspension to adsorb to the oppositely charge patterns and not to like-charged regions. However, the situation is not always as straight-forward as just depicted, since often other forces influence pattern formation.

2.4.2 Capillary Forces

In Section 2.3, it was discussed how capillary forces act on adsorbed particle arrays: thus, if particles (also very small nanoparticles) adsorb on a surface (e.g. by electrostatic interactions), capillary forces are present during the drying step and tend to influence the particle array produced in suspension. Here, the situation is not as straight-forward as with electrostatic interactions. For each system, the question must be answered whether the particle-surface interaction is strong enough to prevent capillary forces from having an influence or not. But this does not only depend on particle-surface interactions but also on other parameters, such as interparticle distance of the adsorbed particles on the surface. In Fig. 2.10 a hypothetical situation of 5 particles was depicted and discussed why capillary forces will affect certain particles and not others. In an actual system, changing the adsorption parameters slightly (for example adding a little more salt), will affect the interparticle distance such, that it is suddenly low enough for capillary forces to start acting. Clustering in such a system will then occur where it has not been observed before. The question of particle mobility is thus a crucial point in almost all systems and can usually not be predicted easily.

Also, capillary forces are the reason why sometimes large differences are observed between patterned and unpatterned surface regarding particle adsorption. Patterning of a surface usually involves creating chemically different surfaces, that might also exhibit different wetting properties. On such a pattern, drying will not occur homogenously as on an unpatterned sample and as a consequence, three phase contact lines on the sample may be formed (for example at pattern edges). Such three phase contact lines will largely influence particle arrays during drying. In some cases these effects are highly undesired and are sought to be minimized with appropriate counter-measures (Chapter 6), in other cases capillary forces and their effect is exploited to use their power to form particle structures otherwise not achievable (Chapter 5). Thus, in most of the cases where capillary forces are used in a favorable way, some sort of patterning is applied, to deliberately create three phase contact lines. These water contact lines are then able to direct particle adsorption in a powerful way. Some examples of the possibilities that are offered by the use of capillary forces are discussed in the next section.

2.4.3 Specific Binding of Colloidal Particles

In some cases, if neither electrostatic nor capillary forces can be used to immobilize particles on a surface in a desired way, other particle assembly methods have to be used. This is for example the case if particles carry no charges or are functionalized in a specific way that does not allow adsorption by electrostatic forces or if a surface pattern is produced that has no wettability contrast and therefore capillary forces may not be used to assemble particles as wished. An alternative strategy to bind particles to a surface is the use of specific interactions between the particle and the surface. Such an interaction might for example be a protein-ligand system, a high chemical affinity system (e.g. gold particles on thiolated surface) or DNA-based assembly systems, that use the hybridization power of the DNA molecule to bind particles coated with a single stranded DNA to a surface containing its complementary strand. In such systems, particle and substrate (pattern) will have to be functionalized specifically, which at the same time offers the possibility to tailor the function of both particle and substrate as desired. Such systems posses very high binding free energies, which also allows for the immobilization of particles on the surface. But again, care must be taken while drying such systems since capillary forces are of course also present in this case and may have an influence on the end-result.

2.5 Self-Assembling of Colloidal Particles on Patterned Surfaces

There are only a few basic principles how colloids can be immobilized on a surface (see the previous section). But a vast number of real systems can be designed, where these principles play together in a new and different way. Especially when particles aim to be immobilized on a patterned sample in a tailored way, many different possibilities arise of which some of the most successful ideas and strategies will be discussed here.

2.5.1 Surface Pre-Patterning and Particle Self-Assembly

Generally, the pre-patterns that are used will consist of structures which will interact with the particle in a specific way and a background which usually is resistant to particle adsorption. These structures are commonly in the micrometer range — but can easily be scaled up and with less ease be brought to the nanometer range [53] — and can be produced using virtually any micro-fabrication technique that is known today — from conventional photolithography to softlithography or imprinting methods.[54, 55] Often, chemical functionalization or an etching step is necessary to provide the surface structure with the necessary chemical or topographical properties that are needed to self-assemble particles on it. Note that several attempts are also undertaken to directly pattern colloidal particles to a surface, for example by μ-contact printing of colloidal particles [56, 57] or other methods. Such processes are, however, inherently top-down processes and will not be reviewed here in great detail.

The second step in this process is the interaction between a nanoparticle suspension and the patterned surface. Depending on the chemical properties of the substrate and the suspension a variety of different effects can occur. The particles can adsorb to the pattern and not to the background or it is possible to have no interaction between particles and the substrate pattern, etc. Thus, tailoring the interaction profiles between particles themselves (necessary to maintain a stable suspension), the particles and the pattern and the particles and the background is an important part in the production of nanoparticle arrays or monolayer.

The third step is the drying process, which is an inherent part of all colloidal fabrication processes. In this step, the solvent evaporates while the particles remain on the surface. The drying process is of equal (or even greater) importance than step two because capillary forces acting on the particles during this step may significantly alter the structure of the particles on the patterned substrate if capillary forces exceed the colloid-substrate adhesion forces. For this reason, capillary forces are a major concern in self-assembly processes of colloidal particles. However, they can also be used intentionally to guide the self-assembly process provided a suitable template is used.

2.5.2 Particle-Assembly by Electrostatic Adsorption

One of the most straight-forward ideas is to pattern a surface with positive and negative charges. A particle suspension with, say, negatively charged nanoparticles will adsorb electrostatically on the positive areas, being repelled from the negative surface background. The charged structures on the surface can be obtained via a variety of surface patterning methods, all of them producing a charge-pattern in the micrometer range. Among these are μ-contact printing,[13, 14, 18, 19, 58] charging of a surface with a focused ion beam [59], vapor phase or solution deposition of a charge-carrying molecule on a photolithographically produced photoresist-surface contrast and subsequent removal of the photoresist [20, 60]. In most of these examples it becomes evident, that capillary forces pose a problem during the formation process of these colloidal pattern on the surface: the particles adsorb electrostatically to the charge-pattern in the first place, however, during drying of the solvent, it is often observed that capillary forces influence the pattern formation.[14, 20]

2.5.3 Particle-Assembly using Capillary Forces

Capillary forces occur in all particle self-assembly processes as soon as the evaporating solvent layer is thinner then the particle diameter. As mentioned before, they will under most circumstances also influence the colloidal pattern formation in cases where other strategies are employed in the first place to assemble colloidal particles on a substrate. For this reason, a lot of work was done using the capillary forces themselves, since they cannot be avoided in the assembly process, to produce colloidal particle arrays on pattern. For 2D and 3D colloidal assemblies (colloidal monolayers and crystals) the mechanisms governing their assembly have been established.[12, 61–63] It is a two step mechanism, where in the first place immersion capillary forces as discussed in section 2.3 attract nearby particles and start to form the nucleus of a monolayer. The second step of that process is the formation of a colloidal monolayer or crystal due to the hydrodynamic force which drags particles to regions of thinner liquid layers. The reason for that particle flux is a hydrodynamic flux, which transports matter to regions where evaporation rates are the highest (which is at three-phase contact lines and thus were liquid films are the thinnest).[50] If a drop of a suspension dries, the three-phase contact line will be the edge of the drop and particles will be dragged to the edge of the drop where

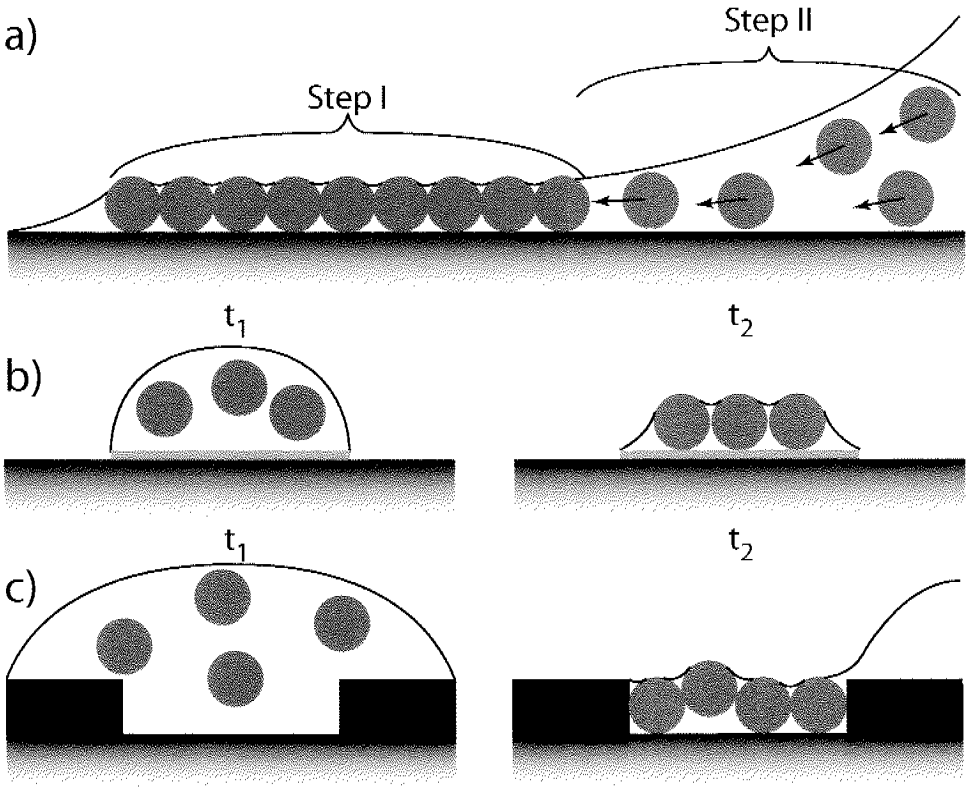

Figure 2.12: Processes of particle self-assembly by capillary forces. a) Particles form dense mono- or multilayer due to attractive capillary forces (section 2.3) if the water contact line is thinner then the particle diameter (step I). Evaporation of solvent in the region of step I leads to a hydrodynamic flux from the bulk to the edge region of the monolayer. This flux is responsible for a constant particle flow (step II) to the edge region which builds up a colloidal (mono-) layer as a consequence. b) capillary forces acting on a hydrophobicity gradient (pattern: hydrophilic, background: hydrophobic). At a given time t_1, most of the solvent has already evaporated, only leaving a small drop of suspension on the hydrophilic pattern. Further evaporation of the liquid leads to an situation similar to a) step I and particles are forming a dense layer on the hydrophilic pattern. c) a topographical contrast is also able to arrange particles into a distinct structure: at t_1, the particle suspension covers the whole sample. If the drying front moves along the sample, particles are dragged into the holes by capillary forces and at t_2 an array of particles captured in the holes of a topographical pattern is achieved.

they assemble. A famous example illustrating this effect is a spilled drop of coffee that dries on a surface and forms ring-like deposits of coffee-powder.[63, 64] More precisely, both of the mentioned processes, which are illustrated in Fig. 2.12a), lead to the formation of such "coffee-ring" structures. The hydrodynamic force moves particles near the edge region of a drop (or to another region with a high evaporation rate) (Fig. 2.12a (Step II)) and capillary forces in the drying region lead to a dense particle monolayer or crystal (Fig. 2.12a (Step II)). In principle, the described mechanisms also apply for patterned substrates. Furthermore, hydrophilic micro or nanopattern offer also a way to selectively deposit nano- or femtoliter amounts of liquid at desired positions, something which is not possible with current dispensing techniques. Biebuyck and Whitesides used this possibility to deposit organic liquids on the hydrophobic parts of such a pattern. The organic polymer was then cured and thus lenses of this organic compound were formed on the hydrophobic regions of the pattern.[65] Dip-coating of a wettability pattern and the exact formation of liquid-filled structures was also studied theoretically.[66] Today, two main approaches are applied to produce colloidal assemblies on patterned substrates using capillary forces as the driving force. Both of them are shortly reviewed in the following sections.

Particle-Assembly on a Hydrophobicity Pattern

A chemical pattern on a surface may exhibit very different wetting behavior. For example, the pattern might have a hydrophilic character, whereas the background is hydrophobic. If a suspension is applied to such a structure, the hydrophobic regions will have the tendency to de-wet, while the hydrophilic regions remain wetted for a longer time. At one point, a situation as depicted in Fig. 2.12b) (t_1) is achieved, where only hydrophilic areas are covered with suspension, the hydrophobic background is solvent-free. Upon further evaporation (t_2), capillary forces start to act and form a particle layer on the hydrophilic surface pattern. Note, that the "size" of the droplet on the hydrophilic area depends on a) the contact angle of the liquid on that surface and b) the size of that pattern. On a small pattern, only a small droplet will exist. This effect can be utilized to "sieve" a colloidal suspension that consists of different particle size fractions.[67] On a small pattern, only small particles can be deposited as sketched in Fig. 2.12b), whereas on larger pattern, also larger colloids will be deposited. Thus, if a suspension with two particle sizes is dipped on a

substrate with "small" structures, only the "small" colloids will be adsorbed.[67] If particles interactions with the initial pattern are minimized in the suspension (e.g a pattern consisting of uncharged or like-charge surfaces only), it will be only capillary forces that produce the particle assemblies during drying. One interesting feature of the wettability pattern is the pinning of the three-phase contact line which occurs at the edge of the pattern (as depicted in Fig. 2.12b) (t_2). The contact line is "pinned" at the edge of the pattern, which leads to similar effects as described above, only on a much smaller scale (pattern scale is in the range of μm). However, this also poses the problem, that particle distribution on a single pattern might be non-uniform with particles enriching in edge regions.

In current literature, a "mixture" between electrostatic adsorption and pattern formation through capillary forces is often observed because the two effects are not separable.[14, 18, 20] In such a case, the pattern carries charges that attract particles in the suspension and capillary forces during drying modify the particle pattern. This restructuring can have unwanted [20] or desirable effects, such as perfectly centering particles on a circular pattern [14], using a hydrophilic / hydrophobic contrast to precisely position particles or solution droplets at desired positions [68] or helping in the formation of particle lines and dense pattern [18, 69].

Particle-Assembly on Templates with Topography Pattern

Topographical pattern can act as excellent template materials for the production of colloidal complexes and other structures. The idea is depicted in Fig. 2.12c)(t_1). If a topographical structure is removed from a suspension (or the solvent evaporated), a drying front will be established (Fig. 2.12c)(t_2) that drags colloidal particles in the holes mainly due to capillary forces. Xia and co-workers have done an extensive amount of work on such structures. For example, they have tailored the holes such that only a specific number of particles fitted into the holes, thus producing particle singlets, doublets, triplets and so forth.[70] A review on their activities using templates with topographical pattern was published recently.[7] Notably, this approach also works for nanoparticles, which is not obvious since the capillary force diminishes with their size and a 2 nm particle will have a capillary force in the order of kT.[49] Chen et al. used a topography pattern to increase the regularity of adsorbing particles. The same principle was applied there, particles move into the cavities of the topography pattern and thus a regular array of particles is achieved

compared to particles adsorbing on a unpatterned substrate.[71] Sun et al. also used a similar idea (topography pattern of PDMS), to *in situ* show how particles assemble in the grooves of the pattern during drying by lateral capillary forces as depicted in Fig. 2.12.[72]

2.5.4 Particle-Assembly via Specific Binding

Instead of a charge-pattern consisting of differently charged regions on a substrate that interacts with charged colloids, one can also imagine to use specific interactions between colloids and surface pattern. The most common of these system is without doubt the gold-thiol system. Gold was found to have a very high binding affinity for thiol-containing molecules. This type of interaction as well as similar systems with silanes on metal oxides for example gave rise to the advent of self-assemble molecular monolayers which use long thiolated or silanated alkane chains that form highly ordered, dense monolayers on gold or metal oxide surfaces. Likewise, gold colloids can be used to interact with thiolated pattern structures on a surface.

Functionalized gold nanoparticles that use another prominent binding system were developed recently: DNA-oligomers were attached to gold particles, which then hybridize to a complementary DNA strand immobilized on the surface. Niemeyer et al. used this technique to form particle arrays on a DNA chip: Au colloids functionalized with a specific DNA oligonucleotide only hybridize to surface regions where the complementary strand is immobilized thus forming highly selective gold pattern on the surface.[73] With the same concept, Au colloids can also be directly functionalized with proteins [74] or proteins can be immobilized on a patterned surface instead of Au particles [75]. A similar approach was chosen by our group, where we patterned a surface with the MAPL technique — which was also used in this thesis (see section 3.5 and Chapter 6 for details of this technique). Then, complexes of neutravidin and biotinylated single-stranded DNA were adsorbed to that MAPL pattern and subsequently, Au colloids with the complementary DNA strand were selectively immobilized on the patterned surface.[76] The highly selective properties of DNA strands to hybridize with their complementary strand was used to an even larger extend by Le et al., who formed DNA arrays in a puzzle-like way to pattern a surface with a "DNA carpet". This DNA carpet has special binding sites designed to again bind Au colloids carrying the matching complementary DNA strand to the surface.[77] The same concept was also used by Li et al. There, long DNA triple

strands were produced by combining many small strands. Some of these strands were modified with biotin groups, that allowed the decoration of these long strands with Au colloids.[78] These few examples (and many more [79, 80]) show, that among specific binding systems, the powerful and highly selective binding capabilities of DNA or oligonucleotide single strands to their complementary counterparts provides one of the most convenient means to specifically adsorb functionalized particles to a substrate surface (pattern).

Another prominent specific binding system is the streptavidin-biotin linkage system. This protein-ligand binding system was originally discovered in investigations on the vitamin H complex, where avidin (a close relative to streptavidin)[19] was responsible for a nutritional deficiency in rats, because streptavidin binds so strongly to vitamin H (which is biotin).[81] The binding of biotin by streptavidin is accompanied by one of the largest decreases in free energy yet observed for a noncovalent interaction between a protein and a small ligand in aqueous solution.[82] Streptavidin is a homotetrameric protein with a molecular mass of $\tilde{4}$x15'000 kDa. Each of the four "arms" is able to bind one biotin molecule with an extremely high affinity constant ($10^{13}\ M^{-1}$). This binding system is common for many applications in biotechnology where biotinylated species (molecules, proteins, vesicles, particles and so on) are specifically interacting with another biotin function via the streptavidin linkage.

2.5.5 Potential Applications of Nanoparticle Arrays

As discussed in the previous sections, scientists are in the course of developing various methods to immobilize nanoparticles on substrates as monolayers,[83 86] photonic crystals,[8, 10, 70, 87, 88] patterned particle arrays,[13, 20, 67, 69, 70, 72, 89–94] or as single particles,[19, 68, 95] thereby opening up the possibilities for applications of particle-modified surfaces in many research areas. While 3D crystals of particles are today widely researched for their potential to form photonic band gap materials which may find applications in opto-electronic devices,[8, 88, 96] less information is available on possible uses of patterned particle arrays or particle monolayers. One common application for particle monolayers is their use in anti-reflective coatings,[97, 98] but beside that, not much in terms of concrete applications

[19]Streptavidin is carbohydrate-free and has a slightly acidic IEP (5-6) compared to avidin. It is also for these reasons, that the crystallographic structure is more easily obtained for streptavidin then for avidin.[81]

has been published. While it is often mentioned, that new physical properties (e.g. optical, catalytic or magnetic) evolve when the particle size is reduced to the few-nanometer regime,[85, 99] and such particle-nanostructures will exhibit new physical features, only little experimental evidence of functioning "devices" is available that supports those ideas today.

There is no doubt, that particle-based patterning techniques are a very attractive tool to fabricate various nanostructures as also shown in this thesis, however, concrete applications of such particle arrays are sparse. In the next few paragraphs, pathways and ideas for possible future applications (of particle arrays or monolayer) as well as complications and restrictions that hamper the way there will briefly be discussed. The focus lies hereby on (nano-)biotechnological applications for colloidal particle arrays, since in this field, the properties of such particle arrays are potentially very attractive (e.g. for the development of new or improved biosensing devices). In general, three different ways in which nanoparticles may impact relevant nanopattern formation can be imagined:

1. Nanoparticles can be used to produce nanopatterns with a function on substrate surfaces either directly through the adsorption of single (functionalized) particles, patches of particles, or monolayers of particles, or indirectly by acting as a mask as in colloidal lithography.[83, 84, 100–103] This latter use of nanoparticles presents one of the most promising ways by which nanoparticles can be used to pattern biologically useful nanopatterns.

2. Colloidal nanoparticles may be used as a platform for the adsorption of (bio-)molecules for use in sensing devices or as markers.[152, 163-169] The role of the particle, in this case, may be two-fold: nanoparticles can be used as an integral part of such a biosensing device, e.g. providing conductivity by using conducting particles,[166, 170-172] or by incorporating particles into a system that have a target biomolecule (pre-)adsorbed to its surface.[173]

3. Colloids functionalized with (bio-)molecules (e.g. DNA or as done in Chapter 6 of this thesis) can be used to attach particles at specific locations on a pattern using biological recognition systems. This is a promising bottom-up approach for the fabrication of for example gold nanowires and devices: this, however, is rather an elaborate nanofabrication tool, than a technologically useful application.

Nanosphere Lithography

One application for nanoparticle monolayer or particle arrays is their use as a "mask" for a subsequent deposition process. This idea was introduced in the early eighties by Fischer et al.[104] and soon after extended by Deckman et al.[83] Initially termed 'natural lithography', particle monolayers were first used as masks for contact imaging and later used as masks for etching and material deposition.[83] The basic idea of this process is straight-forward. First, a monolayer of particles is formed on a substrate. In a second step, a material is deposited on top of the particle layer. The particle layer thereby acts as a mask such that material is only deposited in the empty spaces of the hexagonal particle assembly. After lift-off of the particles, hexagonal nanostructures of deposited material then remain on the surface. At a later stage, Hulteen et al. developed double layer masks over relatively large areas (10-100 μm) to produce nanoparticle arrays, as characterized by AFM.[84] In recent years, a variety of systems have been studied and the technique has attracted increasing interest due to its advantages: it is an inexpensive, inherently parallel, high-throughput nanofabrication technique. For an interesting feature article on advances in particle or nanosphere lithography, refer to Heynes et al.[105]

Despite these advances, the difficulty to produce defect-free particle monolayers remains and this in turn restricts the large-scale production of nanosphere lithographic patterns and limits the number of substrate materials that can be used to, primarily, glass substrates and silicon wafers. Several ways of producing particles monolayers and the study of the formation processes that lead to such 2D crystals have been reported, including spin-coating,[84, 106] drop drying,[12, 107] and evaporation of the solvent using a Peltier element [85, 108]. Wang et al. used a slightly more complicated way of producing their monolayers, which yields monolayers of comparable quality.[86] Ormonde et al. have used convective self-assembly of the nanospheres to increase the pattern fidelity of the particle mask compared to drop coating of the particles.[109] However, it remains the case that the number of achievable patterns by a monolayer of particles is limited and is defined by the particle monolayer and the interparticle holes formed in that layer. In recent years, progress has been made to decrease the size of these features not only by using smaller particles but also by tilting the substrate with the particle monolayer relative to the deposition direction. This significantly decreases the interparticle spacing which can be patterned.[110] Alternatively, Snoeks et al. used an ion-beam to deform the particle monolayers

such that the interparticle spacing was reduced (by 'squeezing' the particle layer together) and consequently smaller nanopatterns could be produced,[111] while Sun et al. used a laser to locally change the morphology of the resulting nanopatterns effectively.[106] An alternative approach to 'classic' nanosphere lithography was presented by Michel et al. to produce biologically relevant nanostructures.[101]. Note that in their case the particles are interacting electrostatically with the surface, and as such form arrays of randomly adsorbed, separated particles. This is in contrast to standard nanosphere lithography, in which interactions between the colloidal particles and the substrate are minimized such that capillary forces drag the particles together during the drying process to form hexagonal colloidal crystals.

Furthermore, colloidal lithography was also used by Garno et al. to directly pattern protein nanostructures on various substrates. A mixture of BSA (or IgG) and latex particles was prepared and adsorbed on a substrate. After dissolution of the latex particles, hexagonal protein nanostructures could be observed on the surface covering the free areas between the particles.[102] This shows how structuring techniques with nanoparticles can provide a useful tool to produce functional nanostructures.

Single Particles as "Detectors" in Biosensing Applications

As mentioned above, nanoparticles are often characterized by interesting physical properties, be they optical,[103, 112] magnetic,[113] or electronic,[114] that change upon adsorption of for example biomolecules such that they can also be used to read-out signals in (bio-)sensing devices. Haes et al. and Frederix et al. used exactly this approach to explore the potential of using a nanosphere patterned surface for biosensors.[115, 116] In this case, polystyrene beads were used to produce a colloidal monolayer and subsequent deposition of Ag onto that monolayer lead to colloid nanostructures. The effect that they take advantage of for their biosensor is termed localized surface plasmon resonance (LSPR), an effect that originates from the extraordinary optical properties of nobel metal nanoparticles. The LSPR refers to the ability of e.g. Ag nanoparticles to oscillate their conduction electrons collectively, which induces strongly enhanced electromagnetic fields surrounding the nanoparticle and will, in turn, determine the sensing volume in which sensing can occur.[116] This LSPR effect, not present in bulk Ag or Au,[117] will also affect resonant Rayleigh scattering, with an efficiency equivalent to that of 10^6 fluorophores, and absorption with extremely large molar extinction coefficients.[116] It is this ex-

tinction, which is extremely sensitive to molecules adsorbed onto the surface of the particles, that can be measured and enables the transduction of chemical binding events into optical signals (for details see references in [116]). Thus, Ag nanodots prepared by nanosphere lithography act as effective chemical and biological optical nanosensors. By simply monitoring changes in the UV/Vis absorption band of the nanoparticles, adsorption of chemical or biological species could be detected. These very sensitive biosensors usually function by first adsorbing a mixed SAM monolayer onto the Ag nanodots. Then, a protein of interest is adsorbed to that molecule and as a last step an antibody that interacts with the protein is introduced. Each of these steps is observable by UV/Vis spectroscopy due to a slight change in the extinction maxima of the LSPR spectra.[103] As a first practical system, a biosensor based on this working principle, for the possible detection of Alzheimer disease, was developed and tested.[116]

Nanoparticles as "Markers" / "Signal Enhancers" in Optical Biosensors

Nanoparticles have also contributed to biosensing and biovisualization as markers. For example, nanoparticles have enabled detection of single molecule interactions by visualizing individual gold colloid labels optically [118] or by means of scanning force microscopy [119]. In both cases, nanoparticles functionalized with antibodies [118] or DNA [119] have been used to later image these particles after they had bound to the protein and complementary DNA, respectively. This idea could be expanded of using colloidal particles as markers could be expanded in several directions. For example, spotting differently functionalized particles (each e.g. carrying an antibody for a specific molecule) on a surface, might create a variety of highly sensitive sites for protein adsorption on a single substrate chip. Another idea with a similar background is the use of nanoparticles as signal-enhancers. The basic concept is to use the large surface area of nanoparticles to increase the surface area available for the detection of — say — specific proteins on a protein chip. Nanoparticles can therefore significantly enhance the properties of existing biosensing devices.[120] It is also this concept, which was investigated in Chapter 7 of this thesis, were an approach is presented to increase the sensitivity of current biosensing devices (based on optical waveguide techniques) through the use of nanoparticles.[93]

Creating Tailored Surface Topographies with Nanoparticles

Another interesting idea is to use the inherent topography of adsorbing particles to produce substrates with distinct topographies for cell biological experiments. Colloidal lithography as mentioned above can be used as an efficient parallel way of producing various nanostructures. Such colloidal structures can be completely covered with a given layer of material and thereby creating a surface of nano 'bumps'. Such surfaces were produced and used in cell experiments to examine the reaction of cells to nanostructured surfaces.[121] In Chapter 4, a similar approach was taken to develop an easy-to-produce, (largely) material-independent technique based on the use of nanoparticles, which is able to create gradients of colloidal particles on a substrate.

The future of nanoparticles assemblies on surfaces

These examples illustrate a general trend. It appears for example, that patterned or single particle arrays have the biggest impact in the field of biosensing, where their unique properties indeed can shine the most. It is also obvious, that in very recent years, tremendous progress has been made in arranging particles on surfaces (in almost every imaginable way), but generating large-scale particle assemblies that are useful for a specific application is still far from trivial. This is all the more so if the particle assembly have to have specific features (e.g. resistant to biomolecule adsorption, having a specific binding affinity for biomolecules, etc.). As a general trend, we see ways to very precisely position particles (single particles, few particles, particle assemblies) on surfaces but these often lack the needed surface functionalization properties for the use in real (nanobiotechnology) applications. On the other hand, when particle (and substrate) do have the properties needed for such applications, arranging these particles becomes less trivial. It will be the combination of these two aspects, i.e.: precise control of particle positioning and tunable, biologically relevant particle and substrate functionalization, that will open the path to further nanoparticle applications, specifically in nanobiotechnology.

Bibliography

[1] Bain, C. D., Troughton, E. B., Tao, Y. T., Evall, J., Whitesides, G. M. and Nuzzo, R. G. Formation of Monolayer Films by the Spontaneous Assembly of Organic Thiols from Solution onto Gold. *Journal of the American Chemical Society*, **111**(1), 321–335, 1989.

[2] Ulman, A. Formation and structure of self-assembled monolayers. *Chemical Reviews*, **96**(4), 1533–1554, 1996.

[3] Brovelli, D., Hahner, G., Ruiz, L., Hofer, R., Kraus, G., Waldner, A., Schlosser, J., Oroszlan, P., Ehrat, M. and Spencer, N. D. Highly oriented, self-assembled alkanephosphate monolayers on tantalum(V) oxide surfaces. *Langmuir*, **15**(13), 4324–4327, 1999.

[4] Terfort, A., Bowden, N. and Whitesides, G. M. Three-dimensional self-assembly of millimetre-scale components. *Nature*, **386**(6621), 162–164, 1997.

[5] Bowden, N. B., Weck, M., Choi, I. S. and Whitesides, G. M. Molecule-mimetic chemistry and mesoscale self-assembly. *Accounts of Chemical Research*, **34**(3), 231–238, 2001.

[6] Oliver, S. R. J., Clark, T. D., Bowden, N. and Whitesides, G. M. Three-dimensional self-assembly of complex, millimeter-scale structures through capillary bonding. *Journal of the American Chemical Society*, **123**(33), 8119–8120, 2001.

[7] Xia, Y., Yin, Y., Lu, Y. and McLellan, J. Template-Assisted Self-Assembly of Spherical Colloids into Complex and Controllable Structures. *Advanced Functional Materials*, **13**(12), 907–918, 2003.

[8] Vlasov, Y. A., Bo, X. Z., Sturm, J. C. and Norris, D. J. On-chip natural assembly of silicon photonic bandgap crystals. *Nature*, **414**(6861), 289–293, 2001.

[9] Yin, Y., Li, Z. Y. and Xia, Y. Template-directed growth of (100)-oriented colloidal crystals. *Langmuir*, **19**(3), 622–631, 2003.

[10] Velikov, K. P., Moroz, A. and van Blaaderen, A. Photonic crystals of core-shell colloidal particles. *Applied Physics Letters*, **80**(1), 49–51, 2002.

[11] Wang, D. Y. and Caruso, F. Lithium niobate inverse opals prepared by templating colloidal crystals of polyelectrolyte-coated spheres. *Advanced Materials*, **15**(3), 205–+, 2003.

[12] Denkov, N. D., Velev, O. D., Kralchevsky, P. A., Ivanov, I. B., Yoshimura, H. and Nagayama, K. Mechanism of Formation of 2-Dimensional Crystals from Latex- Particles on Substrates. *Langmuir*, **8**(12), 3183–3190, 1992.

[13] Tien, J., Terfort, A. and Whitesides, G. M. Microfabrication through electrostatic self-assembly. *Langmuir*, **13**(20), 5349–5355, 1997.

[14] Aizenberg, J., Braun, P. V. and Wiltzius, P. Patterned colloidal deposition controlled by electrostatic and capillary forces. *Physical Review Letters*, **84**(13), 2997–3000, 2000.

[15] Hayward, R. C., Saville, D. A. and Aksay, I. A. Electrophoretic assembly of colloidal crystals with optically tunable micropatterns. *Nature*, **404**(6773), 56–59, 2000.

[16] Chen, K. M., Jiang, X., Kimerling Lionel, C. and Hammond Paula, T. Selective self-organization of colloids on patterned polyelectrolyte templates. *Langmuir*, **16**(20), 7825–7834, 2000.

[17] Himmelhaus, M. and Takei, H. Self-assembly of polystyrene nano particles into patterns of random-close-packed monolayers via chemically induced adsorption. *Physical Chemistry Chemical Physics*, 4(3), 496–506, 2002.

[18] Masuda, Y., Itoh, M., Yonezawa, T. and Koumoto, K. Low-dimensional arrangement of SiO2 particles. *Langmuir*, **18**(10), 4155–4159, 2002.

[19] Lee, I., Zheng, H. P., Rubner, M. F. and Hammond, P. T. Controlled cluster size in patterned particle arrays via directed adsorption on confined surfaces. *Advanced Materials*, **14**(8), 572–577, 2002.

[20] Jonas, U. and Krüger, C. The Effect of Polar, Nonpolar, and Electrostatic Interactions and Wetting Behavior on the Particle Assembly at Patterned Surfaces. *Journal of Supramolecular Chemistry*, **2**(-), –, 2003.

[21] Lyklema, J. *Volume I: Fundamentals*, volume 1 of *Fundamentals of Interface and Colloid Science*. Academic Press, 1991.

[22] Russel, W., Saville, D. and Schowalter, W. *Colloidal Dispersions*. Cambridge University Press, Cambridge, 1989.

[23] Myers, D. *Surfaces, Interfaces and Colloids*. Wiley-VCH, 1999.

[24] Faraday, M. The Bakerian Lecture: Experimental Relations of Gold (and Other Metals) to Light. *Philosophical Transactions Series I*, **(147)**, 145–181, 1857.

[25] van der Waals, J. PhD thesis, State University of Leyden, 1873.

[26] London, F. The General Theory of Molecular Forces. *Transactions of the Faraday Society*, **33**, 8–26, 1937.

[27] Derjaguin, B. V., Churaev, N. V. and Rabinovich, Y. I. The modern state of the macroscopic theory of molecular forces and the results of its experimental verification for thin interlayers. *Advances in Colloid and Interface Science*, **28**, 197–244, 1988.

[28] Gregory, J. The calculation of Hamaker constants. *Advances in Colloid and Interface Science*, **2**(4), 396–417, 1970.

[29] Bergstrom, L. Hamaker constants of inorganic materials. *Advances in Colloid and Interface Science*, **70**(1-3), 125 169, 1997.

[30] Ackler, H. D., French, R. H. and Chiang, Y. M. Comparisons of Hamaker constants for ceramic systems with intervening vacuum or water: From force laws and physical properties. *Journal of Colloid and Interface Science*, **179**(2), 460–469, 1996.

[31] Lyklema, J. *Volume II: Solid-Liquid Interfaces*. Fundamentals of Interface and Colloid Science. Academic Press, 1995.

[32] Debye, P. and HÃ¼ckel, E. Zur Theorie der Elektrolyte. I. Gefrierpunktserniedrigung und verwandte Erscheinungen. *Physikalische Zeitschrift*, **24**(9), 185–206, 1923.

[33] Norde, W. *Colloids and interfaces in life sciences*. Marcel Dekker, Inc., New York, 2003.

[34] Ninham, B. W. On progress in forces since the DLVO theory. *Advances in Colloid and Interface Science*, **83**(1-3), 1–17, 1999.

[35] Gray, J. J. and Bonnecaze, R. T. Adsorption of colloidal particles by Brownian dynamics simulation: Kinetics and surface structures. *The Journal of Chemical Physics*, **114**(3), 1366–1381, 2001.

[36] Mackor, E. L. A Theoretical Approach of the Colloid-Chemical Stability of Dispersions in Hydrocarbons. *Journal of Colloid Science*, **6**(5), 492–495, 1951.

[37] Hesselink, F. T., Vrij, A. and Overbeek, J. T. Theory of Stabilization of Dispersions by Adsorbed Macromolecules .2. Interaction between 2 Flat Particles. *Journal of Physical Chemistry*, **75**(14), 2094–2103, 1971.

[38] Flory, P. J. and Krigbaum, W. R. Statistical Mechanics of Dilute Polymer Solutions. II. *The Journal of Chemical Physics*, **18**(8), 1086–1094, 1950.

[39] Mackor, E. L. and Vanderwaals, J. H. The Statistics of the Adsorption of Rod-Shaped Molecules in Connection with the Stability of Certain Colloidal Dispersions. *Journal of Colloid Science*, **7**(5), 535–550, 1952.

[40] Miguez, H., Meseguer, F., Lopez, C., Mifsud, A., Moya, J. S. and Vazquez, L. Evidence of FCC Crystallization of SiO_2 Nanospheres. *Langmuir*, **13**(23), 6009–6011, 1997.

[41] van Blaaderen, A., Ruel, R. and Wiltzius, P. Template-directed Colloidal Crystallization. *Nature*, **385**, 321–324, 1999.

[42] Miguez, H., Meseguer, F., Lopez, C., Blanco, A., Moya, J., J., R., Mifsud, A. and Fornes, V. Control of the Photonic Crystal Properties of fcc-Packed Submicrometer SiO_2 Spheres by Sintering. *Advanced Materials*, **10**(6), 480–483, 1998.

[43] Dushkin, C. D., Nagayama, K., Miwa, T. and Kralchevsky, P. A. Colored Multilayers from Transparent Submicrometer Spheres. *Langmuir*, **9**(12), 3695–3701, 1993.

[44] Jiang, P., Bertone, J. F., Hwang, K. S. and Colvin, V. L. Single-Crystal Colloidal Multilayers of Controlled Thickness. *Chem. Mater.*, **11**(8), 2132–2140, 1999.

[45] Kralchevsky, P. A., Paunov, V. N., Ivanov, I. B. and Nagayama, K. Capillary meniscus interaction between colloidal particles attached to a liquid-fluid interface. *Journal of Colloid and Interface Science*, **151**(1), 79–94, 1992.

[46] Kralchevsky, P. A. and Nagayama, K. Capillary Forces between Colloidal Particles. *Langmuir*, **10**(1), 23–36, 1994.

[47] Paunov, V. N., Kralchevsky, P. A., Denkov, N. D. and Nagayama, K. Lateral Capillary Forces between Floating Submillimeter Particles. *Journal of Colloid and Interface Science*, **157**(1), 100–112, 1993.

[48] Nishikawa, H., Maenosono, S., Yamaguchi, Y. and Okubo, T. Self-assembling process of colloidal particles into two- dimensional arrays induced by capillary immersion force: A simulation study with discrete element method. *Journal of Nanoparticle Research*, **5**(1-2), 103–110, 2003.

[49] Kralchevsky, P. A. and Nagayama, K. Capillary interactions between particles bound to interfaces, liquid films and biomembranes. *Advances in Colloid and Interface Science*, **85**(2-3), 145–192, 2000.

[50] Kralchevsky, P. A. and Denkov, N. D. Capillary forces and structuring in layers of colloid particles. *Current Opinion in Colloid and Interface Science*, **6**(4), 383–401, 2001.

[51] Serizawa, T., Takeshita, H. and Akashi, M. Electrostatic adsorption of polystyrene nanospheres onto the surface of an ultrathin polymer film prepared by using an alternate adsorption technique. *Langmuir*, **14**(15), 4088–4094, 1998.

[52] Kampes, A. and Tieke, B. Self-assembly of carboxylated latex particles at charged surfaces: influences of preparation conditions on the state of order of the monolayers. *Materials Science and Engineering C - Biomimetic and Supramolecular Systems*, **8-9**, 195 204, 1999.

[53] Chen, Y. and Pepin, A. Nanofabrication: Conventional and nonconventional methods. *Electrophoresis*, **22**(2), 187–207, 2001.

[54] Xia, Y. N. and Whitesides, G. M. Soft lithography. *Annual Review of Materials Science*, **28**, 153–184, 1998.

[55] Whitesides, G. M., Ostuni, E., Takayama, S., Jiang, X. and Ingber, D. E. Soft lithography in biology and biochemistry. *Annual Review of Biomedical Engineering*, **3**(1), 335–373, 2001.

[56] Hidber, P. C., Helbig, W., Kim, E. and Whitesides, G. M. Microcontact printing of palladium colloids: Micron-scale patterning by electroless deposition of copper. *Langmuir*, **12**(5), 1375–1380, 1996.

[57] Shin, H., Yang, H., Jung, Y. and Kim, S. Direct patterning of silver colloids by microcontact printing: Possibility as SERS substrate array. *Vibrational Spectroscopy*, **29**(1-2), 79–82, 2002.

[58] Zheng, H. P., Lee, I., Rubner, M. F. and Hammond, P. T. Two component particle arrays on patterned polyelectrolyte multilayer templates. *Advanced Materials*, **14**(8), 569–572, 2002.

[59] Fudouzi, H., Kobayashi, M. and Shinya, N. Assembly of microsized colloidal particles on electrostatic regions patterned through ion beam irradiation. *Langmuir*, **18**(20), 7648 7652, 2002.

[60] Jonas, U., del Campo, A., Kruger, C., Glasser, G. and Boos, D. Colloidal assemblies on patterned silane layers. *Proceedings of the National Academy of Sciences of the United States of America*, **99**(8), 5034–5039, 2002.

[61] Denkov, N. D. Two-dimensional crystallization. *Nature*, **361**(6407), 26, 1993.

[62] Zhou, Z. C., Li, Q. and Zhao, X. S. Evolution of interparticle capillary forces during drying of colloidal crystals. *Langmuir*, **22**(8), 3692–3697, 2006.

[63] Park, J. and Moon, J. Control of colloidal particle deposit patterns within picoliter droplets ejected by ink-jet printing. *Langmuir*, **22**(8), 3506–3513, 2006.

[64] Deegan, R. D., Bakajin, O., Dupont, T. F., Huber, G., Nagel, S. R. and Witten, T. A. Capillary flow as the cause of ring stains from dried liquid drops. *Nature*, **389**(6653), 827–829, 1997.

[65] Biebuyck, H. A. and Whitesides, G. M. Self-Organization of Organic Liquids on Patterned Self- Assembled Monolayers of Alkanethiolates on Gold. *Langmuir*, **10**(8), 2790–2793, 1994.

[66] Darhuber, A., Troian, S., Davis, J. and Miller, S. Selective dip-coating of chemically micropatterned surfaces. *Journal of Applied Physics*, **88**(9), 5119 5126, 2000.

[67] Fan, F. and Stebe, K. Assembly of Colloidal Particles by Evaporation on Surfaces with Patterned Hydrophobicity. *Langmuir*, **20**, 3062-3067, 2004.

[68] Qin, D., Xia, Y. N., Xu, B., Yang, H., Zhu, C. and Whitesides, G. M. Fabrication of ordered two-dimensional arrays of micro- and nanoparticles using patterned self-assembled monolayers as templates. *Advanced Materials*, **11**(17), 1433–1437, 1999.

[69] Fustin, C. A., Glasser, G., Spiess, H. W. and Jonas, U. Parameters influencing the templated growth of colloidal crystals on chemically patterned surfaces. *Langmuir*, **20**(21), 9114–9123, 2004.

[70] Yin, Y. D. and Xia, Y. N. Self-assembly of monodispersed spherical colloids into complex aggregates with well-defined sizes, shapes, and structures. *Advanced Materials*, **13**(4), 267–271, 2001.

[71] Chen, J. Y., Klemic, J. F. and Elimelech, M. Micropatterning microscopic charge heterogeneity on flat surfaces for studying the interaction between colloidal particles and heterogeneously charged surfaces. *Nano Letters*, **2**(4), 393–396, 2002.

[72] Sun, Y. J. and Walker, G. C. Two-dimensional self-assembly of latex particles in wetting films on patterned polymer surfaces. *Journal of Physical Chemistry B*, **106**(9), 2217–2223, 2002.

[73] Niemeyer, C. M., Ceyhan, B., Gao, S., Chi, L., Peschel, S. and Simon, U. Site-selective immobilization of gold nanoparticles functionalized with DNA oligomers. *Colloid and Polymer Science*, **279**(1), 68–72, 2001.

[74] Niemeyer, C. M. and Ceyhan, B. DNA-directed functionalization of colloidal gold with proteins. *Angewandte Chemie-International Edition*, **40**(19), 3685-+, 2001.

[75] Niemeyer, C. M., Boldt, L., Ceyhan, B. and Blohm, D. DNA-directed immobilization: Efficient, reversible, and site-selective surface binding of proteins by means of covalent DNA-streptavidin conjugates. *Analytical Biochemistry*, **268**(1), 54–63, 1999.

[76] Staedler, B., Huwiler, C., Solak, H., Textor, M. and Voeroes, J. Selective patterning and manipulation of gold colloids. *Proceedings of the 5th IEEE Conference on Nanotechnology*, **5**(3), 215–219, 2005.

[77] Le, J. D., Pinto, Y., Seeman, N. C., Musier-Forsyth, K., Taton, T. A. and Kiehl, R. A. DNA-templated self-assembly of metallic nanocomponent arrays on a surface. *Nano Letters*, **4**(12), 2343–2347, 2004.

[78] Li, H. Y., Park, S. H., Reif, J. H., LaBean, T. H. and Yan, H. DNA-templated self-assembly of protein and nanoparticle linear arrays. *Journal of the American Chemical Society*, **126**(2), 418–419, 2004.

[79] Bandyopadhyay, K., Tan, E., Ho, L., Bundick, S., Baker, S. M. and Niemz, A. Deposition of DNA-functionalized gold nanospheres into nanoporous surfaces. *Langmuir*, **22**(11), 4978–4984, 2006.

[80] Sharma, J., Chhabra, R., Liu, Y., Ke, Y. G. and Yan, H. DNA-templated self-assembly of two-dimensional and periodical gold nanoparticle arrays. *Angewandte Chemie-International Edition*, **45**(5), 730–735, 2006.

[81] Green, M., Wilchek, M. and Bayer, E. Avidin and streptavidin. *Methods in Enzymology*, **184**, 51–67. Academic Press, 1990.

[82] Miyamoto, S. and Kollman, P. A. Absolute and relative binding free energy calculations of the interaction of biotin and its analogs with streptavidin using molecular dynamics/free energy perturbation approaches. *Proteins: Structure, Function, and Genetics*, **16**(3), 226 245, 1993.

[83] Deckman, H. W. and Dunsmuir, J. H. Natural lithography. *Applied Physics Letters*, **41**(4), 377 379, 1982.

[84] Hulteen, J. C. and Van Duyne, R. P. Nanosphere lithography: A materials general fabrication process for periodic particle array surfaces. *Journal of Vacuum Science and Technology A: Vacuum, Surfaces, and Films*, **13**(3), 1553–1558, 1995.

[85] Burmeister, F., Badowsky, W., Braun, T., Wieprich, S., Boneberg, J. and Leiderer, P. Colloid monolayer lithography-A flexible approach for nanostructuring of surfaces. *Applied Surface Science*, **145**, 461–466, 1999.

[86] Wang, X. D., Summers, C. J. and Wang, Z. L. Large-Scale Hexagonal-Patterned Growth of Aligned ZnO Nanorods for Nano-optoelectronics and Nanosensor Arrays. *Nano Letters*, **4**(3), 423 426, 2004.

[87] Zeng, F., Sun, Z. W., Wang, C. Y., Ren, B. Y., Liu, X. X. and Tong, Z. Fabrication of inverse opal via ordered highly charged colloidal spheres. *Langmuir*, **18**(24), 9116 9120, 2002.

[88] Zhao, Y. X., Wostyn, K., de Schaetzen, G., Clays, K., Hellemans, L., Persoons, A., Szekeres, M. and Schoonheydt, R. A. The fabrication of photonic band gap materials with a two-dimensional defect. *Applied Physics Letters*, **82**(21), 3764–3766, 2003.

[89] Liu, J., Lee, T., Janes, D. B., Walsh, B. L., Melloch, M. R., Woodall, J. M., Reifenberger, R. and Andres, R. P. Guided self-assembly of Au nanocluster arrays electronically coupled to semiconductor device layers. *Applied Physics Letters*, **77**(3), 373 375, 2000.

[90] Santhanam, V. and Andres, R. P. Microcontact printing of uniform nanoparticle arrays. *Nano Letters*, **4**(1), 41–44, 2004.

[91] Masuda, Y., Itoh, T., Itoh, M. and Koumoto, K. Self-assembly patterning of colloidal crystals constructed from opal structure or NaCl structure. *Langmuir*, **20**(13), 5588–5592, 2004.

[92] Masuda, Y., Itoh, T. and Koumoto, K. Self-Assembly and Micropatterning of Spherical-Particle Assemblies. *Advanced Materials*, **17**(7), 841–845, 2005.

[93] Huwiler, C., Halter, M., Rezwan, K., Falconnet, D., Textor, M. and Voeroes, J. Self-assembly of functionalized spherical nanoparticles on chemically patterned microstructures. *Nanotechnology*, **16**, 3045–3052, 2005.

[94] Juillerat, F., Solak, H. H., Bowen, P. and Hofmann, H. Fabrication of large-area ordered arrays of nanoparticles on patterned substrates. *Nanotechnology*, **16**(8), 1311–1316, 2005.

[95] Cui, Y., Bjork, M. T., Liddle, J. A., Sonnichsen, C., Boussert, B. and Alivisatos, A. P. Integration of colloidal nanocrystals into lithographically patterned devices. *Nano Letters*, **4**(6), 1093–1098, 2004.

[96] Xia, Y., Gates, B., Yin, Y. and Lu, Y. Monodispersed Colloidal Spheres: Old Materials with New Applications. *Advanced Materials*, **12**(10), 693–713, 2000.

[97] Hattori, H. Anti-Reflection Surface with Particle Coating Deposited by Electrostatic Attraction. *Advanced Materials*, **13**(1), 51–54, 2001.

[98] Koo, H., Yi, D., Yoo, S. and Kim, D. A Snowman-like Array of Colloidal Dimers for Antireflecting Surfaces. *Advanced Materials*, **16**(3), 274–277, 2004.

[99] Abkarian, M., Nunes, J. and Stone, H. A. Colloidal Crystallization and Banding in a Cylindrical Geometry. *J. Am. Chem. Soc.*, **126**(19), 5978–5979, 2004.

[100] Hanarp, P., Sutherland, D., Gold, J. and Kasemo, B. Nanostructured model biomaterial surfaces prepared by colloidal lithography. *Nanostructured Materials*, **12**(1-4), 429–432, 1999.

[101] Michel, R., Reviakine, I., Sutherland, D., Fokas, C., Csucs, G., Danuser, G., Spencer, N. and Textor, M. A novel Approach to Produce Biologically Relevant Chemical Patterns at the Nanometer Scale: Selective Molecular Assembly Patterning Combined with Colloidal Litography. *Langmuir*, **18**(22), 8580–8586, 2002.

[102] Garno, J. C., Amro, N. A., Wadu-Mesthrige, K. and Liu, G. Y. Production of periodic arrays of protein nanostructures using particle lithography. *Langmuir*, **18**(21), 8186–8192, 2002.

[103] Haes, A. J. and Van Duyne, R. P. A Nanoscale Optical Biosensor: Sensitivity and Selectivity of an Approach Based on the Localized Surface Plasmon Resonance Spectroscopy of Triangular Silver Nanoparticles. *J. Am. Chem. Soc.*, **124**(35), 10596–10604, 2002.

[104] Fischer, U. C. and Zingsheim, H. P. Submicroscopic pattern replication with visible light. *Journal of Vacuum Science and Technology*, **19**(4), 881–885, 1981.

[105] Haynes, C. L. and Van Duyne, R. P. Nanosphere Lithography: A Versatile Nanofabrication Tool for Studies of Size-Dependent Nanoparticle Optics. *J. Phys. Chem. B*, **105**(24), 5599–5611, 2001.

[106] Sun, F., Cai, W., Li, Y., Duan, G., Nichols, W. T., Liang, C., Koshizaki, N., Fang, Q. and Boyd, I. W. Laser morphological manipulation of gold nanoparticles periodically arranged on solid supports. *Applied Physics B: Lasers and Optics*, **81**(6), 765–768, 2005.

[107] Hulteen, J. C., Treichel, D. A., Smith, M. T., Duval, M. L., Jensen, T. R. and Van Duyne, R. P. Nanosphere Lithography: Size-Tunable Silver Nanoparticle and Surface Cluster Arrays. *J. Phys. Chem. B*, **103**(19), 3854–3863, 1999.

[108] Burmeister, F., Schafle, C., Matthes, T., Bohmisch, M., Boneberg, J. and Leiderer, P. Colloid monolayers as versatile lithographic masks. *Langmuir*, **13**(11), 2983–2987, 1997.

[109] Ormonde, A., Erin, D., Hicks, M., Castillo, J. and van Dyne, R. Nanosphere Lithography: Fabrication of Large-Area Ag Nanoparticle Arrays by Convective Self-Assembly and Their Characterization by Scanning UV-Visible Extinction Spectroscopy. *Langmuir*, **20**(16), 6927–6931, 2004.

[110] Haynes, C. L., McFarland, A. D., Smith, M. T., Hulteen, J. C. and Van Duyne, R. P. Angle-Resolved Nanosphere Lithography: Manipulation of Nanoparticle Size, Shape, and Interparticle Spacing. *J. Phys. Chem. B*, **106**(8), 1898–1902, 2002.

[111] Snoeks, E., van Blaaderen, A., van Dillen, T., van Kats, C. M., Velikov, K., Brongersma, M. L. and Polman, A. Colloidal assemblies modified by ion irradiation. *Nuclear Instruments and Methods in Physics Research Section B - Beam Interactions with Materials and Atoms*, **178**, 62–68, 2001.

[112] Feldstein, M. J., Keating, C. D., Liau, Y. H., Natan, M. J. and Scherer, N. F. Electronic Relaxation Dynamics in Coupled Metal Nanoparticles. *J. Am. Chem. Soc.*, **119**(28), 6638–6647, 1997.

[113] Shi, J., Gider, S., Babcock, K. and Awschalom, D. D. Magnetic Clusters in Molecular Beams, Metals, and Semiconductors. *Science*, **271**(5251), 937–941, 1996.

[114] Andres, R. P., Bielefeld, J. D., Henderson, J. I., Janes, D. B., Kolagunta, V. R., Kubiak, C. P., Mahoney, W. J. and Osifchin, R. G. Self-Assembly of a Two-Dimensional Superlattice of Molecularly Linked Metal Clusters. *Science*, **273**(5282), 1690–1693, 1996.

[115] Frederix, F., Friedt, J. M., Choi, K. H., Laureyn, W., Campitelli, A., Mondelaers, D., Maes, G. and Borghs, G. Biosensing Based on Light Absorption of Nanoscaled Gold and Silver Particles. *Anal. Chem.*, **75**(24), 6894–6900, 2003.

[116] Haes, A. J., Hall, W. P., Chang, L., Klein, W. L. and VanDuyne, R. P. A Localized Surface Plasmon Resonance Biosensor: First Steps toward an Assay for Alzheimer's Disease. *Nano Letters*, **4**(6), 1029–1034, 2004.

[117] Riboh, J. C., Haes, A. J., McFarland, A. D., Ranjit Yonzon, C. and Van Duyne, R. P. A Nanoscale Optical Biosensor: Real-Time Immunoassay in Physiological Buffer Enabled by Improved Nanoparticle Adhesion. *J. Phys. Chem. B*, **107**(8), 1772–1780, 2003.

[118] Schultz, S., Smith, D. R., Mock, J. J. and Schultz, D. A. Single-target molecule detection with nonbleaching multicolor optical immunolabels. *Proceedings of the National Academy of Sciences of the United States of America*, **97**(3), 996–1001, 2000.

[119] Moller, R., Csaki, A., Kohler, J. and Fritzsche, W. DNA probes on chip surfaces studied by scanning force microscopy using specific binding of colloidal gold. *Nucl. Acids Res.*, **28**(20), e91, 2000.

[120] Cai, H., Xu, C., He, P. and Fang, Y. Colloid Au-enhanced DNA immobilization for the electrochemical detection of sequence-specific DNA. *Journal of Electroanalytical Chemistry*, **510**(1-2), 78–85, 2001.

[121] Andersson, A.-S., Backhed, F., von Euler, A., Richter-Dahlfors, A., Sutherland, D. and Kasemo, B. Nanoscale features influence epithelial cell morphology and cytokine production. *Biomaterials*, **24**(20), 3427–3436, 2003.

Seite Leer /
Blank leaf

CHAPTER 3

Methods and Materials Characterizations

3.1 Characterization Techniques

3.1.1 ζ-potential measurements

The ζ-potential is one of the most important parameters describing a colloidal suspension. Stability and adsorption properties of colloidal particles are to a large part depending on the size and sign of the ζ-potential. In 2.2.4, the theoretical interpretation of the ζ-potential was deduced and in real systems it can often be set equal to the Stern-potential ψ_d, that plays a key role in the strength of the repulsive force in a colloidal suspension. Since the ζ-potential is located at the shear plane of an electric double layer some distance away from the particle surface (see Fig. 2.6), it can only be measured using elektrokinetic methods, where particles are moved in the liquid. In this work, the ζ-potential was measured using a DT 1200 (Dispersion Technology, Bedford Hills, USA), a device that characterizes the ζ-potential by means of a specially designed probe that uses ultrasound as a driving force for generating an electroacoustic effect.[1] The probe is a stainless steel cylinder 3 *cm* in diameter and 10 *cm* long. A piezo-electric crystal inside of the probe converts an electric pulse generated by electronics into an acoustic pulse of 3 MHz frequency. The ultrasound pulse generates an electric current between two electrodes built into the probe due to the motion of either ions or particles, or both. The measured potential between the electrodes induces a current which is called "Colloidal Vibration Current" (CVI).[2] The potential difference arises because the particle is forced to move (by the ultrasonic excitation) leaving part of his ion cloud behind (the part

outside of the outer Helmholtz plane). Since the ion cloud has an excess charge (negative or positive depending on the charge of the particle), a small electric potential develops in the suspension which can be measured between the electrodes. This potential will change rapidly with the frequency of the ultrasonic pulse. The colloidal vibration current is defined as follows:

$$I_{CVI} = C\,\phi\,\mu_e \frac{\rho_p - \rho_m}{\kappa^*\,\rho_m} \frac{Z_g - Z_s}{Z_g + Z_s} \tag{3.1}$$

where C is a constant, ρ_p and ρ_m are the the densities of the particle and the medium, ϕ is the volume fraction of particles in the solution and Z_g and Z_s are the impedances of the sonic transducer and the particle suspension, respectively. The electrophoretic mobility μ_d [3] is an important system parameter that can itself be useful (e.g. for determining the IEP) but it can also be related to the ζ-potential by applying Henry's equation:

$$\mu_e = \frac{2}{3}\frac{\epsilon\epsilon_0\zeta}{\eta} f(\kappa a) \tag{3.2}$$

where η is the viscosity of the suspension and $f(\kappa a)$ is Henry's number (which varies between 1 and 1.5 depending on which approximation model is chosen). The ζ-potential device used measures the ζ-potential with a accuracy of $\pm$ 2 mV and the IEP is determined with $\pm$ 0.2 pI units. With the built-in titration unit the ζ-potential measurements can be carried out over the desired pH range including the recording of titration data for charge calculations.

3.1.2 X-ray Disc Centrifuge (XDC)

Two methods were used in this thesis to assess particle distributions. For one, particle sizes from SEM images were analyzed resulting an average diameter with a standard deviation. To gather more information about particle size distribution with better statistics, x-ray disc centrifuge measurements were conducted. The instrument was an XDC from Brookhaven Instruments in Holtsville, USA. The x-ray disc centrifuge, which is basically a sedigraph, is a very precise measurement technique which allows the measurement of the particle size distribution with high accuracy (with optimization and experience usually within $\pm$ 1 nm). A schematic

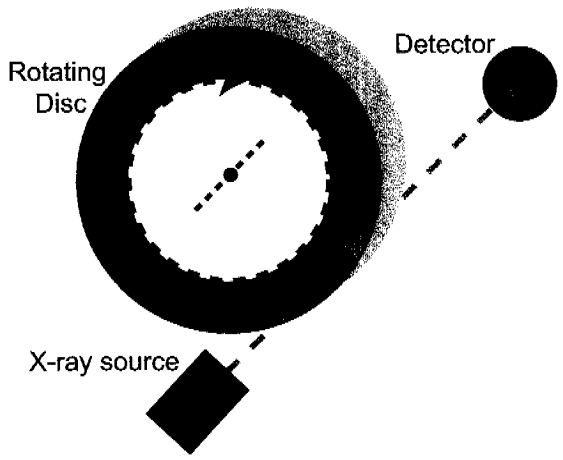

Figure 3.1: X-ray disc centrifuge experimental setup. A disc with inner radius r_i and outer radius r_a is filled with the particle suspension and rotated. Particles are forced to sediment and pass the x-ray beam which is located near the outer edge of the disc. This changes the intensity that passes to the detector and using Eq. 3.3 the particle diameter as a function of time (and thus the particle size distribution) can be calculated.

view of the x-ray disc centrifuge technique is given in Fig. 3.1. A disc with an inlet for the suspension on the inside is rotated at defined, high speeds (few thousand rounds per minute). This rotation forces particles to sediment at the outside of the disc. The x-ray beam penetrates the disc close to the outer edge. Sedimenting particles pass the x-ray beam and cause an intensity change which is recorded over time in the detector. Using Stoke's law, the following expression for the particle diameter can be found and is used in the software to calculate particle size D as a function of time t and frequency of the disc f:[2]

$$D^2 = \frac{ln(\frac{r_a}{r_i})\,18\,\eta}{t(\rho_p - \rho_m)\,4\,\pi^2\,f^2} \tag{3.3}$$

where r_a and r_i are the outer and inner radius of the disc, η is the viscosity of the suspension and $\rho_p - \rho_m$ is the density difference between the particle and the medium. The particle sizes which can be measured are in the range of 5 nm to 5 μm, although at small particle sizes signal-to-noise ratios get small and the error is increased, especially if the density difference between particles and medium is not large.

3.1.3 Contact Angle Analysis / Microdroplet Density measurements

To determine the contact angle of a drop of liquid (usually water) on a substrate surface a measuring device was used, which consists of two main parts: a syringe with a needle which is placed near the surface through which the liquid is pumped out onto the surface and a digital camera to observe the drop simultaneously. The liquid can not only be squeezed out through the syringe but also sucked back through the needle as desired. This allows the measurement of the advancing contact angle (by increasing the drop size continuously) as well as the receding contact angle (by continuously removing the liquid) in a single experiment. To determine the contact angle, the camera is positioned such that it can monitor the substrate with the drop on top of it from the side. Then, movies of the growing or decreasing drop can be made and a special software allows the determination of the contact angle of each frame of that movie giving sufficient statistical data.

Microdroplet density measurements were performed to observe the wetting behavior of patterned surfaces. To do so, the sample was mounted on top of a metal plate which had a liquid-cooling system integrated. A video camera is monitoring the sample from the top. Ice-cooled water is circulated through the cooling system and the metal plate as well as the sample on top of it are cooled down relatively fast. This cooling effect induces the condensation of vapor on the sample. This condensation behavior is monitored using video camera and information on the wetting behavior can be found. Note, that with this setup no direct information is gathered on the contact angle of the condensing water droplets, only the wetting behavior of the surface can qualitatively be described.

3.1.4 Optical Waveguide Lightmode Spectroscopy (OWLS)

A technique was required in this work, that allows to *in situ* monitor and quantify the adsorption kinetics of colloidal particles as well as other molecules such a polymeric ad-layers and specific adsorption of proteins to the surface. Optical waveguide lightmode spectroscopy (OWLS) was selected for that purpose. In OWLS, the adsorbed mass is calculated *in situ* from the change of the refractive index in the vicinity of the surface upon adsorption of particles or molecules from solution onto a waveguiding substrate.[4, 5] The waveguiding substrate consists of planar optical

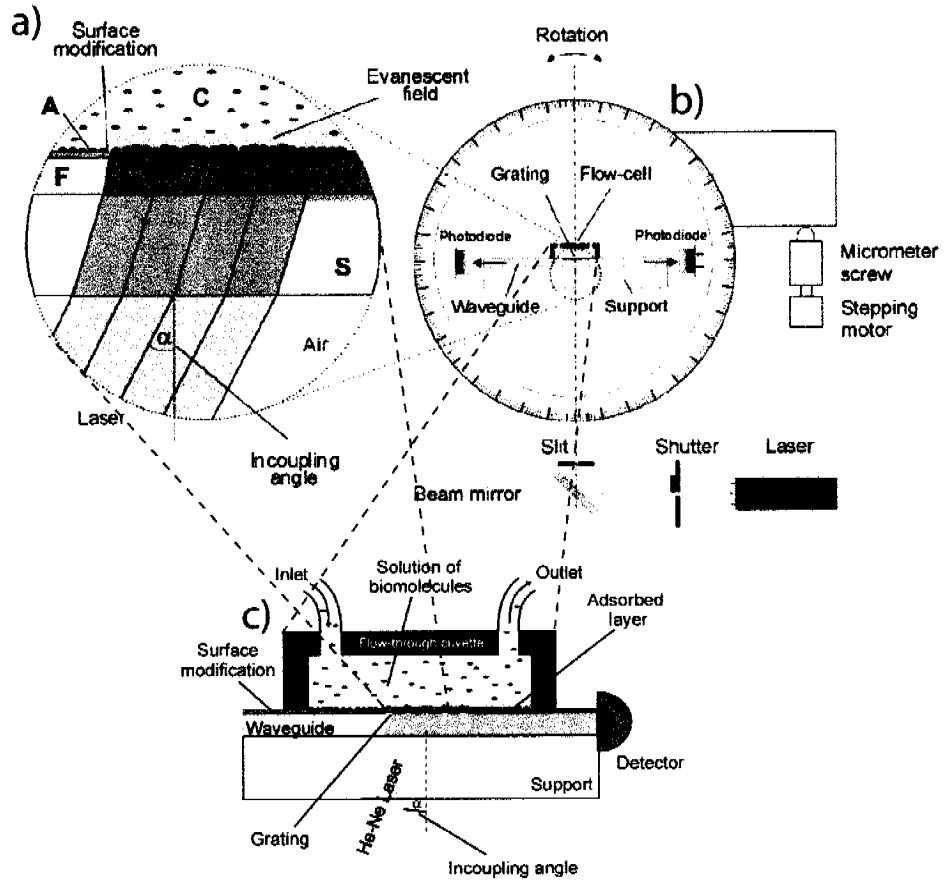

Figure 3.2: Schematic overview of the OWLS experimental setup. a) shows the incoupling of the laser light at a distinct incoupling angle α. S is the glass substrate, F the waveguiding layer and C shows a solution containing adsorbing molecules. b) gives an overview of the total setup with the laser beam line, the photodiodes used to monitor the incoupled laser intensity and the stepping motor which rotates the waveguide to find the incoupling angle α with microradian precision. c) shows the flow-cell with in- and outlet.

waveguides of dimension 8 by 12 *mm* (Schott AF45 glass substrate) coated with a SiO_2-TiO_2 waveguiding layer of approximately 160 *nm* thickness, deposited by the sol gel technique. The optical grating consists of 2400 lines per *mm* with a grating structure height of approximately 10 *nm* (type BV2400 supplied by MicroVacuum Ltd., Budapest, Hungary). On top of the waveguiding layer, a thin film of the required oxide for the experiment was coated (e.g. a 6 *nm* film of niobia).

In the OWLS, plane-polarized light is coupled into the waveguide by the optical grating present on the top of the thin film so that a diffracted wave propagates in the waveguide via multiple total internal reflection. This produces an evanescent field

extending 100-300 nm from the surface. In case of a laser with 633 nm wavelength and water-based solutions, the evanescent field has a decay-length of approximately 180 nm. This field is exponentially decaying and essentially determines the sensing depth for the instrument. The sensitivity of the instrument, however, decreases with the square of the strength of the evanescent field, which reduces the sensing depth to half of the value of the decay length of the evanescent field. Also, the sensing depth of the instrument will be changed if a layer of particles (with a different diffractive index) adsorbs on the surface. Depending on that refractive index, the sensing depth may be significantly reduced or increased.

For each polarization mode of the light (transverse electric, TE, and transverse magnetic, TM) there are discrete incoupling angles α_{TE} and α_{TM} corresponding to maximum constructive interference for the diffracted light detected at the photodiode. Adsorption or desorption of molecules or any other processes involving change of refractive index (e.g. pH changes) within this evanescent field changes the incoupling angle α. From these changes in incoupling angles for TE and TM, the change in effective refractive index of the adlayer is calculated. In turn, from the change of the refractive index upon adsorption, the adsorbed mass can be inferred. The sensitivity of the OWLS technique is typically 1-2 ng/cm^2.[5] In Fig. 3.2, a schematic overview of the OWLS experimental setup is given.

To finally calculate the adsorbed mass density M (in ng/cm^2), the thickness d_A and the refractive index n_A of the adlayer have to be analytically determined.[1] Using de Feijter's approximation [6] and assuming a very thin adlayer and a concentration proportional to the refractive index, the following equation for the adsorbed mass is derived:[5]

$$M = d_A \frac{n_A - n_C}{\mathrm{d}n/\mathrm{d}c} \tag{3.4}$$

Here, $\mathrm{d}n/\mathrm{d}c$ is the incremental change of the refractive index with changing concentration and values for $\mathrm{d}n/\mathrm{d}c$ (in cm^3/g) were taken from [7] (see also 3.1.4).

[1] For which in our lab also many values exist from experience

Cleaning of Waveguides

The niobium oxide coated waveguides were first cleaned ultrasonically in 0.1 M HCL, 2-propanol (Merck, Germany) and Millipore water, for 10 *min* respectively. This was followed by blow drying with nitrogen and then oxygen plasma cleaning (Harrick, Ossining, USA) for 2 minutes.

Protocols for *in situ* particle and polymer adsorption

The waveguides were soaked overnight with the buffer used in the experiment in order to attain a good baseline. They were then setup in the OWLS flow cell in the OWLS instrument (MicroVacuum Ltd., Hungary). A BIOS-1 integrated optical scanner (Artificial Sensing Instruments, Zurich, Switzerland), using a monochromatic, polarized light beam (He-Ne laser, wavelength $\lambda = 632.82\ nm$) was used as the laser source. The incident angle of the laser was varied with microradian precision by a computer-driven stepping motor. The incoupled light was detected by two photodiodes at each end of the waveguide. *In situ* particle, polymer and protein adsorption was studied using a flow-through cell with a volume of 16 μL (8 x 2 x 1 mm^3). Cleaned waveguides were inserted in the flow cell and the experiment was allowed to proceed only after a stable baseline was obtained at room temperature (which was monitored and varied only between 22 and 26°C). Then, the buffer solution was replaced by a polymer, protein or colloidal solution with the same buffer to avoid shifts in the refractive index that are attributed to changes in buffer composition rather then adsorption of species to the surface. Buffer washes were given after each deposited layer had been saturated to remove non-specifically adsorbed particles, polymer or proteins, before the next component was injected. After an experiment, cleaner solution (Cobas Integra, Roche) was used to clean the waveguide and the flow cell *in situ* after the experiment. The flow cell was removed and cleaned again as per the protocol given above and so was the waveguide. However, if the waveguide was required to be investigated by SEM, it was nitrogen blow dried and stored separately. The refractive index increment values of dn/dc were linearly interpolated between 0.13 cm^3/g for pure PEG) and 0.18 cm^3/g (pure PLL) for the different PLL-g-PEG polymers and were taken from the PhD thesis of Pasche as was the published value of 0.182 cm3/g that was used for the proteins in serum as well as for the other proteins.[7] For colloidal suspensions, a dn/dc-value of 0.150 was used.

3.1.5 Scanning Electron Microscopy (SEM)

Scanning electron microscopy (SEM) is one of the most versatile and well-known analytical imaging techniques. As compared to conventional optical microscopy, an electron microscope offers advantages including ultra high magnification, large depth of focus, great resolution and ease of observation. In contrast to an optical microscope, electrons generated from an electron gun (of high energy and thus short wavelength) instead of visible light is used to image the surface. This highly condensed electron beam is scanning across a specimen surface. The energy of the primary electrons can be set by the acceleration voltage (EHT), ranging from 0.3 kV to 30 kV for the LEO1530 from Zeiss which was used for SEM microscopy work. As the beam scans pixel by pixel on the surface, it interacts with the specimen surface. It is usually necessary to coat non-conductive samples with a thin conducting layer, to reduce the charging caused by absorbed primary electrons. In this work, a Pt-film of a few nanometer thickness was applied using a sputter coater. To coat the SEM specimen, the current was set to 40 mA, sputter time was 30 s and the vacuum reached about 6x10^{-2} $mbar$.

There are different signals emerging from the interaction of the electron beam with the surface. Low energy (< 50 eV) so-called secondary electrons (SE) are the most commonly used signal source. If primary electrons get reflected in the specimen surface they are called backscattered electrons (BSE). BSE contain more information about the material whereas SE contain more topographical information. Depending on the information needed, either SE, BSE or both (in a selected mixing ratio) can be detected and counted in different detectors. In the course of this work, most SEM imaging was done using secondary electrons, however, in some cases better results were obtained by mixing SE and BSE electron signals. A pixel in the final picture is bright, if a lot of electrons come out of the surface. After one pixel is acquired, the primary electron beam hops to the next pixel. The dwell time of each pixel can be changed in a wide range. Higher dwell times result in better signal-to-noise ratio, but can lead to charging and/or specimen damage. The depth from which secondary electrons originate is usually below 50 nm, where as BSE electrons can come from several hundred nanometers below the sample surface. For high resolution imaging (as done in this work), only SE electrons can usually be considered. It is also noteworthy that the contrast in an SEM image stems from either topographical features, differences in material or from different crystallographic orientations. For

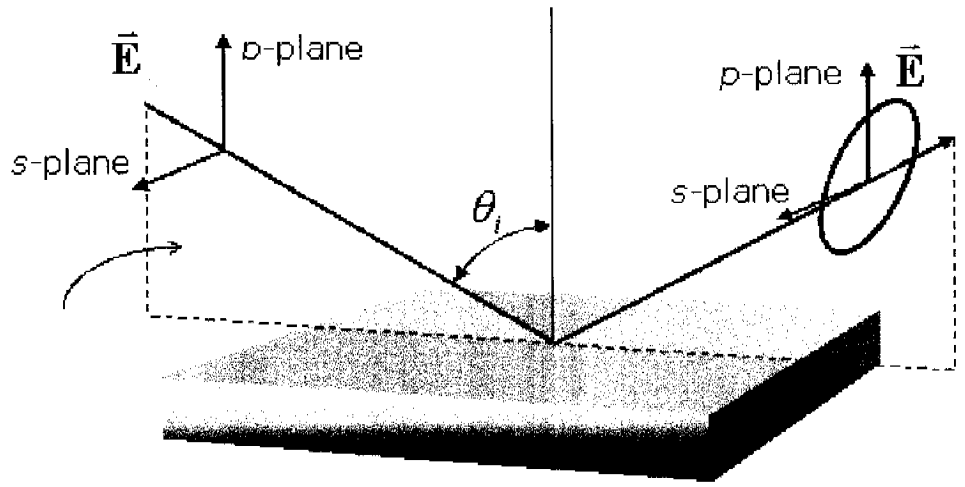

Figure 3.3: Sketch of the functional principle of an ellipsometer. An incoming, lineraly polarized beam of light is reflected on the sample and the dielectric interface is responsible for a phase change of the transmitted light. This phase change is dependent on the refractive index of the material.

SE images, the contrast is mainly attributed to topography (e.g. edges appear very bright), where as the contrast in BSE images mostly originates from material differences. This is another reason, why mostly SE electrons were used in this work.

3.1.6 Ellipsometry

Ellipsometry is used to measure the refractive index and the thickness of semi-transparent thin films. The instrument relies on the fact that the reflection at a dielectric interface depends on the polarization of the light while the transmission of light through transparent layer changes the phase of the incoming wave depending on the refractive index of the material (Fig. 3.3). Optical constants, such as refractive index n and extinction coefficient k, are not constant over varying wavelengths. They change their value as a function of the wavelength λ. The measured values are ellipsometric angles ψ and Δ. For a single layer system, these values are related to the ratio of Fresnel reflection coefficients, R_p and R_s for p and s-polarized light, respectively as below:[8]

$$\tan(\psi)\, e^{i\Delta} = \frac{R_p}{R_s} \tag{3.5}$$

ψ values range from 0 to 90°, Δ values range from 0 to 360°. When ψ and Δ are determined as a function of the wavelength λ, the thickness of the layer can be determined only by comparing the obtained results with theoretical curves of $\psi(\lambda)$ and $\Delta(\lambda)$. However, an assumption model is required and finally the film thickness and optical constants must be extracted through a model-based analysis using Fresnel reflection coefficients, Snell's law, etc. Ellipsometry can be used to measure layers less than 1 *nm* thick up to layers which are several microns in thickness, although this is dependent on the precision with which the data fits the theoretical models.

Besides measuring the thickness and refractive indices, ellipsometry can also be used to estimate the porosity of a layer.[9] Hence, it was used in this work in Chapter 7 to investigate the percentage surface area coverage with colloids, as adsorbed colloids can be viewed as a "porosity" system. For layers that are fairly uniform in nature with well-known material properties, one can use Eq. 3.6 (first-order rule of mixtures) for calculating the porosity.[10] However this linear interpolation method is not highly accurate. Hence, in the course of this thesis an effective medium approximation (EMA) model[2] was used for determining the void surface area, where the dispersive optical properties were modelled using the Cauchy equation (Eq. 3.6).[10]

$$n(\lambda) = A + \frac{B}{\lambda^2} + \frac{C}{\lambda^4} \tag{3.6}$$

where n is the refractive index, A, B and C are Cauchy coefficients and λ is the wavelength. Once the data is measured and the model is made with an assumed layer structure with known or estimated optical constants n and k, the model can be modified by regression analysis. The aim is to vary some parameters in this model such that ellipsometric data calculated from the model matches the experimental data as closely as possible i.e. minimizing the mean squared error (MSE). For a more detailed insight into ellipsometry measurements see the doctoral thesis of Laurent Feuz.[11]

[2]In this model, a linear mixing model is assumed, of the type: $n_A\psi(A) + n_B\psi(B)$, where ψ is the volume fraction and n the refractive index as modelled in Eq. 3.6

3.2 Materials Characterization

3.2.1 Colloidal Silica Particles

The silica colloidal particles used in this work were supplied as dispersed aqueous suspensions with a weight percentage of particles of 30 $wt\%$ (Clariant, France). This value was stated by the manufacturer and found to be exact by evaporation experiments for all suspensions used. To do so, the exact weight of the suspension and of the remaining particles were measured after evaporation and the weight percentages were calculated. Three particle sizes were used, stated to be 12, 40 and 80 nm in size and the suspensions were available in two versions: one in a "native" state with no additives (pH = 2.4) and one with added base (NaOH) to adjust the pH to 9.1 to better stabilize the suspensions. The 40 and 80 nm suspensions, however, were stable in both cases (at pH 2.4 and 9.1) over years time. The 12 nm particles were less stable and formed a gel in a few month.

Adjustment of Ionic Strength

Ultrapure Millipore water (organic content <5 ppb and a conductivity of 18.2 $MOhm/cm$) was used for the preparation of all aqueous suspensions. Adjustment of the ionic strength of the suspension was performed using 4-(2-hydroxyethyl)piperazine-1-ethane-sulfonic acid (Hepes) based buffer (Fluka, Buchs, Switzerland). The pH of this buffer solution was adjusted to pH 7.4 with $6M$ NaOH (Fluka, Buchs, Switzerland). The ionic strength of the Hepes buffer was either 10 mM or 160 mM (increased by adding 150 mM NaCl to the solution) for most experiments. The pH was controlled prior to experiments. If a suspension with a native pH was used, diluting the suspension to 1 $wt\%$ usually was enough to bring the pH to the buffered value of 7.4. If suspensions were used that had their pH adjusted to 9.9, diluting the original 30 $wt\%$ suspension to 0.1 $wt\%$ brought the pH to the buffered value of 7.4. If no salt at all was needed, ultrapure Millipore water was used to dilute the suspensions to their desired weight percentages.

Characterization of the Silica Nanoparticles

The colloidal particles were studied thoroughly prior to their modification or their use in self-assembly experiments. pH, size distribution, ζ-potentials are key param-

eter needed for the characterization of the particle systems. In Tab. 3.1 some key properties of the colloids used in this work are collected. Note that only colloid suspensions which were used for self-assembly experiments are in this table (e.g. the 12 *nm* silica colloids proved to be not stable enough for this purpose). Particle sizes given in Tab. 3.1 are values taken from the evaluation of scanning electron microscopy (SEM) images. At least 300 particles were measured on different images to get a reliable average for the size. Note that the value given in Tab. 3.1 is a slight overestimation of the particle size since a thin platinum layer was sputtered onto the colloidal particles (2-5 *nm*).

Table 3.1: Properties of colloids used in this work

	density[a]	**particle size**[b]	**particle size**[c]	**ζ-potential**[d]	**pH**[e]
PL150H50	2.26	73 ± 7	66	-49 ± 2	2.36
PL1508-35	2.25	39 ± 4	33	-40 ± 2	9.91
30H50	2.26	72 ± 6	65	-47 ± 2	9.5

[a]Dry density of colloids
[b]From SEM image analysis
[c]d_{50} value from XDC
[d]At pH 6
[e]As received

Not only average particle sizes are of interest but also the particle size distributions, since e.g. in ordering processes a wide distribution of particle sizes is obstructive. By means of x-ray disc centrifuge (XDC) measurements, particle size distributions for the 40 and 73 *nm* particles were recorded and are presented in Fig. 3.4. The size distributions for both systems are rather narrow, the 40 nm particles exhibiting an exceptionally narrow distribution. The 73 *nm* silica particles have somewhat broader size distribution. The d_{50}-values (e.g. the size below and above which 50% of the particles are situated) is lower for both particle systems (34 and 66 *nm*) compared to the values gathered from SEM image analysis (Tab. 3.1). Two factors might attribute to this difference: on the one hand, in SEM image analysis the thin platinum film must be taken into account which leads to a slight overestimation of the particle size. On the other hand, in XDC experiments, the density of the particles enters as a constant factor (which was set to 2.2 g/cm^3). If the actual density is lower in the particle then 2.2 g/cm^3, this would also result in a lower value for d_{50}. Such deviations from the density of silica might arise if the surface has a slight porosity or if swelling of the particles occurs. Especially the existence

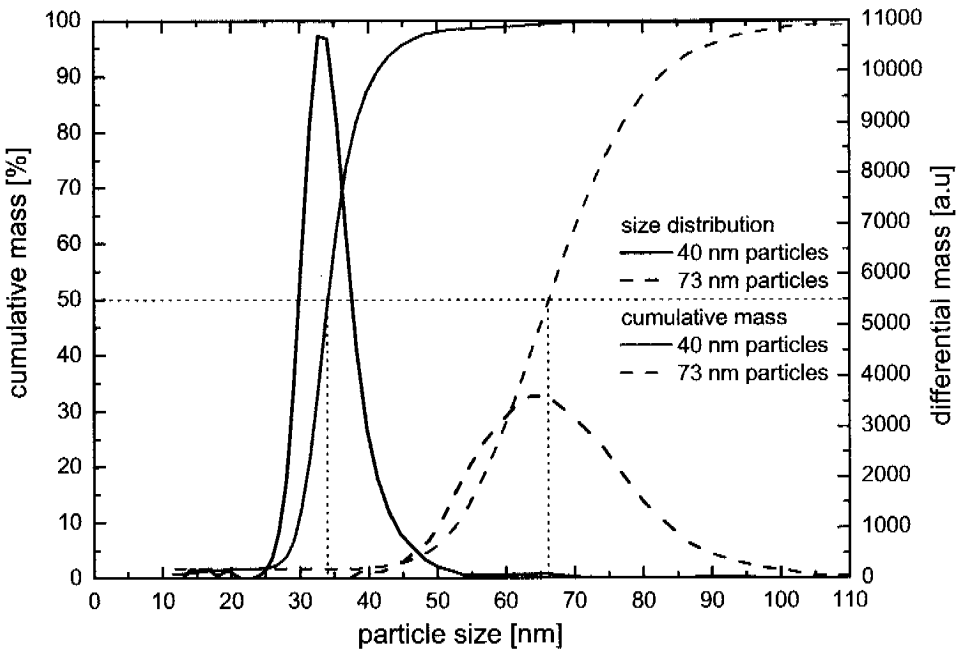

Figure 3.4: Particle size distribution measured by x-ray disc centrifugation for the 73 *nm* (PL150H50)(—) and 39 *nm* particles (PL-1508-35)(- - -). Note that the d_{50}-value is not at 73 and 39 *nm*, respectively. Instead, when a density of 2.2 is assumed in the experiments, these values are slightly shifted to lower values (34 and 66 *nm*).

of surface porosity can not be completely excluded in our case. However, since the difference between the two measured average sizes for the silica particles is not very large, the main contribution might in fact be the thin platinum film on the particle surface present in SEM images.

Beside particle size, pH and ionic strength another important parameter in colloidal science is the surface charge of the particle. This charge determines to a large extent the interactions between particles and surfaces. Since the surface charge is not a directly measurable quantity (as discussed in Chapter 2), measurements of the ζ-potential are usually conducted to gather information about the electrostatic charges which are not shielded on a colloidal particle. The results are shown in Fig. 3.5 for three different colloidal silica systems. The isoelectric point of all three suspension is relatively close to 3 or slightly below. Also, all suspensions used in this work are carrying more and more negative charge with increasing pH.

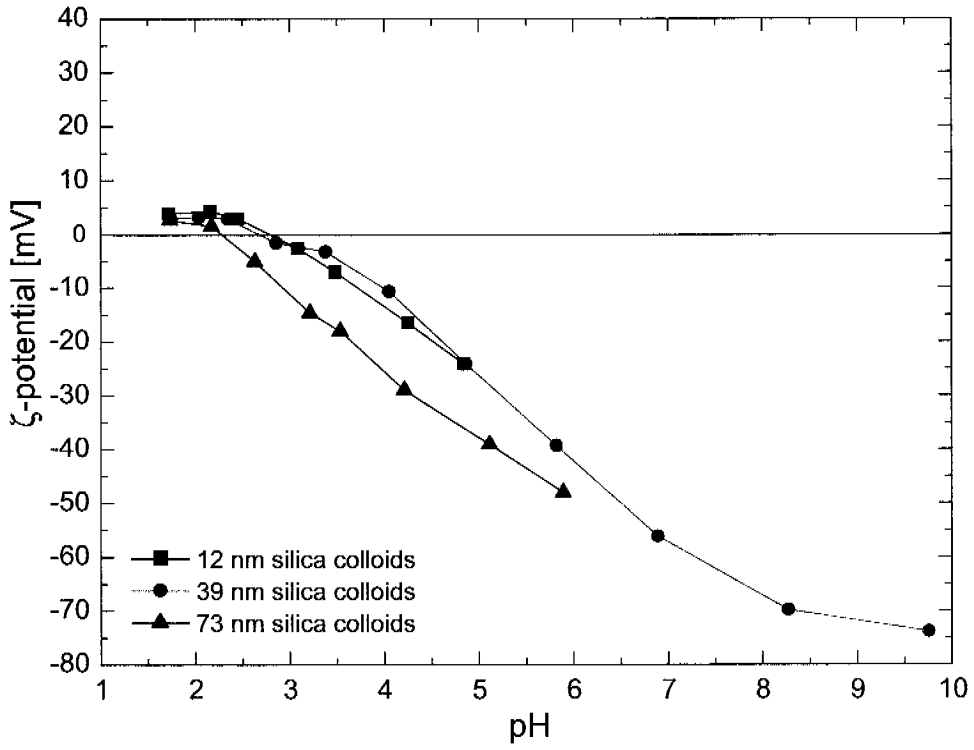

Figure 3.5: ζ-potential measurements on three different sizes of silica nanoparticles. All three suspensions show very similar behavior, which is typical for silica particles. The IEP is around or slightly below a pH of 3 and particles are getting more negatively charged at higher pH values. Suspensions were diluted with pure water and then titrated while simultaneously measuring the ζ-potential.

Coating of Colloidal Particles

The process to coat colloidal particles consists of two main steps. First, the mixing of particles with suitable amounts of the coating molecules which then adsorb in a stable layer to the particle and second, the purification process (often referred to as "washing") which removes all non-adsorbed molecules from the suspension and only leaves the coated particles in the suspension. This purification step is achieved by centrifugation and re-dispersion of the particles in the solvent. A schematic overview of this process is given in Fig. 3.6. Specifically, the steps for coating silica particles with PLL-*g*-PEG/PEG-biotin were performed as follows:

1. The mass of the coating materials required for a given surface area was known from OWLS measurements and this was used to calculate the amount needed for a specific surface area coverage of the colloidal particles. For example,

the specific surface area of the 73 nm particles was 51 m^2/g and the average amount of PLL-g-PEG/PEG-biotin adsorbed on niobia was around 150 ng/cm^2. With these parameters the amount of materials needed to coat a given amount of particle concentration was calculated. Generally, a two to three-time excess of coating material was used to ensure complete coating of all particles.

2. To achieve uniform mixing of particles and coating material, a suspension with twice the final particle concentration and a solution with twice the final coating molecule concentration was produced and these were then mixed together. Usually, a few milliliter of coated particles with a particle concentration of 1-2 $wt\%$ were produced at once.

3. The colloidal solution was then centrifuged for 15 minutes at 10,000 rpm to separate the coated colloids from the excess and unbound components. The effective acceleration due to gravity g with these parameters was xx in the used centrifuge (type Beckmann JA-25 50).

4. The supernatant was removed and the colloids redispersed in the buffer solution to obtain again a particle suspension. Suspensions were stored at room temperature. The particle sediment was relatively strongly attached to the centrifugation tube and light scratching with a spatula was necessary to redisperse the particles. Then, particles could be redispersed by vortexing the suspension.

5. The centrifugation step was repeated twice, since UV/VIS measurements still showed some free PLL-g-PEG/PEG-biotin in the supernatant after the first centrifugation.

3.2.2 Polymers

Poly(L-lysine)-g-poly(ethylene glycol) (PLL-g-PEG)

The patterning system used to specifically assemble functionalized nanoparticles on protein resistant substrates as presented in Chapter 6 relies to a large extent on the extraordinary properties of the grafted polyelectrolyte copolymer used

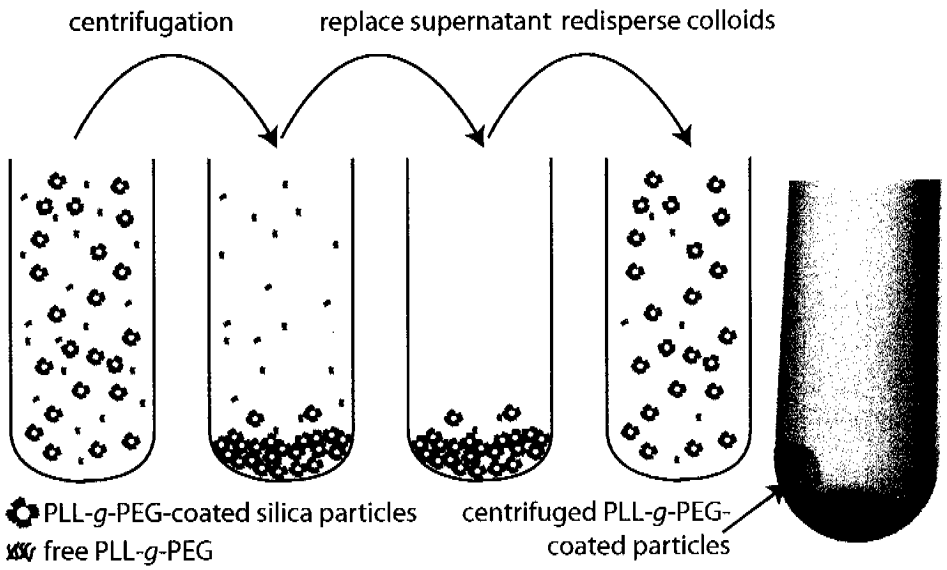

Figure 3.6: Schematic illustration of the silica nanoparticle coating process. Mixing of equal amounts of particle suspension (with twice the final concentration) and solution with the coating molecules (also twice the final concentration) lead to a suspension with coated particles and some free excess coating molecules. Centrifugation leads to sedimentation of particles. The supernatant (containing free molecules) is replaced by fresh buffer solution. This centrifugation step is repeated to remove all free coating molecules. The photograph shows a centrifugation tube containing sedimented particles (the sediment is not at the bottom because the centrifuge had a given angle at which the tubes where inserted)

there: poly(L-lysine)-*g*-poly(ethylene glycol) (PLL-*g*-PEG).[12] In this copolymer, polyethylene glycol (PEG) chains are grafted to amino-terminated side chains of a polycationic poly(L-lysine) (PLL) backbone. The chemical structure of PLL-*g*-PEG is shown in Fig. 3.7. The grafting ratio g describes the ratio of lysine monomeric units divided by the number of grafted PEG chains. Thus, low grafting ratios correspond to higher PEG-densities on the surface since more PEG-chains are grafted to the PLL backbone on average. During synthesis, the molecular weight of both, the PLL backbone and the PEG side chains may be varied, as can the grafting ratio *g*.[7, 13] To indicate the specific architecture of the polymer, the molecular weight of the used PEG and PLL(in kilo dalton) and the grafting ratio are sometimes added in brackets: PLL(20)-*g*[3.5]-PEG(2). In the course of this work, different polymer architectures are occasionally used (where indicated) but in most cases a "standard" PLL-*g*-PEG copolymer was used with a grafting ratio of 3.5, PEG side chains with a molecular weight of 2 kDa and a PLL backbone of 20 kDa. While most PLL-*g*-PEG polymers show good resistance to protein adsorption, the chosen polymer architecture has an exceptionally high ability to resist protein adsorption.[7, 14] The

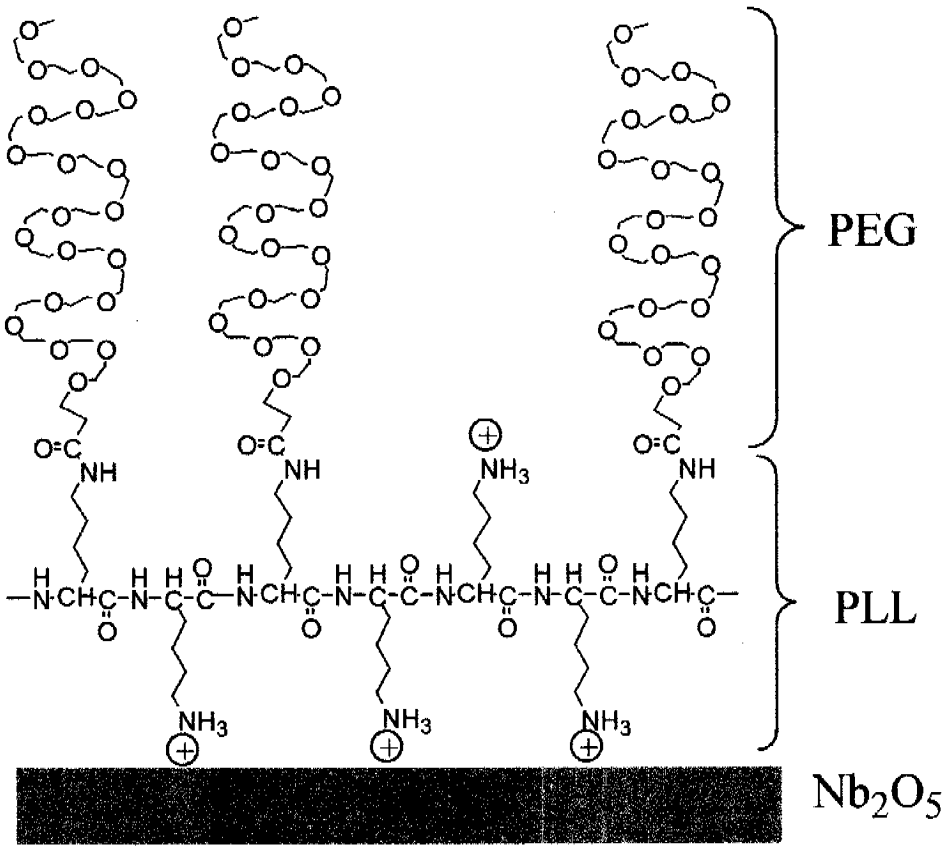

Figure 3.7: Chemical structure of poly(L-lysine)-*g*-poly(ethylene glycol). The poly(L-lysine) (PLL) backbone is positively charged due to protonated amino groups (at neutral pH) and adsorbs readily to negatively charged metal oxide surfaces (such as niobia, silica or titania). PEG chains are grafted to the each n^{th} lysine monomer unit of the backbone, n being the grafting ratio g of PLL-*g*-PEG.

polymer powders were stored at -20°C and stock solutions (0.1 mg/ml PLL-*g*-PEG in Hepes 1 or 2 buffer) at +4°C.

One of the reasons that make PLL-*g*-PEG especially attractive for many uses is the possibility to end-functionalize the PEG side chains. This allows the incorporation of a specific function to the PLL-*g*-PEG copolymer. In this work, two different functionalizations have been utilized. A biotinylated version of PLL-*g*-PEG was used in conjunction with streptavidin as a linker in Chapter 6 and a PLL-*g*-PEG version modified with nitrilotriacetic (NTA) was used in Chapter 7. The structure of PLL-*g*-PEG/PEG NTA is given in Fig. 3.9, that of PLL-*g*-PEG/PEG biotin is shown in Fig. 6.2 in Chapter 7.

Table 3.2: Properties of copolymers used in this work

Polymer	mol. weight [kDa]	Funct. chains (%)
PLL-*g*-PEG	PLL(20)-*g*-PEG(2)	0
PLL-*g*-PEG/PEG-biotin	PLL(20)-*g*-PEG(2)/PEG-biotin(3.4)	50
PLL-*g*-PEG/PEG-NTA	PLL(20)-*g*-PEG(2)/PEG-NTA(3.4)	96
PEI (poly(ethylene imine)	25	-

Poly(ethylene-imine) (PEI)

Poly(ethylene-imine) (PEI) is a positively charged polyelectrolyte which is used in this work to render a surface positive (for example to allow negatively charged silica particles to adsorb). Ellipsometry was used to check the layer thickness of a PEI film on a silica surface. The results are shown in Fig. 3.8 and indicate that with increasing salt content, the PEI layer thickness increases. In this work, PEI was applied in Hepes 1 buffer for 20 *min* to form a positively charged layer of around 6 Å.

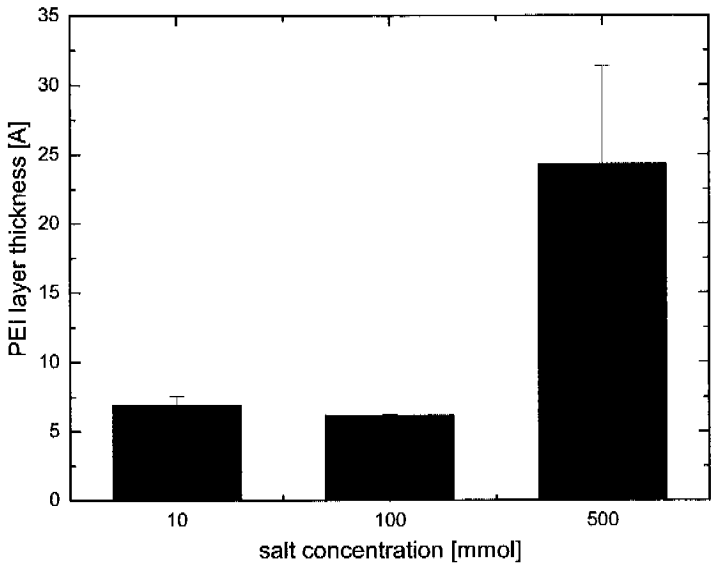

Figure 3.8: Poly(ethylene-imine) (PEI) layer thickness as a function of salt concentration on a silica surface. Higher salt concentrations lead to increased layer thickness of the PEI layer. The layer thickness of the PEI layer with Hepes 1 is around 6 Å.

3.2.3 Alkane Phosphate SAMs

Alkane phosphate self-assembled monolayers were used in this work to functionalize titania surfaces to increase the hydrophobicity of the surface to around 110° (see Chapter 5). To form these SAMs, the protocol developed by Samuele Tosatti was followed: first, piranha-cleaned containers were ultrasonically cleaned before use in a water bath for two times 7 *min*. After drying the container under nitrogen flow, 15.01 *mg* of the $CH_3(CH_2)_{11}PO_4(NH_4)_2$-salt were added. Then, 100 *ml* of ultrapure water was added to the $DDPO_4(NH_4)_2$. At 50°C, the solution is stirred until the $DDPO_4(NH_4)_2$-salt has completely dissolved (which takes around 30-45 *min* rather than the 10 *min* indicated in the protocol). To form the SAMs, the substrates were cleaned in isopropanol (2x7 *min* in the ultrasonic bath) and after drying under nitrogen flow they were treated in an UV/Ozone chamber for 30 *min* (UV Clean 135500, Boekel, Feasterville, USA). The samples are then stored in 24-well plates and around 1 *ml* of the $DDPO_4$-solution was poured onto the sample in the well-plate. The well-plates were sealed with parafilm and aluminum foil and after 48 *h*, the samples were removed from the $DDPO_4$-solution, rinsed with ultrapure water and dried under nitrogen flow.

3.2.4 Biomolecules

Streptavidin

Streptavidin is a tetrameric protein (4 x 13 *kDa*) that has various biochemical applications. The reason for this is the high affinity of the protein to biotin. Each streptavidin molecule binds to four molecules of biotin. Aliquots of streptavidin (Sigma Aldrich, USA) of 20 $\mu g/ml$ in milli Q grade water were stored at -20°*C*.

Green Fluorescent Protein 6xHis-tagged (GFP-6His)

Green fluorescent proteins (GFP) are stable intrinsically fluorescent proteins and are well established as a marker of gene expression and protein targeting in intact cells and organisms.[15] GFP tagged with 6-histidine sequences were used, which bind reversibly with Ni^{2+} ions immobilized via the chelator nitrilotriacetic acid (NTA) present on the PLL-g-PEG/PEG-NTA molecule.[16] Fig. 3.9 shows a sketch of NTA-functionalized PLL-*g*-PEG, which is activated by Ni^{2+} ions. This complex is then

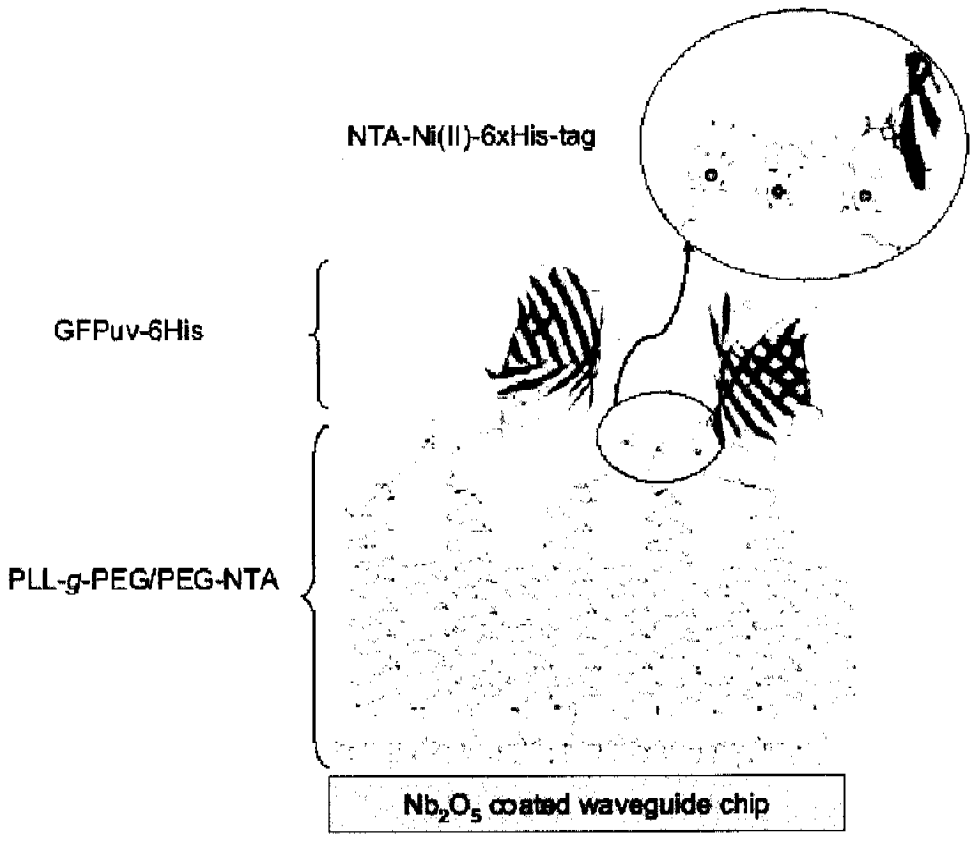

Figure 3.9: GFP-6xHis attachment to Ni^{2+}-NTA complex. The NTA is covalently linked to the end of the PEG chains. The inset shows the interaction of the Ni^{2+}-NTA complex with the six histidine tags.[16]

able to bind any 6xHis-tagged protein (in this case GFP. The GFP protein (1 μM) in Hepes 1 buffer was stored at $4°C$. The Ni^{2+} ions for the chelate were provided by $NiCl_2$ (5 mM stored at $4°C$).

Other Proteins

Various other proteins (antibodies and target proteins) were used in Chapter 7 and for protein resistance tests.

- Human serum (Roche Diagnostics GmbH, Mannheim, Germany) was used to test the protein resistance of surfaces. The powder was dissolved into Milli-Q water and after 30 min, the solution was aliquoted (0.5 ml) and stored at -20°C.

- Rabbit anti-human Fibrinogen (aFb) (Dako, Denmark) was used as a capture agent for Human Fibrinogen. Immunogen is Fibrinogen isolated from human serum. Stock solutions stored at $4°C$.
- Rabbit anti-human Albumin (Dako, Denmark) was used as a capture agent for Human Albumin. Immunogen is Human serum albumin. Stock solutions stored at $4°C$.
- Human Fibrinogen (SigmaAldrich, USA) was used as an immunogen for the antibody rabbit anti-human fibrinogen. Aliquots of 0.5 ml, 50 $\mu g/ml$, stored at -20$°C$
- Human Serum Albumin (SigmaAldrich, USA) was used as an immunogen for the antibody rabbit anti-human albumin. Aliquots of 0.5 ml, 50 $\mu g/ml$, stored at -20$°C$

3.2.5 Buffer solutions

Ultrapure water (organic content < 5 ppb), purified in a Milli-Q gradient A10 System (Millipore Corporation, Billerica, USA). was used for the preparation of all aqueous buffers. Adsorption of PLL-g-PEG and PEI as well as all other experiments requiring buffered solutions or suspension were conducted in 4-(2-hydroxyethyl)piperazine-1-ethane-sulfonic acid (Hepes) based buffer (Fluka, Buchs, Switzerland) adjusted to pH 7.4 with 6M NaOH (Fluka, Buchs, Switzerland). The ionic strength of the Hepes buffer was either kept at 10 mM (Hepes 1) or increased with NaCl to 160 mM (Hepes 2, total ionic strength, 10 mM Hepes and 150 mM NaCl). Colloidal suspension were diluted with either ultrapure water, Hepes 1 or Hepes 2 to the concentration needed. Buffer solutions were filtered with a filter of 0.2 μm pore size (Sigma-Aldrich) before addition of colloids or polymer and stock solutions were stored at $4°C$.

3.3 Photolithography for SMAP and MAPL

The photolithography process to produce any desired pattern in the micrometer range was the same for the SMAP and the MAPL process. All the necessary

steps for photolithography were conducted in the FIRST laboratory, the technology and cleanroom facility for advanced micro- and nanotechnology at ETH Zuerich. The masks for photolithography were drawn on a technical construction software (Autodesk Mechanical Desktop), and developed by Delta Mask (Enschede, Netherlands). These positive 5 inch chromium masks were then used to transfer the pattern into the photoresist in a MA6 mask aligner (Suess Microtec, Munich, Germany). Before, the photoresist (S1818, Shipley) was spin-coated undiluted at a speed of 4000 *rpm* for 2 *min* on either silicon wafer (Wafernet Inc., San Jose, USA) or pyrex wafer (SensorPrep Services Inc., Alabama USA). The wafer was heated to 115°*C* for 2 *min* to evaporate surface water before the spin-coating process as well as after the process to evaporate the solvent from the photoresist. The wafers were pre-coated with either two transparent sputter-coated metal oxide layers (a 100 *nm* SiO_2 layer followed by a 12 *nm* TiO_2 layer on top) (for SMAP samples) or a 12 *nm* thick Nb_2O_5 coating (for MAPL samples). Magnetron sputtering of these metal oxide layers was conducted at the Paul-Scherrer-Institut, Villigen, Switzerland.

After a short cooling, the spin-coated wafers were illuminated for 10 *s* with a UV-light intensity of about 13 mW/cm^2 through the mask of choice (contact mode in vacuum). After illumination, the wafer were developed for 1 *min* in a developer solution (1:1 mixture of water and microposit developer concentrate (Röhm und Haas, Germany) and kept in a water bath for 15 *min* and spin-dried afterwards.

3.4 Production of Wettability Contrast Pattern (SMAP)

The SMAP process was developed by Roger Michel in our group.[17] For a sketch and details on this process see Fig. 5.1 and Chapter 5 in general. In this section, only experimental details and parameters will be provided.

After photolithography of a wafer with a 100 *nm* SiO_2 layer followed by a 12 *nm* TiO_2 layer on top (Section 3.3), a reactive ion etching process was performed to etch selectively through the 12 *nm* titania layer in areas where no photoresist is present.

The reactive ion etching was performed on a Oxford Instruments RIE 80+ (Oxford Instruments, Oxon, UK) at the FIRST lab at ETH Zurich. If possible, three complete wafer were inserted and etched at once. The gas concentrations were 20 *sccm*

of CHF_3 and 20 *sccm* of O_2. After pumping to a vacuum of $2x10^{-5}$ *mtorr*, the etching was performed at 100 *mtorr* and a DC bias of 230 *V* for 150 *s*. Note that etching parameters are very sensitive and if less samples are in the etching chamber, the parameters must be adjusted.

Lift-off of the S1818 photoresist was done by first immersing the samples in an N-methylpyrrolidone (NMP) solution for twice 10 *min* (undiluted), followed by a 10 *min* immersion in isopropanol and an additional 10 *min* in millipore water. All these steps were performed in an ultra sonicator bath. These steps were performed on the whole wafer, before the wafer was cut into 1x1 *mm* samples using a wafer cutting saw. Before the dodecyl phosphate SAM was assembled on the titania background, the samples were cleaned as follows: 2x 7 *min* in isopropanol ultra sonication, millipore water rinsing, 1 *min* oxygen plasma. Then, the dodecyl phosphate SAM was produced according to the protocol given before.

3.5 Production of Patterned Surfaces for Specific Binding of Colloidal Particles (MAPL)

The MAPL process was developed by Didier Falconnet during an earlier thesis in this group.[18] For a sketch and details on this process see Fig. 6.3 and Chapter 6 in general. In this section, only experimental details and parameters will be provided.

After photolithographic patterning of a 4 inch wafer coated with 12 *nm* niobia (Section 3.3) and cutting of the wafer in 1x1 *cm* samples, these MAPL samples were cleaned before the patterning process by 10 *min* of ultrasonication in millipore water. After rinsing with millipore water and blow-drying, the samples were put in an oxygen plasma cleaner for 10 *s*. The clean samples were then put in well-plates (Nunc, Danmark) and around 1 *ml* of a 0.1 *mg/ml* PLL-*g*-PEG/PEG-biotin (50%) in Hepes 2 buffer was added for 40 *min*. Then, the samples were rinsed and blown dry again and the photoresist lift-off step was performed.

The photoresist lift-off process consists of several rinsing steps with N-methylpyrrolidone (NMP). First, the sample is held upside down such that NMP from a squeeze bottle can be flushed over the surface. The sample is held for around 10-20 *s* and NMP is flushed over the surface for this time. This step already removes much of the photoresist. Then, the sample is put in a piranha cleaned glass beaker

which is filled with 2 *ml* NMP. The beaker is ultrasonicated and after 1 *min*, 1 *ml* of the solvent is exchanged with 1 *ml* of new NMP. After another minute, the sample is transferred in a new glass beaker with 2 *ml* NMP and the step is repeated. As a last step, the sample is immersed in a glass beaker with a 1:1 mixture of millipore water and NMP, again sonicated for 1 *min* and then stored in a water bath for 5 *min*. The MAPL chip is rinsed with water and blown dry with nitrogen and stored in a well-plate.

The well-plates are then filled with 1 *ml* of PLL-*g*-PEG and after 40 *min* the samples are removed, rinsed with water and blown dry with nitrogen and stored under ambient conditions in a sealed box (24 well-plates wrapped with parafilm).

Bibliography

[1] Dukhin, A. S., Ohshima, H., Shilov, V. N. and Goetz, P. J. Electroacoustics for Concentrated Dispersions. *Langmuir*, **15**(10), 3445–3451, 1999.

[2] Rezwan, K. *Protein treated aqueous colloidal oxide particle suspensions: driving forces for protein adsorption and conformational changes.* Doctoral Thesis, ETH Zurich, 2005.

[3] Dukhin, A. S., Shilov, V. and Borkovskaya, Y. Dynamic Electrophoretic Mobility in Concentrated Dispersed Systems. Cell Model. *Langmuir*, **15**(10), 3452–3457, 1999.

[4] Kurrat, R., Textor, M., Ramsden, J. J., Boni, P. and Spencer, N. D. Instrumental improvements in optical waveguide light mode spectroscopy for the study of biomolecule adsorption. *Review of Scientific Instruments*, **68**(5), 2172–2176, 1997.

[5] Voros, J., Ramsden, J. J., Csucs, G., Szendro, I., De Paul, S. M., Textor, M. and Spencer, N. D. Optical grating coupler biosensors. *Biomaterials*, **23**(17), 3699–3710, 2002.

[6] de Feijter, J., Benjamins, J. and Veer, F. *Biopolymers*, **17**, 1759–1772, 1978.

[7] Pasche, S. *Mechansims of protein resistance of adsorbed PEG-graft co-polymers.* Doctoral thesis, ETH Zurich, 2005.

[8] Hook, F., Voros, J., Rodahl, M., Kurrat, R., Boni, P., Ramsden, J. J., Textor, M., Spencer, N. D., Tengvall, P., Gold, J. and Kasemo, B. A comparative study of protein adsorption on titanium oxide surfaces using in situ ellipsometry, optical waveguide lightmode spectroscopy, and quartz crystal microbalance/dissipation. *Colloids and Surfaces B-Biointerfaces*, **24**(2), 155–170, 2002.

[9] Xie, H., Wei, J. and Zhang, X. Characterisation of Sol-gel Thin Films by Spectroscopic Ellipsometry. *Journal of Physics: Conference Series*, **28**, 95–99, 2006.

[10] Burden, A. P., Anguita, J. V. and Silva, S. R. P. Microstructural characterisation of carbonaceous dust generated during the deposition of diamond-like carbon coatings. *Thin Solid Films*, **332**(1-2), 252–256, 1998.

[11] Feuz, L. *On the coformation of graft-copolymers with polyelectrolyte backbone in solution and adsorbed on surfaces.* Doctoral Thesis, ETH Zurich, 2006.

[12] Huang, N. P., Michel, R., Voros, J., Textor, M., Hofer, R., Rossi, A., Elbert, D. L., Hubbell, J. A. and Spencer, N. D. Poly(L-lysine)-g-poly(ethylene glycol) layers on metal oxide surfaces: Surface-analytical characterization and resistance to serum and fibrinogen adsorption. *Langmuir*, **17**(2), 489–498, 2001.

[13] Elbert, D. L. and Hubbell, J. A. Self-assembly and steric stabilization at heterogeneous, biological surfaces using adsorbing block copolymers. *Chemistry and Biology*, **5**(3), 177–183, 1998.

[14] Pasche, S., De Paul, S. M., Voros, J., Spencer, N. D. and Textor, M. Poly(L-lysine)-graft-poly(ethylene glycol) assembled monolayers on niobium oxide surfaces: A quantitative study of the influence of polymer interfacial architecture on resistance to protein adsorption by ToF-SIMS and in situ OWLS. *Langmuir*, **19**(22), 9216–9225, 2003.

[15] Tsien, R. Y. The Green Fluorescent Protein. *Annual Review of Biochemistry*, **67**(1), 509–544, 1998.

[16] Zhen, G., Falconnet, D., Kuennemann, E., Voeroes, J., Spencer, N., Textor, M. and Zurcher, S. Nitrilotriacetic Acid Functionalized Graft Copolymers: A Polymeric Interface for Selective and Reversible Binding of Histidine-Tagged Proteins. *Advanced Functional Materials*, **16**(2), 243–251, 2006.

[17] Michel, R., Reviakine, I., Sutherland, D., Fokas, C., Csucs, G., Danuser, G., Spencer, N. and Textor, M. A novel Approach to Produce Biologically Relevant Chemical Patterns at the Nanometer Scale: Selective Molecular Assembly Patterning Combined with Colloidal Litography. *Langmuir*, **18**(22), 8580–8586, 2002.

[18] Falconnet, D., Koenig, A., Assi, T. and Textor, M. A combined photolithographic and molecular-assembly approach to produce functional micropatterns for applications in the biosciences. *Advanced Functional Materials*, **14**(8), 749–756, 2004.

CHAPTER 4

Colloidal Gradients on Metal Oxide Surfaces

4.1 Introduction

Surfaces with a continuously changing surface parameter (a gradient surface) have some distinct advantages for certain applications. It for example allows for rapid screening tests or combinatorial and diagnostic studies performed on a single sample, of particular importance in biotechnology or medicine. The surface parameters of interest range from crystallinity [1] to porosity [2] and surface chemistry. Among surface chemistry parameters, wettability gradients are the most common today. In such a gradient, the wettability changes gradually along the length of the sample due to a controlled change in surface chemistry. Different methods have been developed to produce such wettability gradients.[3–6] Most of them involve the functionalization of a metal oxide or gold surface with organic molecules that have either methyl-terminated endgroups (for hydrophobic surfaces) or hydroxyl endgroups (for hydrophilic surfaces). The gradient is produced by either controlled (liquid or gas phase) diffusion of the molecules on the surface,[3] cross-diffusion of two different molecules (one hydrophilic, one hydrophobic) from two sides,[5] via radiofrequency plasma discharge treatment by exposing the polymer surface for varying times to oxygen plasma [4] or by a simple dip-and-rinse process where the wettability gradient forms by continuously changing the immersion time in the hydrophobic alkane thiol (in this case) solution.[6]

Another parameter plays a crucial role in many cases: surface morphology. It is for example known for a long time, that surface roughness over a wide range of length

scales affects the biological response to surfaces, e.g. cell adhesion, proliferation and differentiation. Also parameters related to surface contact effects (such as tribological or adhesion phenomena) will be influenced by a varying surface topography. However, only little progress has been made in producing large-scale topographical gradients. Crystallinity gradients of a polymer film due to a temperature gradient-stage have been described before,[1] as have been gradients of pore sizes in silicon by etching in an anisotropic E-field. Only very recently, an approach was presented by Kunzler et al.[7] that allows the production of stochastic roughness gradients over centimetre length scales with topographical features in the nanometer and micrometer range by sand-blasting the samples (to give an initial roughness) and then applying a polishing step (in which the sample was continuously withdrawn from the sample). Parts that were immersed for longer times, were polished smoother, parts being removed in the beginning of the withdrawal process retained their initial roughness.

Another approach is to use the self-assembly potential of colloidal particles to form particle gradients. However, the only particle gradient materials, that have been produced recently are colloidal crystals for the use as photonic band gap material. Most of these colloidal crystal gradients use polymer-infiltration techniques, where a polymer with a gradually changing refractive index is infiltrated into the colloidal crystal, thus no "particle" gradient has to be produced. For example, Park et al. fill the background of a colloidal crystal with a polymer matrix whose background refractive index is changing gradually using an interfacial gel polymerization technique.[8] Also, von Freymann et al. produced vertical particle gradients by plasma etching of a colloidal crystal, which reduces the particle size of the top layer of the crystal.[9] It was not until recently, that the first colloidal crystal gradients were produced that where able to introduce a gradient along the sample using colloidal methods.[10–12] However, no gradients in particle density as presented here were reported in literature to the authors knowledge.

In this thesis, the knowledge gained from colloidal silica adsorption experiments on positively charges surfaces was used to develop an alternative way of producing a morphology gradient on a surface. In a simple dip-coating process, a gradient in nanoparticle density is achieved on the substrate, which can be varied from a complete (sub-)monolayer at one end of the gradient to only a few particles per square micrometer on the other. Not only is this method very universal regarding materials (e.g. the substrate material can be most metal oxide (or otherwise negatively

chargeable material), but also — with a simple heat treatment — the shape of the colloidal particles on the substrate can be varied in a wide range. Furthermore, this heat treatment also increases the adhesion of the particles to the substrate at the same time, providing the necessary robustness that such particle gradients might be used in replication techniques and / or in experiments that need a well-established morphology gradient (e.g. in cell biology experiments).

4.2 Experimental

Colloidal Particle

Silica nanoparticles with an average particle size of 73 nm were obtained in suspension(Klebosol, Clarient, France). The initial 30 $wt\%$ suspension was diluted with either ultra pure water (18 $M\Omega$ resistance and an organic content of less then 5 ppm, Millipore) or Hepes 1 or Hepes 2 buffer to a concentration range between 0.01 and 0.001 $wt\%$. Thus, particle suspensions were kept in either 10 mM salt buffer (Hepes 1) or in 160 mM salt buffer (10 mM salt from buffer and 150 mM NaCl) at a pH of 7.4 (Hepes 2) (see Section 3.2.5 for details).

Substrate Preparation

Silicon wafers (Wafernet Inc., San Jose, USA) were cut into 3 by 1 cm samples and cleaned by ultrasonication (10 min in isopropanol, then in Millipore water for another 10 minutes). After rinsing the samples with pure water and blow drying with nitrogen, the samples were cleaned in oxygen plasma chamber for 3 min. Cleaned samples were then immersed in 1 mg/ml filtered poly(ethylene imine) (PEI) (Fluka Chemie, Switzerland) Millipore water solution for 30 min in a laminar flow box. After adsorption of the PEI polyelectrolyte, samples were removed, rinsed with water, blown dry under nitrogen flow and stored at room temperature.

Colloidal Gradient Preparation

The PEI-coated substrates were mounted on a linear motion drive device as shown in Fig. 4.1. The samples were first immersed about 2 mm into the suspension and held

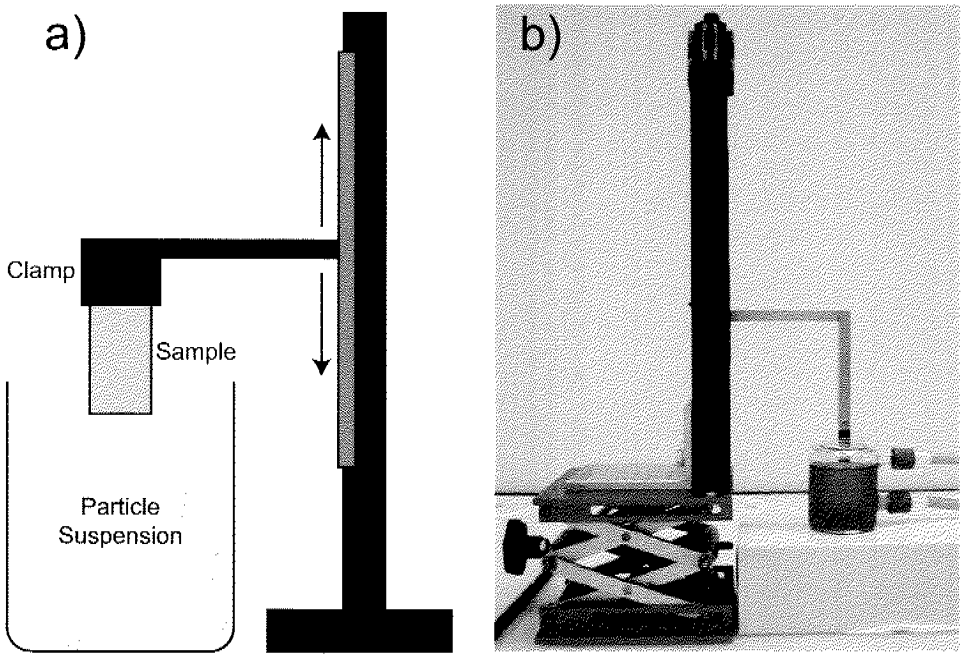

Figure 4.1: Sketch (a) and photograph (b) of the linear motion drive device (LMD) used in this work. The sample is clamped into the LMD stage and placed above the particle suspension. The sample is then immersed into the suspension at a given, computer-controlled speed-profile (as shown in Fig. 4.8).

there for about 15 *min*. This procedure was chosen because at the first contact of the sample with the suspension, the water film will — due to capillary forces — "jump" onto the sample, which would result in an uncontrolled starting situation. For this reason, the samples were immersed some distance into the suspension to avoid these irregularities. The point, where the sample was kept for 15 *min* was marked and from this point on, the experiment was started. This procedure has the additional advantage that within these first few millimeters the saturation density of colloidal particles on the sample can be investigated. After the start of the experiment, the sample is immersed at a given, computer-controlled immersion profile. This profile can be chosen to be almost any linear, polynominal or exponential function as needed. At the end of the experiment, when the full 2 *cm* of gradient have been immersed, the beaker containing the suspension is flushed with large amounts of water (500-1000 *ml*). This is necessary to replace the particle suspension with water containing (almost) no colloids anymore. With this step, it is made sure, that no colloids can adsorb during the drying process and disturb the colloidal gradient

produced in suspension. After the water rinse, the gradient sample is removed from the solution, rinsed under Millipore water and dried under nitrogen flow.

Sintering of the gradient samples was achieved in a high-temperature oven under ambient atmosphere. Samples were heated at 10 $°C/min$ to the desired end-temperature, held for 2 h and then slowly cooled down to room temperature.

Gradient Analysis

Adsorption of silica nanoparticles was investigated *in situ* using Optical Waveguide Lightmode Spectroscopy (OWLS). Colloidal gradients were analyzed using SEM and AFM imaging. To evaluate the colloid density along the gradient, SEM images taken at a known position on the gradient were analyzed using an image analysis program (ImageJ). For details of the experimental techniques, see Chapter 3.

4.3 Results and Discussion

4.3.1 Adsorption of Colloidal Particles on Charged Surfaces

Negatively charged silica particles (see Fig. 3.5) will adsorb readily to a positively charged surface by electrostatic attractions. To provide such a positively charged surface, poly (ethylene imine) (PEI) was adsorbed to a silicon wafer surface. PEI is a cationic, branched, polyelectrolyte which adsorbs spontaneously to the negatively charged silica surface and renders this surface positive.[13] Indeed, 73 nm silica particles will then adsorb to this surface in a controllable way as shown in Fig. 4.2. Depending on the concentration of the colloidal particles in the suspension, a monolayer of particles adsorbs to the PEI coated silica surface very rapidly or over the time-span of several minutes. With a particle concentration of more than 1 $wt\%$, adsorption of a monolayer takes place in less than a minute. For dilute suspensions, say 0.01 $wt\%$, adsorption takes over an hour to produce a complete monolayer. However, at such low concentrations wall-effects (particles adsorbing to the tube and flow-cell walls in addition to the sample surface) play a certain role in OWLS experiments, which causes the kinetics of adsorption to be disturbed to some extent. A fact which is observed in Fig. 4.2, where the low concentration adsorption curves show slight deviations over time.

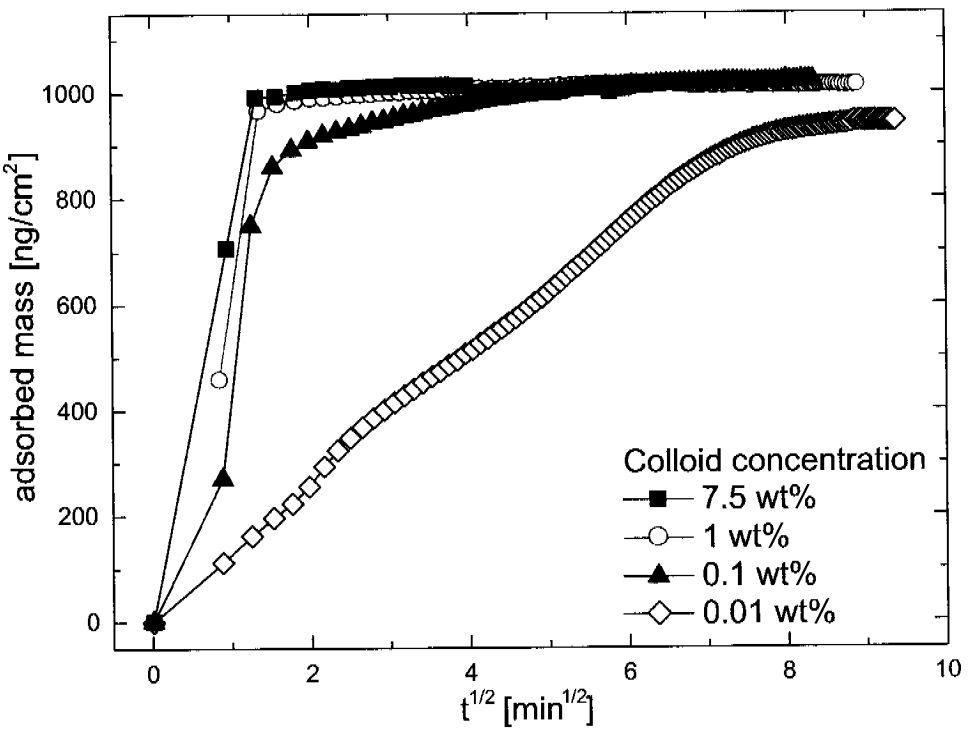

Figure 4.2: Influence of colloid concentration on the adsorption behavior of 73 nm silica colloids buffered in Hepes 1 at pH 7.4 on a poly(ethylene imine) coated silicon wafer observed by OWLS. The negatively charged silica nano colloids adsorb electrostatically to the positively charged PEI coated surface.

The adsorption of colloidal particles by electrostatic interactions may be viewed as a one-step process, where a particle adsorbs electrostatically to the substrate and may not be moved on the surface anymore. Particles thus irreversibly adsorb randomly to the surface and since they can also not be moved on the surface, a "complete" monolayer (in the sense of densely-packed) will never be achieved.[1] Such processes are often referred to as irreversible "random sequential adsorption" (RSA). Mathematically, this problem is simply described as "putting one disk after another randomly on a surface. If it overlaps with a placed disk, it will be removed and the next disk is put on the surface". One immediate conclusion is, that there must exist a jamming limit for the surface coverage, which is lower then that for a surface where particles are close-packed. Indeed, that jamming limit is found to be 0.547.[14, 15] Which means, that the theoretical maximum surface coverage for the system used in this work may not exceed 54.7%. However, this value may in reality not be reached, since the particles have not only their "physical" size but also the electric

[1] Obviously, overlapping of particles is not possible as well

double layer around themselves. This double layer has a finite thickness as well which must be added to the particle's physical diameter. Thus, the "thicker" the electric double layer, the lower will the particle surface coverage at the jamming limit be. The thickness of the electric double layer can — as discussed later — readily be influenced by pH and ionic strength. In Fig. 4.3, a schematic representation of the RSA model is given and corresponding SEM images are shown to illustrate the situation in a real system. At the jamming limit (Fig. 4.3b), no more particles (or disks) may be deposited without moving particles on the surface (some of the forbidden particle positions are indicated). In real systems, it is often not the case that particles can not be moved on the surface. This is the most common deviation from RSA models. In the SEM images of Fig. 4.3, some particles are clustered together and as a consequence, some free space is produced on the surface. However, the particles can only move under the influence of capillary forces during drying. As long as the particles are in suspension, they will randomly adsorb as predicted by the RSA theory and stick to the surface by electrostatic forces. During drying, capillary forces (stemming from water bridges that form between two particles as discussed in the introductory chapter and sketched in Fig. 2.10) may eventually be as high as the electrostatic forces holding the particles in place and therefore move some particles together and form clusters of particles as observed in Fig 4.3.

As mentioned above, two main parameter have long been identified to influence particle adsorption in cases where electrostatic interactions are the main contributor to the adsorption process: pH and ionic strength. These parameters were also tested in the silica nanoparticle — PEI system that was used in this work. In Fig. 4.4 and 4.5, the influence of pH on adsorption of 73 and 40 nm particles is shown. In both cases, the dependence of the adsorption on pH is obvious. At or very near the IEP of the silica particles (2.3), the particles carry only little charge. They are still slightly attracted to the positively charged PEI surface, but only repel each other very little (in fact, particles in this situation are very unstable and have a very high tendency to agglomerate). This leads to situations as shown in Fig. 4.4a) and 4.5a), where even double layer of particles can be adsorbed due to the low charge situation. The situation does not change even for slightly higher pH (Fig. 4.4b) and 4.5b), but already, the occurrence of double layers is less distinct. If pH is increased, particles carry more and more negative charges (because Si-OH groups get deprotonated with increasing pH), repelling each other more and more and thus the end coverage on the

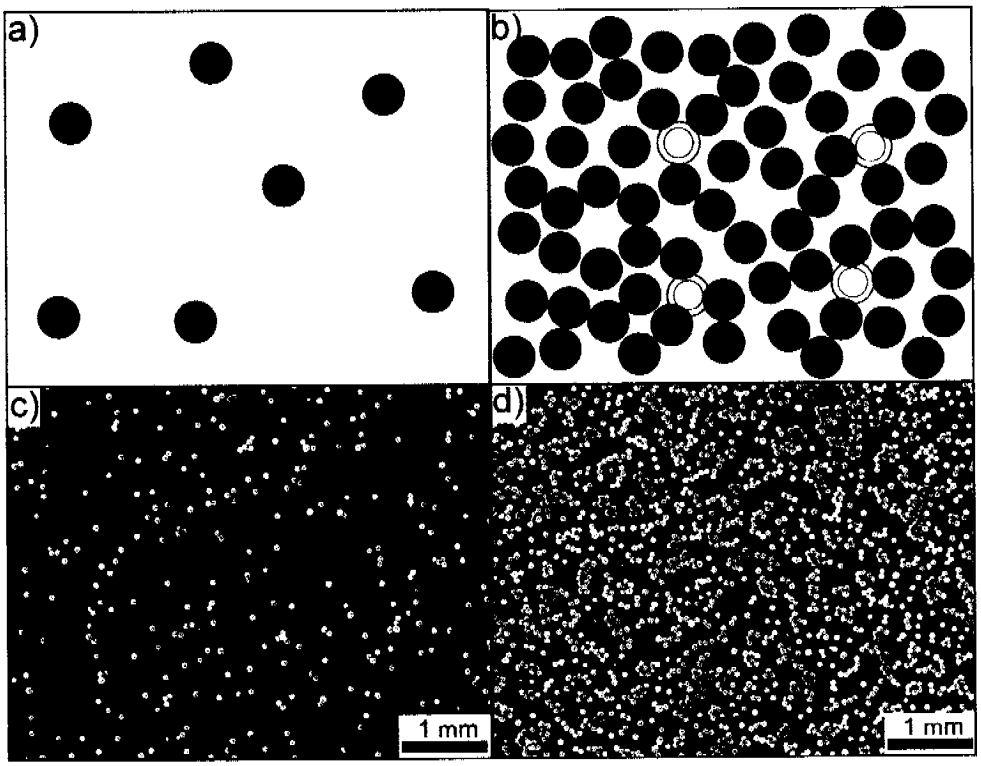

Figure 4.3: Random sequential adsorption model sketch and SEM images illustrating two stages of the process. a) after short times (and depending on particle concentration), a few particles have irreversibly adsorbed to the surface. They cannot be moved on the surface, since they are strongly bound by electrostatic forces. b) At or near the jamming limit of the RSA model: no further particles can be deposited, since they would overlap (some of the forbidden positions are indicated with red, hollow spheres). It is important to note, that the "radius" of the particle is not only the particle itself but also the ion cloud that it carries (symbolized by the grey ring around each black particle). This electric double layer (characterized by the Debye length) can be changed by varying pH or ionic strength of the solution. Increasing the Debye length therefore lowers the actual particle density on the surface. c) and d) SEM images of 73 *nm* silica particles adsorbing on a positively charged PEI surface. c) After short times, a few particles have adsorbed on the surface. Already, some deviation of the RSA model can be observed, such as clustering of a few particles. d) After longer adsorption times (30 *min*), a complete RSA "monolayer" forms as shown in b). But also in this image, deviations between the ideal situation in b) and the system used in this work (d) can be seen. These deviations (clustering of particles and free space on the surface) are artifacts from the drying process which modifies the pattern formed in suspension.

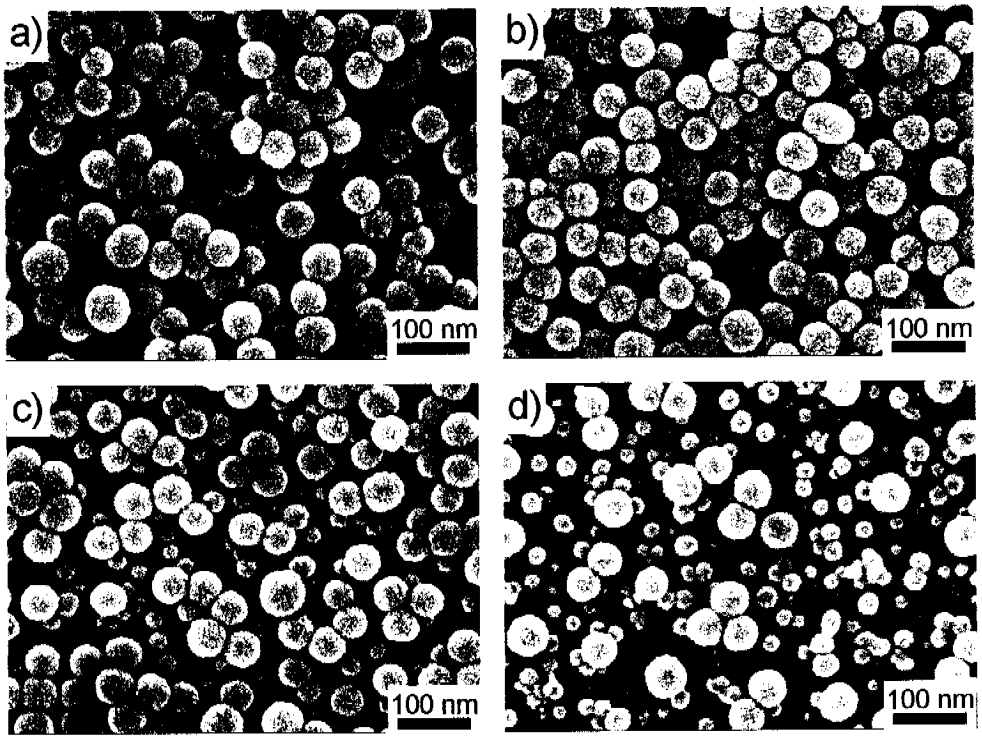

Figure 4.4: Influence of pH on 80 *nm* silica nanoparticle adsorption on a positively charged PEI layer (in ultrapure water as medium). a) ph = 2.4 b) pH = 5.5 c) pH = 8.5 d) pH = 11.1. With increasing pH, less particles adsorb due to the increased stability of the suspension because of the higher surface charge of the silica particles. Note that although the fraction of small particles in the suspension is very small, the polydispersity of the suspension is "increased" near the surface due to the fact that the small particles adsorb much more rapidly and therefore are visible on c) and d).

surface is decreased. Increasing the pH and therefore increasing the surface charge of the particle is equivalent to increasing the effective size as discussed in Fig. 4.3d).

Of similar importance for the adsorption behavior is the ionic strength of the suspension as discussed in Chapter 2. Changing the ionic strength from ultra pure water to 10 mM to 160 mM (as shown in Fig. 4.6), increases the amount of adsorbed particles significantly. While in ultra pure water (and also at a slightly lower pH), particles still adsorb by forming a monolayer of individually adsorbed particles, adding more and more salt increases the tendency for the particles to agglomerate and form denser particle structures upon adsorption. Using Hepes 1 (with moderate salt concentrations of 10 mM leads to a similar situation as with ultra pure water, but already much more clusters of particles have formed. Also, these particles adsorb with a smaller particle-particle distance as the Debye-length responsible for

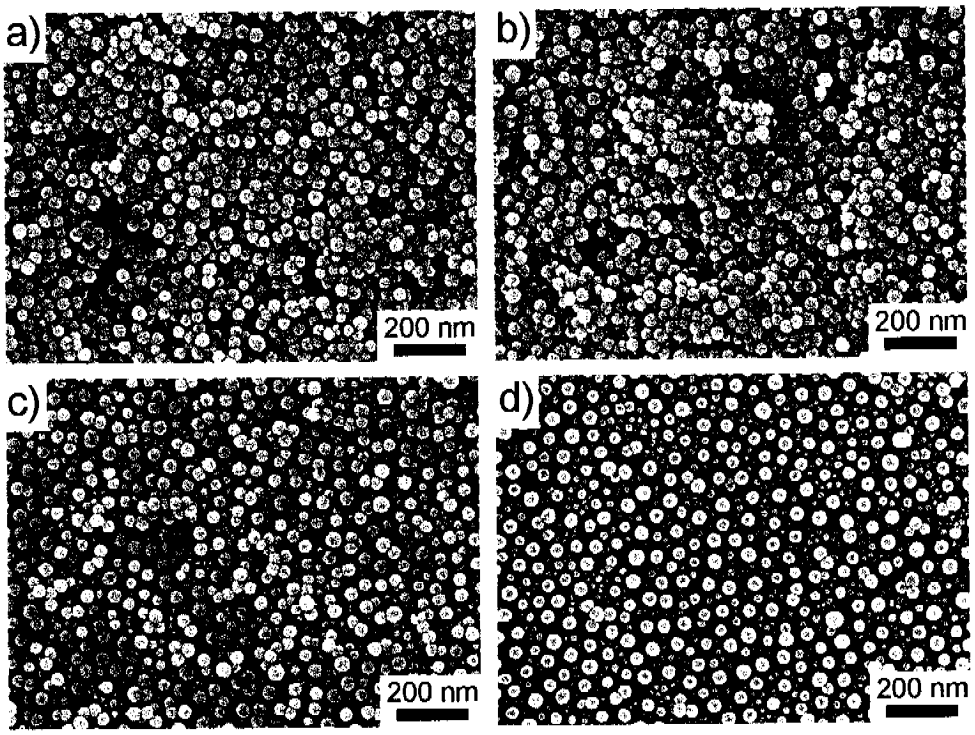

Figure 4.5: Influence of pH on 40 *nm* silica nanoparticle adsorption on a positively charged PEI layer. a) pH = 2.5 b) pH = 6.4 c) pH = 8.3 d) pH = 10. With increasing pH, the concentration of particles on the surface decreases steadily due to the increased inter-particle repulsive forces and the increased stability of the suspension. The behavior is very similar to that observed for 80 *nm* particles in Fig. 4.4.

the separation of particles is decreased significantly. Hepes 2 buffer has a high salt concentration of 160 mM.[2] This results in a very short Debye-length and therefore only little repulsion between particles. The tendency for such suspensions to agglomerate is high. A fact, that is also verified by looking at the respective SEM image in Fig. 4.6. There, multilayers of nanoparticles adsorbed to the surface and form a loosely packed structure because the repulsive interaction potential of these particles is largely reduced due to the high salt concentration. The Debye-length for the present cases as calculated from Eq. 2.16 are below 1 nm for the 160 mM NaCl suspension, around 3 nm for a 10 mM salt suspension and around 10 nm for an ultra pure water suspension (assuming a salt concentration of 1 mM). These numbers already indicate that results as shown in Fig. 4.6 can be expected, since the Debye-length determines the distance over which the repulsive forces between

[2]This is equivalent to the salt concentration in the body, which makes it an often used buffer for physiological experiments

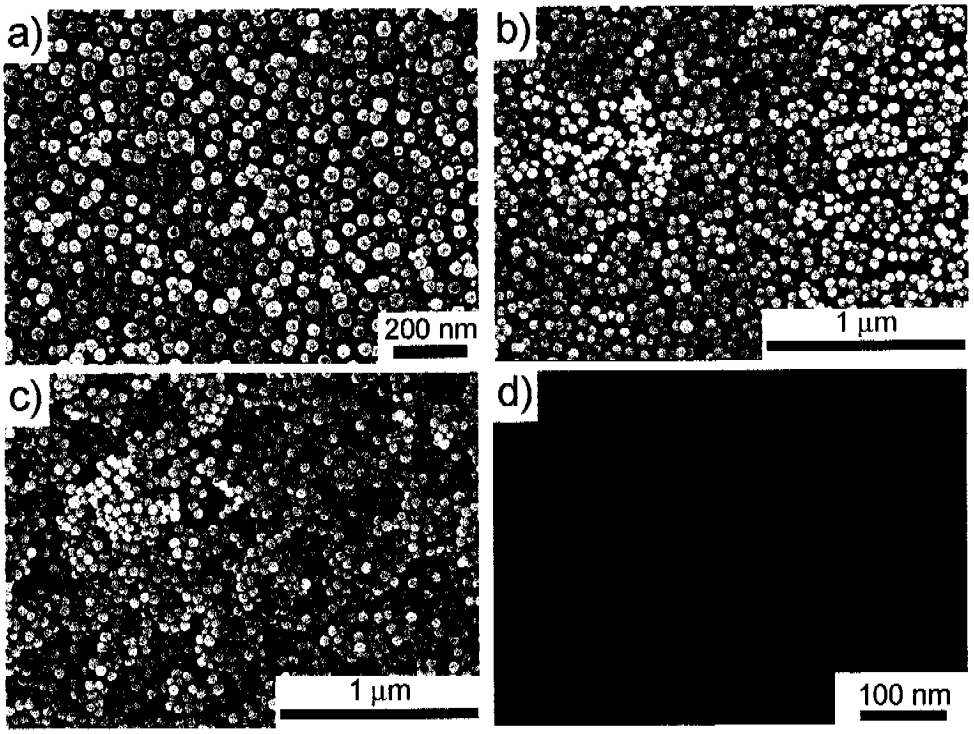

Figure 4.6: Influence of ionic strength on the adsorption behavior of 40 *nm* silica particles on a PEI coated surface. a) SEM image of silica nanoparticles adsorbed from an ultra pure water suspension at pH 8.3 b) Hepes 1 buffered colloid suspension (pH 7.4, 10 *mM* ion concentration) and c) Hepes 2 buffered colloid suspension (pH 7.4, 160 *mM* salt concentration). d) SEM image showing a control surface where also the particles have been coated with PEI (thus rendering them positively charged). Consequently, the silica nanoparticles no longer adsorb in this case.

particles are still active. However, it is not only the Debye-length but also the overall stability of the suspension which decreases at low pH (close to the IEP) or at high salt concentrations. A less stable suspension will have a higher tendency to form multilayer or clusters upon adsorption. That the forces obviously are of electrostatic nature is demonstrated in Fig. 4.6d, where the silica particles where coated with PEI so that they gain a positive surface charge. None of these positively charged particles adsorb to the same PEI surface anymore.

With these *in situ* OWLS experiments and the SEM analysis of adsorbed particle layers under various conditions, the adsorption kinetics of the nano silica particles and the influence of important parameters such as pH and ionic strength were investigated. These insights allowed for the development of a topographical gradient patterning technique using colloidal particles as discussed in the following sections.

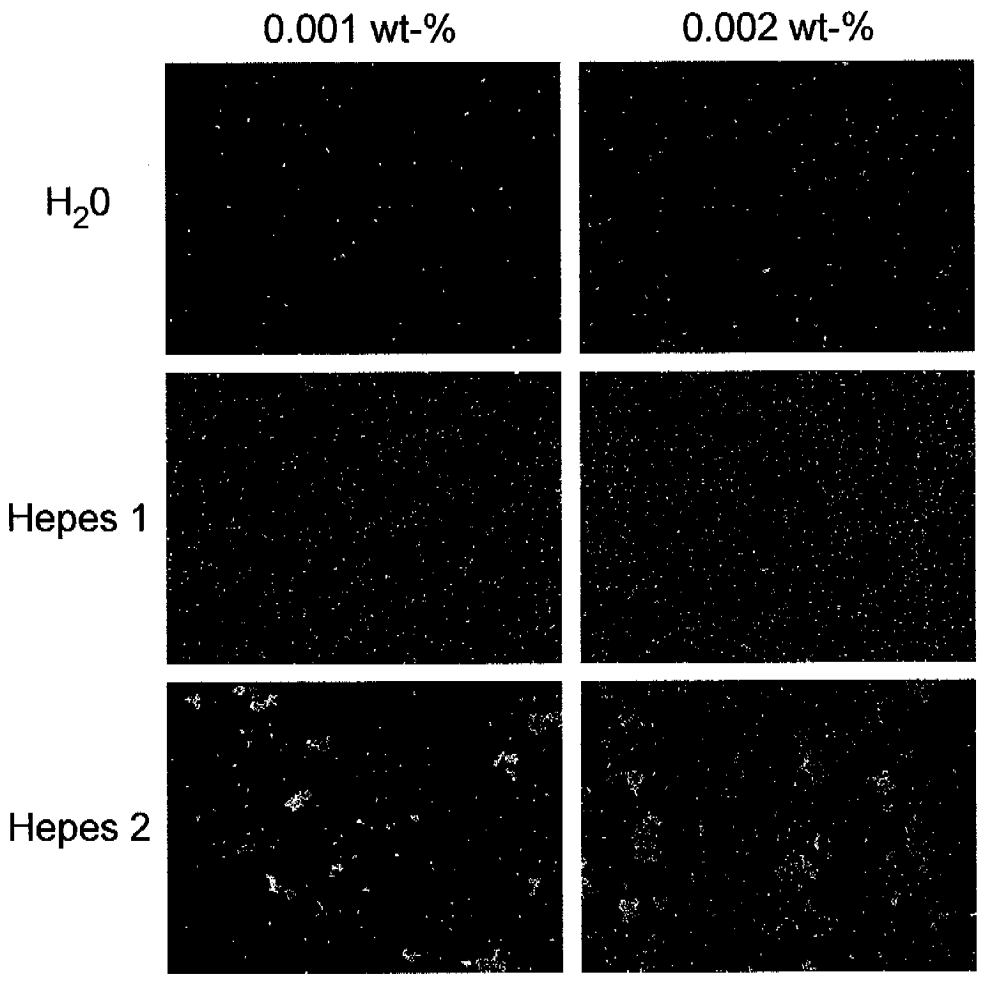

Figure 4.7: Nano silica suspensions (73 *nm* particles) adsorbing for 30 *min* in different solvents (pure water, Hepes 1 and Hepes 2) and with two different concentrations (0.001 and 0.002 *wt%*). Note that the pH is slightly different for the water-based suspension (9.9), while the Hepes-based suspensions were buffered at 7.4.

4.3.2 Colloidal Gradients

The basic idea to produce colloidal gradients is to expose a surface for a specific time interval to a colloidal suspension with known properties. If the surface and the particles interact electrostatically, particles will start to adsorb and form an incomplete particle layer with more or less particles adsorbed to it depending on the time which the particles were allowed to adsorb. This process was already sketched in Fig. 4.3, were a) shows the situation after short adsorption times and b) is equal to the jamming limit of the monolayer (which is reached after a longer time interval — depending on particle concentration). For example, Fig. 4.7 shows a series of

adsorption experiments which were all interrupted after 30 *min*. Solvent as well as particle concentrations were altered as indicated in the figure caption. For all three suspensions, an increased amount of particles adsorb from 0.002 *wt*% compared to 0.001 *wt*% suspensions, as expected. Again, it can be seen, that Hepes 2 buffer suspensions tend to agglomerate and heavy clustering can be observed in this case. Hepes 1-buffered suspensions, on the other hand, show a surface homogeneously covered with particles, with almost no clustering of particles. Particle coverages are rather low, however. In the case of the 0.001 *wt*% suspension, a particle coverage of only 2.9 % is reached after 30 *min*. If the concentration is doubled, the particle coverage after 30 *min* increases to 4.9 %. Similar results were obtained for water-based suspension, however, significantly less particles adsorbed in this case compared to Hepes 1 suspensions (0.5 % in case of the 0.001 *wt*% suspension and 0.9 % using the 0.002 *wt*% suspension). The reason for this is not completely understood. On the one hand, the water-based suspension was buffered at pH 9.9 in this case to prevent an otherwise unavoidable change of pH while changing particle concentration. On the other hand, at such low particle concentrations, local concentration differences or turbulences in the suspension might significantly influence particle adsorption. This is even more probable since the suspensions were not stirred during these experiments. The low amount of adsorbed particles for these suspensions is also consistent with OWLS measurements, as shown in Fig. 4.2. There, it was observed that a 0.01 *wt*% suspension of 73 *nm* silica particles in Hepes 1 already takes around 100 *min* to form a monolayer. And even after a 100 *min*, the layer is still not completed. Thus, low particle coverages for diluted particle suspensions are expected and in fact, OWLS experiments of 0.001 *wt*% suspensions showed that indeed within 100 *min* only a fraction of a monolayer is formed.

The challenge to form a colloidal topographical gradient on a substrate can therefore be tackled by exposing different parts of the substrate for increasing times to a colloidal suspension. This is most conveniently done by simply dip-coating the substrate into the colloidal suspension very slowly. By doing so, the side of the sample, which is immersed in the first place, stays much longer in the suspension than the end of the substrate, which is immersed only during the last part of the dipping process. The dip-coating device is shown in Fig. 4.1. After initial testing of this idea, several issues evolved, which have to be considered in this fabrication process. At first, it had to be determined whether the sample should be dipped into the suspension or removed from the suspension. Testing both possibilities

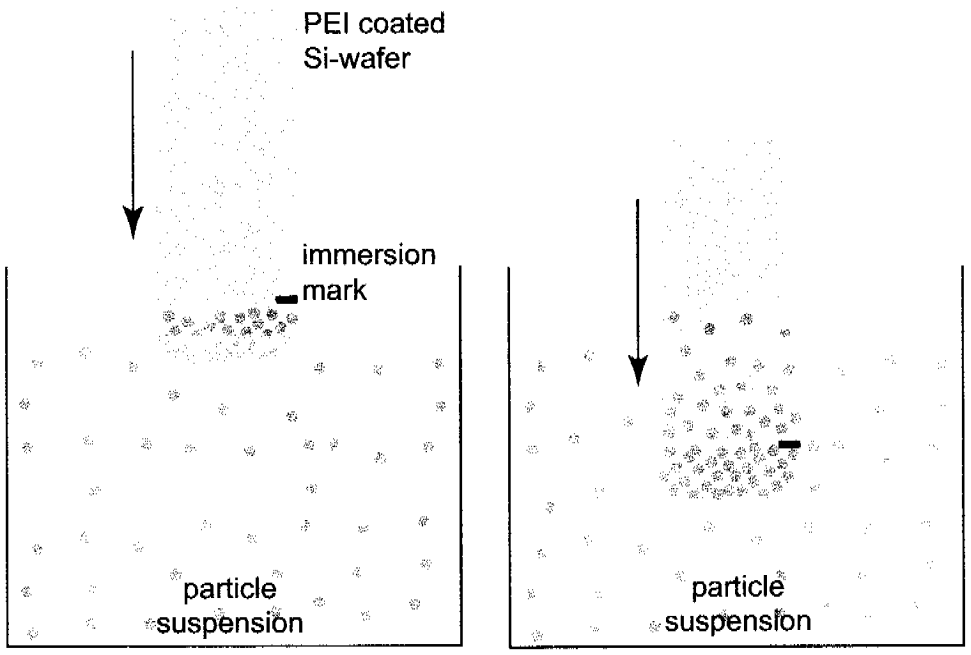

Figure 4.8: Schematic drawing of the situation, when the dip-coating process is started. The sample is immersed a few millimeter into the suspension to avoid unfavorable edge effects and provide an area where a dense RSA monolayer can form. The immersion mark placed on the sample indicates the line, from which on the actual dip-coating process starts.

and recalling theoretical considerations from the introduction chapter made clear, that capillary forces influence a colloidal pattern at the three phase contact line. Removing a sample from the suspension is therefore not advisable, since in this case, a drying front would inevitably form, where the sample leaves the suspension. This situation would not only be able to disturb the colloidal structure itself, but more importantly, additional colloidal particles would be dragged to the three-phase contact line (see Section 2.5.3). This would lead to a situation where particles are not only adsorbed by electrostatic interactions but also by capillary forces, an undesired and less controllable process. Thus, the substrate sample has to be immersed into the suspension. Immersing a substrate surface (in this case a 3x1 *cm* wafer chip coated with PEI) is best done in the following way. The substrate should be immersed about 3-5 *mm* into the suspension and be kept there for a given time interval.[3] Only then, the sample is immersed into the suspension with the speed needed. Fig. 4.8 gives a schematic of the situation prior to the start of the dip-coating process on the left and the situation at the end of the dip-coating process on the right. This procedure

[3]In the presented experiments, this interval was usually 15 *min*

has two advantages: first, it minimizes the influence of edge effects that occur when a sample is immersed into the suspension. For example, a "jump" occurs when the sample first touches the suspension surface and contacts the substrate: the water film wets the sample very rapidly to form the water meniscus as depicted in Fig. 4.8 schematically. If the sample would not be immersed a few millimeter into the suspension before the start of the experiment, such edge effects may affect the formation of the particle gradient. Second, the area where the sample was immersed in the first place, is a good domain to determine the jamming limit of the suspension later on, since this area was kept for a long time in the suspension and a RSA monolayer of particles was allowed to form. An immersion mark is added to find the line (in SEM microscopy imaging), from where the dip-coating process has been started.

Another critical point is the end of the dip-coating process. It must be the aim, to avoid drying effect on these samples as much as possible and therefore, the sample should not be removed through the suspension-air interface. This would cause similar problem as mentioned above, when the sample would be removed from the suspension instead of dipped into it. The best way to perform the experiments was found to be as follows: at the end of the dip-coating process the sample is immersed completely into the suspension. As soon as this point is reached (right hand side of Fig. 4.8), the beaker with the suspension is carefully flushed with extensive amounts of water. By doing so, the beaker overflows and the suspension is rapidly diluted. Only after the suspension is diluted so much that — ideally — no more colloids are in it, the sample is removed from the suspension (or the water, more precisely), rinsed with more water and dried under nitrogen flow. With this process, the influence of capillary forces during the drying process can be minimized efficiently and only few particle are allowed to adsorb during the drying step.

It is not an easy task to assign numbers to the capillary and electrostatic interaction energies due to the inherent assumptions that are made in the existing models which are not always fulfilled in real systems. Nevertheless, the attractive capillary interaction energy between two particles was calculated to be in the order of $4.4x10^6kT$ (see Chapter 5 for details). Using Eq. 2.37, the electrostatic interaction energy between the surface (assuming a ζ-potential of 100 mV) and a particle (ζ-potential of -65 mV, as measured) is around 10^2kT (in contact of the two, rapidly decaying if the separation distance is increased). Which shows, that capillary forces are very strong compared to the electrostatic interaction energies. In fact, judging from the

calculated values, they are several orders of magnitude higher then the electrostatic attraction of the particles to the surface. This is especially true if the particles are only separated by small distances. Capillary forces therefore gain in importance at high colloid densities on the surface, while they are relatively insignificant at low particle concentrations on the surface. These numbers also rationalize why very often in these experiments, doublets, triplets or small clusters of particles are found on the surface instead of well-separated particles. As soon as two, three or more particles are electrostatically adsorbed at relatively close separation distances, it is almost inevitable that these particles are clustering together, since the capillary forces in these situations exceed the electrostatic interactions significantly.

The behavior just described can also be observed on colloidal gradients that were produced during this work. Fig. 4.9 shows an example of a colloidal gradient produced with 73 nm particles at a concentration of 0.002 $wt\%$. An almost perfectly linear increase in particle concentration along the 1 cm gradient can be observed, from very few particles adsorbed on the one end, to a complete RSA-monolayer on the other end. While there is almost no visible influence of capillary forces on the low particle concentration images, clustering of particles increases as the concentration of particles on the surface increases. This behavior is consistent with the force estimations made above, because as soon as the inter-particle distance decreases, capillary forces gain in importance and tend to influence the resulting pattern stronger. At low particle concentrations, the particles are far enough separated that capillary forces may drag these particles towards each other, the particles remain separated and stay on the surface as single particles. The immersion profile used (see figure caption in Fig. 4.9) has a second order polynomial shape to account for the fact, that particle adsorption kinetics is faster in the beginning and becomes slower for longer times (as observed in Fig. 4.2). At high particle concentrations on the surface (the part of the sample which is immersed in the beginning), much more time is needed to further increase the surface coverage, while at low particle concentrations (the end of the sample) the increase in coverage happens much more rapidly. More specifically, in Fig. 4.2, it is observed that nanoparticle adsorption follows a diffusion-controlled $\sqrt{t}$-law, which requires a second order polynomial immersion profile function to account for that fact. The combination of a second order polynomial immersion profile and the $\sqrt{t}$ dependence of the particle adsorption leads to a linear particle gradient in theory and also in the real system this linearization of the particle gradient proved to work rather successful as observed in Fig. 4.10.

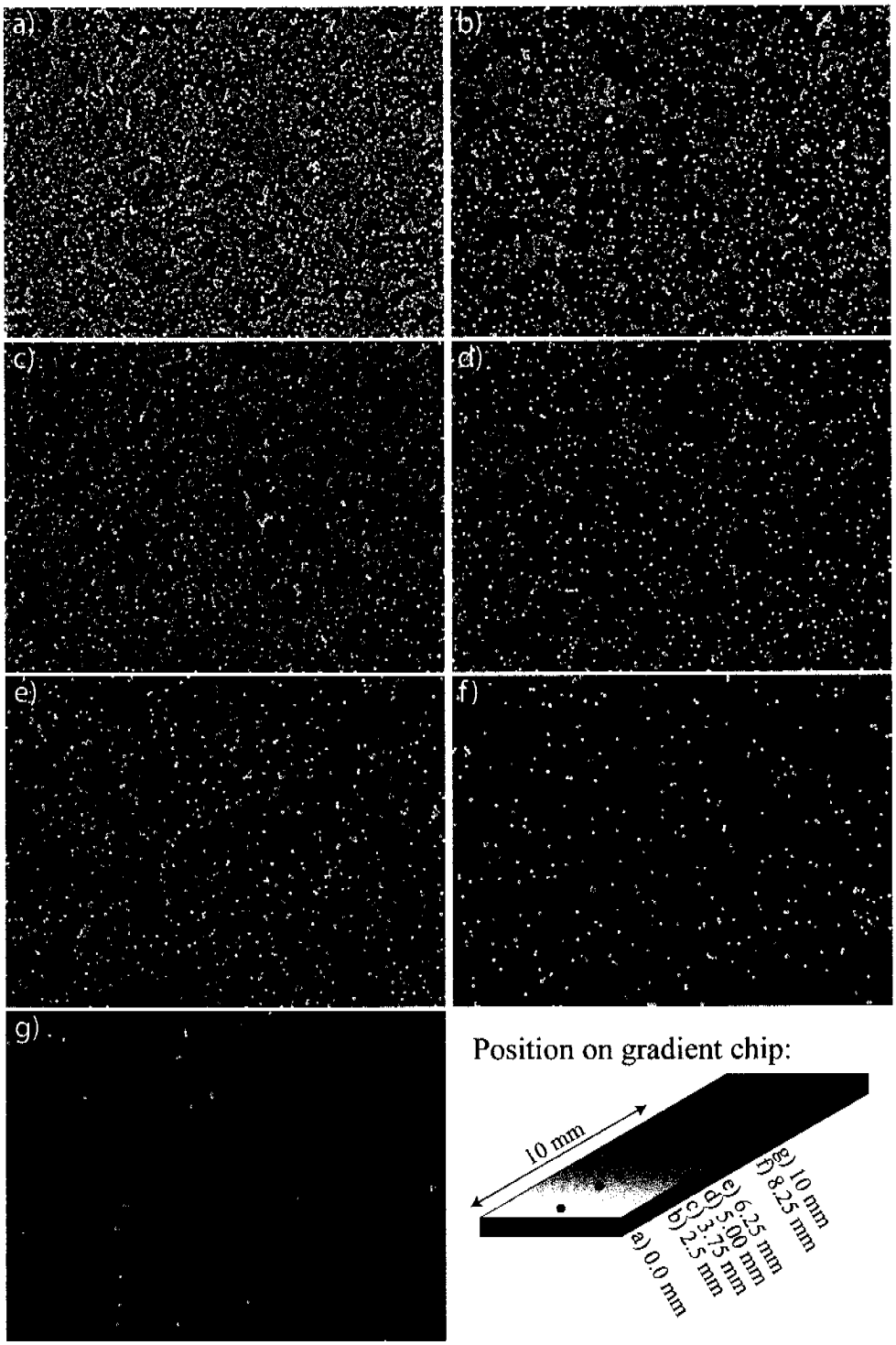

Figure 4.9: SEM images of a colloidal gradient and a sketch of the position of these images on the 1 *cm* gradient. Particle size was 73 *nm* and a particle concentration of 0.002 *wt*% was used in a pure water suspension. The suspension was slightly stirred during the dip-coating process, which lasted for 30 *min* at a designed immersion profile. The immersion profile was set to $x(t) = a(t-u)^2$, where $x(t)$ is the position on the gradient at the time t, which was running from 0 to $1800s$, $u = -100s$ (a parameter needed only for technical reasons) and $a = -3x10^{-6}m/s^2$.

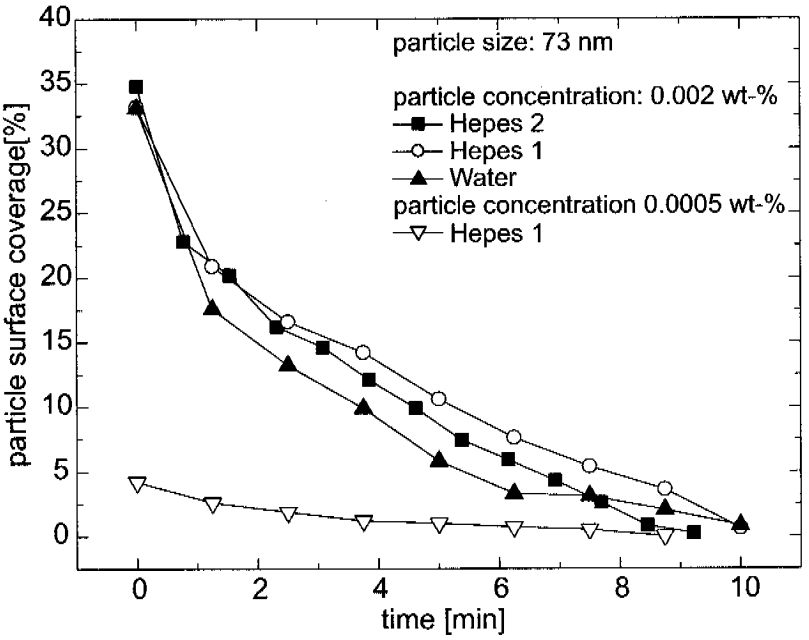

Figure 4.10: Colloid coverage of selected 1 cm gradients as a function of position on the gradient. Statistical evaluation of SEM images from different positions on the colloidal gradients yields the colloid coverage over the whole gradient. Particle suspensions with 0.002 *wt%* 73 *nm* silica particles were used in different solvents. There is no significant difference between Hepes 1 and 2 buffered suspensions and water suspensions (which were at pH 9.9). The end coverages reached values between 32-37%. The end coverage was measured in the area below the "immersion mark" indicated in Fig. 4.8. This explains the fact, why this first point (at 0 *cm*) is slightly higher than expected from the other values on the gradient, which lie on a rather straight line. If particle concentration was 4 times lower than for the first 3 experiments, the end coverage was significantly lower (around 5%), but the gradient still shows very linear behavior but in a narrower coverage range.

To check the exact evolution of the particle concentration profiles, SEM images were analyzed and statistical examination of these images with an imaging software yielded the particle concentration as a function of the position on the gradient. Some of this data is shown in Fig. 4.10. It is observed that indeed the particle gradients evolve nearly linearly over the whole 1 *cm* gradient. The gradient can be expanded to 2 *cm* by simply adopting the parameters such that instead of 10 *mm*, 20 *mm* will be dip-coated during the 1800 *s*. The value for the highest particle coverage (at 0 *cm*) is taken within the area below the "immersion mark" (see Fig. 4.8) and is therefore a little higher than one would expect from the extrapolation of the other values. This first value can be considered the particle coverage near the jamming limit and in this work was found to be in the range of 32-37%. This value is considerably lower than the theoretical value of 54.7%. For one, in the theoretical model

no electric double layer is taken into account, which must be added to the particle diameter. On the other hand, capillary forces disturb the pattern formation to some extent near the jamming limit, such that statistical analysis underestimates the true particle coverage. In Fig. 4.10, there is no clear distinction visible between particle arrays obtained in water, Hepes 1 (10 mM salt) and Hepes 2 (160 mM salt). This was to be expected for most of the particle gradient, since the shielding of the charge of the particles is not as crucial (as long there is sufficient charge) in this process. The negatively charged silica particles (whose charge is shielded more or less by the different salt concentrations in the suspension) will still adsorb to the surface and as long the coverage is not near the jamming limit of the particle layer, the situation is similar for water, Hepes 1 or Hepes 2 suspensions. However, near the jamming limit (at distance 0 in Fig. 4.10), differences were expected between the three different suspensions, because the jamming limit is affected by the salt concentration of the suspension. Indeed, in Fig. 4.7, such differences between different ionic strength suspensions were observed in situations were homogeneous samples were prepared without any stirring. While in our gradient experiments such differences were also expected, they were not observed in a significant extent (Fig. 4.10). One of the reasons for this is the fact, that Hepes 2 suspensions did show considerably more clustering effects not only due to capillary forces but also because the high salt content in this suspension makes the suspension weak in terms of colloidal stability. The clustering effects on the sample lead again to a slight under-estimation of the true particle coverages. For comparison, in Fig. 4.10 a colloidal gradient with less distinct differences in particle coverages is shown. The particle concentration in this case was 4-times lower than that used for standard experiments (0.0005 $wt\%$ compared to 0.002 $wt\%$). As a consequence, even for relatively long particle adsorption times, only few particles adsorb and the observed end coverage was only 4.2%. However, even in this case, almost linear colloidal gradients could be achieved.

With the presented technique, we are able to produce colloidal gradients with adjustable properties in the mm to a few cm range. Depending on particle concentrations, particle sizes, the dip-coating speed profile, salt concentration and others, particle gradients can be produced in a straight-forward way. Importantly, this technique is not restricted in any way to specific materials (be it of the particle or the substrate). In fact, almost any metal oxide and colloidal particle combination will work with this approach. Since the surface is simply coated with a positively charged polyelectrolyte, the underlying material is of limited influence on the end-pattern

(as long as the IEP of the used substrate material is below pH 7). Furthermore, also the particle suspension only has to fulfill 2 basic requirements: it must be stable and carry enough charge on the particle to adsorb electrostatically with the positive charges of the surface. As shown before, the influence of salt (and pH, to some extent) in these experiments is limited because for the most part, particle adsorption takes place in a regime where only sub-monolayers are adsorbing and thus the Debye-length of the particles is less of a factor. Note also, that stirring of the suspension during the process has a distinct influence on the particle gradient formation. In Fig. 4.7, the adsorption behavior of suspensions as used later in the gradient production process was shown. There, even after 30 *min*, only few particles were adsorbed, while in our experiments with gradients, the same conditions (but with stirring!) led to much higher coverages. Without stirring, particle coverages on the surface reached not more than 5% (Fig. 4.7, while in case of the gradient experiments more then 30% coverage was obtained. This drastic difference is associated with depletion effects, that play an important role in this low-particle-concentration regime. Particle diffusion is limited without stirring and around the substrate, a depletion layer forms, which makes subsequent particle adsorption slower. Stirring, on the other hand, makes these depletion layers thinner and increases adsorption drastically.

To conclude, the above discussed possibilities make this approach a very versatile and simple way of producing large-scale, mostly material-independent colloidal gradients. Playing with factors such as colloid concentration in the suspension or dip-coating speed profile allows the production of any type of particle gradients (in this case linear) covering a range from very high colloid coverages (to around 40%) to very dilute coverages (below 1%).

4.3.3 Heat Treatment of Nanoparticle Gradients

The presented method offers another convenient way of changing the morphology of the produced particle gradients besides simply changing the particle size. Since the process was accomplished on a polyelectrolyte modified wafer chip using nano colloidal silica particles, this offers the possibility to subject the colloidal gradient to a heat treatment. Such a heat treatment will have two effects on the particle gradients. For one, all organic components which were used during the production of the gradient will be burned off and, secondly, the colloidal particles will start to

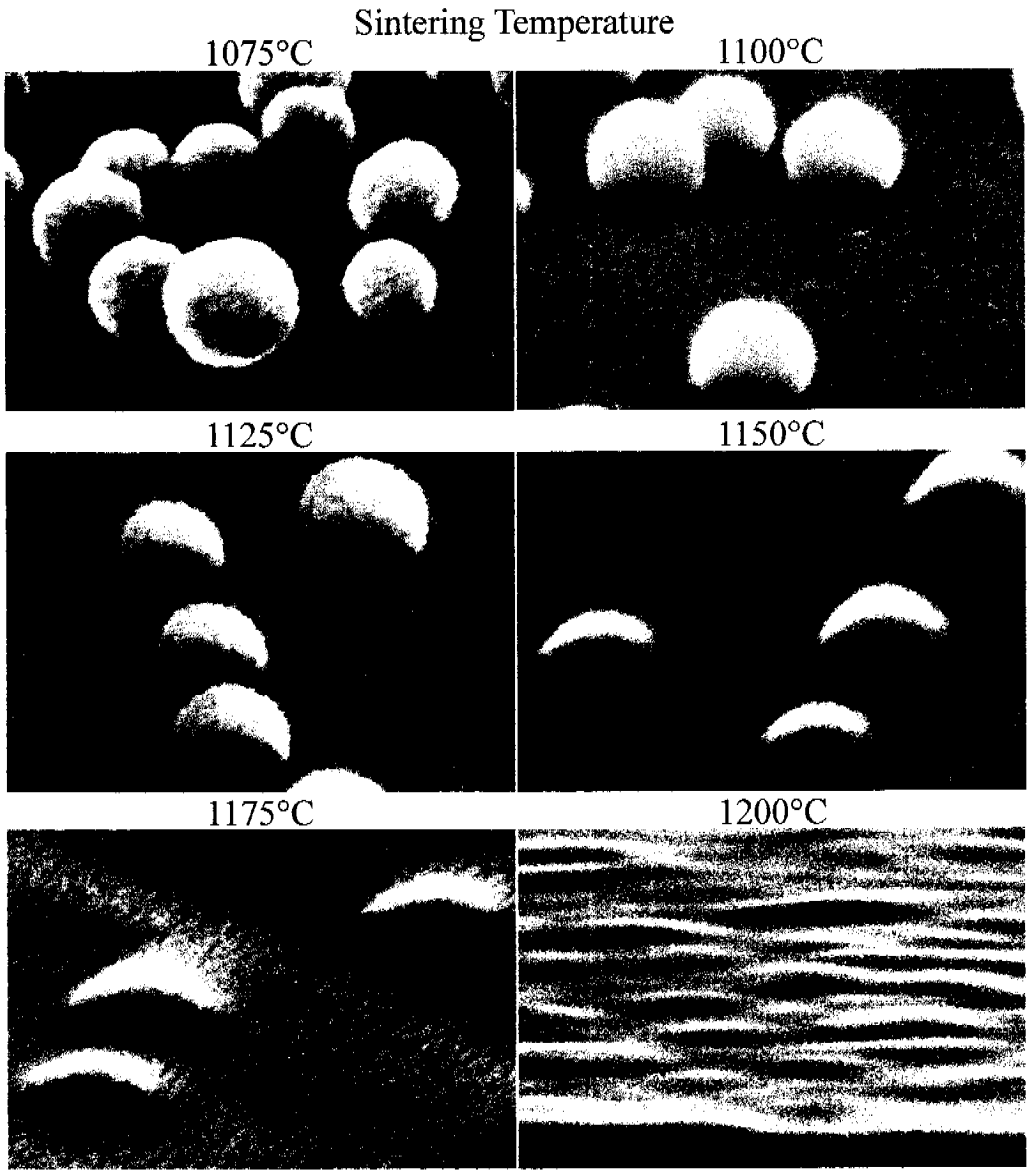

Figure 4.11: SEM images of heat treated colloidal silica particles (73 nm)(tilted view). Heat treatment consisted of heating the samples to the desired temperature (with about $10°C/min$), holding at the end temperature for 2 h and passive cooling (which took several hours). In the interesting temperature regime ($1075°C$ to $1200°C$), particle morphology changes continuously with increasing sintering temperature as observed in the images. Below $1075°C$, the temperature is not high enough to induce surface diffusion on the silica particles and no change in particle morphology was seen. Temperatures above $1200°C$ are sufficient to sinter the particles completely together with the Si-wafer surface, while at $1200°C$ traces of the particles are still seen.

sinter to the substrate. This sintering process will have two effects: on the one hand, mechanical stability of these gradients is increased considerably and — controlling the sintering conditions — the morphology of the gradients may be changed in a desired way. Fig. 4.11 shows the influence of such a sintering treatment on the evolution of the particle morphology. Surface diffusion in the silica nanoparticles was starting to be activated at temperatures around 1100°C. Below 1075°C there was no evidence of sintering and the particles remained in a spherical shape on the surface. With increasing temperature, the particles started to sinter to the surface. At 1100 and 1125°C the effects are not as dominant, but already there, a slight "neck-formation" was observed. This neck-formation is typical for the onset of the sintering process and is associated with the diffusion of surface atoms from the colloidal particle to the contact region of the particle with the substrate. The surface diffusion of atoms alone will not lead to shrinkage of the particles as observed for temperatures higher then 1150°C. At these temperatures also other diffusion mechanisms are active, such as volume diffusion (matter is transported from the bulk of the particle to the neck region) and diffusion along the particle-substrate interface. Both of these diffusion transport mechanisms are responsible for the shrinkage of the particles at higher temperatures. The driving force for these sintering / diffusion processes is related to the minimization of the free surface energy that can be achieved when the spherical particles gradually "minimize" their surface area. The end point of this process is reached for temperatures of more than 1200°C, where the particles loose their entity and have completely diffused into the surface. Fig. 4.11 visualizes these steps and depending on the sintering conditions, the morphology of the particle gradient can be tailored as desired (Fig. 4.12). The apparent "contact angle" of the particle with respect to the surface as determined from SEM image analysis is plotted versus the sintering temperature. A linear relation between the two is found which allows the precise tuning of the morphology of our particle gradients. Corresponding to this change in contact angle, a change in the height of the colloidal particles is observed. The particle height changes similar as the contact angle. At low temperatures, the particle height is equal to the particle diameter and decreases with increasing sintering time. At high temperatures (above 1200°C), the particle height decreases to 0 and the topography pattern vanishes. Thus, the heat treatment is an effective way of changing the particle topography on the gradient, from large, spherical particles to small "hill-like" structures at higher temperatures. During the heat treatment step in this work the temperature was always kept constant for

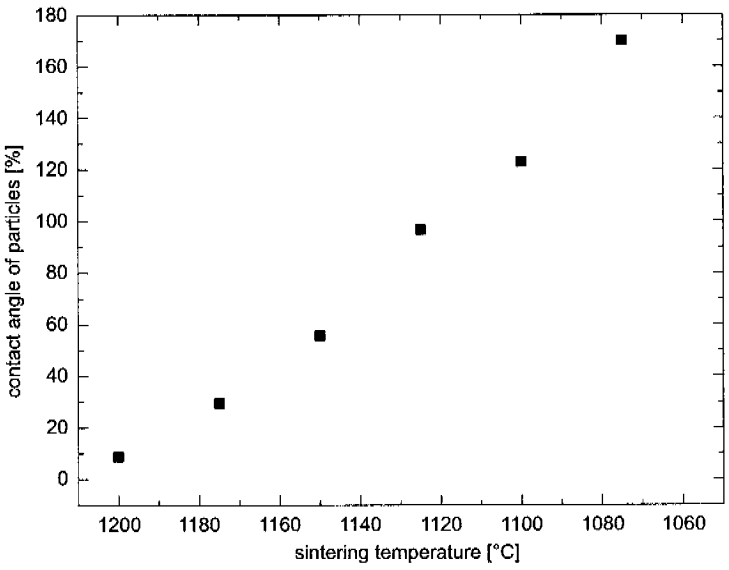

Figure 4.12: Graph of apparent contact angle of particle on a colloidal gradient versus sintering temperature. A linear relation between the contact angle (as determined from SEM images as presented in Fig. 4.11) and the sintering temperature is observed. Sintering at higher temperatures allows the spherical silica particles to diffuse much better into the surface and the spherical particles can decrease their large surface area efficiently at higher sintering temperatures. This surface area reduction upon sintering is the driving force for the sintering process and as soon as surface diffusion processes are activated, the particle morphology starts to change. At lower sintering temperatures, less diffusion processes are activated and consequently only little influence on the particle morphology is observed.

2 h at the chosen sintering temperature. Since the diffusion processes involved in this sintering process are time-dependent, similar results can be achieved by simply varying the sintering time instead of the temperature. The overall morphology of the particles is the product of sintering time and temperature.

Beside the adjustability of the morphology of the particle gradients that is offered by this sintering process, the mechanical stability is increased drastically: the particles are no longer simply adsorbed but densely sintered onto the surface. This fact makes these gradients also interesting for a number of applications, for which particle arrays were not previously suited, for example as molding materials in replication techniques. For example, choosing appropriate sintering conditions such that the contact angle of the particles is below 90° (particles appear as half-spheres on the sample) allows such samples to be used as templating material since no "undercutting" during a replication process (for example casting in PDMS) would be observed.

4.4 Conclusions

Combining the knowledge gained from particle adsorption experiments as a function of particle concentration, pH and ionic strength with a dip-coating process led to the development of a colloidal patterning method that allows the production of colloidal gradients with specifically adjustable parameters on *cm*-length scales. Oppositely charged particles and substrates and the electrostatic attraction between the two are used to produce colloidal gradients which are largely independent on particle and substrate material. The positive surface charge of the silica surface is introduced by a simple coating of the surface with a polyelectrolyte (PEI) and the silica particles already exhibit a negative surface charge at neutral pH. However, almost any material combination can be used in a similar way to produce this kind of particle gradient given the adsorption kinetics is known and can be controlled as shown in this chapter. In this work, silica nanoparticles were assembled in a gradient on a silicon wafer, but for example no significant difference is expected when the substrate material is changed to a different metal oxide.[4] Coating of the substrate with a titania layer prior to PEI adsorption, should for example not affect the gradient formation, but after the sintering process (which removes the organic components), a SiO_2-TiO_2 surface pattern could be produced, where the SiO_2 is present in form of a topography on a TiO_2 substrate. Such material combinations may be used in the future for further specific modifications. (See for example Chapter 5 in this thesis, how such a SiO_2-TiO_2 contrast may be modified and used).

The subsequent sintering process proved to be an efficient way of altering the morphology of the colloidal gradients. The globular shape of the adsorbed particles can be continuously changed depending on the exact sintering conditions. Furthermore, this heat treatment provides a good means of stabilizing the colloidal array on the surface by sintering the particles to the surface. Thus, mechanically stable, topographical gradients were produced using a versatile technique that may find applications in various fields due to their tunable properties.

A first example of how such particle gradients can be useful is shown in Fig. 4.13. There, rat calvarial osteoblasts (rco) cells were cultivated for 7 days on a particle gradient as shown in Fig. 4.9.[5] To achieve a more cell-friendly surface environment,

[4]Provided it has an IEP of less then 6

[5]Seeding denisty: 6000 $cells/cm^2$ in alpha-DMEM + 10% foetal bovine serum + 1% antibiotics medium, incubation for 7 days at $37°C$, 7% CO_2, 100% humidity

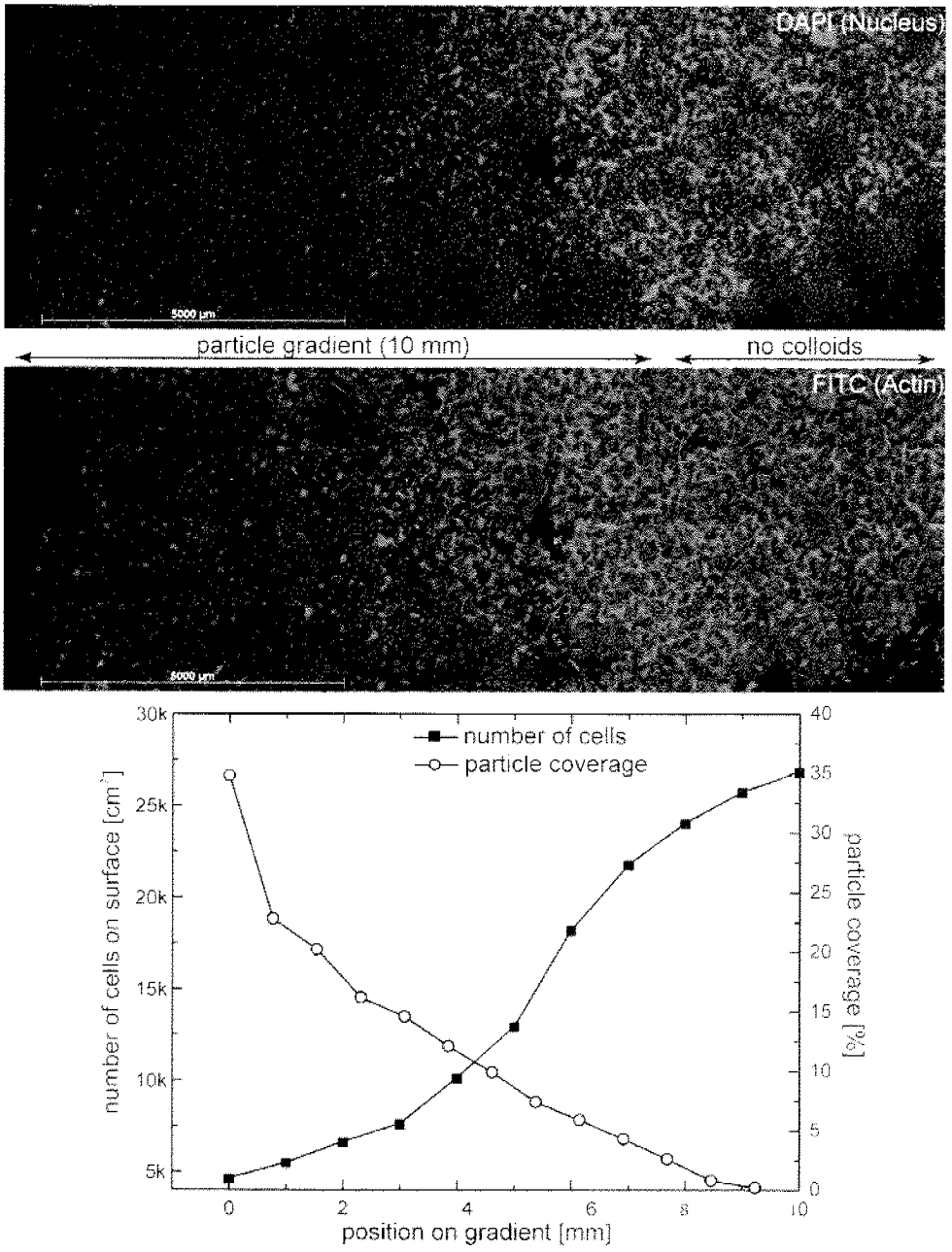

Figure 4.13: Fluorescent microscopy images of stained actin filaments (FITC) and cell nuclei (DAPI) on a particle gradient (0.002 *wt*% in H_2O). The particle gradient was uniformly coated with PLL-*g*-PEG/PEG-RGD, a polymer that introduces the RGD function to the particle gradient surface, a peptide sequence known to induce cells growth. At high particle surface coverages (to the left of the images), only few cells adhere and spread on the surface, while with decreasing particle density (moving to the right hand side of the fluorescent microscopy images) the number of cells increases significantly. Quantitative analysis (graph below the images) shows how indeed a reciprocal relation exists between particle surface coverage and the number of rat calvarial osteoblasts cells growing on the substrate.

the whole particle gradient was dipped in a PLL-*g*-PEG/PEG-RGD solution. The RGD-peptide sequence is end-grafted to the PLL-*g*-PEG copolymer[6] and is known to promote cell attachment by interacting with cell integrins.[16, 17] Fluorescent labelling of the actin filaments and the nuclei of these cells is shown in the top two fluorescent microscopy images. It is observed, that cell adhesion and spreading is largely reduced in areas where the density of particles on the surface is high (left side of fluorescent images). With decreasing particle density, the number of cells growing on the substrate increases significantly and reaches the highest number in the areas where no particles were on the surface (on the right hand side of the fluorescent images). The graph in Fig. 4.13 quantifies these results and indeed an inverse dependence of cell number with particle density is found. These results are rather surprising since osteoblast cells are generally known to adhere to rough surfaces ("rugophilia") rather than to flat substrates. Note, that these are first and promising results of cell biology experiments with this kind of colloidal gradients and more detailed studies are currently conducted in the course of another PhD giving insight into the adsorption behavior of osteoblast cells on such particle gradients. However, this experiment is a good example of how (particle) gradient surfaces will help in rapid screening tests or how combinatorial and diagnostic studies can be performed on a single sample in the future. The technique presented in this chapter may help fabricating suitable particle gradients for this kind of application in a straight-forward and customizable way.

[6]More information on PLL-*g*-PEG is given in Chapter 3 and 6

Bibliography

[1] Washburn, N. R., Yamada, K. M., Simon, C. G., Kennedy, S. B. and Amis, E. J. High-throughput investigation of osteoblast response to polymer crystallinity: influence of nanometer-scale roughness on proliferation. *Biomaterials*, **25**(7-8), 1215–1224, 2004.

[2] Karlsson, L. M., Tengvall, P., Lundstrom, I. and Arwin, H. Back-side etching - A tool for making morphology gradients in porous silicon. *Journal of the Electrochemical Society*, **149**(12), C648–C652, 2002.

[3] Elwing, H., Welin, S., Askendal, A., Nilsson, U. and Lundstrom, I. A Wettability Gradient-Method for Studies of Macromolecular Interactions at the Liquid Solid Interface. *Journal of Colloid and Interface Science*, **119**(1), 203–210, 1987.

[4] Lee, J. H., Kim, H. G., Khang, G. S., Lee, H. B. and Jhon, M. S. Characterization of Wettability Gradient Surfaces Prepared by Corona Discharge Treatment. *Journal of Colloid and Interface Science*, **151**(2), 563–570, 1992.

[5] Liedberg, B. and Tengvall, P. Molecular Gradients of Omega-Substituted Alkanethiols on Gold - Preparation and Characterization. *Langmuir*, **11**(10), 3821–3827, 1995.

[6] Morgenthaler, S., Lee, S., Zurcher, S. and Spencer, N. D. A Simple, Reproducible Approach to the Preparation of Surface-Chemical Gradients. *Langmuir*, **19**(25), 10459–10462, 2003.

[7] Kunzler, T., Drobek, T., Sprecher, C., Schuler, M. and Spencer, N. Fabrication of material-independent morphology gradients for high-throughput applications. *Applied Surface Science*, **in press**, 2006.

[8] Park, J.-H., Choi, W., Koo, H. and Kim, D. Colloidal Photonic Crystal with Graded Refractive-Index Distribution. *Advanced Materials*, **17**(7), 879–885, 2005.

[9] vonÂ Freymann, G., John, S., Kitaev, V. and Ozin, G. Enhanced Coupling to Slow Photon Modes in Three-Dimensional Graded Colloidal Photonic Crystals. *Advanced Materials*, **17**(10), 1273–1276, 2005.

[10] Abkarian, M., Nunes, J. and Stone, H. A. Colloidal Crystallization and Banding in a Cylindrical Geometry. *J. Am. Chem. Soc.*, **126**(19), 5978–5979, 2004.

[11] Zhang, J., Xue, L. and Han, Y. Fabrication of Gradient Colloidal Topography. *Langmuir*, **21**(13), 5667–5671, 2005.

[12] Li, Y. and Han, Y. Optical Intensity Gradient by Colloidal Photonic Crystals with a Graded Thickness Distribution. *Langmuir*, **published on web**, 2006.

[13] Pericet-Camara, R., Papastavrou, G., Behrens, S. H., Helm, C. A. and Borkovec, M. Interaction forces and molecular adhesion between pre-adsorbed poly(ethylene imine) layers. *Journal of Colloid and Interface Science*, **296**(2), 496–506, 2006.

[14] Hinrichsen, E. L., Feder, J. and Jossang, T. Geometry of random sequential adsorption. *Journal of Statistical Physics*, **44**(5 - 6), 793–827, 1986.

[15] Evans, J. W. Random and Cooperative Sequential Adsorption. *Reviews of Modern Physics*, **65**(4), 1281–1329, 1993.

[16] Ruoslahti, E. RGD and other recognition sequences for integrins. *Annual Review of Cell and Developmental Biology*, **12**, 697–715, 1996.

[17] Schuler, M., Owen, G. R., Hamilton, D. W., De Wilde, M., Textor, M., Brunette, D. M. and Tosatti, S. G. P. Biomimetic modification of titanium dental implant model surfaces using the RGDSP-peptide sequence: A cell morphology study. *Biomaterials*, **27**(21), 4003–4015, 2006.

CHAPTER 5

Self-assembly of Nanoparticles on Microstructured Wettability Contrasts

5.1 Introduction

In the introductory chapter, the two main forces that act during the formation of a nanoparticle array on a patterned surface were introduced: on the one hand, the particles interact with the surface pattern in suspension (most dominantly by electrostatic forces but also others), then, during the drying step, capillary forces evolve between the particles on the surface, which influences the colloidal pattern formation. In this chapter, a colloidal patterning technique is presented, that relies on the latter forces to self-assemble nanoparticles on a structured surface. The main idea is to produce a surface pattern, which reduces particle-surface interaction in suspension to avoid the (electrostatic) adsorption of particles to the surface and at the same time exhibits a distinct hydrophobicity contrast. This hydrophobicity contrast is able to direct the self-assembly process of the nanoparticles during the drying step. Capillary forces provide the driving force for this self-assembly process and are responsible that the hydrophobic structures are particle-free due to de-wetting during the drying step and particle assemblies form on hydrophilic structures. During the course of this thesis, several groups have published similar concepts of arranging colloidal particles on surfaces with a wettability contrast.[1–4] This contrast can be produced in a number of different ways, basically every patterning method that allows the tailored chemical functionalization of a surface (photolithography with a subsequent chemical functionalization step,[2, 3] softlithography techniques,[1, 4]

selective etching among other) can be used to produce a suitable surface pattern as long as the pre-requisites of such a pattern are met. It is also noteworthy, that capillary forces may also be used to assemble particles on a topography contrast.[5 7] In such a case, nanoparticles are dragged into the grooves and holes during the drying step and particle assemblies can be formed as well. For a more detailed overview of current work in other groups refer to section 2.5.3 of the introductory chapter. Here, an approach is chosen which uses standard photolithography and a subsequent reactive ion etching step to produce a metal oxide contrast (of SiO_2 and TiO_2). This contrast can then easily be turned into a hydrophobicity contrast by specifically modifying the titania structures with a hydrophobic alkane phosphate SAM.

5.2 Experimental

In the Selective Molecular Assembly Patterning Process (SMAP), which was developed by Roger Michel during his PhD thesis in our Laboratory,[8] a photoresist film is spin-coated onto two transparent sputter-coated metal oxide layers (a 100 nm SiO_2 layer followed by a 12 nm TiO_2 layer on top). The desired geometrical features are transferred into the photoresist using standard photolithography (Fig. 5.1a). This pattern is then locally etched through the TiO_2 by reactive ion etching (RIE) (Fig. 5.1b). After removal of the photoresist (and cleaning of the sample), the SiO_2/TiO_2 metal oxide pattern is immersed in an aqueous solution of 0.5 mM ammonium dodecyl phosphate ($CH_3(CH_2)_{11}PO_4(NH_4)_2$) ($DDPO_4$)[9] for 48 h and rinsed with high-purity water. This produces a well-defined hydrophobic self-assembled alkane phosphate monolayer (SAM) specifically adsorbed on the TiO_2 patches while leaving the SiO_2 areas entirely uncovered. By this process, a wettability contrast pattern is achieved with the hydrophobic SAM covering the TiO_2 regions and the hydrophilic silica areas in the background. For a more detailed experimental section on SMAP sample production, please refer to Chapter 3.4.

Colloid adsorption experiments on 1 cm^2 samples patterned with the SMAP technique were carried out under controlled conditions to study the parameters that govern the colloidal self–assembly processes. Particles were either adsorbed by drying a 50 μl drop of Hepes 1 buffered colloid suspension of 0.1 or 0.01 $wt\%$ particle concentration under ambient conditions (10 mM ionic strength (NaCl) and pH = 7.4)

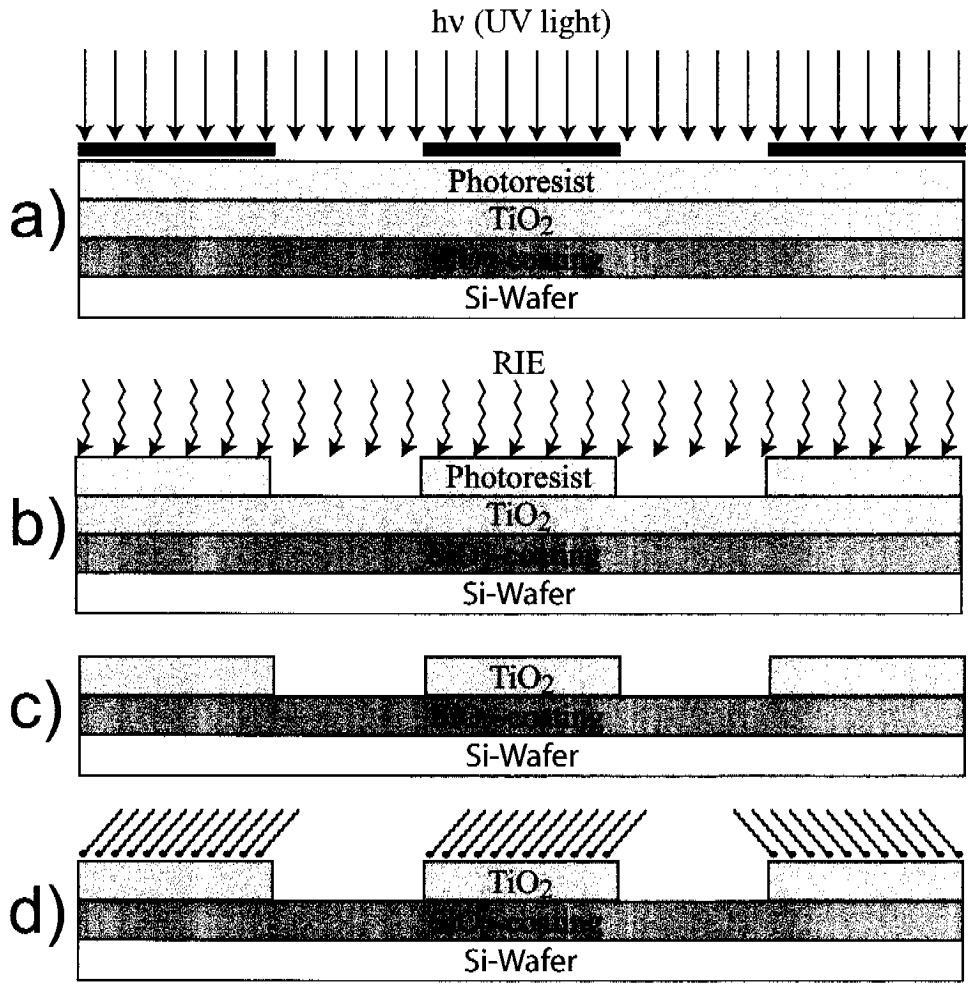

Figure 5.1: Schematic illustration of the Selective Molecular Assembly Patterning Process (SMAP) process used to achieve a distinct wettability contrast: a) layered substrate before standard photolithography. b) reactive ion etching of the photoresist contrast to etch through the TiO_2 top layer. c) Lift-off of the photoresist. d) Selective chemical modification of the TiO_2 surface area by an alkane phosphate SAM. Sketches are not drawn to scale.

(drop drying) or by immersing the sample into the suspension for 15 min, removing it from the suspension with a controlled speed, rinsing it with Millipore water and blowing it dry under nitrogen flow (dip coating). Drop dried samples were not rinsed before scanning electron microscopy (SEM) investigations. All high resolution SEM investigations were performed on samples sputter-coated with a Pt-film of approximately 4 *nm* thickness.

5.3 Results and Discussion

5.3.1 Wettability Contrast Characterization

The first colloidal patterning approach developed in this thesis uses a hydrophobicity contrast created by the Selective Molecular Assembly Patterning Process (SMAP).[8] By this process, a wettability contrast pattern is achieved with hydrophilic silica pattern and a hydrophobic SAM covering the TiO_2 background. This hydrophobicity contrast serves later as a template for the self-assembly of nano colloids by capillary forces in controlled drying and dip-coating experiments.

In a first set of experiments the contact angle of homogeneous substrates was checked in order to confirm the high contact angle of a $DDPO_4$ self-assembled monolayer and the relatively low contact angle of the silica substrate. The results of these experiments are summarized in Fig. 5.2. On a smooth titania surface ($R_a = 0.44\ nm$[10]), an advancing contact angle of 109.4° was found and this contact angle only decreased little over time (after 20 days of storage under ambient conditions, the contact angle was 98°). On silica substrates, a very low advancing contact angle of below 10° was found. These results agree well with those reported earlier from our group.[9] In Fig. 5.2, the advancing and receding contact angle observed on a patterned SMAP chip are shown as well. In this case, samples were produced containing 60 by 60 micron silica squares in a $DDPO_4$ background. It can be seen, that the advancing contact angle is similar to that of a homogeneous $DDPO_4$ surface, whereas the receding contact angle is significantly lower than that observed for a pure $DDPO_4$ surface. To explain this behavior, a schematic overview of how contact angle experiments are conducted is given in Fig. 5.3. An "advancing" contact angle refers to a situation depicted in Fig. 5.3a). Liquid (ultrapure water) is squeezed through the nozzle and the drop increases in size, the angle Θ measured is called advancing contact angle

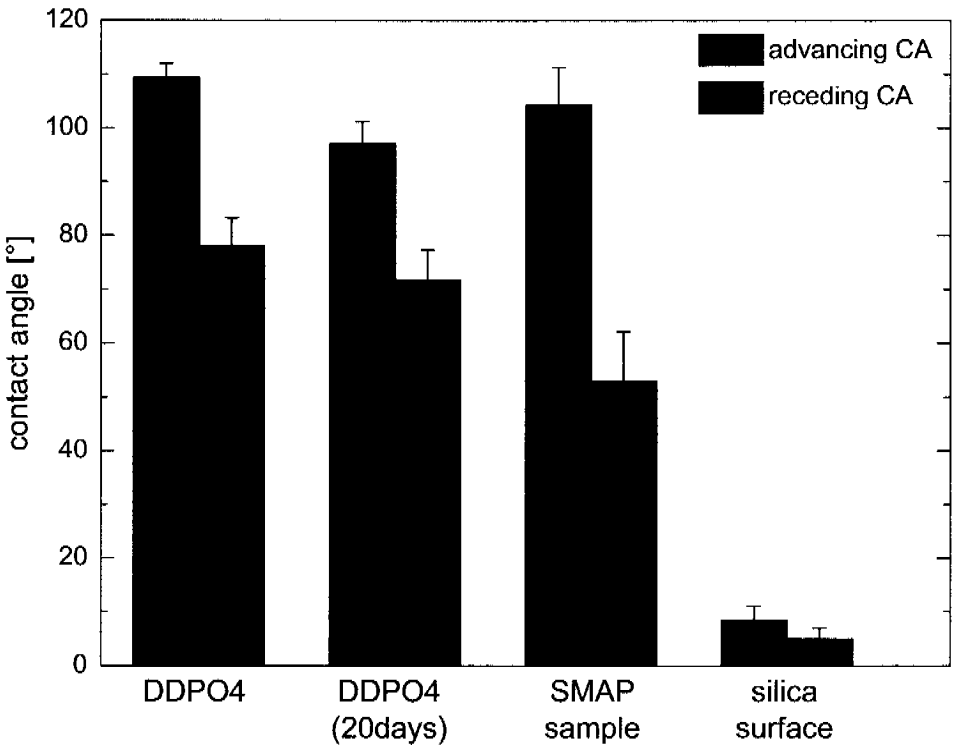

Figure 5.2: Graph of advancing and receding contact angles of different substrates used in this work. Dodecyl phosphate self-assembled monolayers on titania exhibit contact angles of 109.5°. These SAMs are stable upon storage under ambient conditions, the contact angle only decreases to about 98°. Silica surfaces generally exhibit rather low contact angles (below 10°), representing their hydrophilic character. The contact angle of a SMAP chip (made up of silica squares of 60 by 60 microns in a $DDPO_4$ background) shows high advancing contact angles but much lower receding contact angles due to pinning of the water droplet on the patterned surface.

Θ_a. If the liquid is sucked back into the nozzle, the drop decreases in size and the receding contact angle Θ_r is observed. The difference between Θ_a and Θ_r is called contact angle hysteresis. As discussed in Chapter 2.3, this difference stems from surface irregularities due to composition heterogeneities, surface roughness or other imperfections as well as the wetting of the surface with a water film[1]. Thus, the more such irregularities a surface contains and the better the surface can be wetted, the higher the contact angle hysteresis will be. A patterned sample obviously contains many "surface irregularities" — the pattern — and therefore it is expected that the contact angle hysteresis is larger on a patterned sample. Indeed, the contact angle

[1]The wetting of the surface occurs during the measurement of the advancing contact angle and if the receding contact angle is measured, the drop recedes often on a film of water which changes the contact angle compared to the dry sample

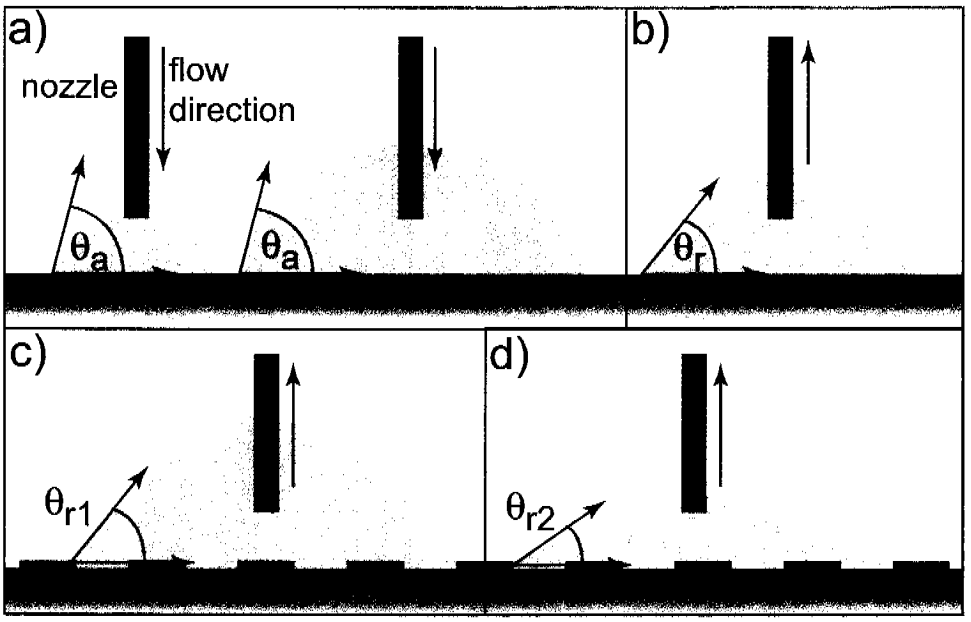

Figure 5.3: Schematic illustration of contact angle measurements: a) advancing contact angles measured by increasing the drop of water on the surface by an out-flow of water through the nozzle. b) receding contact angle observed by decreasing the drop on the surface. c) receding contact angle on a patterned sample. Red squares indicate a hydrophobic area, black squares are hydrophilic. The water drop contact line is pinned at an edge of a hydrophilic area and a given receding contact angle is observed (Θ_{r1}). d) If water is sucked back through the nozzle, the contact line stays in place, which leads to a decrease in the receding contact angle (Θ_{r2}). If the pinning line reaches the contact angle Θ_{r2}, the drop "jumps" to the next hydrophilic spot and reaches again Θ_{r1}.

hysteresis is much larger on the patterned sample then on the homogeneous ones, as shown in Fig. 5.2. The mechanism leading to the larger contact angle hysteresis is depicted in Fig. 5.3c) and d). The decreasing drop (water is sucked back through the nozzle), is "pinned" at pattern edges and the contact angle therefore decreases until the drop "jumps" back to the next pattern on the surface. Overall, this results in a smaller receding contact angle compared to a homogeneous substrate. The same idea holds, if a drop is increased and the advancing contact angle is measured. Even though roughly a fourth of a patterned sample consists of hydrophilic surface patches, the overall contact angle measured is still more or less the same as if the surface only was hydrophobic. Again, the increasing drop is pinned at the pattern edge and the advancing contact angle increases until the drop moves forward to the next pattern edge.

As such, contact angle measurements only offer limited insight into the wetting behavior of a patterned sample. A related technique, microdroplet density measure-

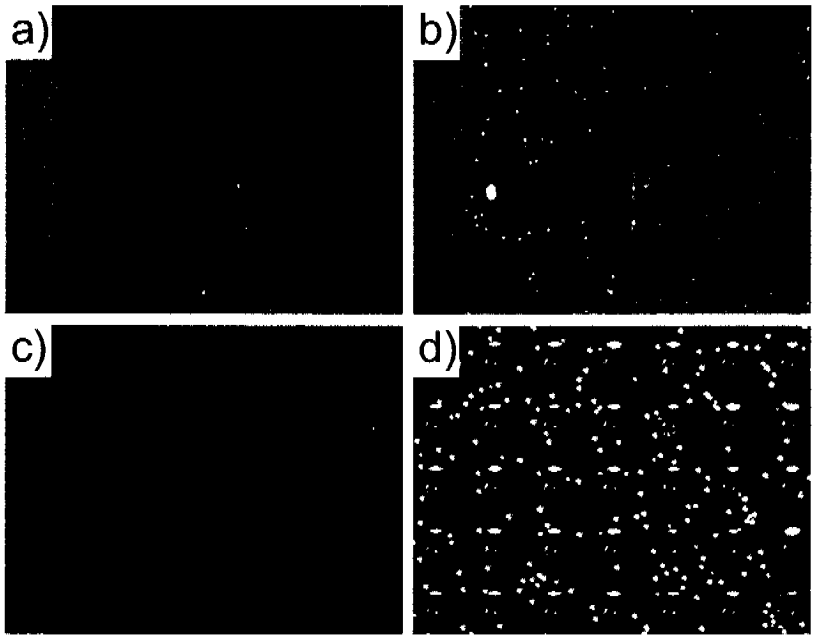

Figure 5.4: Microdroplet density measurements illustrating the wettability behavior of a SMAP surface. Images are of low quality because they are still shots from movies showing the condensation of water on a SMAP sample. On all samples, structures consist of SiO_2 and TiO_2 covered with a $DDPO_4$ SAM is on the background. a) and b): SMAP sample of lines showing that the water condenses preferentially on the hydrophilic structures. a) SMAP sample before water condensation takes place. b) Lines are completely filled with water after condensation, only few drops (bright spots) are visible on the background. Furthermore, the spherical shape of the drops on the background indicates that indeed the background surface is very hydrophobic. c) and d): 60 by 60 μm squares before (c) and after (d) water condensation. Again, the squares are completely filled with water, a drop sits on each square exactly limited by the edges of the square pattern. A few drops also be observed on the hydrophobic background.

ment, allows the qualitative analysis of the wetting behavior of a patterned sample. With this technique, the condensation behavior of water vapor on a patterned sample is observed. The sample is cooled on a microscopy stage indirectly (by means of ice-cooled water flowing through the stage upon which the sample is positioned), which allows water droplets to condense on the patterned sample. Depending on its wetting behavior, condensation takes place on different areas of the pattern and evolves differently. Fig. 5.4 shows two examples of microdroplet density measurements on line a) and b) and square structures c) and d). In both cases the structures consist of hydrophilic SiO_2, while the titania background of the samples is covered with a hydrophobic $DDPO_4$ SAM. Before condensation takes place, the pattern contrast is already visible in the light microscope due to interference effects and the

material contrast (Fig. 5.4a) and c). As soon as cooled water is circulated through the microscope stage, water vapor starts to condense on the samples. Condensation will start at surface imperfections (on a patterned sample mainly on edges) and continuously wet the sample. Preferentially, however, hydrophilic areas will be wetted in the progress of the experiment. Hydrophobic regions (the background in Fig. 5.4) will not get wetted for as long as possible. Thus, as observed in Fig. 5.4b) and d), the patterned structures are wetted completely while the background only shows little condensation of water. And if water does condense on the background, it has a very spherical form, indicating that the background is very hydrophobic. Water condensing on the pattern, however, immediately wets the pattern and fills the whole structure. As soon as the edge of the hydrophilic pattern is reached, the spreading is stopped and additional condensing water accumulates on the pattern. This leads to a situation as observed in Fig. 5.4d), where large drops of water are confined on the 60x60 μm squares. With these experiments it can be confirmed that SMAP samples exhibit a distinct hydrophobicity contrast between the SiO_2 structures and the very water repellant $DDPO_4$ coated TiO_2 background.

5.3.2 Nano Colloidal Arrays on Wettability Contrast Pattern

Drop Drying on Wettability Contrast Pattern

There are two basic ways of producing nano colloidal arrays of particles on a wettability contrast pattern: dip-coating and drop-drying. In the former case, a patterned sample is dipped into the particle suspension and withdrawn at a known and constant speed, while in the latter case, a defined amount of particle suspension is brought onto a patterned substrate and the solvent is given time to evaporate. Drop drying is straight-forward, fast[2] and easy but has some obvious drawbacks. For one, a drying drop on a surface is an uncontrolled situation in the sense that the drying front is ill-defined and the progression of the drying front is difficult to control. In Fig. 5.5 the different steps, which might be involved in the drying process of a drop on a patterned sample are sketched. A drop of suspension is placed on a patterned sample. The drop will move into a position with a certain contact

[2]In the sense, that a large number of samples can be produced in parallel. Evaporation of the solvent, however, takes several hours / days.

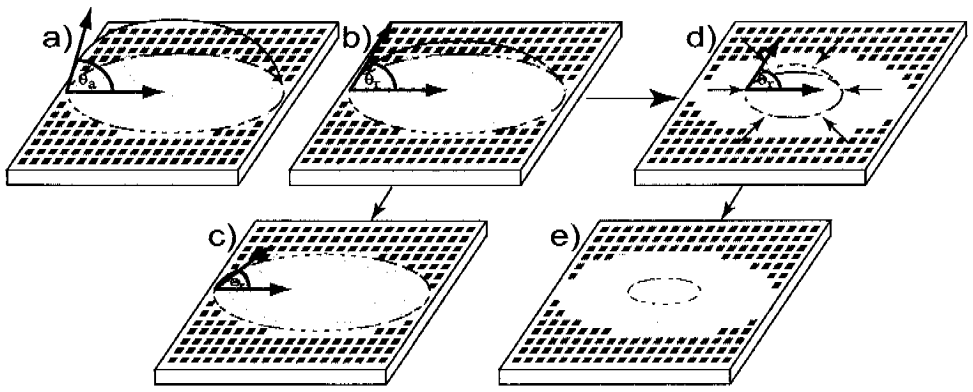

Figure 5.5: Sketch of the processes during a drop-drying experiment. A drop of suspension is placed on a patterned substrate adopting a given contact angle (advancing contact angle) Θ_a (a). b) evaporation of the solvent starts, the drop maintains its contact line on the substrate, which must lead to a decrease of the contact angle until the receding contact angle is reached Θ_r. Depending on the exact value of Θ_r, two situations may occur: c) if Θ_r is very low, the drop remains fixed and particles start to move towards the edge of the drop and a "coffee ring" starts to form (which is nothing but a colloidal crystal in the edge regions of the particle). d) if Θ_r is larger, the drop will start to shrink and decrease. In this case, the drying front moves over the pattern and the hydrophilic squares are filled with suspension. In this region, colloidal arrays are able to form. e) but also in this case (rather large Θ_r), at some point a colloidal crystal will form (given the particle concentration is sufficient) and the drop will dry off.

angle Θ_a (Fig. 5.5a). This contact angle is equivalent to the advancing contact angle that one would measure on that pattern. Then, the solvent is slowly evaporating and after some time, a situation as depicted in Fig. 5.5b) is reached. The contact angle decreases to a value Θ_r, which is identified with the receding contact angle. Then, depending on the experimental conditions, different situations may occur. For example, the drop can uniformly shrink (as shown in Fig. 5.5d) and leave hydrophilic squares filled with suspension behind (indicated by the light blue color of the squares). These squares will after drying of the solvent — then be filled with particles. However, it is also possible that the edge of the drop stays pinned and the solvent evaporates further (situation in Fig. 5.5c). In such a situation, a "coffee ring" will form, where the particles in the suspension are dragged towards the edge of the drop. In this coffee ring, a colloidal crystal will form and the substrate is covered by this crystal, which will obstruct the formation of a colloidal array in this region. But also in the case where the drop was shrinking uniformly a similar situation will occur at some point and a colloidal crystal will start to form (sketched in Fig. 5.5e). In most situations, where drop-drying experiments were conducted in this work, a situation as depicted in Fig. 5.5e) was observed: the drop of suspension

first looses some of the solvent, then uniformly shrinks. During this uniform shrinkage, the pattern is filled with suspension where the contact line of the drop passes and a colloid pattern is achieved. However, since we have only limited control over the speed with which the drop moves over the sample during this phase (for example by changing the evaporation rate via temperature), it is possible that the pattern is not completely filled with particles. Then, at some point, a colloidal crystal will form on the pattern and cover the remaining substrate. If particle concentration is low, the colloid crystal is only present in the edge region and the middle of the drop is depleted of colloids (just as sketched in Fig. 5.5d) and e). In this middle region, the pattern can again be filled with colloids but this situation offers little control over particle deposition.

The effects described in Fig. 5.5 were observed experimentally by SEM imaging of SMAP-patterned samples. In Fig. 5.6, a selection of SEM images is presented. If a 73 nm silica suspension with a relatively high particle concentration (1 $wt\%$) is used, drying of a 50 μl drop of that suspension will produce a colloidal crystal over a substantial region of the sample (Fig. 5.6a). A region in the middle of the drop was depleted of colloidal particles (indicated by the circle), since the particles were dragged towards the edge of the drop during the drying process. Crack formation in the crystal is observed, a very common and almost unavoidable problem in colloidal crystal formation.[11] These cracks form — similar to cracks in dried-out landscapes or cracks in old oil paintings — by capillary pressure, which is released by the formation of a crack. In some parts in Fig. 5.6a), pieces of the colloidal crystal are broken away during the sample preparation steps after drying, revealing the patterned surface below (two of them are indicated with arrows). Interestingly, a colloidal pattern also forms below the colloidal crystal, however, the morphology differs completely from colloidal arrays formed by capillary forces during drying. In fact, it is possible to remove the whole colloidal crystal and reveal the patterned colloidal arrays on the surface pattern which where formed below the colloidal crystal. To elucidate this different behavior, in Fig. 5.6b) and c) two drop-dried samples are shown, where parts of the colloidal crystal are still visible. The right hand side (red) in this image was initially covered by a colloidal crystal, while the left hand side (green) was not. This situation corresponds to the sketch in Fig. 5.5d), where the drop was retracting for some distance before the movement stopped, the drop was pinned and a colloidal crystal was formed. In the green region, the drop moved over the sample during drying and the hydrophilic squares remained filled with suspension after the drying

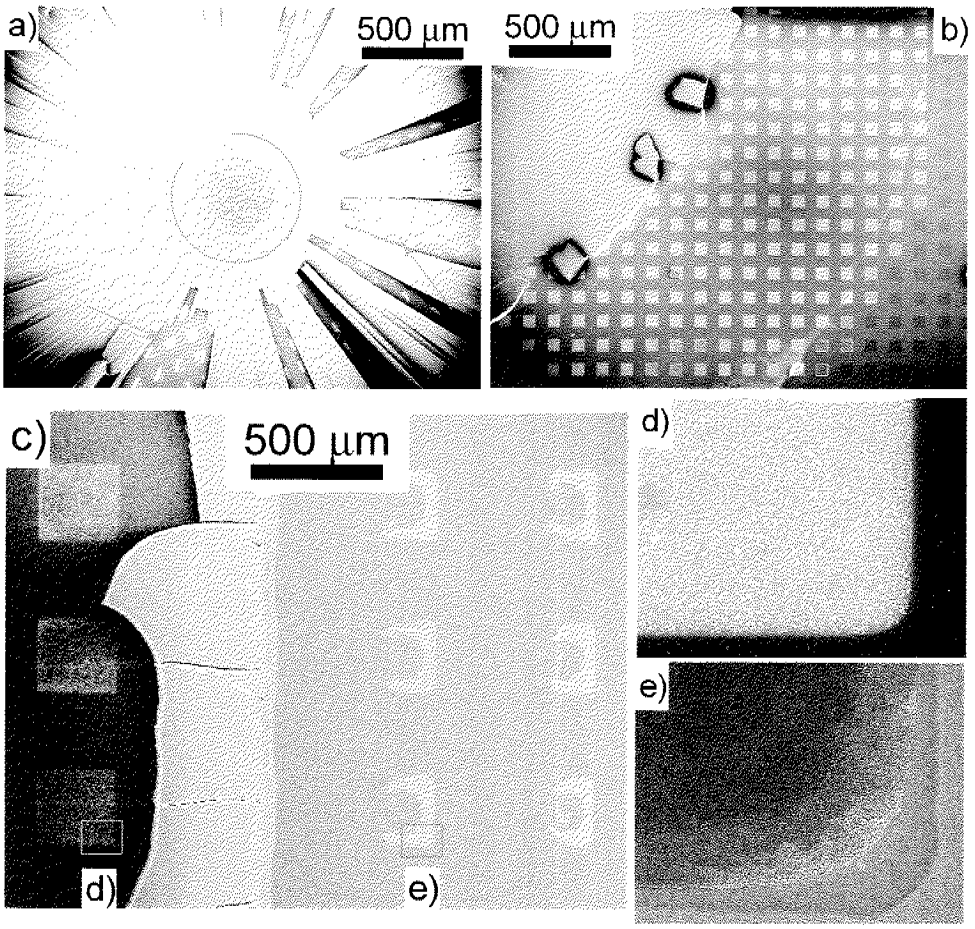

Figure 5.6: SEM images of drop-dried 73 *nm* silica particles on a 60x60 *µm* square SMAP pattern. 50 *µl* drops of Hepes 1 buffered suspension were dried on the pattern at slightly elevated temperatures (50°*C*). Particle concentration was 1 *wt%* for a) and 0.1 *wt%* for all other images. a) colloidal crystal formed by drying a drop of suspension on a SMAP pattern. The outside of the crystal is much thicker (coffee ring effect), while the inside (red circle) is depleted of particles. The arrows highlight two of several regions were the colloidal crystal was broken away during sample handling after drying. b) drop drying experiment of a more diluted drop of suspension. An outer region formed, over which the drop was passing while the drop was shrinking. (green highlighted area). At some point, the shrinkage of the drop ceases and a colloidal crystal is again formed (red area). c) shows a similar region but at higher magnification. Parts of the colloidal crystal are still visible, the rest — originally covering the whole left hand side — was broken off. Red and green highlighted areas have the same meaning as in b). d) and e) show inserts of c) revealing the completely different colloidal arrays that form depending whether the particle assembly was formed by capillary forces during drying (e) or by adhesion of colloidal particles to the silica squares and not the $DDPO_4$ background below the colloidal crystal (d).

front has passed. The hydrophobic background was dewetted, thus no suspension was able to dry on the background. The particles on each square finally dried off and the squares are filled with colloidal silica particles. However, if the drying front moved too fast, the squares could not be filled completely and only partially filled squares were observed (Fig. 5.6c), right hand side and insert e). In this insert, it can be observed that indeed capillary forces were responsible for the pattern formation, since the packing of the colloidal particles is very tight and also multilayers of particles were produced. In contrast, Fig. 5.6d) shows a square filled with particles that was previously hidden below a colloidal crystal. Also in this case, the colloidal silica particles were adsorbed selectively on the hydrophilic silica squares, but obviously the governing force were not of capillary origin. Rather, the adhesion of the particles to the squares is favored compared to the hydrophobic background and upon the removal of the colloidal crystal, which was above that pattern, some silica particles remain adsorbed to the silica pattern, while no particles were adhering to the $DDPO_4$ background. The reason for this fact is not completely understood but it is most likely attributed to the hydrophilic character of the silica squares. During drying of the colloidal crystal, the silica surface will be in contact with the silica particles (because both are equally wettable) and the particle will therefore remain in contact with the silica surface. It is also possible, that salt in the suspension dries at the particle necks and particles are "glued" to the silica squares (and each other. The hydrophobic $DDPO_4$ background on the other hand will be de-wetted during drying of the crystal and no connection between particles and background is established. Interestingly, this effect can be used to form different structures than achieved by the particle self-assembly via capillary forces (as observed Fig. 5.6). It can even be imagined to pattern particle layers by simple forming a large colloidal crystal on the wettability pattern and remove this crystal after drying. This method might allow the patterning of nanoparticles in a straight-forward way, avoiding some of the problems described in this chapter.

An interesting region in the formation process of colloidal arrays is found in the middle of the drop. The middle of a drop is usually depleted of colloidal particles (because of the particle out-flux to the edge regions of the drop), such that there are not enough colloidal particles to form a crystal. Obviously, the size of this region where no colloidal crystal forms, mainly depends on the particle concentration of the suspension. But unfortunately there is still a large margin of error, because the crystal does not always starts to form at the same position. In some cases (on a

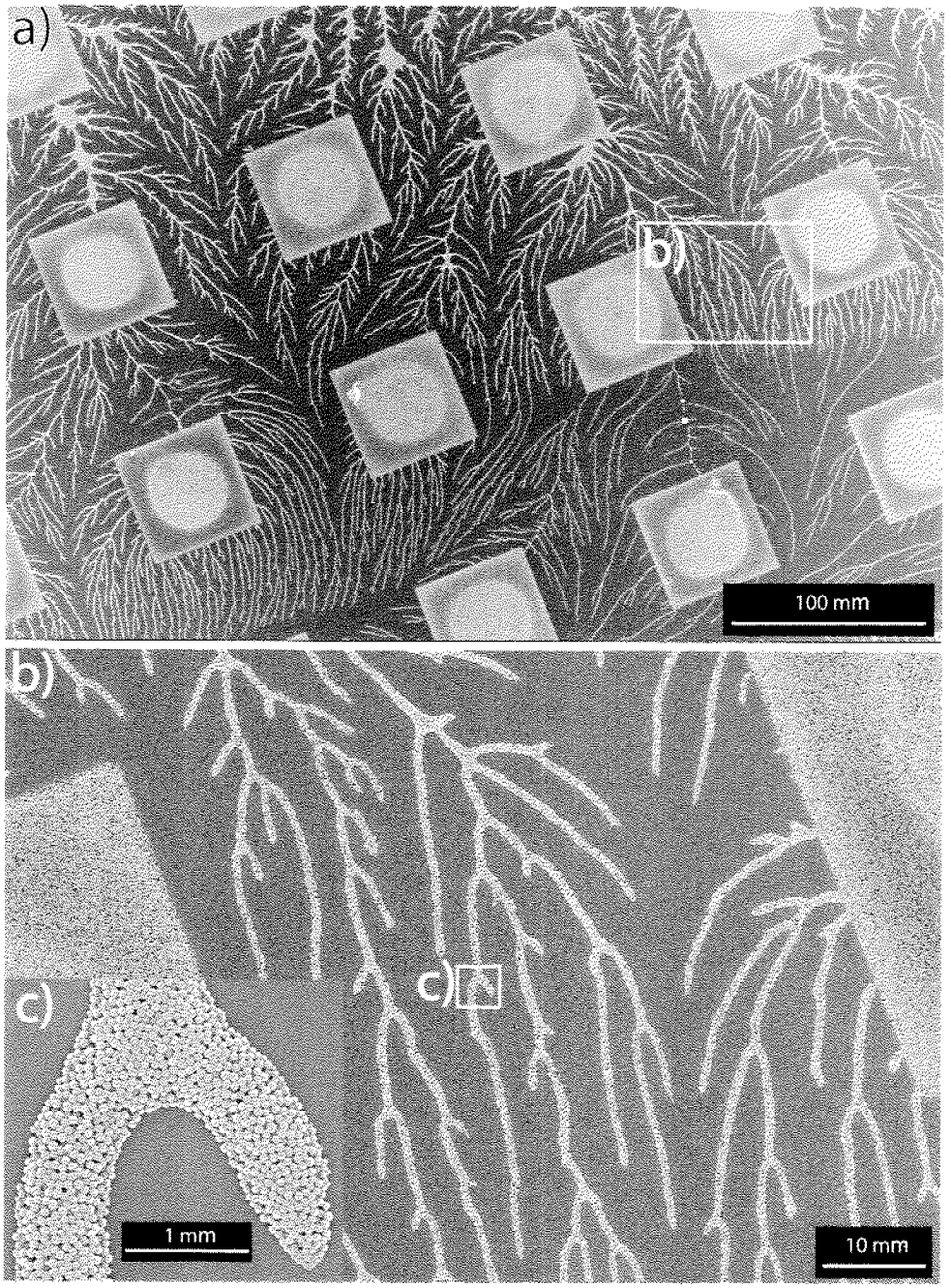

Figure 5.7: SEM micrographs of 73 nm silica colloidal particles on a hydrophobicity contrast pattern produced by SMAP (see text). A small 50 μl drop of a 0.2 wt% suspension was deposited and dried. The hydrophobic background SAM is particle free apart from the observed colloid structures due to the de-wetting that occurs upon drying. Colloidal particles completely fill the hydrophilic SiO_2 areas (60 x 60 μm squares). After filling of the pattern with nanoparticles during drying, remaining silica colloids line-up and form branch-like structures on the hydrophobic background. Thickness and range of these structures may show substantial variations from area to area on a sample; the branched structure, however, is always observed. b) and c): inserts revealing the detailed structure of these drying structures.

similar pattern), a drop is immediately pinned and a colloidal crystal starts to form, while in other cases the drop first shrinks considerably before the formation of a colloidal crystal was observed. However, it is within this middle region, where in our experiments capillary forces formed a colloidal pattern of good quality and often, interesting branch-like structures of colloidal particles were found. An example of such structures is given in Fig. 5.7. As mentioned, these structures were only present in the central region of a dried drop, where the hydrophilic silica squares are completely filled with a monolayer of the 73 nm silica particles (Fig. 5.7a). The branched structures of colloidal particles are observed on the hydrophobic background. These branches consisting of several layers of particles (insert of Fig. 5.7) have a fractal type structure always originating at the edge of the silica squares. While their width is typically in the range of several hundred nanometers to several microns, their length varies between a few μm to several hundreds of microns depending on the experimental conditions. Presently, we have no clear explanation for the described phenomenon. It seems plausible that these branches are formed during the last stage of the drying process when the large drop of water breaks up and de-wetting of the background competes with drying of the minute amount of liquid still present at the surface. However, the presence of the branches in these structures suggests that the branches grow out of the silica squares. A plausible explanation might be, that the center region of the drop dries off very evenly. Compared to a well-established drying-front (for example in a dip-coating process as explained later), the situation in the center of a drop is very different. At some point, the drop height will reach the height of the colloidal particles. As soon as the particles protrude out of the water drop (which at this point is rather a film than a drop), immersion capillary forces (as discussed in Section 2.3.3) will start to act and drag the particles towards the hydrophilic squares because at the same time, the hydrophobic background is starting to de-wet. Since this process happens in a rather large region at the same time, the first particles to come fill the hydrophilic squares and remaining particles — in the attempt to also move towards the hydrophilic squares — will be "lined-up" around the square as observed in Fig. 5.7. If a defined drying front was present, the particles which now appear lined-up on the hydrophobic background could have "escaped" back into the liquid phase, but since in this situation, the film dries off over a large area at the same time, no such "escape route" for the particles was available.

In conclusion, drop drying of a drop of suspension on a wettability contrast pattern offers the potential to observe a variety of different processes that lead to very different colloidal arrays on the substrate. For example, in the outer region of a dried drop, capillary forces produce well-defined colloidal structures on the pattern, while in regions that were covered by a colloidal crystal, loosely packed pattern of particles may be achieved. In the center region of the dried drop, even more exotic colloidal structures were produced. The obvious drawback of this method is the low reproducibility of these processes. The drying process of a drop on a sample is a relatively uncontrolled process, and results will vary from sample to sample. There may be ways to reduce this irreproducibility. Working in a clean room and under perfectly controlled evaporation conditions, for example.[3] Therefore, such experiments are of great interest from a theoretical point of view to help elucidate the formation behavior of such nano colloidal particle assemblies on patterned samples but their use in large-scale applications, where precise nano colloidal structures are needed, is problematic.

Dip-Coating on Wettability Contrast Pattern

A much more controllable way of producing particle assemblies on micron sized wettability contrast patterns is the use of a dip-coating process. The setup used is the same as presented in Chapter 4 (Fig. 4.1). A SMAP chip is dipped into the colloidal suspension, which is slightly stirred. Then, the sample is removed at a controlled speed from the suspension. The biggest advantage of that approach compared to a simple drop-drying experiment lies in the very well-established drying front that evolves at the point where the pattern leaves the suspension. By dip-coating, large-scale (cm^2) homogeneous colloidal patterns were produced. In Fig. 5.8 two of the achieved colloidal patterns are shown. On the left, a 1 cm^2 sample patterned with the SMAP technique was immersed into a 2 $wt\%$ suspension of 41 $\pm$ 5 nm silica colloids in 10 mM Hepes buffer for 30 min, removed from the suspension at a speed of 2.5 $\mu m/s$, rinsed with Millipore water and dried under nitrogen flow. The formation process of these square structures differs to some extent from lined samples. In the case of squares, the hydrophobic background is de-wetted just outside the drying front, the hydrophilic squares are still filled with suspension. Subsequent evaporation

[3]This work was done under a chemical hood mainly and evaporation took place in an oven or in air (in the chemical hood

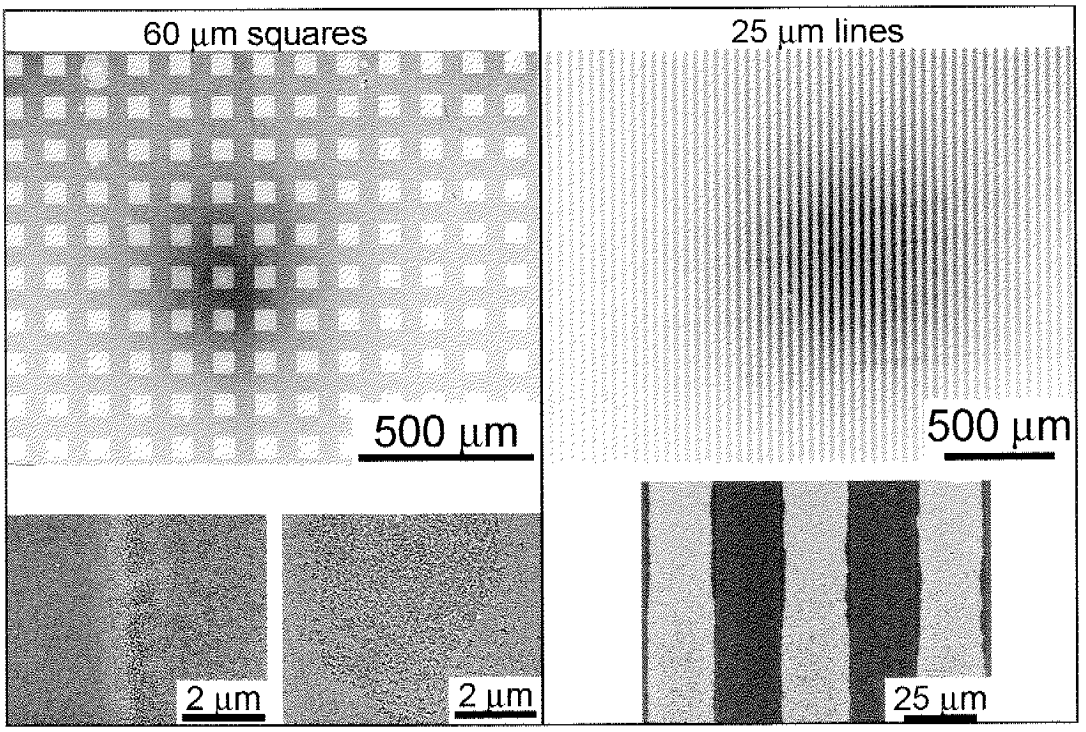

Figure 5.8: SEM images of two different examples of nano colloidal microarrays obtained on SMAP chips by dip-coating. The background consists of TiO_2 modified with a hydrophobic alkane phosphate self-assembled monolayer and is particle free due to the hydrophobic character of this surface and the de-wetting that therefore occurs during drying. Well-ordered silica colloid arrays can be obtained with this method choosing suitable particle concentration and dip-coating conditions. On the left, 60x60 μm silica squares filled with 40 nm colloidal silica particles (in Hepes 1) after dip-coating with a speed of 2.5 $\mu m/s$. Inserts show how particles form dense mono- or multilayer close to the edge regions and in the middle of each square depletion effects are observed, where only a sub-monolayer of particles remains on the surface. On the right hand side, 25 μm lines also filled with 73 nm colloidal particles (but only 1 $\mu m/s$ dip-coating speed and a 0.1 $wt\%$ suspension).

of the solvent on each of these hydrophilic squares leads to the colloidal arrays observed in Fig. 5.8a). The droplet left on such a square outside the drying front is pinned at the three-phase contact line around the edge of the square, where therefore the highest rate of evaporation is observed (see sketch in Fig. 5.12c). This results in a liquid flux dragging the particles towards the three-phase contact line, as discussed in the introductory chapter. For the same reason, edge regions of a hydrophilic square typically have very dense mono- or multilayers while the center region is depleted of colloidal particles (see inserts of Fig. 5.8) or consists of a lower number of layers compared to the edge regions. We found that depletion effects could not be completely inhibited on such hydrophobicity contrast patterns. While

the number of colloid layers formed on each individual hydrophilic square depended mainly on the particle concentration and dip-coating speed and could be controlled rather reproducibly, the depletion effects observed in the middle of a square were more difficult to control systematically.

On the right, 25 μm lines were patterned with the same technique. The lines are completely filled with particles, while the hydrophobic background again is particle free. However, contrary to the square-patterned samples, no depletion effects are visible in the center of the lines. The pattern formation of lined samples is more clearly observed in the tilted SEM images of Fig. 5.9. There, two different line widths, 50 and 10 μm, are shown and the evolution of the particle layer is observed on a cleaved sample. It can be seen, that the 10 μm lines consist of only a monolayer with a double layer of particles in the middle of the line, the 50 μm lines have 2-5 layers on average (4 and 5 layers are not seen on the presented images). The inserts of the top images show several interesting points. For one, the dense particle layers only start a few micrometers within the actual pattern edge. This is actually expected since during drying a water film is covering the whole hydrophilic line. If this water film dries, the film thickness at the edge of the line will be smaller than the particle diameter at some point. While in the middle of the line pattern, the film thickness will still be much larger. At this time, particles near the edge region will be moved to the middle region of the line due to capillary forces. The particles then finally assemble there as all the solvent evaporates over time. Note also, how the transition from single to double layers is very smooth and evolves over the distance of several particles (inserts of Fig. 5.9f). In this transition region between layers, often a deviation from the usually observed hexagonal packing is seen. In this transistion region, fcc-packed particles were sometimes observed. This phenomenon, occurring to compensate for the gradually changing film thickness due to the liquid meniscus slope and favoring the fcc-(100) surface orientation, is known for other systems and has been explained by Dushkin et al.[12] This is also consistent with the concept of a drying water film that spans the whole hydrophilic line in a "semi-spherical" form. It is also for this reason, that the number of particle layers depends on the width of the line. On a larger line, a thicker water film evolves before drying, which contains more particles that subsequently assemble on this line. Fig. 5.10 shows some more examples of how the particle arrays develop on different structures. For example, it is possible to form particle arrays with a gap of only 1 μm. Even such a low gap size is sufficient for the background to be dewetted and to form a stable particle

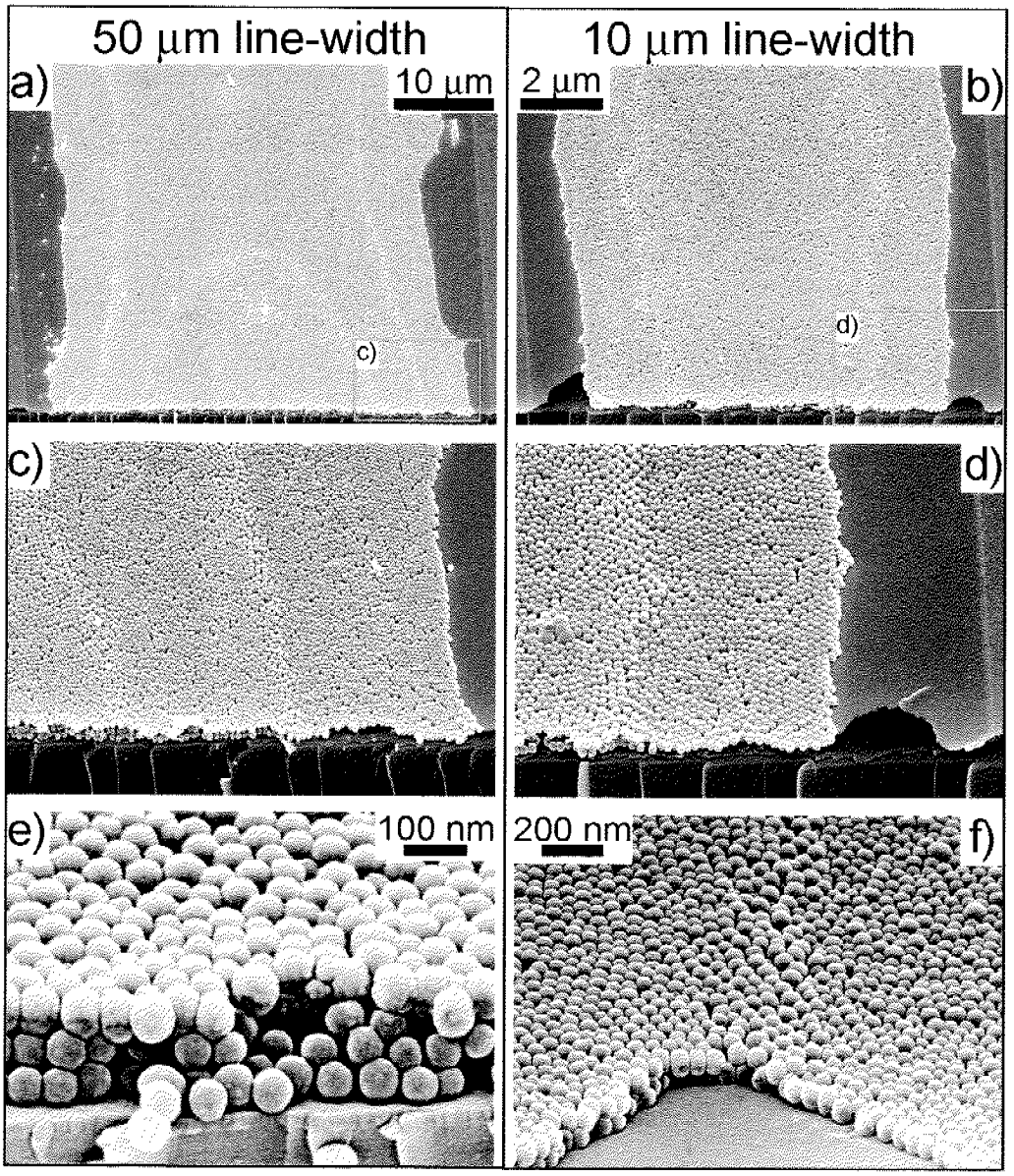

Figure 5.9: SEM images offering a side view of nano colloidal assemblies on SMAP sample with two different line-widths, 50 and 10 μm. For a detailed description of the images see text.

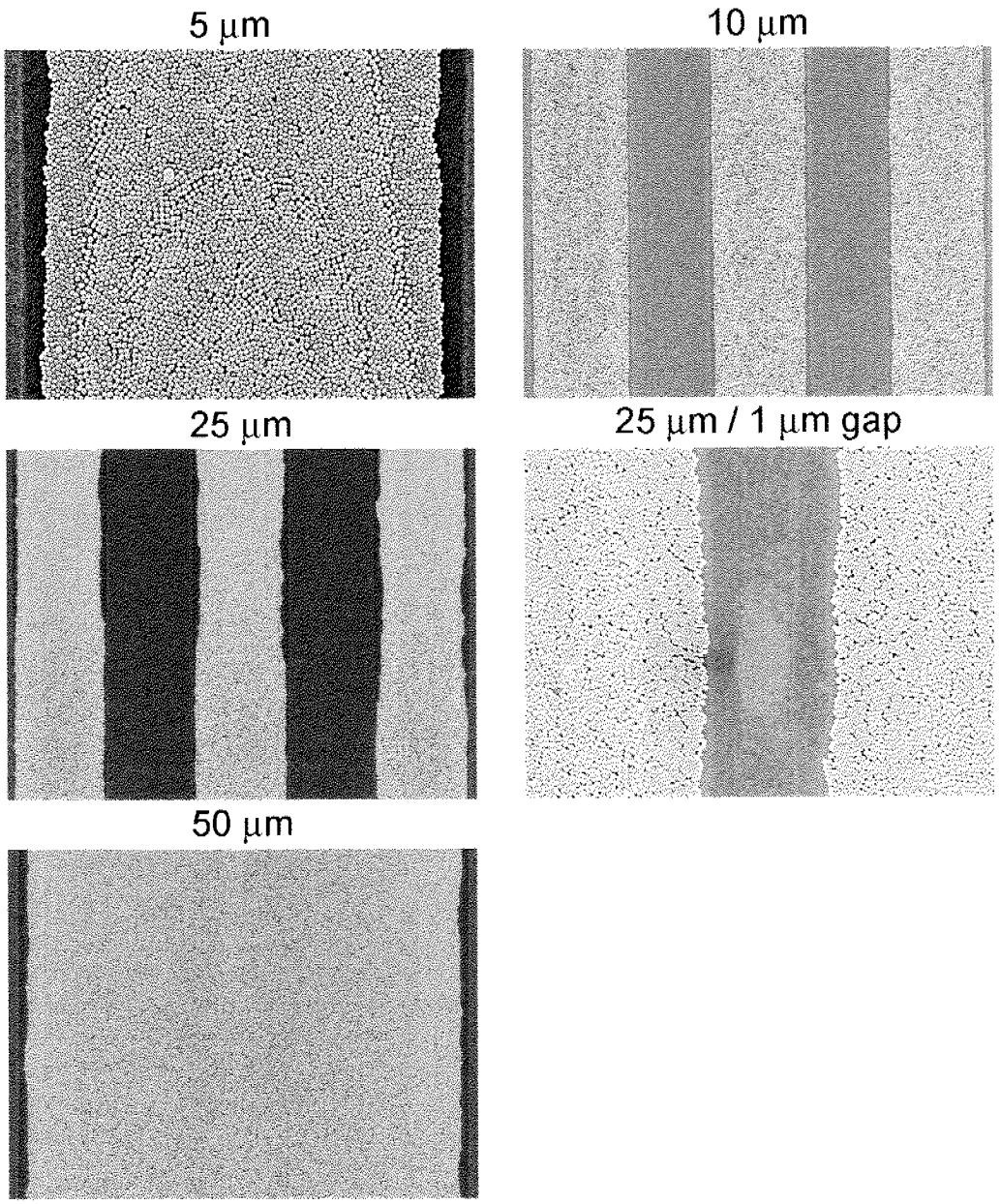

Figure 5.10: SEM images of different examples of nano colloidal assemblies on SMAP structures with 73 nm particles, dip-coated at 1 $\mu m/s$ in a 1 $wt\%$ suspension. Details see text.

layer. On the other hand, no stable particle assemblies could be produced with line width below 2 μm. For 5 μm however, colloidal self-assembly is achieved without problems as observed in Fig. 5.10. A value slightly lower than those reported by Fustin et al. recently for a similar system.[13] They also found a similar increase in particle layers from the edge to the center and with increasing the line width or particle concentration as in this work. The number of particle layers on a pattern with a given line width can in principle be calculated. Dimitrov and Nagayama presented an equation which relates the number of particle layers k to the length of the meniscus L (see Fig. 5.12c).[14]

$$k = \frac{\beta L j_e \phi}{0.605 v d (1 - \phi)} \tag{5.1}$$

β is the ratio between particle and fluid movement (and taken to be 1), ϕ is the volume fraction of particles, j_e the solvent evaporation rate, d the particle size and v is the array growth rate (= withrawal speed). However, this equation was derived for homogeneous samples and therefore, especially the determination of L will be troublesome and deviations must be expected. In fact, below 100 μm line width Eq. 5.1 will loose its practical benefits [13] because the meniscus lenght L cannot be deduced easily and other factors[4] start to govern the formation of the particle layers.

5.3.3 Capillary and Hydrodynamic Forces in the Self-Assembly Process of Particles on a Wettability Pattern

The dominance of capillary forces in the self-assembly of particles on a wettability contrast pattern as the main driving force for particle self-assembly was mentioned several times in the last sections. In this section, some more details on these mechanisms will be provided. First, another experiment was conducted to confirm the importance of the capillary interactions in the formation of these colloid assemblies. To do so, a patterned SMAP chip was immersed into the suspension. Then, large proportions of water were carefully filled in the beaker with the sample, letting the water overflow for several tens of seconds. By doing so, the suspension was diluted

[4]Such as pattern edge effects, relative contact angles of hydrophilic / hydrophobic regions, etc.

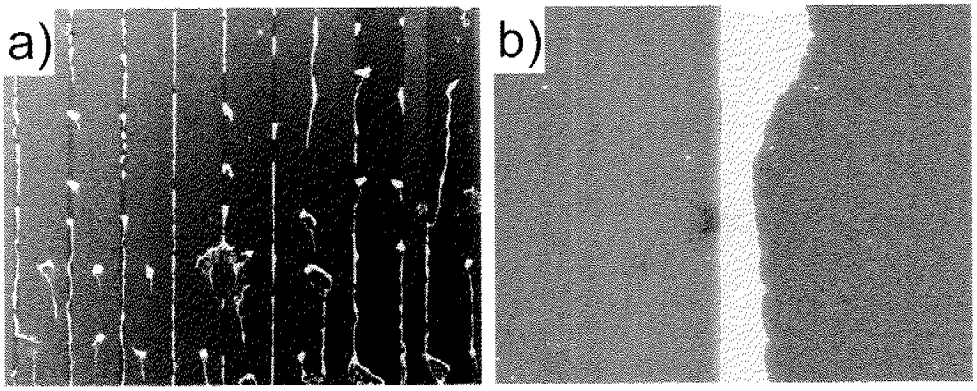

Figure 5.11: SEM images of colloidal particles self-assembled on a SMAP chip which was not coated with a $DDPO_4$ SAM on the titania background. Therefore the hydrophobicity contrast between pattern and background is not developed sufficiently and particle self-assembly does not work as on a standard SMAP chip. However, some ordering of particles, especially near the edges of the line pattern, is still visible in a) and b). This ordering may be attributed to two effects. For one, there is still a slight difference in hydrophobicity between the hydrophilic silica lines and the slightly more hydrophobic titania background. On the other hand, there exists a small difference in height of the pattern (of approximatly 15 *nm*) between the etched silica pattern and the background. These "steps" at pattern edges provide a favorable position of particle assembly (by capillary forces) during the drying step.

until ideally no particles were left in the beaker with the SMAP chip. After removal of the immersed chip, no colloidal particles were found on the surface by SEM. Similar results were also obtained by OWLS, where silica particles neither adsorbed to a $DDPO_4$ coated surface nor to a silica surface in suspension. This indicates that the colloidal particles did not interact to a significant degree with neither the hydrophobic nor the hydrophilic (silica) areas of the SMAP surface in suspension. This was also expected since ζ-potential measurements of the silica colloids showed an IEP of around pH 2.3 (see Chapter 4 for details) and the colloidal particles are therefore negatively charged at all used pH values as is the silica substrate. It can therefore be conclude that, in this case, capillary forces indeed dominate the self-assembly process. In fact, the absence of particle-surface interactions is one important prerequisite for the formation of this kind of particle arrays.

Another set of control experiments was conducted to check whether the $DDPO_4$ SAM was indeed necessary to assemble particles on (lined) SMAP chips. These experiments showed, that the large hydrophobicity contrast obtained by the $DDPO_4$ SAM together with the hydrophilic silica pattern is really of high importance as shown in Fig. 5.11. There, some examples of structures achieved without the SAM on top of the titania background are presented. The tendency to form structured

arrays is still there to some extent, however, since the hydrophobicity contrast is much less distinct (but still there), no coherent particle arrays could be formed on such samples. Also, the minimal particle structuring observed in these samples is probably due to the small difference in topography of the pattern. The etching process forms steps at the pattern edges which are sites, where particles preferentially assemble during drying. This fact was discussed in the introductory chapter, where examples were presented that use topographical pattern (with higher feature depth) to assemble colloidal particles within such structures. The reason for this is found in the fact that capillary forces drag particles towards these edges during drying and to some extent, particles are able to assemble at these small height differences.

It is also not surprising that no significant influence of a variety of parameters was observed in our experiments, since in the SMAP system capillary forces are dominant over colloid-surface interactions. For example, changing pH (3, 7.4 and 9.9) or ionic strength (10, 160 mM) did not alter the characteristics of the resulting colloid nano-arrays. This was to be expected since the change in the interaction potential between the colloids and the surface and the colloids themselves was small when changing the mentioned parameters compared to the capillary forces present during the drying process. It was only important, that the colloidal particles retain their non-interacting properties with the surface pattern in suspension, because otherwise adsorption of particles to the pattern might occur in suspension, which will then alter the characteristics of the particle arrays during drying.

The above observations again point towards the original forces that are responsible for the nano colloidal self-assembly of particles on wettability contrast pattern: capillary forces that occur when particle layers dry and hydrodynamic forces that move particles together at the water-air-surface three-phase interface. In Fig. 5.12, a schematic overview is given on how capillary forces assemble colloidal particle layer on patterned substrates during the dip-coating process. Fig. 5.12a) and b) show how the three phase contact line evolves if a hydrophilic (or hydrophobic) substrate is slowly removed from a suspension. Depending on the contact angle Θ of the substrate, the water surface is either attracted to the substrate and thus lifted up to form a meniscus, or the water line is suppressed below the normal water level at the substrate if the substrate is hydrophobic. If now a substrate is considered, where a pattern of hydrophobic and hydrophilic stripes are present, the situation will evolve as sketched in Fig. 5.12c. The water meniscus at the contact line will rise due to the low contact angle with water of the hydrophilic lines and wet these

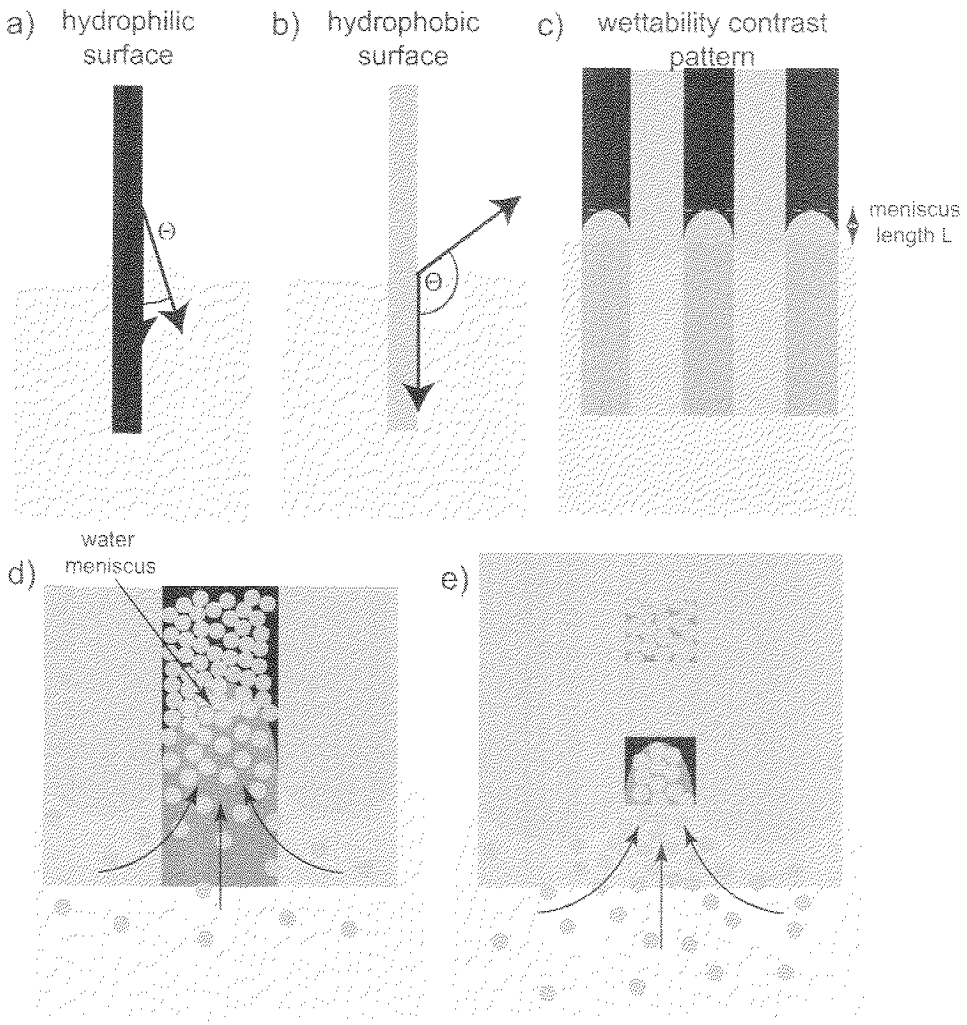

Figure 5.12: Schematic overview of the particle self-assembly processes acting on a patterned sample during dip-coating. a) If a homogeneous hydrophilic pattern is dip-coated in a water-based suspension, a liquid meniscus depending on the contact angle (and also other factors, such as density of liquid) develops at the water contact line. b) The inverse situation evolves if a hydrophobic pattern is slowly removed from the solvent. The water contact line is suppressed below the normal water level. If a pattern with a hydrophobicity contrast is considered, a situation as depicted in c) evolves: the water contact line changes gradually when changing from a hydrophilic to a hydrophobic line. The length of the concave water meniscus on the hydrophilic lines depends on the line-width (and is constant and equal to the meniscus in a) if the line-width is above a critical length). d) Close-up of c) with particles indicated. Colloidal particles move into the water meniscus on hydrophilic lines by hydrodynamic flow. This flow is caused by the high water evaporation rate present in the water meniscus. Particles brought into the vicinity of the water meniscus are then arranged and ordered by immersion capillary forces that evolve when the particles protrude out of the water film at the end of this meniscus. e) The same situation as in d) but with a square hydrophilic pattern instead of a hydrophilic line. The mechanism remains essentially the same, however, when such a sample is removed from the suspension, individual squares remain filled with suspension and are detached from the drying front. The suspension on these squares dries off eventually. However, this different drying mechanism on square samples produces fundamentally different particle assemblies. See text for more details.

lines, while at the same time the water contact line is below the water line on the hydrophobic lines. Thus, a curved water interface evolves as sketched. In a closer look, Fig. 5.12d) shows how this situation looks for a single hydrophilic line (this time with particles in the water phase). The wetting of the hydrophilic line leads to a water meniscus that protrudes out of the water edge. At this water meniscus, evaporation of water has its highest value due to the large three phase contact line and the fact that in this region, colloidal particles are enriched, which also increases water evaporation. The high evaporation rate of water at this position causes a water flow towards the hydrophilic lines. This water flow also drags particles in suspension with it, therefore particles will accumulate at hydrophilic lines. If the sample is removed slowly form the suspension, particles that were dragged to the hydrophilic lines will dry on the hydrophilic lines only. The situation is similar on a pattern of square structures. However, in such a case (Fig. 5.12c) a square will usually be filled with suspension (upper square in sketch) and be detached from the drying front because the hydrophobic areas between the squares will be dewetted rapidly and the water front will retract to the next hydrophilic square. Then, the suspension filled square which is out of the drying front will dry-off individually. As a consequence of this process, "coffee ring" like structures are observed in most cases on square pattern. The water on the square dries off and again the highest evaporation rate is found on the edge of the square at the three-phase contact line. Particle on a square will be dragged towards the edge of the square and regions in the middle of a square are subject to depletion effects. This explains the differences found in the evolution of particle arrays between square and line pattern (as for example shown in Fig. 5.8).

Note also, the the deformation of the water contact line caused by the hydrophobic-hydrophilic pattern is limited to not too narrow line widths. As discussed in a previous section, hydrophilic lines of 5 μm could still be patterned successfully, but not below that. The reason for this lies in the fact, that below a certain value of the line width, the water meniscus is no longer as pronounced as for wider lines which hinders the formation of particle arrays. The same must be true for the hydrophobic background lines, but in this case, dewetting was still observed down to 1 μm (which was the resolution limit in our SMAP process).

An estimation of the strength of the capillary forces in the vicinity of the water meniscus can be given using the theoretical equations derived in the introductory

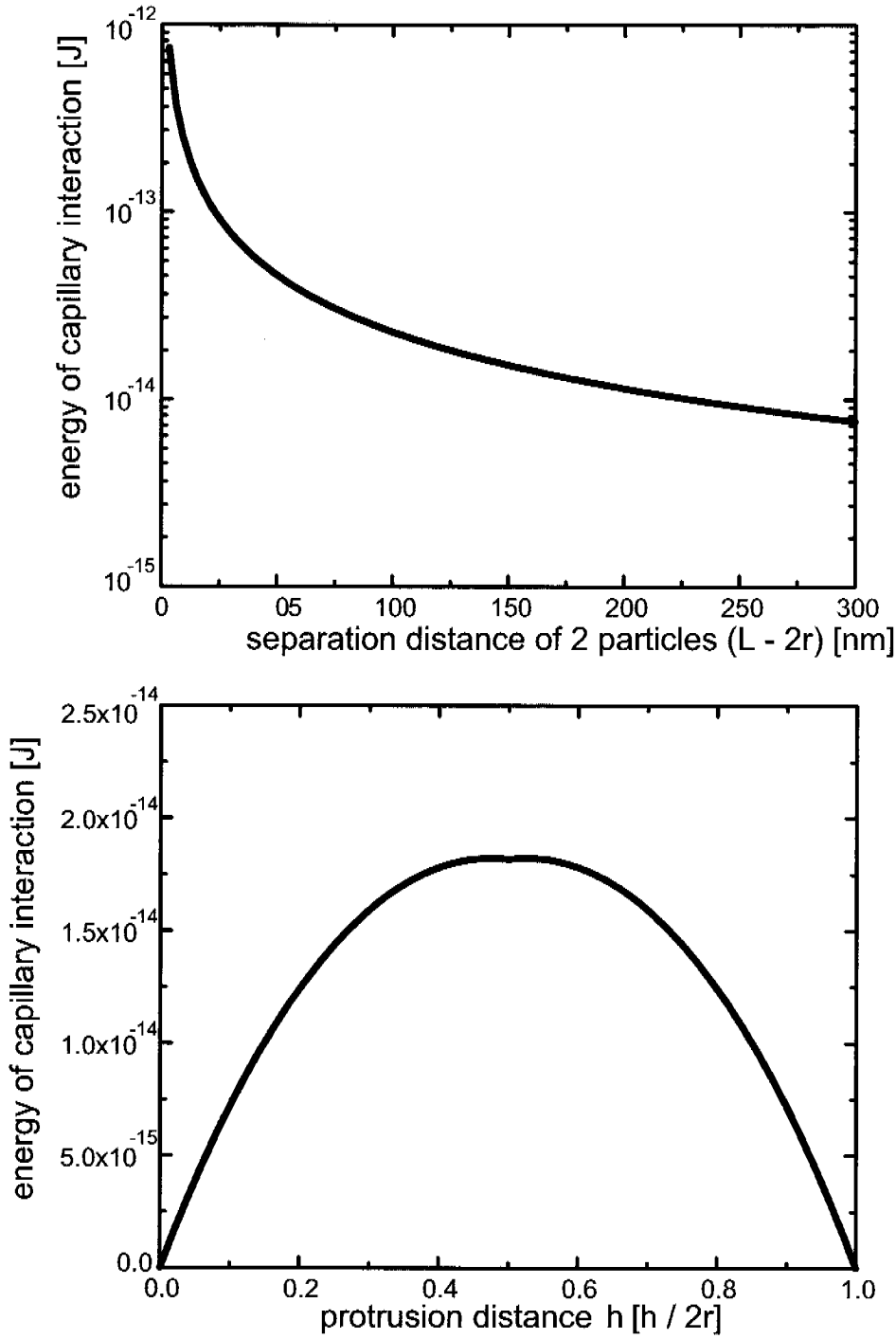

Figure 5.13: Attractive capillary interaction energies as a function of separation distance of the two considered particles (top) and as a function of the water film height h (bottom). Capillary interactions decrease with increasing separation distance L but remain of considerable strength also after several hundreds of nanometers. The protrusion height h describes the position of the water film. At $h = 0$ the water film just covers the particle and at $h = 1$ the water film reaches to bottom of the particle. See Fig. 2.11 for a sketch showing the protrusion height h. The capillary interaction energy therefore increases until the water film has the same height as the particle radius, where it has its maximum and decreases again.

chapter. There, the capillary interaction energy of two particles was defined as follows:

$$\Delta G = 2\,\pi\,\gamma\,\frac{R^2\,\sin^2(\alpha)\,r}{L-2r} \tag{5.2}$$

We assume a particle size of $r = 37\ nm$ and a surface tension of 72 $dynes/cm$ and use the relations for R and α proposed by Aizenberg on the basis of geometrical considerations:[1] $\alpha = arcsin(r/R) - \psi$ and $R = \sqrt{(h(2r-h))}$, where h is the distance which the particle protrudes out of the water film. For example, the interaction energy of two of those particles, separated by $L = 200\ nm$ and protruding out with half of their diameter ($h = 37\ nm$) is around $-1.8x10^{-14}\ J$ or -$4.4x10^6\ kT$. These energies are very considerable and indeed provide a powerful source for the self-assembly of colloidal particles. These values are also in agreement with values found by Juillerat et al. very recently for a similar system.[15] They also concluded, that the capillary forces are the dominating factor in the drying process and are considerably higher than particle-particle forces in suspension. In Fig. 5.13, two graphs further elucidating the power of capillary forces are shown. For one, the dependence of the capillary interaction energy on the separation distance of the two particles is given and it can be seen that the capillary force decreases rapidly with increasing particle distance, but even for relatively long separation distances the force is considerable. Furthermore, particles are generally very concentrated in the regions where drying occurs (due to the hydrodynamic flow that moves them there) and thus the separation distance of particles is usually rather low which further strengthens capillary interactions. Also it is seen in the second graph, that capillary interactions are maximized if the water film is exactly half as thick as the particle diameter. Obviously, the capillary force vanishes as long as the water film is thicker than the particle or if the film disappears completely. This is important in the sense, that hydrodynamic forces can transport colloidal particles in the region of the water meniscus without the influence of capillary forces, as long as the water film is not thinner then the particle's diameter. Thus, transport mechanism (hydrodynamic flow) and compacting mechanism (capillary forces) play together rather nicely to form the colloidal particle assemblies shown in this work.

In conclusion, we can summarize the requirements that are needed to form nano colloidal arrays on a wettability contrast.

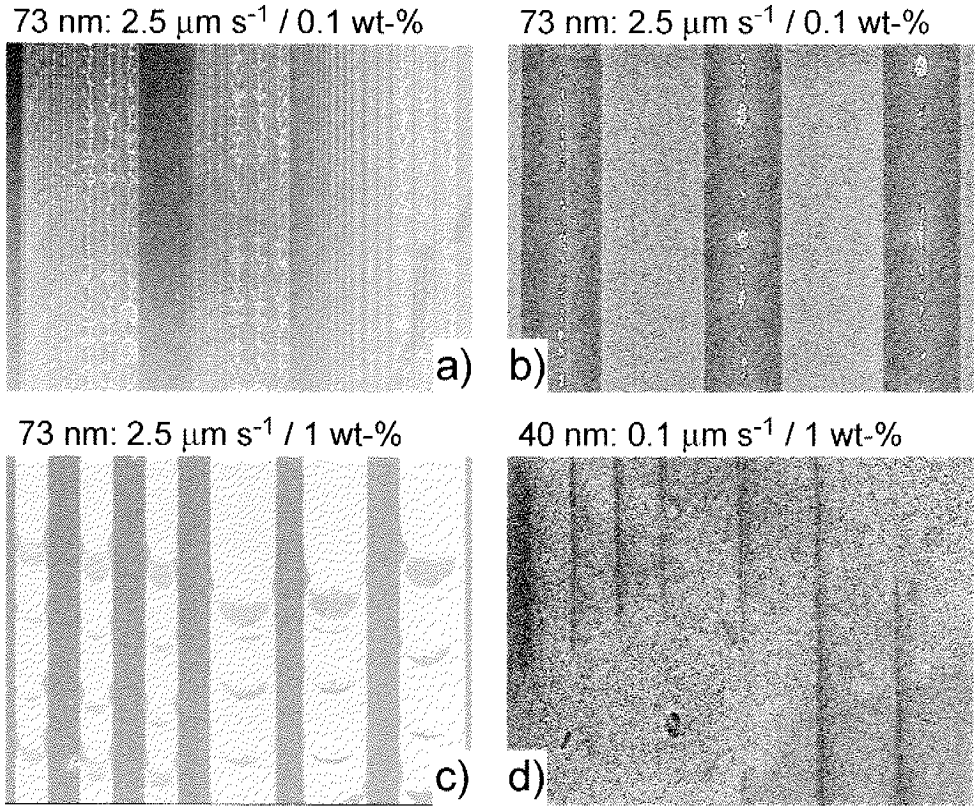

Figure 5.14: SEM images of some common irregularities observed during the production of colloidal particle arrays on wettability contrast pattern. a) and b) at too high withdrawal speeds (or low particle concentration in the suspension), only little particle deposition is observed and not complete particle layer are formed. c) rupturing of films as often observed at rather high withdrawal speeds. d) too slow evaporation rates (withdrawal speeds) result in complete coverage of the sample with thick layers of particles.

1. The hydrophobicity contrast of the pattern must be high and well-established. Particle deposition and array formation is limited to the hydrophilic regions of the pattern and no particles will adsorb on the hydrophobic background.

2. The wettability contrast pattern must be constructed such that particles will not interact with the surface. Adsorption of particles (for example by electrostatic forces) has to be avoided, since this would prevent a) particle flux towards the three-phase interface and b) capillary forces from arranging particles on the surface easily.

3. A stable particle suspension must be formed and maintained

4. Evaporation of solvent has to be restricted to the meniscus of the water-air-interface on hydrophilic areas, such that particle flux is maximized and no disturbances in the pattern are introduced. For example, working under saturated water vapor may help to maintain this condition. If this condition is not met, particle arrays may still be achieved (see the section on drop-drying) but the reproducibility of the pattern will not be acceptable.

5. Water evaporation rate must be in a correct regime. An equilibrium between particle flux, array formation and evaporation rate must be found (in our experiments it was achieved with speeds in the order of 0.1-2.5 $\mu m/s$ for particle concentrations of around 1 $wt\%$).

If the last point is not followed, e.g. too high evaporation rates / withdrawal speeds are chosen, defects and rupturing of colloid arrays may occur. Some examples of such irregularities are shown in Fig. 5.14. If the withdrawal speed is too high (or particle concentration too low), a situation as shown in the top two images of Fig. 5.14 may be observed, where the hydrophilic pattern was not able to be filled completely. On the other hand, even at 1 $wt\%$, rupturing of the particle film may occur due to the rather fast withdrawal speed of 2.5 $\mu m/s$. However, if particle concentration is high and the dip-coating speed low at the same time, too many particles were deposited and instead of only depositing particles on hydrophilic surface, a homogeneous and thick particle film is deposited (Fig. 5.14, bottom right).

However, even if these requirements are fulfilled, many other factors may severely hinder particle array formation. For example, working under ambient conditions (as done in this work) may introduce organic substances into the suspension from air. Such organic molecules may alter the wetting behavior of the solution and cause particle array formation to be disturbed.[14] Particle polydispersity also hinders particle array formation and even more problems may be caused by agglomerates present in the suspension. Stepping motors (as used in here) also are a source of possible problems as well as the slight stirring of the suspension during the dip-coating process. Both of them potentially disturb the colloidal array's leading edge, which in turn may cause the patterning process to fail. It is therefore not an easy task to meet the described theoretical requirements under real laboratory conditions.

5.4 Conclusions

Capillary forces are used as the driving force to assemble silica nanoparticles on wettability contrast pattern. The SMAP patterning technique used here produces first a SiO_2-TiO_2 contrast (through a photolithography process with a subsequent etching step) and then the TiO_2 structures are functionalized with a hydrophobic alkane phosphate monolayer. On these hydrophobicity contrast patterns, silica nanoparticle suspensions were dried with two different methods: on the one hand, a drop of suspension was applied to the substrate pattern and dried off. On the other hand, the substrate was dip-coated in the particle suspension at controlled conditions. Both methods are able to produce distinct particle arrays on the hydrophilic pattern and leaving the hydrophobic background free of particles.

The main advantage of the drop drying method — beside its simplicity — lies in the fact that different mechanisms leading to the formation of the particle arrays may be observed on a single sample due to the character of a drying drop on a patterned sample. Typically, a drying drop will leave several areas where different pattern morphologies evolve: 1. The region on the outside of the drop, where the drop was receding during drying (which leads to densely packed particle arrays on the pattern). 2. A region where a colloidal crystal builds. Below this crystal, particle arrays with very different characteristics form. This finding offers the possibility to form particle arrays on wettability contrast without the influence of capillary forces and may be an interesting way of patterning high-throughput particle arrays. 3. Areas in the middle of the drop, where particle depletion effects lead to interesting drying phenomena on the pattern such as fractal, branched colloidal lines on the hydrophobic background.

Dip-coating a patterned sample in the colloidal suspension is a more controlled way of producing particle arrays on a wettability contrast and leads to large-scale, homogeneous particle arrays of various geometries. Due to the nature of the process, line pattern are especially well-suited for this process and lines of particles between 2 and 500 μm can be formed. The number of particle layers on such a line depends on its width, the dip-coating speed and the particle concentration. The mechanisms and parameters that govern the formation of these particle arrays were studied and discussed in detail. It was shown, that larger line width, higher particle concentra-

tions and slower dip-coating speeds will lead to an increase in the particle layers present on the structure and vice versa.[5]

In conclusion, capillary forces occurring during drying are a powerful means to arrange nanoparticles on a patterned substrate provided the particle-substrate pattern system fulfills some basic requirements, which were deduced and discussed in this work. Both, drop-drying and dip-coating proved to be possible techniques to form such particle layers, however, the production of reproducible, large-scale particle arrays is more promising using a dip-coating process. But even then, care must be taken during all steps of the process and the particle array formation is easily disturbed and some irregularities in these structures are hard to be avoided.

[5]For example, structures with a line width of 10 μm, a dip-coating speed of 0.1 $\mu m/s$ and a particle concentration of 0.1 $wt\%$ will be covered with 2-3 particle layer of 73 nm particles

Bibliography

[1] Aizenberg, J., Braun, P. V. and Wiltzius, P. Patterned colloidal deposition controlled by electrostatic and capillary forces. *Physical Review Letters*, **84**(13), 2997–3000, 2000.

[2] Masuda, Y., Itoh, M., Yonezawa, T. and Koumoto, K. Low-dimensional arrangement of SiO2 particles. *Langmuir*, **18**(10), 4155–4159, 2002.

[3] Jonas, U. and Krüger, C. The Effect of Polar, Nonpolar, and Electrostatic Interactions and Wetting Behavior on the Particle Assembly at Patterned Surfaces. *Journal of Supramolecular Chemistry*, **2**(-), –, 2003.

[4] Fan, F. and Stebe, K. Assembly of Colloidal Particles by Evaporation on Surfaces with Patterned Hydrophobicity. *Langmuir*, **20**, 3062–3067, 2004.

[5] Xia, Y., Yin, Y., Lu, Y. and McLellan, J. Template-Assisted Self-Assembly of Spherical Colloids into Complex and Controllable Structures. *Advanced Functional Materials*, **13**(12), 907–918, 2003.

[6] Yin, Y. D. and Xia, Y. N. Self-assembly of monodispersed spherical colloids into complex aggregates with well-defined sizes, shapes, and structures. *Advanced Materials*, **13**(4), 267–271, 2001.

[7] Chen, J. Y., Klemic, J. F. and Elimelech, M. Micropatterning microscopic charge heterogeneity on flat surfaces for studying the interaction between colloidal particles and heterogeneously charged surfaces. *Nano Letters*, **2**(4), 393–396, 2002.

[8] Michel, R., Reviakine, I., Sutherland, D., Fokas, C., Csucs, G., Danuser, G., Spencer, N. and Textor, M. A novel Approach to Produce Biologically Relevant Chemical Patterns at the Nanometer Scale: Selective Molecular Assembly Patterning Combined with Colloidal Litography. *Langmuir*, **18**(22), 8580–8586, 2002.

[9] Hofer, R., Textor, M. and Spencer, N. D. Alkyl phosphate monolayers, self-assembled from aqueous solution onto metal oxide surfaces. *Langmuir*, **17**(13), 4014–4020, 2001.

[10] Tosatti, S., Michel, R., Textor, M. and Spencer, N. Self-Assembled Monolayers of Dodecyl and Hydroxy-dodecyl Phosphates on Both Smooth and Rough Titanium and Titanium Oxide Surfaces. *Langmuir*, **18**, 3537–3548, 2002.

[11] Lee, W. P. and Routh, A. F. Why Do Drying Films Crack? *Langmuir*, **20**(23), 9885–9888, 2004.

[12] Dushkin, C. D., Lazarov, G. S., Kotsev, S. N., Yoshimura, H. and Nagayama, K. Effect of growth conditions on the structure of two-dimensional latex crystals: experiment. *Colloid and Polymer Science*, **277**(10), 914–930, 1999.

[13] Fustin, C. A., Glasser, G., Spiess, H. W. and Jonas, U. Parameters influencing the templated growth of colloidal crystals on chemically patterned surfaces. *Langmuir*, **20**(21), 9114–9123, 2004.

[14] Dimitrov, A. S. and Nagayama, K. Continuous Convective Assembling of Fine Particles into Two-Dimensional Arrays on Solid Surfaces. *Langmuir*, **12**(5), 1303–1311, 1996.

[15] Juillerat, F., Bowen, P. and Hofmann, H. Formation and drying of colloidal crystals using nanosized silica particles. *Langmuir*, **22**(5), 2249–2257, 2006.

Seite Leer /
Blank leaf

CHAPTER 6

Functionalized Nanoparticle Assemblies through Specific Particle-Surface Interactions

6.1 Introduction

So far, particle assemblies in this work were produced using fundamental particle-surface interactions (electrostatic attraction between particle and surface in Chapter 4, capillary forces that act during drying in Chapter 5). Choosing these routes to direct particle self-assembly is a relatively straight-forward way of arranging particles on a patterned surface. For example, the exact surface chemistry of the used particles (and also the pattern) does not matter in principle (as long as they carry the correct surface charge). However, in biotechnology, for example, control of surface chemistry is of high importance since interactions between biological species (blood, serum, proteins,...) and the surface (of particle and substrate) must be precisely controlled in order to avoid undesired adsorption of biomolecules. Ideally, the properties of a substrate surface are tailored such, that no interactions exist between biomolecules and the substrate unless specifically designed. For example, in the development of a protein biosensing device, surface spots must be produced that specifically interact with a protein of interest. A capturing mechanism must be developed that is able to specifically recognize the target molecule. The background of such a biochip must be completely non-interacting with the biological sample to reduce signal-to-noise ratios and to avoid false-positive signals.

One of the most prominent ways of producing such protein-resistant surfaces is their functionalization with poly(ethylene glycol) (PEG). PEG has several properties

which are essential to promote resistance to protein adsorption on a surface: PEG is uncharged, hydrophilic, soluble in water and organic solvents and is a hydrogen-bond acceptor. If a PEG-coating forms a dense brush on a surface, it is hydrated well and the PEG chains have a good conformational flexibility. Furthermore, the PEG-chains remain sufficiently mobile in the PEG-brush, such that this brush contributes to a steric exclusion effect between PEG chains in water.[1] All these effects combined lead to the excellent resistance to biomolecule adsorption of PEG-brushes on a surface. A range of different techniques have been employed for the immobilization of PEG polymers onto surfaces, in this work we present the approach developed in our lab some years ago. It uses the spontaneous assembly of PEG-grafted copolymers onto a substrate surface. PEG chains are grafted to a poly(L-lysine) backbone, which is positively charged at a pH below 10.3 and adsorbs electrostatically to any negatively charged substrate surface. This PLL-*g*-PEG copolymer has been shown to resist protein adsorption from serum almost completely ($<1\ ng/cm^2$).[1, 2] The structure and a more general overview about this copolymer are given in Section 3.2.2 and in Fig. 3.3.

The potential of producing particle arrays with surface-functionalized nanoparticles is explored in this chapter. Indeed, the nanoengineering of particle surfaces is a growing field due to the interesting properties of such functionalized particles.[3] In this work, the PLL-*g*-PEG copolymer is used as a coating of the particle surface as well as the substrate surface, which inherently renders this system resistant to protein adsorption. However, the PEG coated particles would not be able to adsorb to the PEG-coated surface since they repel each other sterically. For this reason, a different approach of binding the particles to the substrate has to be introduced. This alternative strategy of binding particles to a surface makes use of a protein-ligand binding system. This ligand system is introduced simply by end-functionalizing the PLL-*g*-PEG copolymer with a biotin unit (Fig. 6.2). If both, the particle and the surface, are coated with PLL-*g*-PEG/PEG-biotin, the particles can be bound to the surface by a streptavidin linker. Streptavidin will then bind to the biotin of the PLL-*g*-PEG/PEG-biotin on the surface as well as capture a biotinylated particle from suspension. The following section provides some more information on the biotin-streptavidin system.

As a last step, a surface pattern must be produced to bind the particles to the surface at desired locations. To do so, a patterning technique introduced by Didier Falconnet was adopted, which allows the production of biotinylated and non-biotinylated sur-

face regions.[4] This technique relies on the assembly of biotin-functionalized PLL-g-PEG in a background of PLL-g-PEG. If PLL-g-PEG/PEG-biotin functionalized nanoparticles are introduced in such a system, they can be linked with streptavidin to the surface regions where biotin is present. In the end, functionalized nanoparticles are assembled on specific regions of a PLL-g-PEG / PLL-g-PEG/PEG-biotin pattern.

6.1.1 Biotin-Streptavidin System

One of the most used protein-ligand binding systems is the biotin-streptavidin system. Originally discovered in investigations on the vitamin H complex, where avidin (a close relative to streptavidin)[1] was responsible for a nutritional deficiency in rats, because streptavidin binds so strongly to vitamin H (which is biotin).[5] The binding of biotin by streptavidin is accompanied by one of the largest decreases in free energy yet observed for a noncovalent interaction between a protein and a small ligand in aqueous solution.[6] Streptavidin is a homotetrameric 159 residue protein with a molecular mass of $\tilde{4}$x15'000 kDa. The crystallographic structure of streptavidin is given in Fig. 6.1. Each of the four "arms" is able to bind one biotin molecule with an extremely high affinity constant (10^{13} M^{-1}) and consists of an 8-stranded anti-parallel β-barrel. Biotin is bound in the open end of the twisted barrel, and one surface loop (indicated by $*$ in Fig. 6.1b) folds over the binding site when biotin is bound.[7, 8]

The binding energy of the biotin-streptavidin system was calorimetrically determined to be -76.58 kJ/mol[9] and using molecular dynamics calculations using a thermodynamic free energy perturbation method a value of -83.7 - 92 kJ/mol was found.[6] The exceptionally high binding constants of biotin to streptavidin is attributed to a large number of hydrogen-bonds that may form if biotin is bound in its "binding-pocket". A large negative binding energy indicates that the bound state is much more favorable then the state where streptavidin and biotin are both in solution. Thus, hydrogen bonding in the bound state is enhanced and more effective than hydrogen bonding that is present between streptavidin and water. Also, due to the close contact of the bound biotin, van der Waals forces play an important

[1] Streptavidin is carbohydrate-free and has a slightly acidic IEP (5-6) compared to avidin. It is also for these reasons, that the crystallographic structure is more easily obtained for streptavidin then for avidin.[5]

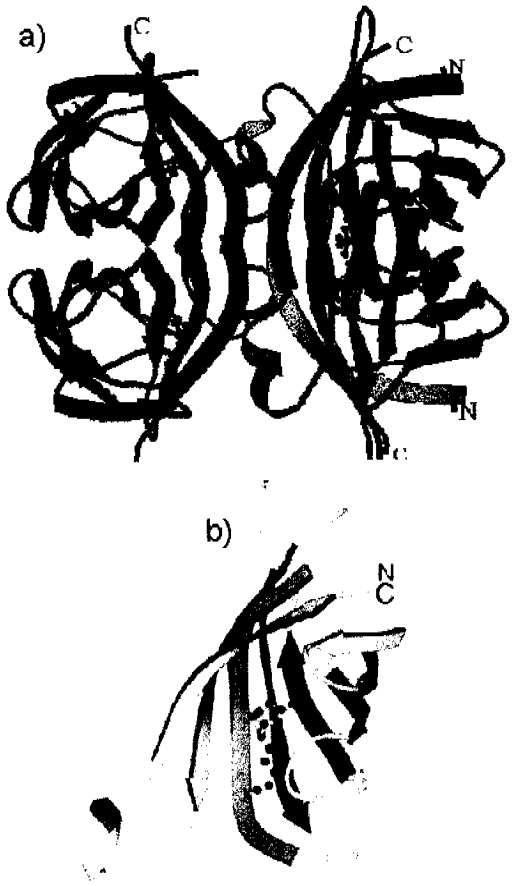

Figure 6.1: Crystallographic structure of streptavidin. a) tetrameric structure of streptavidin. b) each of the four monomers forms β-barrels and has a number of hairpin-loops joining the β-strands. Adopted from [8].

role for the large binding energy between streptavidin and biotin. Furthermore, only little entropic influence on the binding energy was found, it is therefore mostly an enthalpic gain in energy[2] ($\Delta G = -76.5 kJ/mol$ and $\Delta H_0 = 134.0 kJ/mol$).[9] In Fig. 6.2 a sketch of a biotin molecule is drawn indicating all the interactions with streptavidin residues.

6.2 Experimental

The Molecular Assembly Patterning by Lift-Off (MAPL) technique [4] is able to convert a photolithographically prestructured photoresist film into a micropattern

[2]Which leads to a decrease in ΔG

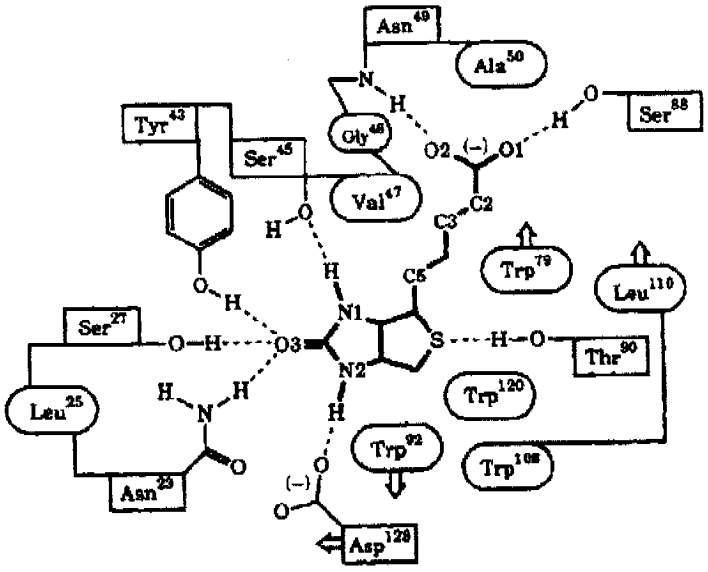

Figure 6.2: A biotin molecule and its interactions with streptavidin residues in the bound state. Residues enclosed in squares represent hydrogen bonding, such enclosed in ellipsoids show van der Waals interactions. Adopted from [6].

of biointeractive and noninteractive regions (Fig. 6.3). Negatively charged niobium- or titanium-oxide surfaces are used as substrates for this process. In a first step, a biotinylated polyelectrolyte copolymer grafted with PEG chains (cationic poly(L-lysine)-graft-poly(ethylene glycol) (referred to as PLL-*g*-PEG-biotin)) is adsorbed by a simple dip and rinse step in an aqueous solution on the photoresist patterned substrate (Fig. 6.3c). At neutral pH, the positively charged amino-terminated backbone of the PLL-*g*-PEG-biotin molecule adsorbs electrostatically to negatively charged metal oxide surfaces, such as niobia, and to the photoresist as well. After lift-off of the photoresist, PLL-*g*-PEG-biotin and bare substrate regions are exposed (Fig. 6.3d). Backfilling of the Nb_2O_5 substrate with non-biotinylated PLL-*g*-PEG is achieved by subsequent immersion of the sample in a PLL-*g*-PEG solution. As a result of the MAPL process, a micro pattern of biotinylated areas (PLL-*g*-PEG-biotin) in a non-adsorbing background (PLL-*g*-PEG) is achieved, for which the non-specific interactions of serum proteins is below 2 ng/cm^2 (Fig. 6.3e).[4] A PLL-*g*-PEG version with a molecular weight of the PLL backbone of 20 kD, a PEG chain length of 2 kD molecular weight and a grafting ratio of 3.5 was used in this work. For a more detailed experimental section, please refer to Chapter 3.5.

Colloidal self-assembly experiments on MAPL samples were performed by first immersing a MAPL sample of 1 x 1 cm into a streptavidin solution (25 $\mu g/ml$ in

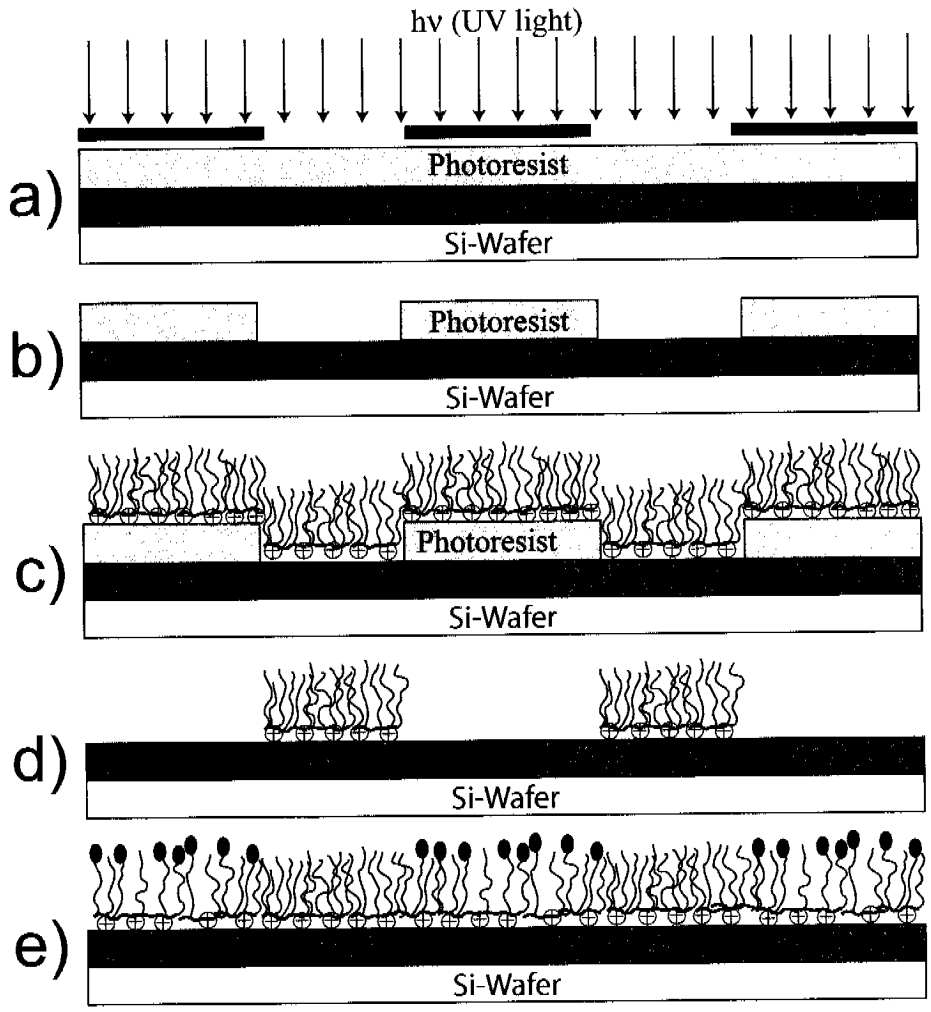

Figure 6.3: Schematic illustration of the Molecular Assembly Patterning by Lift-Off process (MAPL): a) A photoresist layer is spin-coated on a Nb_2O_5-coated wafer and a standard photolithography process produces a photoresist pattern (b). c) This pattern is coated with PLL-*g*-PEG-biotin polymer. d) Photoresist lift-off. e) backfilling of open areas with PLL-*g*-PEG. Sketches are not drawn to scale.

Hepes 1) for 30 *min*. After rinsing and drying of the sample, it was immersed into a Hepes 1 suspension of PLL-*g*-PEG—biotin coated colloidal particles for 30 *min*. The coating of the particles was established as described in Section 3.2.1. Samples were flooded after adsorption with extensive amounts of millipore water to remove all non-adsorbed colloidal particles. They were then rinsed and dried under nitrogen flow.

OWLS experiments (see Section 3.1.4) were conducted to observe *in situ* the adsorbed amounts of species, e.g. PLL-*g*-PEG-biotin on the substrate surface, streptavidin on the biotinylated PLL-*g*-PEG surface and biotinylated colloidal particles on streptavidin. SEM imaging was used to characterize the final colloidal arrays.

6.3 Results and Discussion

The Molecular Assembly Patterning by Lift-Off (MAPL) technique [4] (Fig. 6.3) produces a micro pattern of biotinylated areas (PLL-*g*-PEG-biotin) in a non-adsorbing background (PLL-*g*-PEG), for which the non-specific interactions of serum proteins is below 2 ng/cm^2. Particles functionalized with the same biotinylated polymer can be specifically attached to the biotinylated areas of the MAPL chip using streptavidin as a linker. The background of these pattern has to be rendered non-interactive for the colloidal particles in order to avoid unspecific adsorption of colloidal particles to the background. While in the system discussed in Chapter 5, the nano colloid self-assembly was driven predominantly by guided capillary forces, the colloidal particles are functionalized in the MAPL process to directly interact with the micro-pattern present on the surface. Thus, capillary forces during drying might have an unwanted impact and should be minimized.

6.3.1 Coating of Nanoparticles with PLL-*g*-PEG

In a first step, the colloidal nanoparticles were coated with biotinylated PLL-*g*-PEG co-polymer. This was achieved by mixing equal amounts of colloid suspension with a PLL-*g*-PEG-biotin solution (buffered at pH 7.4 with Hepes 2) as described in the experimental chapter. ζ-potential measurements were conducted to monitor the adsorption of the co-polymer to the colloid surface (Fig. 6.4). The isoelectric point

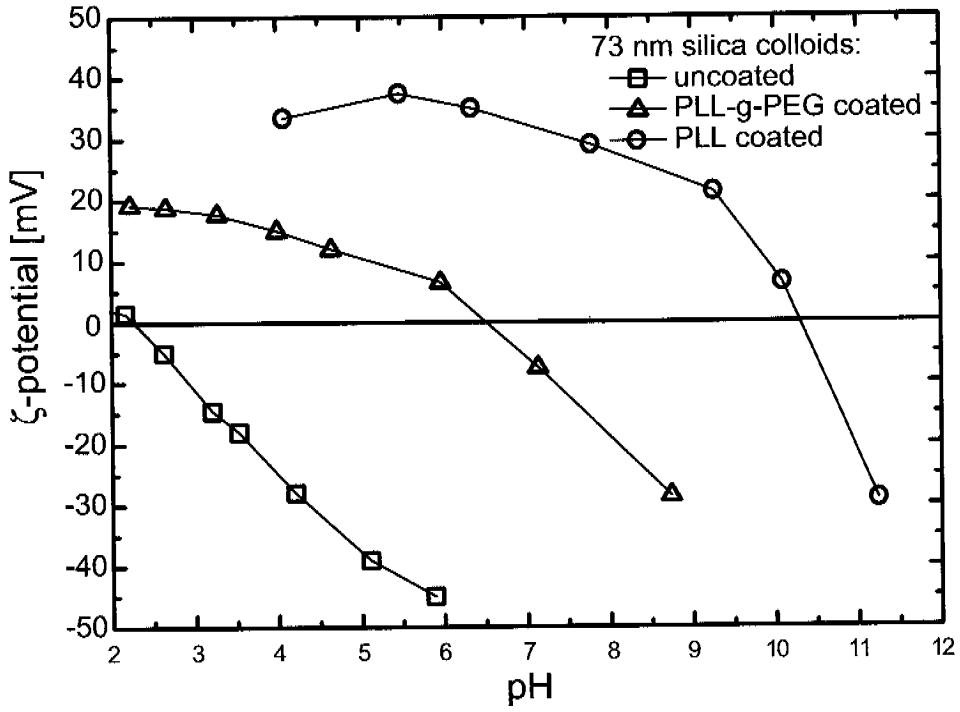

Figure 6.4: Change in ζ-potential upon adsorption of PLL-*g*-PEG and PLL, respectively. The IEP is shifted from a pH of 2.38 for pure silica colloids to 6.8 for the PLL-*g*-PEG-coated colloids and 10.5 for the PLL-coated colloids. Note that there is no notable difference in ζ-potentials between PLL-*g*-PEG- and PLL-*g*-PEG-biotin-coated particles.

(IEP) of the 73 nm silica colloids was determined to be at pH 2.3. Mixing of the colloidal suspension with the co-polymer solution shifted the IEP to pH 6.5, indicating that the surface of the colloidal particles became indeed coated with a PLL-*g*-PEG film. The positively charged polyelectrolyte co-polymer adsorbed to the negatively charged silica particle surface exposing the uncharged, hydrophilic PEG chains. It is the exposed water-like PEG chains that are believed to be responsible for the change in the IEP to values close to pH 7. There is also no distinct difference on the behavior of ζ-potential between PLL-*g*-PEG and PLL-*g*-PEG-biotin coated particles. On the other hand, coating the silica colloids with the positively charged PLL (without the attached PEG chains) rendered the silica surface positive (+35 mV at pH 7) and shifted the IEP to 10.3. From a colloidal stability point of view, the IEP shift of silica particles when coated with PLL-*g*-PEG is an "unfavorable" tendency, since particles are used at pH 7.4 which means their electrostatic repulsion is much lower when coated with PLL-*g*-PEG. However, PLL-*g*-PEG-coated silica suspensions are stable up to several weeks, because the brush-like PEG chains in

the PLL-*g*-PEG molecule have an additional important function: they sterically stabilize the colloid suspension preventing them from coagulating even at pHs close to the IEP (see Fig. 2.8). For this reason, no agglomeration of particles was observed in the experiments, even if the suspensions were kept for several month. Sedimentation of particles did occur, but this was reversed by vortexing the suspension for a minute or two. One advantage of the steric stabilization of PLL-*g*-PEG-coated silica suspension was the fact, that also high salt suspensions (e.g. in Hepes 2 (150 *mM* NaCl plus 10 *mM* ions from Hepes buffer) may be used without a loss of their stability, whereas high salt suspension of pure silica particles tended to agglomerate with time.

6.3.2 Adsorption Behavior of Coated and Uncoated Silica Particles

Not only ζ-potential measurements were conducted to test, whether the coating was successful. OWLS measurements on homogeneous substrates further confirmed that the coating process of the colloidal particles lead to completely non-interacting particles as shown in Fig. 6.5. In this OWLS measurement, PLL-*g*-PEG co-polymer was adsorbed to the niobia surface and after rinsing with buffer — PLL-*g*-PEG-coated silica nanoparticles were introduced in the system. After washing of the flow cell with buffer, no particles remained adsorbed to the PLL-*g*-PEG-coated surface. That the adsorption behavior of coated and uncoated silica particles differs dramatically, can be seen in Fig. 6.6. The uncoated particles readily adsorbed on a PLL-*g*-PEG coated surface within minutes (depending on the concentration) and formed a stable and dense layer as observed by SEM and OWLS (Fig. 6.6b). If the colloidal particles were coated with a PLL-*g*-PEG layer, the adsorption behavior changed completely and the coated particles no longer adsorbed to a PLL-*g*-PEG-coated surface (Fig. 6.6c). Thus, by coating the colloidal silica particles with a layer of PLL-*g*-PEG (or PLL-*g*-PEG-biotin) we can produce silica nanoparticles, that are not only non-interacting with a PLL-*g*-PEG coated surface but also form very stable suspensions due to the steric stabilization of the particles because of the brush-like PLL-*g*-PEG coating.

As shown, uncoated silica particles adsorb to a large extent to a surface covered with PLL-*g*-PEG. This observation is in fact somewhat puzzling at a first glance: a

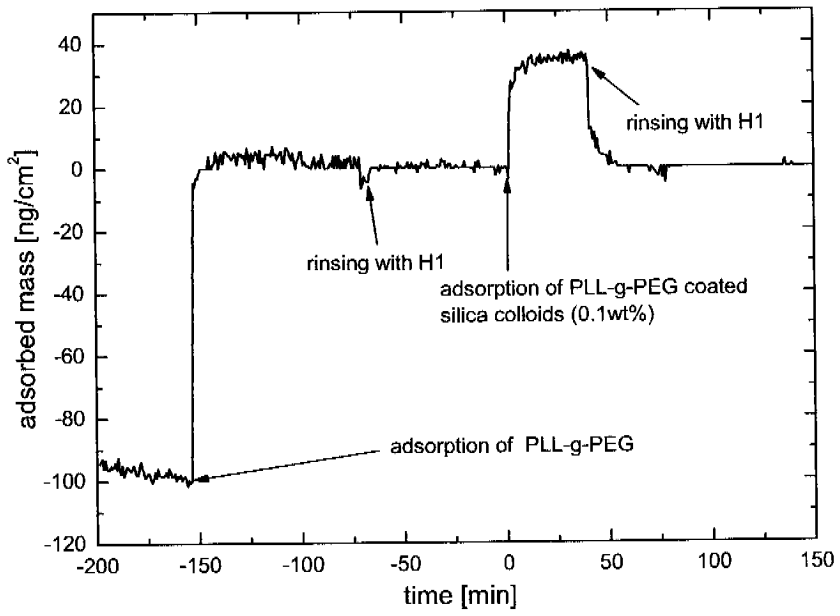

Figure 6.5: OWLS experiment showing how coating the 73 nm silica colloids with PLL-*g*-PEG makes these particles non-interacting with a PLL-*g*-PEG surface.

PLL-*g*-PEG layer[3] on a silica substrate extends about 8-10 nm[10] from the surface forming a strongly hydrated and dense PEG brush. If particles and substrate surface are coated with a PLL-*g*-PEG adlayer, the interaction between particle and surface and between individual particles is efficiently reduced, because PLL-*g*-PEG acts as a stabilizing agent on the surface by providing steric repulsion. The reason why uncoated silica nano colloids do adsorb to a PLL-*g*-PEG coated surface is somewhat less obvious. Theoretical calculations using equation 2.16 show that the Debye-length — the length at which the electric double layer is effective — is ~3 nm for a 10 mM electrolyte solution and < 1 nm for a 160 mM solution. Therefore, the negative charges from the metal-oxide surface should be completely shielded by the ions within the adsorbed 8-10 nm thick PLL-*g*-PEG layer and indeed uncoated SiO_2 micro particles did not interact with PLL-*g*-PEG coated surfaces in colloidal probe AFM experiments,[1] which is contradicting the results found in this work for silica nanoparticles. We have found that, silica particles adsorb to PLL-*g*-PEG-

[3]Of the "standard" architecture PLL(20)-*g*[3.5]-PEG(2)

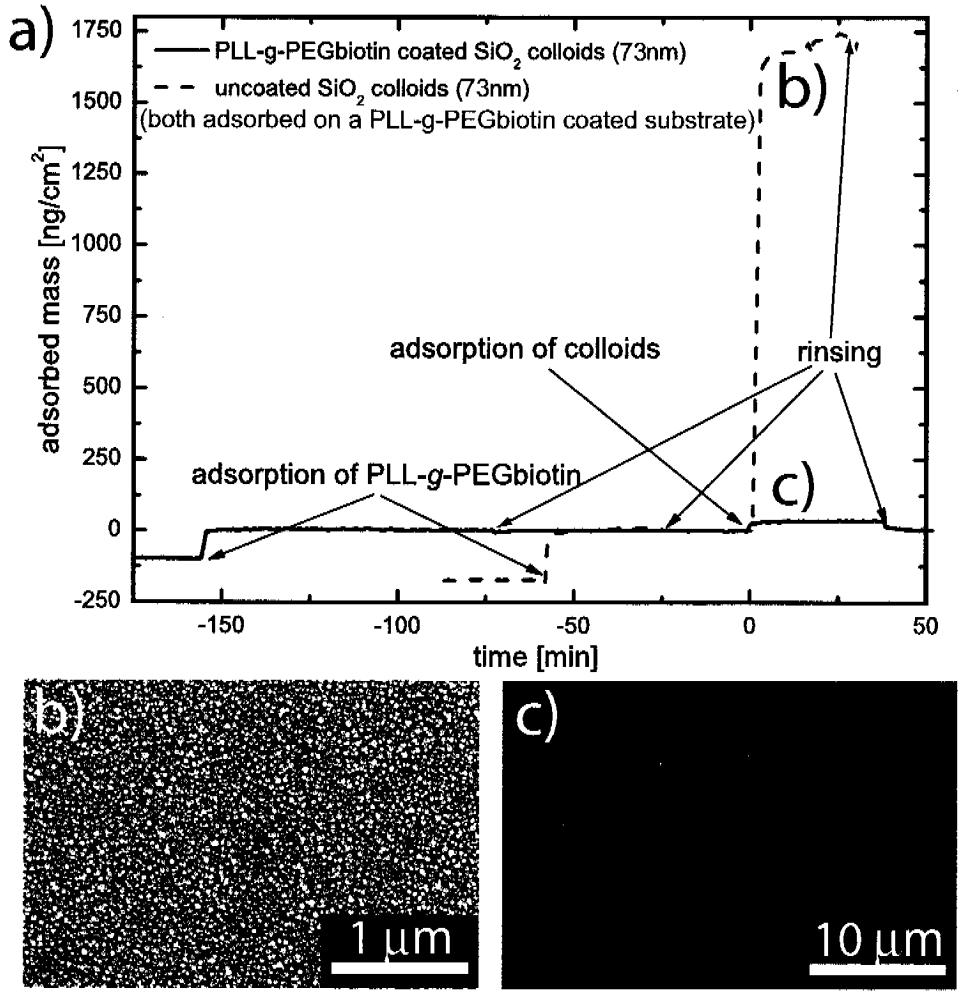

Figure 6.6: OWLS measurements and SEM micrographs showing the drastically different adsorption behavior of PLL-*g*-PEG-biotin coated and uncoated 73 *nm* silica particles on a PLL-*g*-PEG-coated surface. While the silica nanoparticles readily adsorb on such a surface, coating these particles with PLL-*g*-PEG-biotin efficiently reduces the interactions between the colloidal particles and the surface.

coated niobia surfaces and — in fact — the amount of adsorbed particles depends on the specific PLL-*g*-PEG architecture used. In Fig. 6.7 this correlation is shown. It is seen, that the adsorbed amount of colloidal particles increases from the top left to the bottom right. In the case of a pure PLL adlayer (without the PEG side chains), a monolayer of particles adsorbs due to the fact, that the PLL is a cationic polyelectrolyte that reverses the negative charge of the surface. Therefore, the adsorption in this case is electrostatically driven and follows a random sequential adsorption process as discussed in Chapter 4. As soon as PEG side chains are grafted to the PLL, the adsorption behavior will and cannot be purely electrostatic, because a) the number of positive charges on the PLL molecule is reduced (for every PEG chain, a positively charged amino side chain of the PLL molecule is consumed) and b) the PEG side chains shield the remaining charge from the surface and from the PLL molecule. In the top right corner of Fig. 6.7, a high grafting ratio PLL-*g*-PEG version (g=22.6)[4] is used and adsorption of colloidal particles is similar to that of a pure PLL surface. T he loss of electrostatic attraction in this case is made up for by another attractive force. In the bottom left and right corner of Fig. 6.7, higher grafting ratios of PLL-*g*-PEG are chosen (as described in the figure), indicating that more PEG side chains are grafted to the PLL backbone. It is observed, that more nanoparticles adsorb to this kind of surface. If the PEG chain length is varied (from 2 to 5 kD, which is the only difference between the bottom left and right image), again substantially more particles are able to adsorb, even forming colloidal multilayer.

An explanation for the adsorption behavior of silica nano colloids as shown in Fig. 6.7 was suggested by van der Beek et al.[11] They found, that silica surfaces (of nano colloids) may form hydrogen bonds between the protonated oxygen atoms of the silica surface and the oxygen atoms of the PEG layer and thus silica nano colloids can be immobilized on the surface. This has also the consequence that with increasing pH more and more Si-OH groups get deprotonated and less colloids will adsorb due to reduced hydrogen bonding as suggested by Gage et. al.[12] This model can explain why PLL-*g*-PEG coated surfaces with lower grafting ratios (e.g. more EG-groups are present per surface area) exhibit increased colloid adsorption as shown in Fig. 6.7. Indeed, each ethylene glycol unit has four potential hydrogen bond acceptor groups[13] and if the EG-density on the surface is increased (as it is continuously in Fig. 6.7), the number of potential hydrogen bonding sites in-

[4] I.e. fewer PEG side chains per PLL monomer

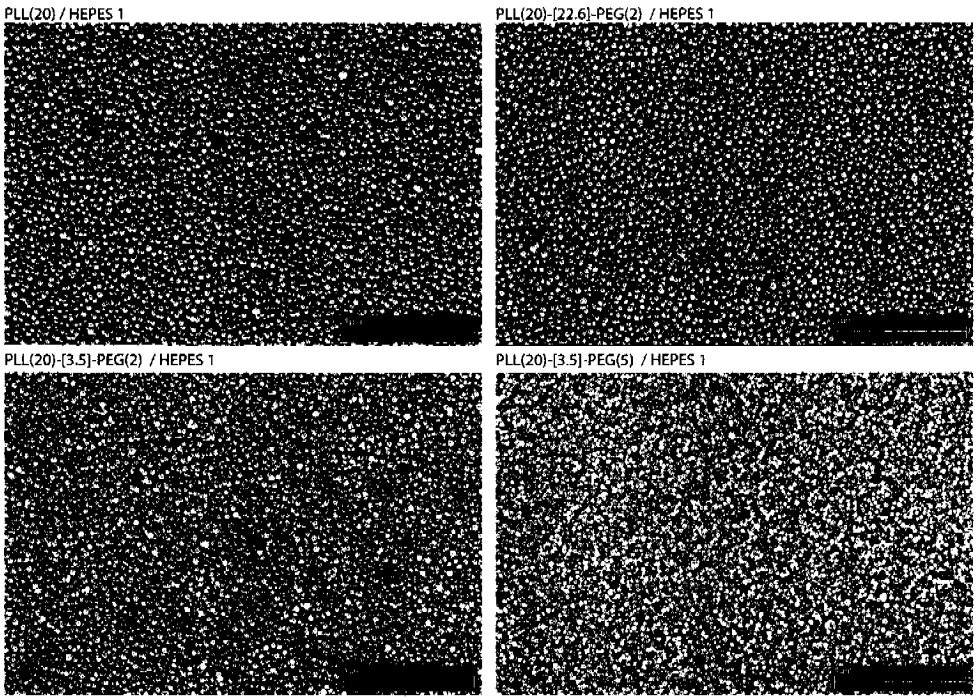

Figure 6.7: SEM micrographs showing the influence of PLL-*g*-PEG architecture on the adsorption behavior of 73 *nm* silica nanoparticles. The amount of adsorbed colloidal particles increases steadily as the grafting ratio of the PLL-*g*-PEG is increased. An increase in the grafting ratio is related to an increase in the ethylene glycol (EG) density on the surface. On the top left, a pure PLL film is used, where particles adsorb electrostatically. On the top right, a very high grafting ratio PLL-*g*-PEG was used and colloid adsorption is already increased. In the bottom left and right, two PLL-*g*-PEG architectures with the same grafting ratio (3.5) are chosen, but in one case the PEG chain length is 5 instead of only 2 *kD*. This also leads to a higher EG-density on the surface and as a consequence more silica nano colloids have adsorbed.

creases. Indeed, the importance of hydrogen bonding in adsorption processes is also found in other systems. For example, Zheng et al. observed that amino-terminated polystyrol particles specifically adsorb to ethylene glycol self-assembled monolayers through hydrogen bonds. These experiments make clear, that adsorption processes of colloidal particles may not simply be viewed in terms of electrostatic interactions. While in most "high surface charge" situations, it is true that electrostatic interactions dominate adsorption processes, for situations where only a low amount of charges is involved (e.g. by charge shielding due to adsorbed co-polymers as in the presented system or in low-surface charge materials) other interaction mechanisms (hydrogen bonding, hydrophobic interactions) gain in importance and may become the driving forces for adsorption processes.

However, this hypothesis struggles with some aspects observed in experiments. For example, multilayer of particles are often seen at very high EG-density samples which can not simply by explained with the presented hypothesis. Another possible explanation might be bridging phenomena which are known to occur with long, adsorbed co-polymers. If bridging occurs, PLL-g-PEG-molecules spontaneously detach partly from the surface and might re-attach at a particle near the surface and attract it to the surface. Such bridging events might also be involved in the adsorption process of silica particles to PLL-g-PEG-coated substrates. At this point, both mechanism same plausible and possibly both will contribute to the phenomena observed.

6.3.3 Production of Functionalized Nanoparticle Arrays using MAPL

Colloidal self-assembly experiments on MAPL samples were performed by first immersing a MAPL sample of 1 x $1cm$ (exhibiting a PLL-g-PEG / PLL-g-PEG-biotin contrast) into a streptavidin solution to adsorb the streptavidin molecules to the biotinylated regions of the MAPL pattern. After rinsing and drying, samples were immersed into a suspension of PLL-g-PEG-biotin coated colloidal particles. Samples were then flooded with water before removal, rinsed with Millipore water and dried under nitrogen flow. In Fig. 6.8, a PLL-g-PEG / PLL-g-PEG/PEG-biotin contrast of 30 μm squares was produced and the PLL-g-PEG/PEG-biotin coated colloidal particles were bound to these squares via the streptavidin linker. Since no unspecific adsorption occurs on the background (Fig. 6.6c and Fig. 6.8), the nano colloid adsorption is restricted to the originally biotinylated areas of the substrate and formation of a monolayer is observed (inserts in Fig. 6.8b). Regions in the center of each biotinylated square, however, typically exhibit drying artifacts such as areas depleted of colloids (Fig. 6.8d). These artifacts originate from the capillary forces that act upon drying and which are not negligible even if the colloids are bound to the surface by biotin-streptavidin interactions. However, we did observe less-extensive multilayer formation on MAPL samples as it was the case for the SMAP samples if particle concentration was increased and dip-coating speed was reduced. This is attributed to the fact that on MAPL chips, there is no distinct hydrophobicity contrast pattern since there is no significant contact angle difference between a PLL-g-PEG-biotin coated and a PLL-g-PEG coated surface and therefore different processes are responsible for the nano colloid array formation in the

two patterning approaches. However, in the last stage of the drying process, when liquid bridges are still present between individual particles and a capillary force is exerted, the particle arrays might still be deformed resulting in the observed drying artifacts (Fig. 6.8d).

In Fig. 6.9 two more examples of a typical colloidal array obtained on MAPL chips with lines are shown. In these samples the biotin density on the substrate was changed from 50% to 5%.[5] In both cases similar colloidal pattern were produced (Fig. 6.9a),b) and c) show images from a sample with 5% biotin on the pattern, d),e) and f) show images from a 50% biotin sample). Even though some particle clusters are present on the background in most samples, the colloidal arrays show good fidelity with those high biotin concentrations. In the course of this work, the dependance of the pattern formation on the biotin concentration was investigated, but due to reproducibility issues (mainly caused by drying effects as explained in the next paragraph) this dependance could not be established consistently. It was clear from these experiments, however, that high biotin concentrations are favorable for the formation of the particle arrays and pattern fidelity decreases if the biotin-concentration on the surface is lower than 5% (as shown in Fig. 6.10).

The influence of capillary forces is observed on high magnification images (c) and f) similar to those seen on samples with square structures (Fig. 6.8). This can be understood, if the forces involved in the formation of the particle arrays in these MAPL chips are estimated: the binding strength of biotin to streptavidin is around -80 kJ/mol,[6, 9] an exceptionally high value for a ligand-binding system, which equals a binding strength in the order of -1.33x10^{-19} J per biotin-streptavidin bond. At high biotin concentrations, more than one biotin-streptavidin bond will form between the biotinylated particles and the biotinylated surface pattern (linked by streptavidin). Calculations show, that in the case of a particle coated completely with PLL-g-PEG/PEG-biotin, each particle carries several hundred PLL-g-PEG/PEG-biotin molecules. Thus, the amount of biotin units on a completely covered particles is around 15-20 thousand. However, only the biotin functions which are in the section of the particle, which is in contact with the surface are able to bind to the surface-bound streptavidin. Also, not all of these functions are available as binding sites due to the distribution of the PEG end groups throughout the polymer

[5]Note, that the PLL-g-PEG/PEG-biotin copolymer has a biotin unit at every second PEG side chain. Thus 50% biotin density is equal to 100% PLL-g-PEG/PEG-biotin, while 5% biotin describes a mixture of 10% PLL-g-PEG/PEG-biotin with 90%PLL-g-PEG.

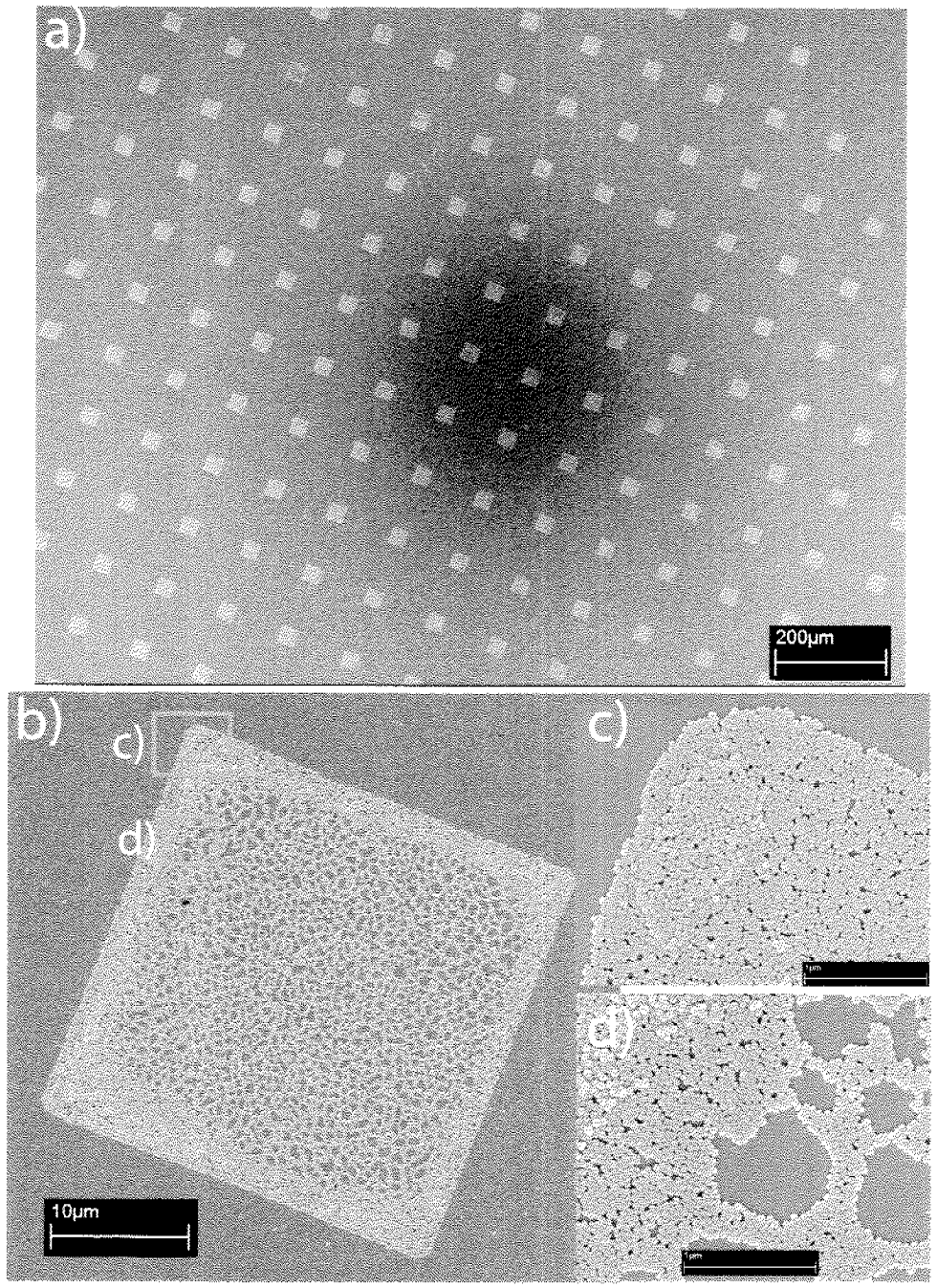

Figure 6.8: SEM micrographs showing colloidal nano-arrays obtained by adsorption of PLL-*g*-PEG/PEG-biotin coated 73 nm silica colloids on a MAPL chip. On this chip, 30 μm squares are coated with PLL-*g*-PEG/PEG-biotin while the PLL-*g*-PEG coating on the background effectively resists particle adsorption. Streptavidin is adsorbed to the biotinylated regions of the substrate and subsequently binds the biotinylated silica colloids. The achieved patterns show good fidelity over a large area (a). Edge regions of the pattern are sharply confined (b/c). Depletion effects in the center regions of an individual square are drying artifacts that are often seen in these colloidal nano-arrays (d).

layer.[14] This distribution problem exist on both, the particle and the surface, thus the effective number of biotin-groups that contribute in the binding of a single particle is probably in the order of some hundred biotin-streptavidin links. However, even if several hundred of these bonds are considered, the binding strength will remain in the order of -1x10^{-17} to -1x10^{-16} J. If this value is compared to the capillary force which arises between two particles during the drying step, it must be concluded that the particle-surface binding strength is several orders of magnitude lower than the capillary forces. The strength of the capillary interaction was estimated in Chapter 5 to be in the order of -1.8x10^{-14} J. This estimation of the effective forces also supports the presented mechanism of how these arrays form. In suspension, the biotin-streptavidin bond by which the particles are bound to the surface are extraordinarily strong (since there is no competing force of similar strength). Therefore, the particles are bound to the biotin surface pattern in an efficient way. As soon as drying of these particle layers proceeds, capillary forces much stronger than the particle-surface interaction may distort the colloidal pattern and structures as shown in Fig. 6.8 and 6.9 are formed.

An interesting phenomenon was repeatedly observed on samples with very low biotin concentrations. To test the specificity of the colloid binding, MAPL chips were produced with no or only a very low biotin concentration on the pattern (instead, unfunctionalized PLL-g-PEG or a mixture of PLL-g-PEG with PLL-g-PEG/PEG-biotin was used). Thus, the patterning process was inherently the same, but instead of a high biotin density on the patterned structures no or little biotin was present. Fig. 6.10 shows particle arrays observed on this kind of pattern. The most astounding observation was that samples containing no biotin at all (effectively being a PLL-g-PEG pattern in a PLL-g-PEG background!) still showed the evolution of particle arrays (Fig. 6.10a). However, the evolution of these particle arrays seems to be exclusively initiated by capillary forces. Indeed, the obtained structures differ significantly from colloidal arrays shown in for example Fig. 6.9. Interestingly, these structures formed by capillary forces seem to nucleate from the edges of the pattern (even though, ideally, there should be no pattern whatsoever in Fig. 6.10). Note also, that the morphology of these particle structures originating from capillary forces could not be controlled and any of the structures depicted in Fig. 6.10 could be observed. The production process of these colloidal layers is such, that the immersed sample is flooded with extensive amounts of water (around 1 l for a sample immersed in 1-2 ml of suspension). By doing so, it was aimed to remove most of the

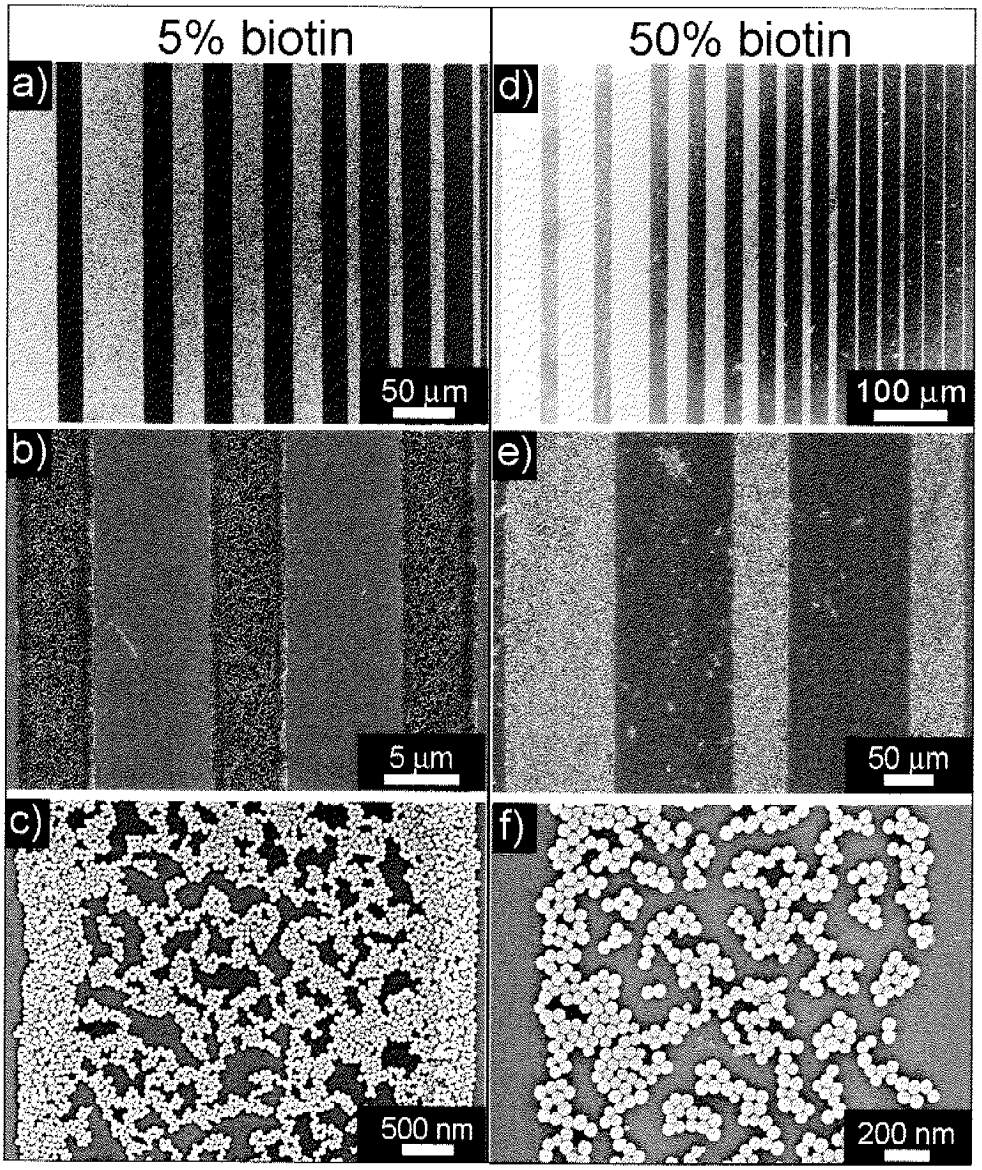

Figure 6.9: Colloidal silica nanoparticle arrays (73 *nm*) self-assembled on a MAPL chip with line structures. a),b) and c) show images of samples with a biotin density of 5% on the line pattern (e.g. a biotin molecule is attached to every 20^{th} PEG side chain). d),e) and f) are images of samples with a biotin density on the lines of 50%. A good pattern fidelity is observed on all samples, however, often particle clusters are also observed on the background. High magnification SEM images (c) and f) reveal the morphology of the particle structures. Typically, clustering of particles on the micron-sized structures is observed due to capillary forces evolving during the drying process. The formation of double layers in the edge regions of the pattern which is sometimes observed is attributed to same effect.

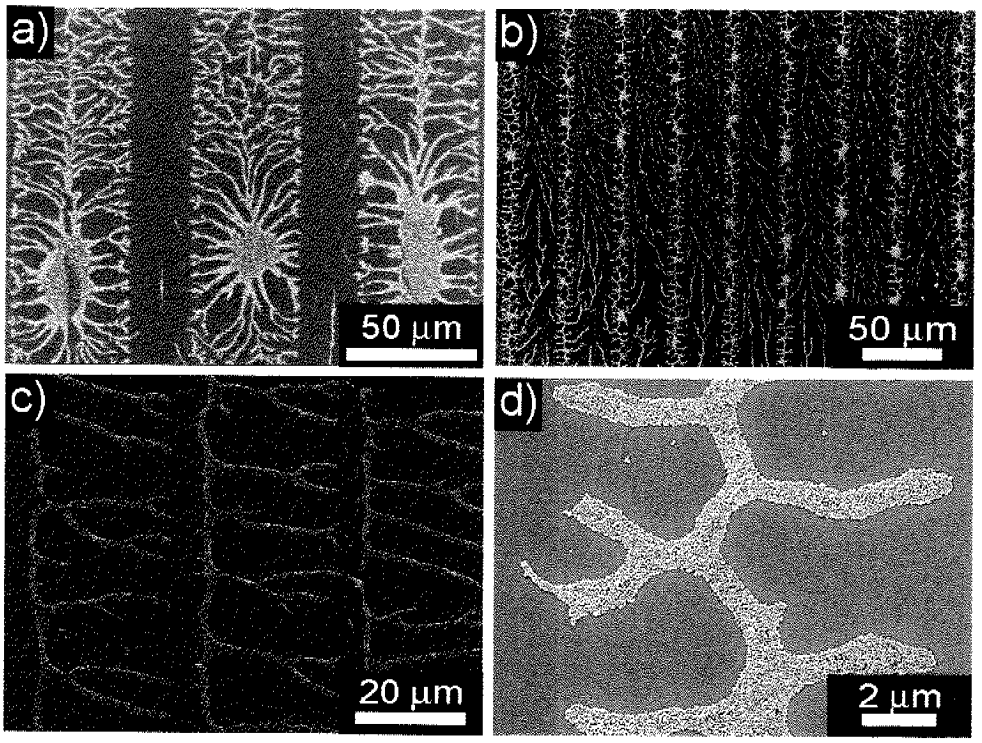

Figure 6.10: Colloidal particle arrays (73 *nm* silica particles) obtained on MAPL chips with line structures with no biotin on the surface (a) or very low biotin densities (b: 0.05% c: 0.5% d: insert of b). Capillary forces form the colloidal structures observed in these images, the biotin concentration is too low to induce the formation of colloidal layers as shown in Fig. 6.9. For more details see text.

non-adsorbed particles from the suspension, a goal which seems not to have been reached in this case. However, it is also probable, that the particles did interact with the surface pattern weakly in suspension, such that the rinsing step was not able to remove these particles form the surface. These weakly interacting particles on the surface will then be present during the drying step. Which case is relevant can not be determined from the data available, however, the evolution of these particle arrays is attributed to the drying process, where the remaining suspension (in which still a considerable amount of particles can be found) dries off on the surface and the structure present is sufficient to induce the formation of the colloidal arrays. In fact, the amount of particles may be approximated to be in the order of only a few thousand times less than the initial amount of particles.[6] Since in 1 *ml* of a 0.1 *wt%* suspension several million particles are present, even after excessive flushing with

[6] 1 *ml* of suspension is added onto the sample, then it is flooded with at least 1 *l* of pure water, diluting it by a factor of at least 1000.

water a considerable number of particles can be found in the suspension which might then forming the structures found on the substrates. Thus, the washing step was not sufficient by itself to completely remove the particles and avoid the adsorption of particles which have not been attached via a biotin-streptavidin linker or — as noted above — the particles were weakly interacting with the surface, in such a case, a washing step will not be sufficient to remove the particles from the substrate. Note that there is no "structure" in Fig. 6.10a) (since the surface should be chemically equal on the whole chip), rather it is suspected that at the edges of the structures inhomogeneities exist originating from the photolithography and lift-off process. These inhomogeneities on the structure edges or on the pattern seem to be large enough to induce a structuring of the drying process. Also, very similar structures are observed if low concentrations of biotin were present on the sample. The structures in Fig. 6.10b) (and d), which is an insert of b) contain only 0.05% biotin on the lines and those in Fig. 6.10c) have a biotin density of 0.5%. Such low biotin densities seem not to be sufficient to bind the particles (in a significant number) to the surface during the 30 *min* of immersion. Only if the biotin concentration is increased to values of 5% or more, structures as shown in Fig. 6.9 rather than those in Fig. 6.10 may be obtained.

The origin of these drying structures is not completely understood, however, a hypothesis may be given: For one, these structures are consistently observed on the biotinylated areas, i.e. the features, where the copolymer was adsorbed in the first place, before the lift-off of the photoresist in the background took place. The removal of the photoresist might in fact slightly disturb the PLL-*g*-PEG/PEG-biotin layer and induce a slight difference in the wetting behavior. The morphology of the structures indicates that some difference in hydrophobicity on the pattern surface evolves, which leads to the observed effects. Also, the edge-effects[7] suggest that at some point during the drying process, the drying front must have been pinned at pattern edges. This again is an indicator that the pattern homogeneity is not perfect and that indeed at edges of the pattern some irregularities evolve and that PLL-*g*-PEG-adlayers that went through the photoresist lift-off process may have a slightly different composition.[8] It might be necessary to study the chemical composition and evolution of the chemical structures on a MAPL-pattern more thoroughly in the future to confirm or disprove this hypothesis.

[7]All particle structures are confined at the edges of the pattern

[8]Otherwise, there is no reason why in Fig. 6.10 *any* pattern formation should be observed

6.4 Conclusions

The assembly of functionalized nanoparticles on a chemically structured surface using a specific ligand binding system was demonstrated. More specifically, PLL-*g*-PEG/PEG-biotin coated silica particles were bound to biotinylated surface regions of a pattern with biotinylated and non-biotinylated areas using streptavidin as a linker. Coating of the particles with PLL-*g*-PEG/PEG-biotin was followed by the investigation of the adsorption behavior of these particles, which indicated that the coating process was successful. The coated particles were no longer interacting with a PLL-*g*-PEG/PEG-biotin-coated surface (in the absence of streptavidin). This coating method allows the production of functionalized silica nanoparticles, which are inherently non-interacting with proteins as well as with a PLL-*g*-PEG-coated surface. Only the specific linkage of the particles using streptavidin is able to bind these particles to the MAPL pattern. Thus, a system was developed where colloidal particles may be specifically adsorbed to a biotinylated area of a pattern in an otherwise non-interacting environment. However, capillary forces that act upon drying may influence the pattern formation considerably since these forces are stronger than the biotin-streptavidin linkage.[9] If the concentration of biotin on the surface is decreased, so is the binding strength of the particle to the surface and the capillary forces are even more dominant and the pattern formation is heavily disturbed. It was also found that having no biotin on the surface (and therefore having no interaction between particles and surface) still produces particle arrays on a MAPL pattern. This finding is attributed to defects which occur in the MAPL process at the edges of the pattern and are sufficient for capillary forces to structure the particles during the drying step. The flushing step which was introduced with the aim to remove all non-adsorbed particles from the suspension before the drying step starts, was not sufficient in this regard. These remaining particles may dry on the substrate pattern and disturb the particle arrays.

While the particle arrays obtained with this process are generally of lower quality than those presented in previous chapters, the main advantage of this system lies in the inherent protein-resistance of these particles as well as the surface pattern. With the presented patterning process, it is therefore possible to form particle assemblies on a surface which will not interact with biological species unless another specific functionality is introduced in the system. Even though challenges remain for the

[9] Even if many of these binding events are considered per particle

large-scale defect-free production of these arrays, they prove to be an interesting concepts, that allows the assembly of specifically functionalized particles to a surface pattern. The following chapter will present concepts and first results of how this kind of particle arrays may be used in the future to enhance the performance of biosensing devices.

Bibliography

[1] Pasche, S. *Mechansims of protein resistance of adsorbed PEG-graft co-polymers.* Doctoral thesis, ETH Zurich, 2005.

[2] Huang, N. P., Michel, R., Voros, J., Textor, M., Hofer, R., Rossi, A., Elbert, D. L., Hubbell, J. A. and Spencer, N. D. Poly(L-lysine)-g-poly(ethylene glycol) layers on metal oxide surfaces: Surface-analytical characterization and resistance to serum and fibrinogen adsorption. *Langmuir*, **17**(2), 489–498, 2001.

[3] Caruso, F. Nanoengineering of particle surfaces. *Advanced Materials*, **13**(1), 11–+, 2001.

[4] Falconnet, D., Koenig, A., Assi, T. and Textor, M. A combined photolithographic and molecular-assembly approach to produce functional micropatterns for applications in the biosciences. *Advanced Functional Materials*, **14**(8), 749–756, 2004.

[5] Green, M., Wilchek, M. and Bayer, E. Avidin and streptavidin. In *Methods in Enzymology*, volume 184, pages 51–67. Academic Press, 1990.

[6] Miyamoto, S. and Kollman, P. A. Absolute and relative binding free energy calculations of the interaction of biotin and its analogs with streptavidin using molecular dynamics/free energy perturbation approaches. *Proteins: Structure, Function, and Genetics*, **16**(3), 226–245, 1993.

[7] Bayer, E. and Wilchek, M. The use of the avidin-biotin complex as a tool in molecular biology. *Methods of Biochemical Analyis*, **26**, 1–45, 1980.

[8] Freitag, S., Trong, I. L., Klumb, L., Stayton, P. S. and Stenkamp, R. E. Structural studies of the streptavidin binding loop. *Protein Sci*, **6**(6), 1157–1166, 1997.

[9] Weber, P. C., Wendoloski, J. J., Pantoliano, M. W. and Salemme, F. R. Crystallographic and Thermodynamic Comparison of Natural and Synthetic Ligands Bound to Streptavidin. *Journal of the American Chemical Society*, **114**(9), 3197–3200, 1992.

[10] Heuberger, M., Drobek, T. and Voros, J. About the role of water in surface-grafted poly(ethylene glycol) layers. *Langmuir*, **20**(22), 9445–9448, 2004.

[11] Vanderbeck, G. P., Stuart, M. A. C. and Cosgrove, T. Polymer Adsorption and Desorption Studies Via H-1-Nmr Relaxation of the Solvent. *Langmuir*, **7**(2), 327–334, 1991.

[12] Gage, R. A., Currie, E. P. K. and Stuart, M. A. C. Adsorption of nanocolloidal SiO2 particles on PEO brushes. *Macromolecules*, **34**(15), 5078–5080, 2001.

[13] Clark, S. L. and Hammond, P. T. The Role of Secondary Interactions in Selective Electrostatic Multilayer Deposition. *Langmuir*, **16**(26), 10206–10214, 2000.

[14] Feuz, L. *On the coformation of graft-copolymers with polyelectrolyte backbone in solution and adsorbed on surfaces.* Doctoral Thesis, ETH Zurich, 2006.

Seite Leer /
Blank leaf

CHAPTER 7

Bi-Functionalization of Colloidal Particles: towards more Sensitive Bio-affinity Assays

7.1 Introduction

7.1.1 Colloidal Nanoparticles and Proteomics?

In the recent past, the use of nanoparticles of various types and characteristics has grown rapidly in the area of drug delivery, bioassay applications, molecular detection etc. Applications are envisaged and are being developed in the area of cancer targeting,[3] drug delivery [4] and for understanding cellular response [5]. A wide variety of materials, which are available in a large structural diversity are being used in such devices.[6] The field of biosensing has also seen use of nanoparticles not just for the high surface area [7] but also for signal amplification,[8, 9] as protein detection and coding (using magnetic particles,[10, 11]as signaling agents,[12] biomolecule harvesting or fractionation [13], detection of pathogenic biomolecules [14] and even facilitating enzyme immobilization and improving enzyme stability [15].

For protein microarrays in proteomics[1], nanoparticles have the potential to be used in several interesting ways. For example it was discussed, that an ideal protein microarray substrate has to offer attributes like limited non-specific binding, high surface area-to-volume ratio and compatibility with available detection methods.[16]

[1]Proteomics is defined as the large-scale study of proteins (with biochemical methods).[1] This usually involves the systematic determination of all proteins, their sequence, quantity, modification state, interaction partners, activity, sub-cellular localization and structure in a given cell type at a particular time.[2]

With the nanoparticle system developed in Chapter 6, some of these requirements can be met in principle. These functionalized nanoparticles offer for example a high area-to-volume ratio, which has the potential to significantly increase the sensitivity of a surface microspot. So far, planar substrates have been traditionally used in this area as they proved to be very successful with the nucleic acid arrays.[17] However, they lack the required surface area per spot for detecting proteins with very low concentrations, like in the femtomolar range, of the analyte proteins.[18] This is where nanoscale particles assembled or spotted on these microspots offer the potential to increase the loading capacity of an individual spot significantly. Furthermore the particles produced in Chapter 6 are inherently non-interacting with biological species and specific capturing agents may be incorporated in the particle surface to selectively bind proteins on these particles. All these aspects and concepts will be outlined in this chapter's results and discussion section in more detail.

In this chapter, possible ways of using high-surface area, bi-functionalized nanoparticles as signal enhancers and analyte-capturing platforms are introduced and discussed. Bi-functionalization of nanoparticles may offer an interesting way of forming *in situ* particle assemblies on desired spots (by using one function to bind the particles to the surface (and / or each other)), while the second function on these particles acts as a capturing agent for a specific analyte. Basic experiments elucidating these concepts and trying to explore these possibilities are presented and their potential for future applications in protein microarrays is assessed. The ideas and concepts developed here are further examined and pushed forward at the time of writing in the doctoral thesis work of Martin Halter, who also contributed his ideas and time to this chapter.

7.2 Experimental

7.2.1 Colloid Assembly Experiments

In the case of serum adsorption experiments on colloid monolayers (see Fig. 7.1 and 7.2), the substrate (SiO_2 coating on an OWLS waveguide) was coated after standard cleaning with a thin layer of poly(ethylene imine) (PEI) (see Section 3.2.2 for details). This coating first renders the SiO_2 surface positive at neutral pH and allows the rapid electrostatic adsorption of negatively charged silica colloids. After

adsorption of the colloid layer for 40 *min*, another layer of PEI was adsorbed to render the colloid sub-monolayer positive again so that serum adsorption on both samples (bare PEI-coated surface and colloid monolayer coated with PEI) could be compared. If more then one layer was produced, the procedure was just repeated for every colloid layer.

Bi-functionalization of the colloidal particles was performed essentially according to the protocol given in Section 3.2.1. However, a slight change was introduced to add a second function to the particles: the amount of PLL-*g*-PEG/PEG-biotin was adjusted such, that theoretically a certain fraction of the colloid surface is coated on average. Then, the second function (either PLL-*g*-PEG/PEG-NTA or anti-human Fibrinogen) was added in excess to the colloidal suspension to backfill the free surface on the colloidal particles. Centrifugation and adsorption of the particles was again performed as outlined in Section 3.2.1.

Adsorption of the particles was done by first coating the substrate with a PLL-*g*-PEG/PEG-biotin layer (20% biotinylated PLL-*g*-PEG / 80% non-biotinylated PLL-*g*-PEG) in Hepes 2. Then, a 25 $\mu g/ml$ streptavidin solution (in Hepes 2) was adsorbed on this layer. Bi-functionalized particles were then immobilized on the PLL-*g*-PEG/PEG-biotin / streptavidin layer.

7.3 Results and Discussion

7.3.1 Increasing Sensitivity by Increased Surface Area of Particle Layers

In a first set of experiments, it was confirmed that increasing the surface area by the presence of a particle layer increases the adsorbed amount of serum. Fig. 7.1 shows OWLS curves of 10% serum adsorbing on substrates with different surface areas prepared by colloid deposition (for SEM images of these experiments see Fig. 7.2). The first curve shows serum adsorption on a PEI coated silicon wafer (—). As expected serum readily adsorbs in considerable amounts to the positively charged polyelectrolyte (around 500 ng/cm^2). If prior to the serum adsorption, a colloidal (sub-)monolayer of 73 *nm* silica particles was adsorbed on the surface, the value of adsorbed serum was increased by a factor of about 2. More than 1000 ng/cm^2

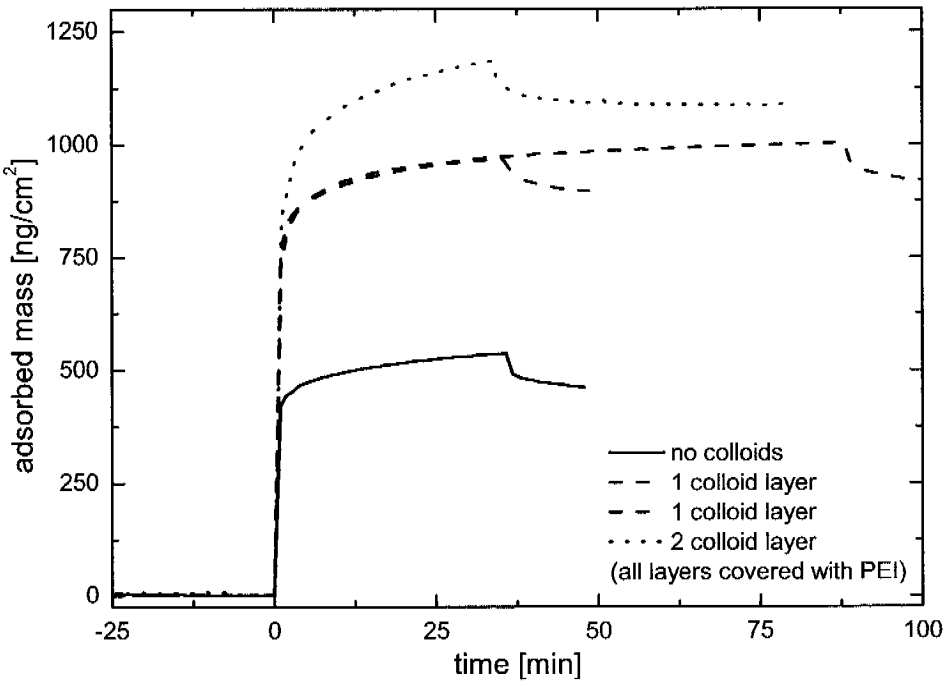

Figure 7.1: OWLS curves showing the adsorption behavior of 10% human serum on a PEI coated SiO_2-coated waveguide (—), on a PEI coated 73 *nm* silica particle layer (- - -) and on two of these particle layers (...). Particle multilayer are simply achieved by alternating adsorption of PEI and silica particles. In the presence of a single particle layer, serum adsorption is roughly doubled and it is further increased on a double particle layer. Also note, that in case of the double particle layer, adsorption kinetics is slower and the rinsing step was interrupting the adsorption process. Given more time, even more serum would have been able to adsorb to the double particle layer. SEM images illustrating the particle layers are presented in Fig. 7.2

of serum adsorbed on a sub-monolayer of particles in these OWLS experiment. Note that the silica colloids were adsorbed on a PEI coated waveguide and after adsorption, the particles were coated with a PEI layer as well to ensure equal surface chemistry. Thus, the change in adsorbed mass can be attributed solely to the change in available surface area. A second experiment for the single particle layer is shown in Fig. 7.1 to demonstrate the good reproducibility of the experiment. A second particle layer further enhances the ability of the system to adsorb proteins. However, the second particle layer only adsorbed about 1250 ng/cm^2 serum. This rather low increase may have two origins: on the one hand, the second particle layer already has a height of more than a hundred *nm* (roughly twice the particle size of 73 *nm*). In this region, the evanescent field induced by the incoupled laser light is already diminished thus not all the information (e.g. not all adsorbed proteins) will be

detected from this outer region. This is also the reason, that for more than 3 particle layers no significant increase in adsorbed serum was detected (data not shown). The decay length of the evanescent field is in the order of 180 *nm* for a 633 *nm* wavelength laser and a water-based suspension on top of the waveguide, which indicates that the sensitivity of the OWLS measurement is in the order of 90 *nm*. Thus, the smaller increase of serum adsorption in the second layer can be expected. However, this rough estimate does not take into account the change in the sensitivity caused by the adsorbing particles[2]. A second reason might be the evolution of diffusion problems that might start to play a role if the number of particle layers is increased. Proteins have to diffuse through the particle layers to be able to adsorb in the first layer or on the substrate surface. However, the 73 *nm* particles used here might be to big to induce such problems.

From a theoretical point of view, the increase in surface area is simply defined by the area available on a colloidal particle plus the surface below that particle ($4\pi r^2 + \pi r^2 = 5\pi r^2$) divided by the area without a particle (πr^2). Thus a factor of 5 is gained in surface area at the location of a particles. In a hexagonally close-packed layer (74% particle coverage) the effective increase in surface area would be 3.7 (0.74 times 5) and if a probably more realistic random sequential adsorption configuration of the particles (coverage of 54.7%) is assumed, the gain is reduced to a factor of 2.75. This factor of increase is relatively close to the factor observed for a particle monolayer in the presented OWLS experiments. Hypothetically, it can also be reasoned, that this factor is a value *per particle layer*, thus with decreasing particle size and increasing layers of particles this factor may be increased considerably.

7.3.2 Protein Resistance of PLL-*g*-PEG/PEG-biotin coated particle layers

For any approach using particle assemblies to be successful in a biosensing / proteomics application, the surface chemistry must be controlled. For example, the surface chemistry of the particles should be tailored such, that no unwanted adsorption of biological species occurs unless it is specifically designed to do so. The prevention of such unwanted interactions is a key factor in such applications since it

[2]The particles will strongly affect the decay length of sensitivity of the OWLS depending on their refractive index

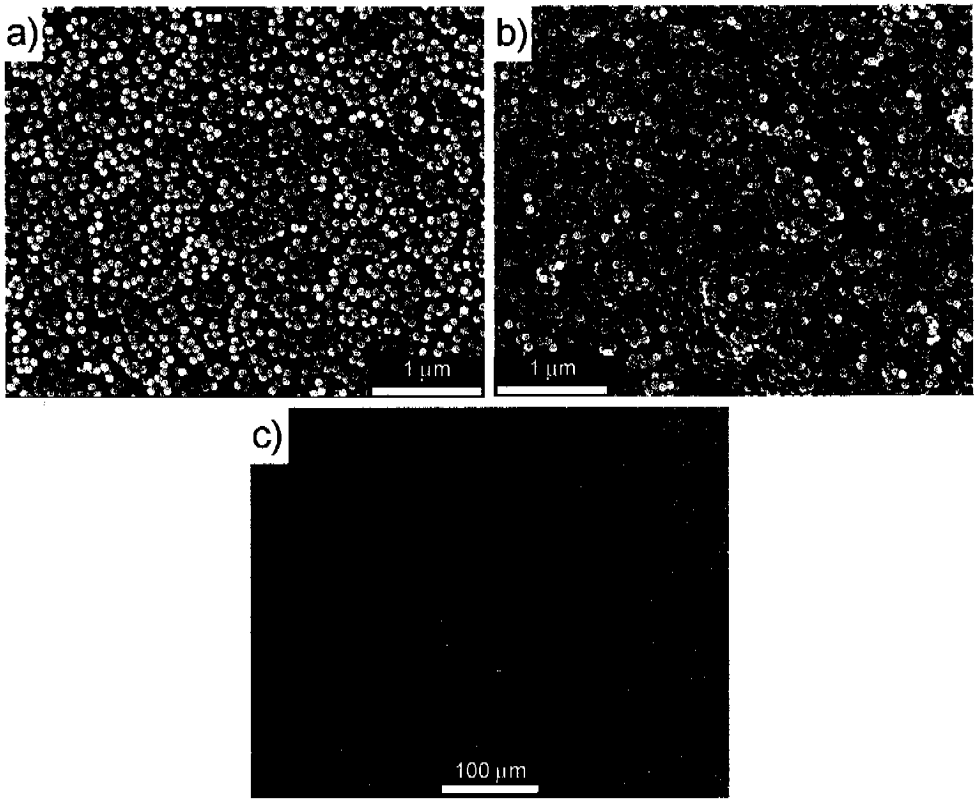

Figure 7.2: SEM images illustrating the particle layers used in the OWLS experiments in Fig. 7.1. a) A single layer of 73 *nm* silica particles adsorbed on a PEI coated waveguide in Hepes 1. A loosely packed monolayer is observed, typical for a random sequential adsorption process. Also, some influence of capillary forces are visible, notable clustering of particles occurs. b) Same as a) but this time with three adsorbed particle layers. Still, a relatively loosely packed structure is produced with no sign of crystallization. c) Smooth PEI coated waveguide surface used as a reference.

does not only significantly reduce the signal-to-noise ratio of the device by avoiding unspecific adsorption but also decreases the amount of "false-positive" signals which are attributed to other biomolecules than the target adsorbing on areas which are reserved to the specific adsorption of target molecules. To prevent unspecific adsorption of proteins onto a surface, poly(ethylene glycol) (PEG) coated surfaces have proven to be extremely successful. In our group the formation of PLL-*g*-PEG adlayers on metal oxide surfaces (as introduced in the previous chapter) has been shown to completely prevent protein adsorption on particle layers even from complex protein solutions like serum. Also, ways of patterning surfaces in the micron- and nano-scale have been developed and were the basic of the colloidal patterning approach presented in the previous chapter. The concept in this chapter for the

production of protein-resistant particle assemblies with specific functionalities therefore build on the knowledge gained with the PLL-*g*-PEG system on flat samples. The first question is, whether we can produce protein-particle layers on a protein-resistant background. This question is of fundamental importance, since only with such a system, further functionalization of particles is a promising way of producing functional particle arrays for biosensing applications.

In Fig. 7.3, a schematic view of the functionalization system and two OWLS curves are presented. 73 *nm* silica colloids coated with PLL-*g*-PEG/PEG-biotin were then immobilized using the streptavidin linkage system on a PLL-*g*-PEG/PEG-biotin functionalized Nb_2O_5 coated waveguide substrate. Fig. 7.3b) and c) show the adsorption of the functionalized colloidal particles monitored by OWLS. In Fig. 7.3b), adsorption of PLL-*g*-PEG/PEG-biotin coated particles on a PLL-*g*-PEG/PEG-biotin adlayer in Hepes 1 is shown.[3] After particle adsorption (only a few 100 nm/cm^2 adsorbed in Hepes 1), human serum is adsorbed to the particle layer to test for protein resistance of this particle layer. If particles are adsorbed in Hepes 1, a small amount of proteins (around 50 ng/cm^2) is still adsorbed on the surface after washing with buffer solution. If the same experiment is repeated in Hepes 2 the situation changes drastically. First, a lot more particles adsorb to the surface than in Hepes 1 buffer. Second, no proteins from human serum adsorb in Hepes 2 as seen after the washing step. This finding is expected, since it has been shown before, that the protein resistance of a PLL-*g*-PEG adlayer is better in Hepes 2 buffer than in Hepes 1. While the higher salt concentration of Hepes 2 is less favorable for the stability of the particle suspension, it is clearly more suitable for the protein resistance of the adsorbed particle layers. Also, the coating of the particles sterically stabilizes the particle in suspension such that the disadvantage of using Hepes 2 as the solvent is largely reduced. In fact, no stabilization problems with Hepes 2 suspensions were observed. Even if the suspension did settle over the course of several days, gentle stirring was sufficient to redisperse the particles in Hepes 2 suspensions. Thus, Hepes 2 was used in the course of this chapter since it showed better protein resistance properties of the particle layer. The good protein resistance of these particle layers[4] is an important finding, since it shows, that with the present system we can produce particle layers that are inherently protein resistant but at the same time offer

[3]Streptavidin is adsorbed on the PLL-*g*-PEG/PEG-biotin before particle adsorption in a separate step

[4]Protein resistance was also excellent for 2 and 3 layers of adsorbed particles

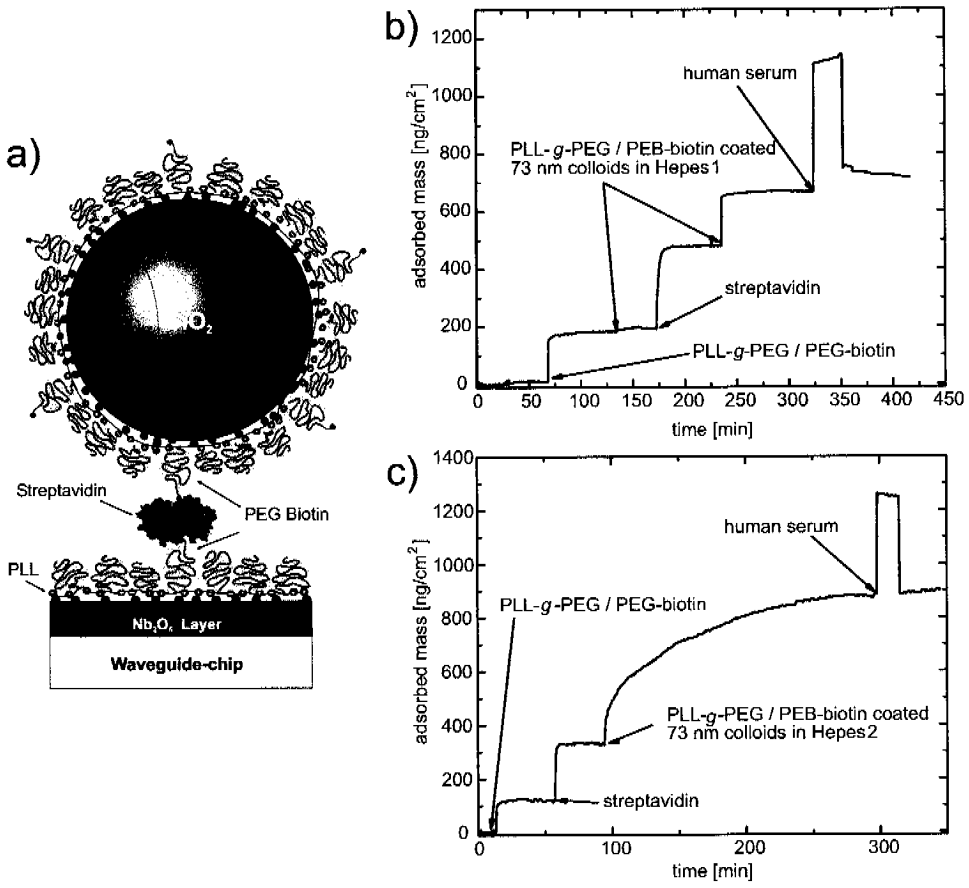

Figure 7.3: Sketch of a silica particle coated with a PLL-*g*-PEG/PEG-biotin adlayer. The coated particle is bound via a streptavidin linker to the PLL-*g*-PEG/PEG-biotin coated surface. The right hand side shows two OWLS experiments with the depicted coated particles showing the resistance of these particle layers to protein adsorption. The experiment shown in the top graph is performed in Hepes 1 (10 *mM* salt concentration) and does not show complete resistance to protein adsorption, while the lower graph shows an experiment done in Hepes 2 (160 *mM* salt concentration). Choosing higher salt concentration buffer leads to completely protein resistant particle layers.

the functionality (via the biotin-function) to be specifically adsorbed on a suitable surface and even into particle assemblies as shown in the previous chapter.

In order to check what biotin-concentration is needed on the particles to achieve a good binding to the surface, OWLS and ellipsometry experiments were conducted. To do so, silica colloids coated with different surface area coverage of PLL-*g*-PEG/PEG-biotin (0, 1, 2, 5, 10, 25 and 50%) were obtained. The desired biotin-coverages were achieved by mixing PLL-*g*-PEG/PEG-biotin with the unfunctionalized PLL-*g*-PEG. The OWLS waveguide or the ellipsometry chip was functionalized with a mixture of 20% PLL-*g*-PEG/PEG-biotin and 80% PLL-*g*-PEG. Since the PLL-*g*-PEG/PEG-biotin used was 50% biotinylated, the final concentration of biotin on the surface was 10%. This coverage has been kept constant throughout this chapter for the coating of the surface, since it was found that a too high biotin concentrations on the surface reduces the activity of the streptavidin.[19] The OWLS and ellipsometry measurements were performed twice for each type of functionalized colloidal solution. The amount of colloids (in ng/cm^2 or %) that were immobilized on the surface were noted for each type of colloidal solution and the summary of these results is given in Fig. 7.4, for both ellipsometry and OWLS experiments. The amount of adsorbed coated particles increases rapidly with increasing biotin concentration on the particles and reaches its maximum at around 10%. Higher biotin concentrations do not have any positive effect and in fact, a slight decrease in adsorbed particle amounts is seen in OWLS experiments with increasing the biotin concentrations above 10%. However, almost no difference in ellipsometry data is observed for higher concentrations (though the error bars are slightly higher). Coating the particles with pure PLL-*g*-PEG shows, that these particles do not interact with the surface at all and no unspecific particle adsorption is found in this case. The same is true if the streptavidin linker is not present: the biotinylated particles also will not interact with the surface. These results show, that already at rather low biotin-concentrations (around 5-10%) on the particle surface a sufficient amount of particles is bound to the surface and high biotin concentrations show no further positive effect. A fact, which will allow to only incorporate a small fraction of biotin binding sites on the particle and leave the larger portion of the surface free for other functionalizations. Note that these results were obtained for homogeneous particle layers. The situations changes somewhat if patterned particle layers are considered (as was shown in Chapter 6). There, a higher biotin coverage on the surface, resulted in better quality colloidal pattern (but not necessarily having much more

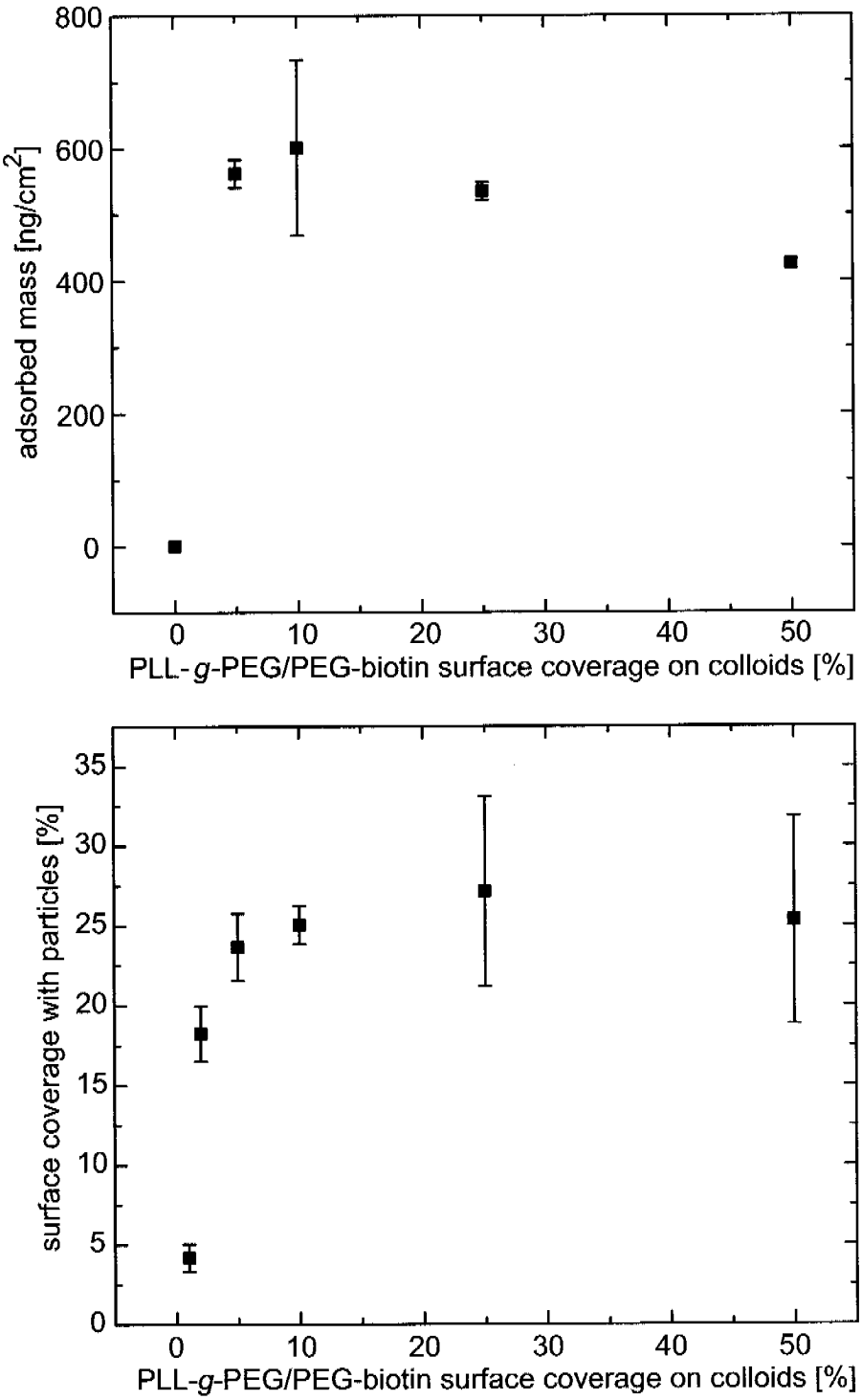

Figure 7.4: OWLS (top) and ellipsometry data (bottom) showing the influence of PLL-*g*-PEG/PEG-biotin concentration on 73 *nm* silica particles on the total adsorbed amount of particles on a PLL-*g*-PEG/PEG-biotin surface layer (in Hepes 2). Both, OWLS and ellipsometry show good agreement and indicate that already a low percentage of PLL-*g*-PEG/PEG-biotin on the particles is sufficient to bind them to the surface. Higher concentrations will not help to adsorb more particles, rather a plateau region is reached after around 10%.

particles adsorbed). However, on patterned particle arrays, capillary forces have a much higher influence than on homogeneous layers, which explains this behavior.

7.4 Bi-Functionalization of Colloidal Particles

So far, it was shown how silica nanoparticles were functionalized with a PLL-*g*-PEG/PEG-biotin adlayer. This adlayer on the one hand rendered those particles protein resistant (as well as non-interacting with a PLL-*g*-PEG coated surface). Furthermore, the biotin functional unit provided an anchoring tool by which the colloidal particles can be immobilized on streptavidin coated surface. This tool allows for example the patterning of colloidal particle assemblies as shown in Chapter 6. However, in a real biotechnology application (such as a biosensing device), a single functionalization of a particle will often not be sufficient. Not only should there be an anchoring functionality (which will bind the particles to the surface), but also a second functionality which is able to capture a target molecule.[5] Fig. 7.5 shows two sketches of such a bi-functionalized particle systems. There, each particle carries two functions. The first function is used to immobilize the particle on the surface, while the second function is used to capture a target molecule from a biological sample. In one case (Fig. 7.5a), the target molecules are 6xHis-tagged proteins (in this work, 6xHis-tagged green fluorescent protein (GFP) was used). The 6xHis-unit specifically interacts with the NTA-Ni^{2+} complex present on the particle surface. The NTA-unit is end-grafted to PLL-*g*-PEG similarly as the biotin. The second scheme uses specific antibody-antigen interactions to bind a target protein. There, anti-human Fibrinogen (aFb) is co-adsorbed to the particle surface together with PLL-*g*-PEG/PEG-biotin. The aFb-proteins are then able to capture human Fibrinogen (Fb) from a biological sample solution.

In Fig. 7.6, the feasibility of a bi-functionalization approach was tested using OWLS to measure *in situ* the adsorbed amounts of the specific target molecules. In these experiments, the system sketched in Fig. 7.5b) was used. First, a mixture of PLL-*g*-PEG/PEG-biotin and anti-human fibrinogen (aFb) was co-adsorbed on a niobia coated OWLS waveguide. The mixing ratio was chosen such, that a relatively low amount of PLL-*g*-PEG/PEG-biotin was on the surface (between 0.1 and 10 *wt*%)

[5]Note that it might be very well possible to have the biotin function performing *both* functions at once: anchoring the particles to the surface and capturing streptavidin-functionalized target molecules

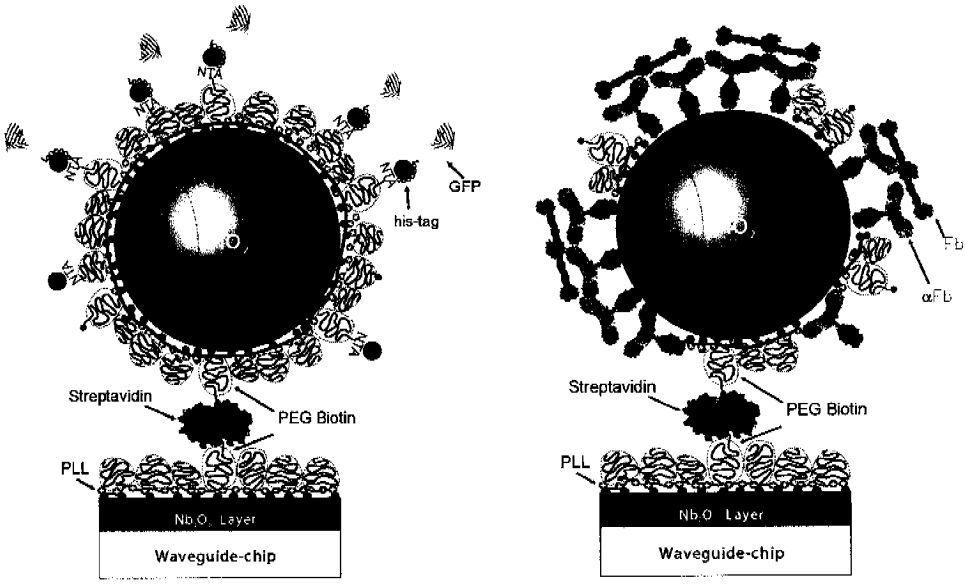

Figure 7.5: Two sketches of bi-functionalization schemes used in this work. The substrate surface is in both cases coated with a PLL-*g*-PEG/PEG-biotin adlayer and biotinylated PLL-*g*-PEG molecules on the particle surface are responsible for binding the silica particle to the surface (via a streptavidin linker), which is the first function. The second function varies in a) and b) but is in both cases used to capture a target protein form a biological sample solution. a) While a small portion of the particle surface is coated with PLL-*g*-PEG/PEG-biotin, the rest of the surface is coated with PLL-*g*-PEG/PEG-NTA. The NTA functionalization offers the possibility to capture any 6xHis-tagged protein (in this case 6xHis-tagged green fluorescent protein (GFP-6xHis)). The NTA unit attached at the end of the PEG chains forms a chelate with Ni^{2+} ions which is then able to bind 6xHis-tagged proteins. For more information on GFP see Section 3.2.4 and Ref [20]. b) The second bi-functionalization scheme also uses PLL-*g*-PEG/PEG-biotin as the first functional unit. The majority of the particle surface, however, is in this case coated with anti-human fibrinogen (aFb). The adsorbed aFb then acts as a capturing agent for the target protein (Human Fibrinogen (Fb)).

and the major part of the waveguide surface was occupied by the aFb. However, the results of these experiments indicate, that producing such bi-functionalized surfaces is far from trivial (even on flat, homogeneous substrates) and some troubling observations were made during the course of these experiments. For example, the adsorbed amounts of the PLL-*g*-PEG/PEG-biotin / aFb mixtures are unexpectedly low. In all four cases tested in Fig. 7.6 amounts below 200 ng/cm^2 were found while an amount of around 200 ng/cm^2 is expected for a PLL-*g*-PEG/PEG-biotin adlayer and aFb was found to adsorb in the order of 500 ng/cm^2 to a niobia surface. Thus, it must be concluded that the surface coating might have an uncertain composition, which impedes the interpretation of these results. Nevertheless, some observations can be made from these experiments. First, regardless of which of the

two functional molecules (streptavidin or fibrinogen) is adsorbed in the first place, the adsorbed amounts of the respective molecules stay the same (Fig. 7.6a) and b). This indicates that the system is specific for both molecules and neither of the two adsorbs non-specifically. Furthermore, tests with human serum albumin in the same graphs showed that no adsorption of this protein occurred (although this is not a sufficient proof of this system's specificity). It was also observed, that changing the mixing ratio of PLL-*g*-PEG/PEG-biotin and anti-human fibrinogen on the surface changes the adsorbed amounts of streptavidin and fibrinogen accordingly. If only very little PLL-*g*-PEG/PEG-biotin is present on the surface, the amount of adsorbed streptavidin decreases drastically (Fig. 7.6d). However, the difference in the adsorption behavior between 5 and 10% PLL-*g*-PEG/PEG-biotin on the surface is less distinct and in fact a certain error in the adsorbed amounts was observed in these experiments (compare Fig. 7.6a) and c), where more fibrinogen adsorbs in the case where 90% aFb was on the surface than in the case with 95%). And again, it must be stressed that these experiments suffer from the lack of knowledge of the precise composition of the surface coating.

This system provides a possibility of bi-functionalizing a surface with two specific functions. Changing the mixing ratios of the two functionalizations on the surface influences the adsorbed amounts of the specifically interacting proteins accordingly. However, some inconsistencies in this system were also observed as mentioned. The situation becomes even more complex, if nanoparticles are coated instead of flat substrates. Experiments with bi-functionalized nanoparticles showed even less conclusive results and difficulties arose during OWLS experiments with bi-functionalized nanoparticles. Fig. 7.7 shows typical OWLS curves obtained with bi-functionalized silica nanoparticles. The PLL-*g*-PEG/PEG-biotin and PLL-*g*-PEG/PEG-NTA system were compared on a flat substrate (a) and on 73 *nm* silica particles (b). It was found, that a good number of particles adsorb to the PLL-*g*-PEG/PEG-biotin coated surface via the streptavidin linker. The adsorbed amounts of GFP-6His (the 6xHis-tagged green fluorescent protein) on the flat substrate and the coated particle layer, however, are in a similar range (around 35-40 ng/cm^2 on the flat substrate and around 50 ng/cm^2 on the colloidal particles). Thus, while the system works in principle, the adsorbed amounts of green fluorescent protein were consistently only slightly higher on a particle layer than on a flat substrate and we could in this system not achieve a considerable increase of the adsorbed target molecules due to the increased surface area of the particle layer.

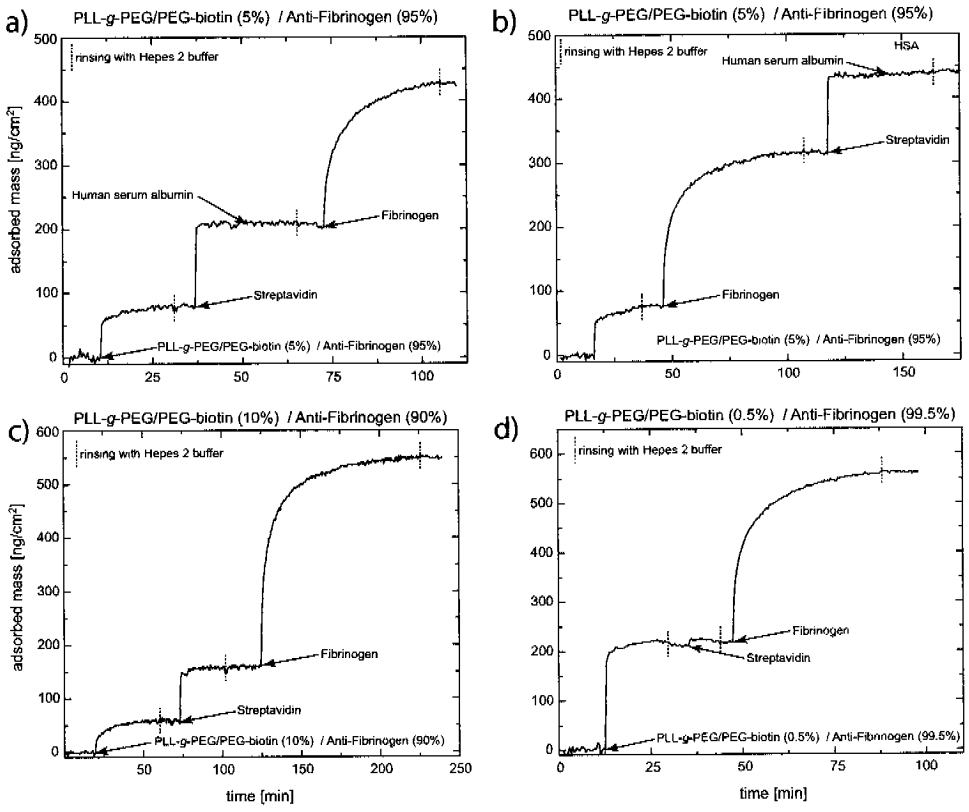

Figure 7.6: OWLS experiments of bi-functionalized (flat) niobia substrates, illustrating the working principle of bi-functionalized surfaces. The first step is in all 4 graphs the adsorption of an indicated mixture of PLL-*g*-PEG/PEG-biotin and anti-human fibrinogen (aFb), covering the substrate with the two functional molecules. Streptavidin adsorbs to the biotinylated areas of the surface and fibrinogen interacts specifically with the anti-human fibrinogen on the surface. Reversing of the adsorption steps of fibrinogen and streptavidin does not change the adsorption properties (a) and b). It is also shown in these two graphs, that human serum albumin does not adsorb to such a surface, demonstrating that the adsorption of streptavidin and fibrinogen is indeed specific and no unspecific adsorption occurs. Changing the mixing ratios of PLL-*g*-PEG/PEG-biotin and anti-human fibrinogen on the surface (c) and d) shows that as a consequence the adsorbed amounts of streptavidin and fibrinogen change.

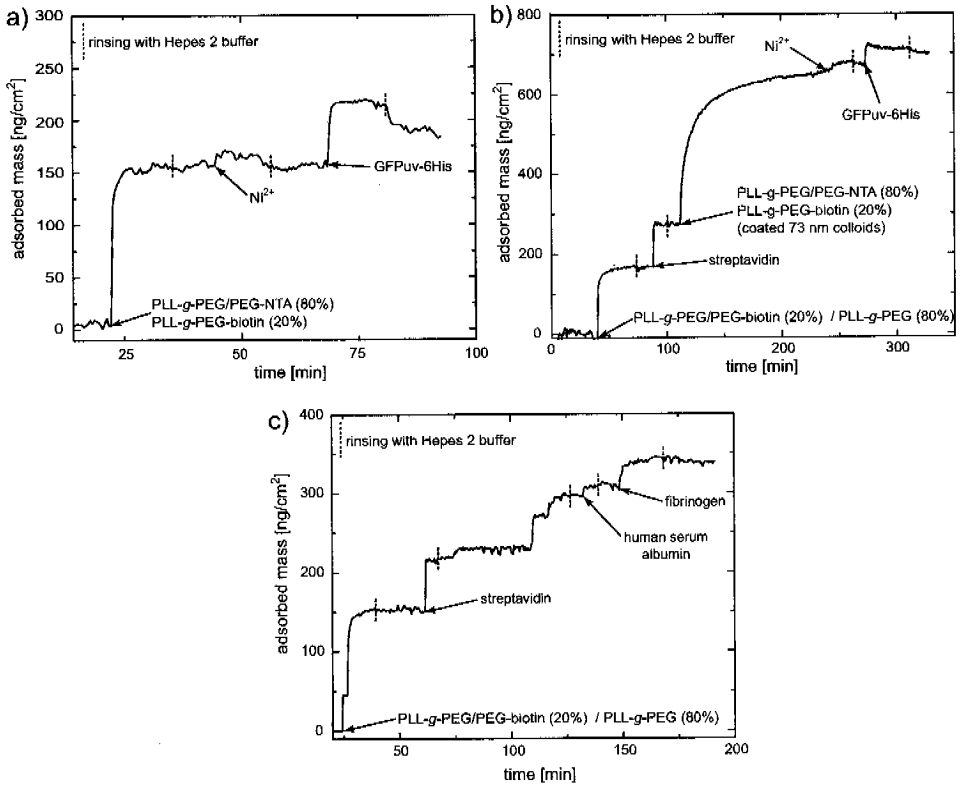

Figure 7.7: OWLS experiments showing the adsorption behavior of GFP-6His to a flat surface bi-functionalized with a mixture of PLL-*g*-PEG/PEG-biotin and PLL-*g*-PEG/PEG-NTA (a). The same experiment but this time with bi-functionalized particles adsorbing on the surface (b). c) shows bi-functionalized particles with PLL-*g*-PEG/PEG-biotin and anti-human fibrinogen co-adsorbed on the surface. However in this case, particle adsorption was very low. Consequently only little fibrinogen was adsorbing to the few particles. The system was still specific since no human serum albumin was found to adsorb.

Also the second system discussed before showed some unexpected behavior. As soon as the colloidal particles were coated with a mixture of PLL-*g*-PEG/PEG-biotin and anti-human fibrinogen only very few particles adsorbed to the surface via the streptavidin linker (Fig. 7.7c). Consequently, the amount of adsorbed fibrinogen remained relatively low as well. No unspecific adsorption occurred, however, as the test with human serum albumin proved. No clear understanding of this unexpected behavior was found at this time. The same system performs considerably better on a flat niobia substrate (as shown in Fig. 7.6) but as soon the transition is made to small silica nanoparticles the experiments become less conclusive. At the time of writing, the silica nanoparticle system is replaced by polystyrene particles which offer a better controllable particle surface compared to the silica particles used here.

Also, since the exact composition of the adlayer on the particle surface is unclear at this time, it might be that the particle surface have a different composition than expected, which would influence the adsorption behavior. Additionally, a number of other factors (signal dependance on colloid surface density / number of binding sites), different binding kinetics and strength of GFP and Fb (and other proteins) leading to unexpected effects (such as desorption / exchange or exclusion effects) may attribute to the inconsistencies still present in the investigated systems.

7.5 Conclusions

Nanoparticles can be used on a flat surface to increase the loading capacity efficiently: a single layer of 73 *nm* silica particles was shown to increase the amount of adsorbed serum by a factor of 2 (particles and surfaces both coated with a PEI layer). Furthermore, the resistance to non-specific protein adsorption of these silica nanoparticle layers could be minimized by coating the particles with a PLL-*g*-PEG/PEG-biotin adlayer. It was also shown that the protein resistance of such particle layers is excellent when using Hepes 2 as a buffer and decreases significantly if Hepes 1 buffer with a lower ionic strength is used. Such functionalized nanoparticle assemblies with their high specific surface area are therefore indeed possible candidates for biosensing devices (such as protein microarrays) since they can provide high sensitivity (due to the high surface area) with at the same time low signal-to-noise ratio (due to the excellent resistance to protein adsorption). The amount of biotin needed on the particle surface was investigated as well. The optimization of the PLL-*g*-PEG/PEG-biotin colloids surface coverage showed that around 5-10% of biotin on the particle surface was sufficient to immobilize the nanoparticles on the chip surface. This finding is of importance since it suggests the a large portion of the particle surface can be used to add a second functionality.

The colloids bi-functionalized with the PLL-*g*-PEG/PEG-biotin and PLL-*g*-PEG/PEG-NTA showed good immobilization on to the functionalized waveguide. However, the lower than expected binding of the GFP-6His was a predicament. The system needs to be investigated to determine how the proximity of the Ni^{2+}-NTA groups on the colloidal surface could improve the binding of the GFP to the colloids to obtain higher signal enhancement compared to a flat substrate.

Colloids coated with PLL-*g*-PEG/PEG-biotin and an antibody (anti-human fibrinogen) produced inconclusive results. The colloids were unable to bind to the streptavidin functionalized waveguide surface in the same amounts as the PLL-*g*-PEG/PEG-biotin functionalized colloids with the same biotin concentration. This could be due to some steric hindrance that the flexible PEG-biotin chains face from the antibodies on the colloidal surface, making the biotin on the colloidal surface unavailable to the streptavidin for binding, thus resulting in a low number of immobilized colloids on the surface.

Both of the tested bi-functionalization approaches suffer from a basic lack of accessability to measure the surface composition and therefore the interpretation of the presented data is troublesome. That the adsorption behavior is rather complex was already concluded from the experiments presented on flat, homogeneous substrates for the PLL-*g*-PEG/PEG-biotin / aFb system, where unexpectedly low amounts of those mixtures adsorbed. In the future, attempts will be undertaken to better understand such bi-functionalized particle systems and the optimization and investigation of these bi-functional particles is on-going work in follow-up projects in our lab.

Despite these complications, bi-functionalization of nanoparticle surfaces will in principle allow the production of nanoparticles which have tailored surface properties. One of the two functions may for example be used to immobilize the particles at specific locations on the surface via suitable patterning methods (as shown in the previous chapter). Then, the second function on the particle acts as a capturing agent for a specific target molecule, while at the same time the whole particle surface is resistant to non-specific interaction with a biological sample. The presented data supports the use and feasibility of such bi-functionalized particles as interesting means of introducing functionality (also as a pattern) on a surface.

To conclude, the basic principle shown here may present a promising way of producing highly functional nanoparticles that may be assembled on a surface (pattern) in a straight-forward way and at the same time provide specific "capturing functions", which allows to selectively bind a target molecule from a biological sample. Such particles may be useful for their use on a flat surfaces to increase the sensitivity of current biosensing devices by increasing the sensing area. The possibilities of such functionalized particles offers a great potential for many different applications in

biotechnology, but to do so the difficulties still existing with these complex systems must be solved to be able to utilize these nanoparticle systems to their full extent.

Bibliography

[1] Pandey, A. and Mann, M. Proteomics to study genes and genomes. *Nature*, **405**(6788), 837–846, 2000.

[2] Editorial - A cast of thousands. *Nat Biotech*, **21**(3), 213–213, 2003.

[3] Kim, G. J. and Nie, S. Targeted cancer nanotherapy. *Materials Today*, **8**(8, Supplement 1), 28 33, 2005.

[4] Pellegrino, P., Kudera, S., Liedl, T., Munoz, A., Manna, J. and Parak, W. On the Development of Colloidal Nanoparticles towards Multifunctional Structures and their Possible Use for Biological Applications. *Small*, **1**(1), 48–63, 2005.

[5] Haruyama, T. Micro- and nanobiotechnology for biosensing cellular responses. *Advanced Drug Delivery Reviews*, **55**(3), 393–401, 2003.

[6] Jianrong, C., Yuqing, M., Nongyue, H., Xiaohua, W. and Sijiao, L. Nanotechnology and biosensors. *Biotechnology Advances*, **22**(7), 505–518, 2004.

[7] Liang, R.-Q., Tan, C.-Y. and Ruan, K.-C. Colorimetric detection of protein microarrays based on nanogold probe coupled with silver enhancement. *Journal of Immunological Methods*, **285**(2), 157–163, 2004.

[8] Nam, J.-M., Thaxton, C. S. and Mirkin, C. A. Nanoparticle-Based Bio-Bar Codes for the Ultrasensitive Detection of Proteins. *Science*, **301**(5641), 1884 1886, 2003.

[9] Nam, J. M., Stoeva, S. I. and Mirkin, C. A. Bio-Bar-Code-Based DNA Detection with PCR-like Sensitivity. *J. Am. Chem. Soc.*, **126**(19), 5932–5933, 2004.

[10] Wang, J., Liu, G. and Jan, M. R. Ultrasensitive Electrical Biosensing of Proteins and DNA: Carbon-Nanotube Derived Amplification of the Recognition and Transduction Events. *J. Am. Chem. Soc.*, **126**(10), 3010–3011, 2004.

[11] Wang, J., Liu, G., B., M., Lin, L. and Zhu, Q. DNA-Based Amplified Bioelectronic Detection and Coding of Proteins. *Angewandte Chemie International Edition*, **43**(16), 2158 2161, 2004.

[12] Geho, D., Lahar, N., Gurnani, P., Huebschman, M., Herrmann, P., Espina, V., Shi, A., Wulfkuhle, J., Garner, H., Petricoin, E., Liotta, L. A. and Rosenblatt, K. P. Pegylated, Steptavidin-Conjugated Quantum Dots Are Effective Detection Elements for Reverse-Phase Protein Microarrays. *Bioconjugate Chem.*, **16**(3), 559–566, 2005.

[13] Geho, D. H., Jones, C. D., Petricoin, E. F. and Liotta, L. A. Nanoparticles: potential biomarker harvesters. *Current Opinion in Chemical Biology*, **10**(1), 56–61, 2006.

[14] Georganopoulou, D. G., Chang, L., Nam, J.-M., Thaxton, C. S., Mufson, E. J., Klein, W. L. and Mirkin, C. A. From The Cover: Nanoparticle-based detection in cerebral spinal fluid of a soluble pathogenic biomarker for Alzheimer's disease. *PNAS*, **102**(7), 2273–2276, 2005.

[15] Tang, F. Q., Li, J. R., Zhang, L. and Jiang, L. Improvement of enzymatic activity and lifetime of Langmuir-Blodgett films by using submicron SiO2 particles. *Biosensors and Bioelectronics*, **7**(7), 503–507, 1992.

[16] Seong, S.-Y. Microimmunoassay Using a Protein Chip: Optimizing Conditions for Protein Immobilization. *Clin. Diagn. Lab. Immunol.*, **9**(4), 927 930, 2002.

[17] Miller, L. D., Long, P. M., Wong, L., Mukherjee, S., McShane, L. M. and Liu, E. T. Optimal gene expression analysis by microarrays. *Cancer Cell*, **2**(5), 353–361, 2002.

[18] Liotta, L. A., Espina, V., Mehta, A. I., Calvert, V., Rosenblatt, K., Geho, D., Munson, P. J., Young, L., Wulfkuhle, J. and Petricoin, E. F. Protein microarrays: Meeting analytical challenges for clinical applications. *Cancer Cell*, **3**(4), 317–325, 2003.

[19] Huang, N. P., Michel, R., Voros, J., Textor, M., Hofer, R., Rossi, A., Elbert, D. L., Hubbell, J. A. and Spencer, N. D. Poly(L-lysine)-g-poly(ethylene glycol) layers on metal oxide surfaces: Surface-analytical characterization and resistance to serum and fibrinogen adsorption. *Langmuir*, **17**(2), 489–498, 2001.

[20] Zhen, G., Falconnet, D., Kuennemann, E., Voeroes, J., Spencer, N., Textor, M. and Zurcher, S. Nitrilotriacetic Acid Functionalized Graft Copolymers: A Polymeric Interface for Selective and Reversible Binding of Histidine-Tagged Proteins. *Advanced Functional Materials*, **16**(2), 243–251, 2006.

CHAPTER 8

Conclusions and Outlook

This thesis investigates the potential of nanoparticles to be self-assembled on patterned samples with various methods. On the one hand, the different processes leading to the self-assembly are identified and investigated. On the other hand, with the knowledge gained from these experiments, silica nanoparticles are assembled on micron-sized patterns produced with two different methods to form particle assemblies. The control and tailoring of the various inter-particle and substrate-particle forces is one key-factor to achieve reliable colloidal assemblies on a patterned surface. Most applications of such particle arrays require a drying step at some point, which is another challenge to master. Capillary forces arising during the drying steps have often a major effect on the nanoparticle distribution. Only if all these processes are understood and controlled, complex particle assemblies on patterned substrates may be reliably achieved.

8.1 Nanoparticle Gradients

Adsorption and kinetic studies were conducted to learn about the behavior of the colloidal nanoparticles upon contact with different surfaces and under various conditions. This knowledge was then used to develop a method, that produces gradients of nanoparticles over several centimeters, where the particle density changes linearly from one end of the gradient to the other (Chapter 4). It is the first time, that such particle gradients are presented as a convenient way of producing morphology gradients on a substrate surface via colloidal methods. The process consists of a

controlled dip-coating step of the substrate in the particle suspension, such that more particles adsorb at the end which is in the suspension for longer times and a lower particle density is achieved on the other end. This technique uses electrostatic interactions between the particles and the substrate to immobilize the nano colloids on the surface. This is achieved by coating the surface with a positively charged polyelectrolyte to which the negatively charged silica particles adsorb during the dip-coating process (Section 4.3.2). OWLS experiments and SEM imaging is conducted to follow the adsorption process *in situ* and after the experiments in order to investigate the adsorption kinetics and to determine the optimal conditions for the production of these gradients. Due to the nature of this method, it is applicable to a variety of systems and not limited to silica particles and silica substrates (as used here). Rather, almost any material combination is possible as long as a few restrictions[1] are obeyed. To further improve the usefulness of this process, a heat treatment step is performed, which is able to tailor the morphology of the colloidal particles on the gradient. During that heat treatment step, particles are partially sintered and consequently the shape of the particles can be continuously changed from spherical to half-spheres and at temperatures above 1200 °C — the particles are finally completely sintered into the substrate (Section 4.3.3). The production of such colloidal gradients is only possible if the adsorption kinetics, the nature of the electrostatic interaction and the sintering kinetics of the heat treatment are investigated in detail.

8.2 Particle Self-Assembly by Capillary Forces

In the course of this work, the importance of capillary forces was stressed many times. Whenever particles on a surface dry, capillary forces drag these particles on the surface towards each other. The strength of these forces is calculated and compared to other forces and it is found, that in most situations, capillary forces overcome these other forces (such as electrostatic forces between the particle and the substrate) by many orders of magnitude. As a rule-of-thumb, capillary forces dominate the assembly process on a substrate. This is the more true, if the substrate exhibits a pattern. Therefore, a patterning system — developed previously in-house — is used to produce a distinct wettability contrast, in order to deliberately

[1]Both, substrate and particles, should be negatively charged at the pH used (i.e. an IEP below 6 is required) and the adsorption kinetics must be known

use the power of the capillary forces to self-assemble nanoparticles on hydrophilic structures (Chapter 5). The mechanisms governing this process are examined and criteria are deduced that must be fulfilled to be able to produce nanoparticle assemblies on patterns with a hydrophobicity contrast (Section 5.3.3). With those parameters, nanoparticle assemblies of various geometries are then produced by either drop-drying or by removing the patterned sample at controlled conditions from the suspension. It is found, that low dip-coating speeds (0.1-1 $\mu m/s$) and moderate particle concentrations (0.1-1 $wt\%$) yield the best results as far as quality of the nanoparticle arrays goes. Furthermore, the line width of the samples (as well as withdrawal speeds and particle concentrations) influence the number of layers formed on a hydrophilic line. Thinner lines, faster withdrawal speeds and low particle concentrations generally lead to fewer layers of particles on a substrate. Lines down to 5 μm could be filled with particles and separation distances of the lines of 1 μm were sufficient to de-wet and thus no particles were found on the background.

8.3 Functionalizing Nanoparticles

In some cases, particle assemblies on a substrate will be useful *per se*. However, for many possible applications, nanoparticles assembled on a surface pattern will need to have a certain function assigned to it. In this work, silica nanoparticles were functionalized with the co-polymer PLL-g-PEG (Chapter 6). First, such a coating introduces a steric barrier on the surface, which is favorable for the stability of the colloidal suspension. Second, the PLL-g-PEG-adlayer on the particle surface renders the particles protein resistant, a fact which will make this kind of functionalized particles interesting for applications in the field of biotechnology. ζ-potential measurements, OWLS experiments and SEM investigations are conducted to observe the properties and the success of the PLL-g-PEG coating. This functionalization step is rather general and may also find applications in various other particle systems (such as e.g. magnetic beads, other metal oxide systems or (with a slightly different approach) gold colloids).

8.4 Arrays of Functionalized Particles

PLL-*g*-PEG functionalized nanoparticles have another interesting feature: at the end of the PEG-side chains, functional units, such as biotin, can easily be incorporated. The biotin-unit of the PLL-*g*-PEG/PEG-biotin coating of the particles is then able to bind to streptavidin molecules, which are for example present on the surface.[2] A patterning method is chosen, based on functionalized PLL-*g*-PEG/PEG-biotin and unfunctionalized PLL-*g*-PEG, were the PLL-*g*-PEG/PEG-biotin particles can be adsorbed specifically to the biotinylated areas of the underlying PLL-*g*-PEG / PLL-*g*-PEG/PEG-biotin pattern via a streptavidin linker (Section 6.3.3). It is shown, how the functionalized silica nanoparticles selectively adsorb to the surface pattern, as long as the biotin density is high enough (above 10%). Furthermore, it was found, that capillary forces tend to disturb the pattern formation, since they are stronger than the biotin-streptavidin interaction between particle and substrate. However, particle arrays of functionalized particles can be obtained and it is proven that these particle layers are indeed resistant to protein adsorption (Section 7.3.2). Based on these protein resistant nanoparticle arrays, concepts are developed which show how such particle arrays may be used in biosensing devices due to their large specific surface area (Chapter 7). For such an application, not one but two independent functions per particle are in some cases necessary.[3] The first function[4] acts as an anchor for the particles to the surface and the second function will be used as a capturing agent[5], that allows the immobilization of a biomolecule of interest. First data on these systems is presented in this thesis.

8.5 Outlook

In the course of this thesis, different ways of organizing nanoparticles on (patterned) surfaces have been investigated. For all these methods, two main directions of future developments may be envisaged. Either, the process itself can be further developed

[2]Note, that this function may also directly act as a "capturing" function to bind target molecules containing a streptavidin-molecule

[3]It might also be possible with a single functionalization, where some of these functional units are used to bind to the surface and other are used to capture target molecules.

[4]The biotin-streptavidin system in this work

[5]PLL-*g*-PEG/PEG-NTA / 6-His-tagged proteins or anti-human fibrinogen / fibrinogen are examples for such capturing agents and their sample molecule

and studied in order to improve the quality and the features of the particle arrays or a more application-oriented approach could be chosen to use the particle-arrays in systems, where their particular properties would increase the performance of a given device. Depending on the progression level of these methods, one or the other way may be more applicable and in the following paragraphs some more detailed ideas are presented.

8.5.1 Nanoparticle Gradients

The presented technique to form nanoparticle gradients is shown to work for 40 and 73 *nm* silica nanoparticles on PEI-functionalized silica substrates. It is mentioned, that almost any material combination will work reliably as long as both, surface and particle, are charged negatively. Thus, this potential might be tested in future work to produce particle gradients of different material combinations. Metal or metal oxides are good choices since they can be heat treated similarly as shown in this work to form stable particle density gradients. For any new system, adsorption kinetics, the optimal concentration regime, immersion profile and sintering conditions have to be re-adjusted, however, the basic parameters are expected to be rather general. Many material combinations may be of interest for such future analysis: gold-nanoparticle gradients (that can be functionalized selectively with various molecular systems) on a selected substrate, titania particle gradients on a silica substrate (or vice versa) to produce nanostructured SMAP[6] samples, the direct adsorption of functionalized particles into gradients (without a heat treatment step if the functionality is of organic origin) or also polymeric particles on various substrates. If polymeric particles are chosen, a heat treatment step at adjusted temperatures can still be applied to "glue" the particles to the surface. Also, systems of different charge signs may be studied, in such a case, the (positively charged) polyelectrolyte on the substrate surface will not be necessary. A suitable testing system may be silica-alumina, where (at neutral pH) positively charged alumina particles will adsorb to the negatively charged silica surface (or — again — silica particles may be used to adsorb to alumina substrates).

Also, functionalized particles as presented in Chapters 6 and 7 might be interesting candidates for the formation of colloidal gradients. The surface would then be cov-

[6]The process introduced in Chapter 5

ered with PLL-*g*-PEG/PEG-biotin/streptavidin in order to bind PLL-*g*-PEG/PEG-biotin coated or even bi-functionalized particles to the surface. Such gradient processes might be even combined with MAPL structures on the surface to have both, a pattern and an overlying particle gradient on one substrate.

The colloidal gradients presented might also be used as a mask to turn the morphological gradient into a chemical contrast. Various methods exist to turn an adsorbed particle layer into a chemical contrast.[1] The presented methods offers a way to efficiently produce a nanoparticle gradient, which could be turned into a chemical gradient with such techniques. The production of this kind of chemical gradients again might find many interesting applications. Using polymeric particles instead of metal oxide particles might also allow the subsequent control of the particle size by applying a plasma process. Projects using plasma treatments to tailor the shape of polymeric particles[7] are currently on the way in our group and a combination with the presented gradient technology may provide interesting results.

Besides the many systems of interest that are worth to be explored with the presented technique, many applications for such particle gradients can be pictured. The advantages of a gradient material may have potential uses in many areas, particularly in biotechnology and medicine, where — for example — such gradient materials will allow for rapid screening tests or combinatorial and diagnostic studies performed on a single sample. A first project is currently on the way in our group, where nanoparticle gradients are used to study osteoblast cell proliferation and growth as a function of the surface topography. This is a classical example, how a gradient material may offer a significant advantage compared to homogenous samples in terms of rapid screening. In a similar fashion, tailored particle gradients may be useful in a number of applications given the broad applicability of the presented process.

8.5.2 Silica Nanoparticle Assemblies

Capillary forces are used to self-organize nanoparticles on wettability contrast pattern. This technique is developed and a number of different geometries are patterned with layers of nanoparticles. For the future, a number of interesting questions remain to be answered. Reproducibility of the self-assembled arrays may be further

[7] also combined with an etching process of the background not coated by the particles

increased with proper procedures. Controlling and studying the influence of temperature and humidity on array-formation as well as working under clean-room conditions may have a positive impact on the particle arrays. Furthermore, the influence of particle size and feature size on the formation of these colloidal structures may be of interest. Interesting results might also be gotten from using bi-modal particle suspensions for the assembly. Essentially, larger colloids can not be self-assembled on small structures, whereas smaller colloids will. Such ideas may also open the road to, for example, colloid fractionation on suitably tailored samples.[3]

Alternatively, ways of tailoring the capillary forces involved in the drying process may be investigated. For one, working with low-surface-tension solvents will reduce these forces and may have an impact. Alternatively, Park et al. showed, that using a mixture of formamid and water instead of pure water suspension is a possible way to suppress "coffee ring" effects,[2] which are also observed in our experiments. This treatment might help to homogenize particle assemblies (especially on square samples, where "coffee ring" effects are common).

8.5.3 Functionalized Nanoparticles

Functionalization schemes for nanoparticles are introduced and arrays of PLL-*g*-PEG-functionalized silica particles on MAPL pattern are produced. However, reproducibility issues are still a problem and capillary forces during drying disturb the colloidal arrays. While these problems cannot completely avoided, certain measures may be undertaken to reduce these issues. For example, the rinsing/drying process so far only dilutes the particles in suspension to a factor where still a considerable amount of particles is present in the suspension. An alternative way of removing the particles may be considered to reduce these problems, like step-wise dilution or working in a flow-cell.

A lot of potential lies also in the bi-functionalization concepts that are introduced in the last chapter. Coating particles with two different functions for the application in biosensing devices is an interesting way of increasing the sensitivity, however, still a lot of work has to be put into the development of a working system. Several problems have to be tackled in order to do so: a detection method has to be found, that allows the (quantitative) assessment of the particle' surface chemistry. OWLS studies on flat substrate (as started in this work) will give useful information, but

it will arguably not be sufficient for the characterization of colloidal particles. Also, the systems presented in this work might turn out to be not optimal for this purpose: at the time of writing, projects are carried-out that assess this problem further by, for example, changing the particle system from silica to latex particles with better defined surface chemistries.

(Bi)-functionalization of other colloidal particles might be of interest. For example, (bi)-functionalization of colloidal gold nanoparticles and the arrangement of these particles on a surface (i.e. with the MAPL process), might be a possible way to form localized surface plasmon resonance (LSPR) sensors.[4, 5]

Also the coating itself, based currently on PLL-*g*-PEG-functionalized copolymers may be changed in order to achieve a better quality of the coating with other systems available from our lab.

Furthermore, the incorporation of functional particles into biosensing devices to show the feasibility of these concepts will be an interesting task. First steps in this direction are currently undertaken in the thesis work of Martin Halter (in our group), who investigates the behavior of colloidal particles in commercially available biosensing devices.

Certainly, the basic concepts presented here offer many possible ways of using such functionalized particles, however, these systems must be further assessed with suitable methods before the most promising directions for the development and application of these systems will arise.

Bibliography

[1] Haynes, C. L. and Van Duyne, R. P. Nanosphere Lithography: A Versatile Nanofabrication Tool for Studies of Size-Dependent Nanoparticle Optics. *J. Phys. Chem. B*, **105**(24), 5599–5611, 2001.

[2] Park, J. and Moon, J. Control of colloidal particle deposit patterns within picoliter droplets ejected by ink-jet printing. *Langmuir*, **22**(8), 3506-3513, 2006.

[3] Fan, F. and Stebe, K. J. Size-Selective Deposition and Sorting of Lyophilic Colloidal Particles on Surfaces of Patterned Wettability. *Langmuir*, **21**(4), 1149 1152, 2005.

[4] Haes, A. J. and Van Duyne, R. P. A Nanoscale Optical Biosensor: Sensitivity and Selectivity of an Approach Based on the Localized Surface Plasmon Resonance Spectroscopy of Triangular Silver Nanoparticles. *J. Am. Chem. Soc.*, **124**(35), 10596-10604, 2002.

[5] Haes, A. J., Hall, W. P., Chang, L., Klein, W. L. and VanDuyne, R. P. A Localized Surface Plasmon Resonance Biosensor: First Steps toward an Assay for Alzheimer's Disease. *Nano Letters*, **4**(6), 1029 1034, 2004.

Acknowledgements

A thesis work is not possible without the support of many people. In about every part of work during my thesis, advice / help / support / criticism / cynicism / reproval / friendship and many other forms of "making-life-easier"-actions were greatly appreciated and needed. It is this section were I have the possibility to thank everybody for their help in the last 4 years.

First, I sincerely thank both my Professors for not only giving me the opportunity to work in their group(s) but also for their continuous support. Prof. Marcus Textor invited me to join his group and guided and supported my in a wonderful way especially during the first year of my thesis. The mixture of scientific knowledge, very large experience in all processes involved in the daily life in a scientific community and the great care and understanding he shows for his students make it a real privilege for me to be able to call him my "Doktorvater". However, technically speaking, this "title" belongs to Prof. Janos Vörös. Janos got continuously more involved in my project over time and soon became my main source of scientific inspiration and advice, especially in the last two years. So I took the opportunity to move with Janos to join his newly formed group and I am proud to be the first PhD student to finish in his exiting group!

I also would like to thank my board of co-referees consisting of Prof. Heinrich Hofmann from the EPF in Lausanne and Dr. Erik Reimhult. Reading through the whole thesis and giving me their valuable comments is highly appreciated. Special thanks go to Erik who, besides thoroughly correcting my thesis, gave so many scientific inputs and really has the gift to see the important points and ask the nasty questions.

Back in the old days, some 3-4 year ago, it was Dr. Fabiano Assi, who was my first Postdoc in charge of me and my project. He was almost as new to the group as me

and his input helped so much to avoid at least the worst mistakes in experiment design in my starting phase. His struggles to teach me the importance of developing a strict working plan and a good lab journal are not forgotten, Fabiano, however...

Dr. Didier Falconnet shared a desk with me for about 2 years and also most of his knowledge about patterning of surfaces. He taught me the MAPL and SMAP techniques (supported by Dr. Roger Michel, who rushed in for some weeks to also give me a crash course on SMAP), which were the basis of much of my work. But also his other remarks about surface science and all other aspects of life in general were (and are) greatly appreciated. I really enjoyed sharing a desk with you!

Speaking about "remarks about surface science and all other aspects of life", I also would like to thank Dr. Samuele Tosatti, lab officer of LSST, who never stopped reminding me about all the mistakes I was making in the lab. Always. And Forever. You are unique and hope you still do like me a little bit. I for sure will never forget your PhD party and now you are only one thing a head of me...

Which brings me to the rest of the people of LSST. I think — or better fear — that it is a rather rare occasion in professional life that you have the opportunity to meet and work with so many like-minded and nice people in one place. The enjoyable atmosphere in the LSST (and LBB) institutes is really the perfect working environment and I'd like to thank all members of the institutes for contributing to this as scientists and friends. Despite the danger of missing someone important, I have to mention and thank a few people specifically: Stéph Pasche and Laurent Feuz for teaching me every little detail about that omnipresent copolymer. Tinu Halter and Thomas Blättler for doing all the lab introductions, lab tours, bureaucratic stuff and social events for me. Duessi for being a even less tidy office mate than me (which made me look less bad) and the mostly valuable discussions about science and life, Brigitte Städler for the constant pressure she put on me by starting new experiments when I was leaving office, knowing every piece of literature and still knowing (and introducing me to) every little rumor the lab has to offer. Thanks for all that and thanks for having become good friends.

Martin Elsener and Jaroslav Vanicek did great jobs in their machine shops for me and helped me a lot with their experience in building home made devices, which I gratefully acknowledge. Also, I'd like to thank Mike Gabi, Dominik Textor and Rohit Mishra, who had the pleasure (I hope) to work for me as Hilfsassistenten or as a master student.

Experiments were partially performed at the clean room facilities in the FIRST Center for Micro- and Nanoscience (ETH Zurich) and also at the Institute of Non-metallic Materials of Prof. Gauckler. A big thank to the people there for their support and help. Any kind of metal oxide coatings were produced at the PSI (Villingen, Switzerland) by Michael Horisberger, who spent many days with me coating hundreds of different substrates. Thank you.

Also, members of other groups, such as Dr. Kurosch Rezwan and Dr. Brandon Buergler of Prof. Gaucklers group and many others were of great help introducing me to equipment I was allowed to use in their Labs (such as ζ-potential devices or the SEM). A big thank to them for the time they spent with me and for being good friends.

A big thanks goes out to all my friends in my hometown Küssnacht and in Zurich, my volleyball team mates, my alternative soccer league friends, all the online-mates from "World of Warcraft" especially Christian Zink and many other people. Don't be angry if I forgot to mention YOU! ;) They were all kind enough to endure my presence, because they knew at one point it would pay out and they would be allowed to call me "Doctor". This time has come. ;)

Finally, I would like to thank my parents for their unconditional support and interest in my work, their patience with me and all the care they showed for me during my whole life. Not to forget my brother Roli, who is actually a really nice brother to have! Last but not least my special thanks go out to Nati, for her constant support, care, comprehension and for accepting me the way I am. I hope we keep having a wonderful time.

ETH Zurich and the Swiss Priority Program for Nanotechnology "Top Nano 21" are gratefully acknowledged for their generous financial support (CTI grant 5971.2).

Seite Leer /
Blank leaf

Curriculum Vitae

Christoph Beat Huwiler

Date of birth:	5^{th} of January, 1975
Citizenship:	Hasle (LU), Switzerland
Marital status:	unmarried
Children:	none
Address:	Bahnmatt 15, CH-6340 Baar
Telephone:	+ 41 41 760 66 08
Mobile:	+ 41 79 293 55 77
E-mail:	chuwiler@gmx.ch

Education

2002 – 2006	**Swiss Federal Institute of Technology, ETH Zurich** Doctoral student at the Laboratory for Surface Science and Technology
1995 – 2001	**Swiss Federal Institute of Technology, ETH Zurich** Studies of "Material Sciences and Engineering" Graduation with the degree Dipl. Werks.-Ing. ETH (masters)
1989 – 1995	**Gymnasium Bethlehem, Immensee** Matura Typus B

Experience

2002 - 2006	Research associate and doctoral student at the Laboratory for Surface Science and Technology of Prof. Spencer and Prof. Textor, ETH Zurich, Switzerland
2001 - 2002	Research associate at the Institute of Nonmetallic Inorganic Materials (Prof. Dr. L. Gauckler), ETH Zurich, Switzerland
2000 - 2001	Diploma Thesis: "Grain Growth of Micron-Sized Grains in Undoped and CoO-Doped Ce0.8Gd0.2O1.9" Institute of Nonmetallic Inorganic Materials (Prof. Dr. L. J. Gauckler),ETH Zurich, Switzerland
1999 - 2000	Assistant in Biomaterials Group of Prof. Wintermantel, ETH Zurich
1998	Internship at ABB Research Center (4 month), Baden-Dättwil, Switzerland
1998	Cambridge Advanced Certificate, San Francisco, USA

Publications

Journal Articles

2006 **Nanopatterns with Biological Functions (Invited Review)**
C. Huwiler, M. Ochsner, B. Städler, T. Blättler, J. Vörös, M. Grandin
Journal of Nanoscience and Nanotechnology **2006**,6(8):2237-2264

Grain Growth of Micron-Sized Grains in Undoped and Cobalt Oxide Doped Ceria Solid Solutions
E. Jud, **C. Huwiler**, L.J. Gauckler
Journal of the Ceramic Society of Japan **2006**,114(11):963-969

Colloidal Gradients on Metal Oxide Surfaces
C. Huwiler, T. Kuenzler, N.D. Spencer, J. Vörös
in Preparation **2006**

2005 **Self-assembly of functionalized spherical nanoparticles on chemically patterned microstructures**

C. Huwiler, M. Halter, K. Rezwan, D. Falconnet, M. Textor, J. Vörös
Nanotechnology **2005**,16(12): 3045–3052.

Sintering Analysis of Undoped and Cobalt Oxide Doped Ceria Solid Solutions
E. Jud, **C. Huwiler**, L.J. Gauckler
Journal of the American Chemical Society **2005**,88: 3013-3019.

Conference Proceedings / Poster Presentations

2005 **Nanocolloidal Microarrays on Chemically Patterned Substrates**
C. Huwiler, D. Falconnet, M. Halter, K. Rezwan, J. Vörös, M. Textor
IEEE Nano 2003, July 13–16, Nagoya, Japan

Self-assembly of nanosized particles via colloidal methods; an economical method for novel multi-dimensional functional materials
F. Juillerat, **C. Huwiler**, H. Solak, P. Bowen, M. Textor, H. Hofmann
NanoEurope, September 13–15, St. Gallen, Switzerland

Nano-Colloid Arrays on Micro-Patterned Substrates for Biosensing Applications
(poster presentation, Poster Prize of the Biosurf VI Conference)
C. Huwiler, D. Falconnet, M. Textor, J. Vörös
BioSurf VI, September 20–23, Lausanne, Switzerland

2004 **Self-assembled Colloidal Nano-Arrays on Structured Surfaces for Biosensor Applications**
C. Huwiler, F. Assi, M. Textor
7^{th} World Biomaterials Congress, May 17–20, Sydney, Australia

New Approach towards Protein Adsorption and Exchange *(poster presentation)*
M. Halter, **C. Huwiler**, G. J. Szöllősi, I. Derényi, J. Vörös
7^{th} World Biomaterials Congress, May 17–21, Sydney, Australia

3D Nanostructured Surfaces for Proteomics
(poster presentation, Poster Prize of the Kolloidgesellschaft)
M. Halter, **C. Huwiler**, M. Textor, J. Vörös
2^{nd} Zsigmondy Colloquium, March 3–4, Berne, Switzerland

2003 **Self-assembling of nano-sized SiO_2-Particles on Patterned Substrates**
C. Huwiler, F. Assi, M. Textor
European Cells and Materials Journal, **2003**, 6(supplement 1)

2002 **Constant Heating Rate Sintering of Ceria-Nanopowders**
C. Huwiler, E. Jud, L. P. Meier, L. J. Gauckler
Proceedings of COST 525 Meeting: Advanced Electroceramics: Grain Boundary Engineering, Avairo, Portugal
British Ceramic Proceedings, "Grain Boundary Engineering of Electronic Ceramics"

Oral Presentations

2004 Self-assembled Colloidal Nano-Arrays on Structured Surfaces for Biosensor Applications
C. Huwiler, D. Falconnet, F. Assi, M. Textor
World Biomaterials Congress, May 17–20, Sydney, Australia

2005 Nanocolloidal Microarrays on Chemically Patterned Substrates
C. Huwiler, D. Falconnet, M. Halter, K. Rezwan, J. Vocroes, M. Textor
IEEE Nano 2005, July 13–16, Nagoya, Japan

Awards

2004 Poster Prize of the Kolloidgesellschaft: 3D Nanostructured Surfaces for Proteomics
M. Halter, **C. Huwiler**, M. Textor, J. Vörös
2^{nd} Zsigmondy Colloquium, March 3–4, Berne, Switzerland

2005 Poster Prize of BioSurf VI Conference: Nano-Colloid Arrays on Micro-Patterned Substrates for Biosensing Applications

C. Huwiler, D. Falconnet, M. Textor, J. Vörös
BioSurf VI, September 20–23, Lausanne, Switzerland